Industrial Doctoral Thesis

Development of new applications of simultaneous vision simulator

Carmen María Lago López

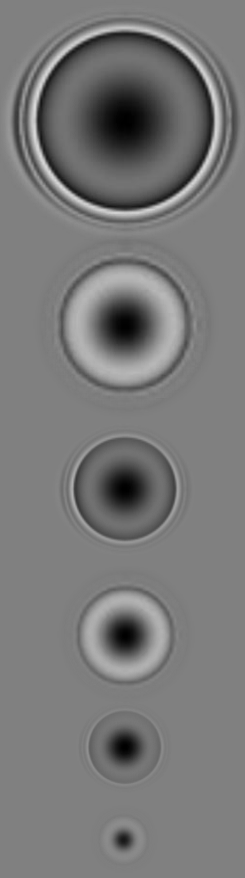

Supervisors

Prof. Susana Marcos Celestino

Dr. Alberto de Castro Arribas

Dra. Lucie Sawides

UNIVERSIDAD COMPLUTENSE DE MADRID

FACULTAD DE CIENCIAS FÍSICAS

TESIS DOCTORAL

Development of new applications of simultaneous vision simulator

Desarrollo de nuevas aplicaciones de un simulador de visión simultánea

MEMORIA PARA OPTAR AL GRADO DE DOCTORA

PRESENTADA POR

CARMEN MARIA LAGO LOPEZ

DIRECTORAS Y DIRECTOR

SUSANA MARCOS CELESTINO

ALBERTO DE CASTRO ARRIBAS

LUCIE SAWIDES

VioBio Lab.
Instituto de Óptica
CSIC

2EyesVision S.L.
Madrid

Departamento de Óptica
Facultad de Ciencias Físicas

UNIVERSIDAD COMPLUTENSE MADRID

DECLARACIÓN DE AUTORÍA Y ORIGINALIDAD DE LA TESIS PRESENTADA PARA OBTENER EL TÍTULO DE DOCTORA

Dña. **Carmen María Lago López**, estudiante en el Programa de Doctorado en Física, de la Facultad de Ciencias Físicas de la Universidad Complutense de Madrid, como autora de la tesis presentada para la obtención del título de Doctor y titulada:

Desarrollo de nuevas aplicaciones de un simulador de visión simultánea

y dirigida por: Prof. **Susana Marcos Celestino**, Dr. **Alberto de Castro Arribas** y la Dra. **Lucie Sandrine Sawides**.

DECLARO QUE:

La tesis es una obra original que no infringe los derechos de propiedad intelectual ni los derechos de propiedad industrial u otros, de acuerdo con el ordenamiento jurídico vigente, en particular, la Ley de Propiedad Intelectual (R.D. legislativo 1/1996, de 12 de abril, por el que se aprueba el texto refundido de la Ley de Propiedad Intelectual, modificado por la Ley 2/2019, de 1 de marzo, regularizando, aclarando y armonizando las disposiciones legales vigentes sobre la materia), en particular, las disposiciones referidas al derecho de cita.

Del mismo modo, asumo frente a la Universidad cualquier responsabilidad que pudiera derivarse de la autoría o falta de originalidad del contenido de la tesis presentada de conformidad con el ordenamiento jurídico vigente.

En Madrid, a 12 de diciembre de 2022

Fdo. LAGO LOPEZ CARMEN MARIA - 77009064G

Firmado digitalmente por LAGO LOPEZ CARMEN MARIA - 77009064G
Fecha: 2022.12.12 12:19:46 +01'00'

Esta DECLARACIÓN DE AUTORÍA Y ORIGINALIDAD debe ser insertada en la primera página de la tesis presentada para la obtención del título de Doctor.

"Si he logrado ver más lejos es porque me he subido a hombros de gigantes"

Isaac Newton

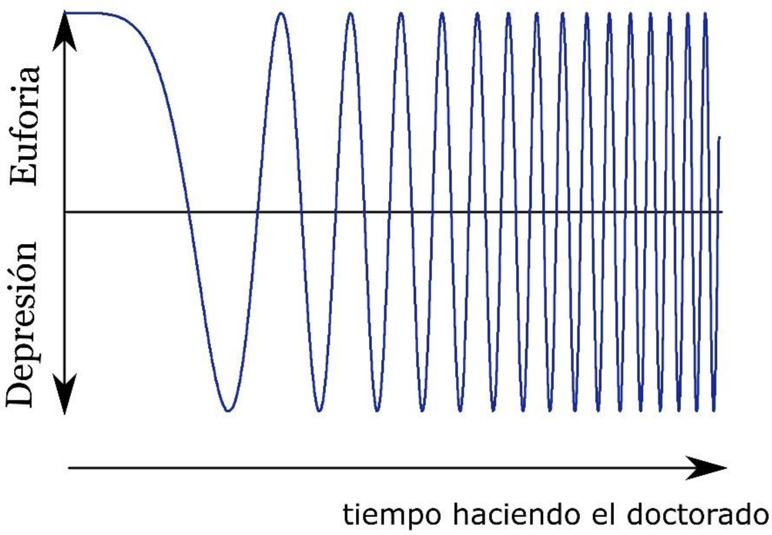

Relación entre estado anímico del doctorando y el tiempo haciendo el doctorado

Científico en España, Guía de supervivencia

Agradecimientos

Al fin llegó este momento, y creo que aún no soy consciente que al fin se acaba. Recuerdo al empezar que muchas veces se define esta etapa como una carrera de fondo, y ahora en este punto sólo puedo confirmarlo. Una carrera que mirando hacia atrás se ve corta y muy larga al mismo tiempo. Una carrera llena de altibajos, de sentimientos encontrados, de aprendizaje, de frustración, de alegría, de soledad, de compañerismo, pasión, impotencia, euforia, stress, felicidad, una pandemia… pero sobre todo de agradecimiento. Muchas son las personas que durante estos años han sido fundamentales para poder llegar a la meta.

A **Susana**, gracias por brindarme esta oportunidad, por la confianza depositada para realizar esta tesis en el grupo. Sigo fascinada cada vez que pienso en esos AO meetings y reuniones en las que en un segundo haces ver los problemas desde una óptica diferente, que nadie más alcanza a ver. Por tu dedicación y pasión que transmites en todo lo que haces.

Quien me diría a mí en 2016 cuando os conocí en el LOUM, que finalmente acabaría en VioBio y vosotros dirigiendo mi tesis, y no creo que nadie podría ocupar mejor ese puesto. **Alberto** ninguna palabra es suficiente para poder agradecerte todo el apoyo, consejos y el conocimiento que me transferiste en estos años. Que con tu libreta y unos esquemas haces que todo se convierta en un mundo más nítido y sencillo. Muchas veces no hacía falta pedirte ayuda porque ya estabas asomado en la puerta después de recibir un mail, tener una reunión… por los increíbles esfuerzos a horas y en días inadecuados para poder llegar a los deadlines de reports, congresos y de esta misma tesis. Si hay algo que te caracteriza es tu humildad y desinterés en un mundo en el que la competitividad es un apellido, donde el foco lo pones soló en avanzar y aprender. **Lucie** ha sido un verdadero placer trabajar a tu lado, eres una gran mentora. Me fascina la impecabilidad y precisión con la que trabajas, eres un todoterreno. Gracias por tu disposición siempre que lo necesité, por todas las correcciones y el esfuerzo que ello conllevaba, y por tu gran apoyo, sobre todo en este último año.

Gracias por supuesto al **AO team**, **Carlos, Susana, Sara, Clara, Ana, María y Merche** sin vosotras esto tampoco sería posible. **Sariña,** quien nos diría en 2016 que nuestros caminos volverían a cruzarse, ¡y como me alegro de que fuese así! Gracias por todas esas horas a oscuras en el AO donde ya no sabíamos en que día u hora estábamos, por enseñarme y ayudarme siempre con esa disposición que te caracteriza, por estar ahí siempre que lo necesité al otro lado de la pared y tus consejos, por ser mi conviviente post pandemia para resucitar ese sistema que tantas alegría y penas nos ha dado. Tendrás una carrera increíble y espero poder seguir de cerca todos tus logros, eso sí, ¡no te olvides de comer! **Clara,** fuiste todo un descubrimiento. La primera persona que conozco que le fascina hablar a grandes públicos jaja. Fue un placer trabajar contigo, aprender a tu lado se hace muy fácil y divertido. Gracias por transmitir ese entusiasmo que tienes por lo que haces, puedo afirmar que el día que esa cubeta funcionó al fin, fue de los más satisfactorios del doctorado y las cañas supieron a gloria. Y aunque nuestros caminos se dividieron, gracias por el apoyo en esta última etapa y tus consejos. Seguiremos con nuestros karaokes y nuestras “ruinas” por mucho tiempo. It was a pleasure sharing these years with you **Lekha**. Thanks for all the helpful talks and fun times shared, and these last months as a “thesis-mate”. I wish you all the best in your new stage!

Como no agradecer a mis industriales también. **Xoana** parece que fue ayer que estábamos en el despacho 302 hablando de cuando llegaría el día de la defensa, y tu ya hace un año que eres Dra Barcala, ¡como pasa el tiempo! ;) aunque compartimos despacho menos tiempo del que me gustaría, gracias por todos tus consejos, sobre todo estos últimos meses que te volví loca con todos los trámites, y por todos los buenos momentos compartidos fuera del trabajo. **Pilariña**, fue un auténtico placer compartir contigo este tiempo, gracias por ser la mejor vice que pude tener en IOPTICA! una pena que la pandemia retrasase el conocernos porque fuiste otro gran descubrimiento. La calma, la pasión con la que transmites a los más peques la ciencia es admirable y la motivación con la que haces todo es contagioso. Compañera de lesiones jaja y que me daba tanto desahogo saber que tenía en la pared de al lado en el laboratorio. No te olvides que los 11F son nuestros :) **Edu,** ese chico que empezó en el despacho trabajando con Carlos y Victor y poco a poco tuve el placer de ir conociendo, gracias por todos los cafeses que nos tomamos despotricando de la vida adulta, que si mudanzas, que si trabajo, que si Madrid no le llega a la suela a Zaragoza y Galicia jaja, y por nuestros viernes de celebración liberados de tuppers en asiáticos y hamburgueserías. Por todo el apoyo y entender que no estaba loca por hablar sola en el despacho día sí y cada día un poco más.

A **Victor**, gracias por comprender que te llamase Jesús los primeros meses ajaja, por ser compañero de desorden de mesa, por conversaciones y por supuesto por esa carrera que nunca olvidaré y me hizo feliz durante meses. **Elena** por tu paciencia infinita en todos los pedidos, dudas, trámites… ya de viajes conmigo te libraste. Por saber escuchar, la psicóloga del grupo. Gracias por todos esos debates posicionados y conversaciones que sientan tan bien, por la calma que transmites. ¡Por todos los buenos momentos de cañas y karaokes, y por muchos más! **Dani** que haríamos en VioBio sin ti, gracias por estar ahí siempre que lo necesitamos, que no fueron pocas veces, da igual que se cayera el techo o un shutter no abriese, siempre tuviste la capacidad de solucionarlo todo y decir “lo que os queda por llorar con este sistema”. **Edu** una lástima que la pandemia separase un poco todo, el tiempo que pude tener la oportunidad de conocerte fue genial, eres la vida de VioBio. Cualquier conversación contigo siempre fue un placer. **Fernando y Alejandra** una lástima que fuese breve el tiempo que tuve para conoceros, pero fue un verdadero placer el tiempo compartido.

Y por supuesto muchas gracias al resto de la gente que formó parte de VioBio durante estos años y tuve el placer de compartirl **Rocío, Nohelia, Mar, Paula, Lupe, James, Iván, Andrés, Amal, Álvaro, Andrea y Judith.**

Gracias por supuesto a toda la gente de 2EyesVision: **Diana, Joshua, Yassine, Álvaro, Cristina, Cándido, Irene y José Ramón.** En especial a **Carlos** tanto por tus consejos y debates en los AO meetings, como después en 2Eyes. Gracias por la pasión y la ilusión que transmites. También la importancia que das a la hora de formación y crear equipo y bienestar que es fundamental. **Enrique** fue un placer trabajar contigo, un aprendizaje continuo. Cada inconveniente se convertía en un debate maravilloso lleno de nuevas posibilidades y soluciones.

Por su puesto gracias a **IOPTICA**; descubrí lo maravillosa y necesaria que es la divulgación y disfrutar con ella como una niña más. Por cada uno de los proyectos, la motivación y el crecimiento personal que me aportasteis, a todos los que dije antes y **Pablo, Miguel, Carlos, Francesca y Néstor**.

A **Justo**, muchísimas gracias por tu confianza sin apenas conocerme, has sido mi motor y parte fundamental en esta última etapa. Gracias por tu apoyo, por tus consejos, tu entusiasmo y tu empatía.

No puedo olvidarme a toda la familia Madrileña, fundamental para mi salud mental y superar un doctorado en medio de una pandemia. **Mele** por acogerme en tu casa y hacerlo nuestro hogar los primeros meses. **Mef** por esos dos años compartidos y todas las mil tundas y consejos al llegar a casa, sobrevivimos a una pandemia encerradas que se dice pronto. **Angeliño** y **mi panito** por todos los descansos y cafés tan reconfortantes, todas las tundas y conversaciones de vida a cualquier hora, conspiraciones, por las mil risas y por hacerme sentir como en casa desde el primer día. **Paula** por todas nuestras cañas eternas por el barrio. A todos mis **pachangadictos**, ¡qué maravilla encontraros en el camino!, en el voley no sólo encontré un deporte sino una familia que hizo que Madrid dejase de ser una ciudad llena de gente con prisa y solitaria, y el domingo pasase a convertirse en el mejor día de la semana, en especial a **Javi, María, Gema, Berto, Edgar y Oli.** Y a mis **PTR** que me permitieron irme de Madrid ganando la liga.

A elas, que pasan os anos e a pesar da distancia sempre están ahí, **María, Pili, Vaz e Vicky. Luchi** polas mil tundas, polo teu apoio e pola incrible muller que es e da que aprendo cada día. **Juls** polas duascentas telecañas, por estar e ser dende cativas, por ser un referente e polos mil desafogos que con poucas palabras ninguén coma ti pode entenderme.

E por último os mais importantes, non a escollemos, pero se tivéramos que facelo non dubidaría en facelo mil veces. Por apoiarme incondicionalmente en cada paso, cada mudanza, cada toleira, en tódalas miñas decisións persoais e laborais, a pesar de non ter claro aínda que é o que fago. A ti **papá** por ser un loitador nato, o meu referente na vida, por estar sempre que o preciso. **Mamá,** por ser tan comprensiva e cálida, estar e ser incondicional dende cativa,sei que unha parte fundamental de seguir este camiño es ti. **Chu**, polas mil conversas ata altas horas e consellos que sempre me das e tanto me axudan. **Xián**, meu pequecho que adoro e sorpréndeme escollendo ciencias divertidas como fai a súa nana. Quérovos, sen vos nada disto seria posible.

Funding

This thesis it was possible thanks to the funding received by public and private institutions:

- Madrid Regional Government (CAM). Industrial PhD Grant IND2018/BMD-9809 to Carmen María Lago.

- Spanish Government Grant FIS2018-2020 to Susana Marcos

- Objective on bench assessment of Alcon EDF IOL: IOL cuvette and AO simulation, 2019-2021

- Computer predictions of Isofocal IOL in realistic model eyes, 2019-2020

- PresbyLASIK ablation patterns simulation with SCHWIND eye tech solutions GmbH

"La vida es fascinante, sólo hay que verla a través de las gafas correctas"

Alexandre Dumas

Summary of the thesis in Spanish

Desarrollo de nuevas aplicaciones de un simulador de visión simultánea

Introducción

La presbicia y la catarata son dos procesos fisiológicos asociados a la edad que afectan a la visión. La presbicia es debida a la pérdida de elasticidad del cristalino que implica una pérdida de la capacidad de enfocar objetos cercanos. Hay múltiples soluciones actualmente en el mercado como gafas progresivas, lentes de contacto multifocales y PresbyLASIK entre otros, pero ninguna restaura completamente el proceso acomodativo. La catarata es una opacificación del cristalino que impide el paso de la luz y puede ocasionar ceguera, su tratamiento se basa en reemplazar el cristalino por una lente intraocular. Hay más de 100 diseños de lentes intraoculares actualmente en el mercado y la lente a implantar se selecciona atendiendo a las aberraciones oculares y el estilo de vida de cada sujeto porque no hay ningún diseño que restablezca la visión a todas las distancias para toda la población.

El simulador visual SimVis Gekko (2EyesVision S.L.), es una tecnología reciente basada el principio de multiplexación temporal (visión simultánea), y permite a los sujetos ver binocularmente a través de diferentes diseños multifocales antes de la cirugía de cataratas. De esta forma, es posible la selección del diseño más adecuado para cada sujeto maximizando el confort visual después de la cirugía y reduciendo problemas de adaptación al diseño seleccionado después de la operación en la clínica.

Las lentes extendidas de foco (EDOF), son una nueva clasificación de diseño de lentes intraoculares. Los programas de diseño óptico permiten diseñar modelos de ojo pseudoafáquicos, convirtiéndose en grandes predictores del comportamiento visual, con diferentes diseños de lentes intraoculares. Ofrecen la posibilidad de explorar distintos grados de libertad para simular casos clínicos generales (como el descentramiento e inclinación de la lente), específicos (como la simulación de la óptica en pacientes operados de LASIK) y de gran interés para los fabricantes (como la estabilidad del diseño en un amplio rango de potencias, o el estudio de su comportamiento con córneas realistas).

Los simuladores visuales basados en óptica adaptativa son una herramienta muy útil que permiten de una forma no invasiva manipular el frente de onda. Permiten el estudio de diseños de lentes intraoculares, antes incluso de que sean fabricadas e implantadas. En esta tesis se utilizan distintos dispositivos como espejos deformables, moduladores espaciales de luz y lentes optoajustables combinadas con la tecnología SimVis para validar la simulación de las lentes intraoculares y para evaluar sus propiedades.

Métodos

En esta tesis se ha utilizado el programa de diseño óptico de Zemax para el modelado personalizado de ojos pseudoafáquicos para el estudio de los lentes EDOF de reciente aparición en el mercado y dos lentes monofocales para comparar el comportamiento visual entre correcciones. Se han realizado diferentes estudios para evaluar las lentes en términos de calidad óptica y profundidad de foco y para evaluar los halos producidos en la retina. Además, se ha estudiado de forma computacional su comportamiento en diferentes casos clínicos: descentramiento e inclinación de la lente con respecto a la córnea, inducción de aberraciones oculares, diámetro pupilar, potencia de la lente y uso en pacientes operados de LASIK.

También, se han realizado estudios en un simulador visual basado en óptica adaptativa y se han estudiado distintas métricas de un paso y de doble paso en sujetos de forma no invasiva simulando dos lentes EDOF y midiendo la calidad visual a través de foco. Estos trabajos han permitido estudiar las distintas posibilidades de simulación de las lentes, con modulador espacial de luz y mediante multiplexado temporal con la tecnología SimVis, teniendo como referencia las medidas de la lente física en una cubeta. Además, se modificó el frente de onda con el espejo deformable del sistema de óptica adaptativa para evaluar la influencia de las aberraciones corneales en la lente.

Por último, se ha utilizado el simulador binocular de visión simultánea SimVis Gekko basado en multiplexación temporal para validar la simulación de patrones de ablación PresbyLASIK en sujetos.

Resultados y Conclusiones

Los estudios realizados con las dos lentes EDOF de forma teórica utilizando los programas de diseño óptico, y experimentalmente mediante medidas de banco óptico y en sujetos con un sistema de óptica adaptativa nos han permitido validar la capacidad de la tecnología SimVis para simular estos diseños suaves y verificar la posibilidad de su uso en el ámbito clínico. Estas conclusiones permiten afianzar su competitividad en el mercado.

La lente Isopure muestra un buen balance entre calidad óptica y profundidad de foco con diferentes diámetros de pupila, grados de inclinación de la lente con respecto a la córnea y potencias y aberración esférica corneales. La lente Vivity se ha estudiado para distintos diámetros de pupila y ha demostrado ser relativamente independiente de la aberración esférica y el coma corneales. Los resultaos muestran que una lente intraocular adecuada para pacientes operados de LASIK, especialmente los operados para corregir miopía.

Con la manipulación del frente de onda en el sistema de óptica adaptativa sobre la lente Isopure, los resultados obtenidos indican estabilidad de su comportamiento frente a la manipulación de aberraciones oculares, confirmando que su diseño es robusto y su profundidad de foco estable.

La tecnología SimVis muestra por primera vez, según lo que sabemos, la capacidad de simular diferentes patrones de ablación PresbyLASIK en sujetos, permitiendo la selección del mejor perfil antes de la cirugía y aumentar el confort y el éxito de la cirugía.

Summary of the thesis in English

Development of new applications of simultaneous vision simulator

Introduction

Presbyopia and cataract are two age-related physiological processes that affect vision. Presbyopia prevents focusing on near objects; multiple solutions to compensate it are currently implemented on the market, such as: progressive lenses, multifocal contact lenses and PresbyLASIK among other examples; but none fully restore accommodation process. The cataract is an opacification of the crystalline lens that leads to blindness. Its treatment is based on the crystalline lens replacement by an intraocular lens (IOL). More than 100 IOLs designs are currently on the market, but according with the individual ocular aberrations and lifestyle of each subject, there is still no design that restores vision for the entire population.

SimVis Gekko (2EyesVision S.L.) visual simulator is a recent technology based on the temporal multiplexing principle (simultaneous vision). It was Introduced on the market throughout this thesis, it allows subjects to see binocularly through different multifocal designs before cataract surgery. It makes possible to select the most suitable design for each subject, maximizing visual comfort after surgery and reducing inadaptation to the selected design after surgery in clinics.

The extended depth of focus (EDOF) is a new IOL classification. Optical design programs allow the design of pseudophakic eye models, becoming great predictors of visual behavior, with different IOLs designs. They offer a great degree of freedom to evaluate clinical cases: general (such as IOL decentration and tilt), specific (post-LASIK surgery subjects) and those which manufacturers have great interest in (e.g., design stability in a wide range of lens powers, aberrations influence in the IOL design).

Visual simulators based on adaptive optics (AO) are a useful tool that allow a non-invasive wavefront manipulation and to study the IOL design before they are even manufactured and implanted. Different technologies as deformable mirrors, spatial light modulators (SLM) and temporal multiplexing tunable lenses (SimVis) make it possible to simulate and validate IOL designs and evaluate them to launch in the clinical setting.

Methods

In this thesis, Zemax OpticStudio optical design program has been used for customized model of pseudophakic eyes to study two EDOF IOLs that have launched in the market throughout this thesis. Two monofocal IOLs also have been studied to compare with the EDOF IOLs. Different studies were carried out to evaluate the IOLs performance in terms of optical quality and Depth of Focus (DOF). In addition, more studies were performed to predict the EDOF IOLs behavior in different clinical reports: IOL decentration and tilt in cataract surgery, ocular aberrations induction, pupil diameter size, IOL power and validation of EDOF IOLs used in subjects with post-LASIK surgery, including halos evaluation.

Experimental studies have been carried out in an AO system, on bench and on subjects' measurements with the two EDOF IOLs. Through focus curves have been measured to validate the IOLs simulation with SLM and temporal multiplexing (SimVis technology) in comparison with the physical IOL in a cuvette as a reference. In addition, the wavefront in the AO system was manipulated with the deformable mirror to evaluate the influence of ocular aberrations in the IOL design.

SimVis Gekko simultaneous binocular visual simulator based on temporal multiplexing was used to evaluate the ability to simulate PresbyLASIK ablation patterns in subjects.

Results and conclusions

In this thesis, different studies of two EDOF IOLs have been performed theoretically through optical design, and experimentally with an AO system which allow us to evaluate the ability of SimVis technology to simulate soft designs, as EDOF IOLs, and verify the possibility of its use in the clinics to strengthen the SimVis technology in the market.

The design of the two EDOF IOLs has been evaluated computationally and they show robustness in their designs. The Isopure IOL shows a good balance between optical quality and depth of focus at: different pupil diameters, when it's tilted, with different corneal power and with spherical aberration induction. In addition, Isopure shows stability in the design for a range of powers in its catalog from 10 to 35 D. The Acrysof IQ Vivity IOL also shows a good balance between optical quality and DOF at different pupil diameters and a great robustness in its design with spherical aberration and coma induction. The results predicted the Vivity as a good candidate to implant in post-LASIK surgery subjects, especially myopic.

When the wavefront was manipulated with the deformable mirror in the AO system over the Isopure IOL; the IOL performance was stable against the manipulation of ocular aberrations. Isopure design shows robustness and stability in the DOF.

SimVis technology shows for the first time, to our knowledge, the ability to simulate accurately different PresbyLASIK ablation patterns in subjects, allowing the selection of the best profile prior to surgery and increasing comfort and success of surgery. Also increase the SimVis technology applications in the clinics and increase its competitiveness in the market.

Keywords

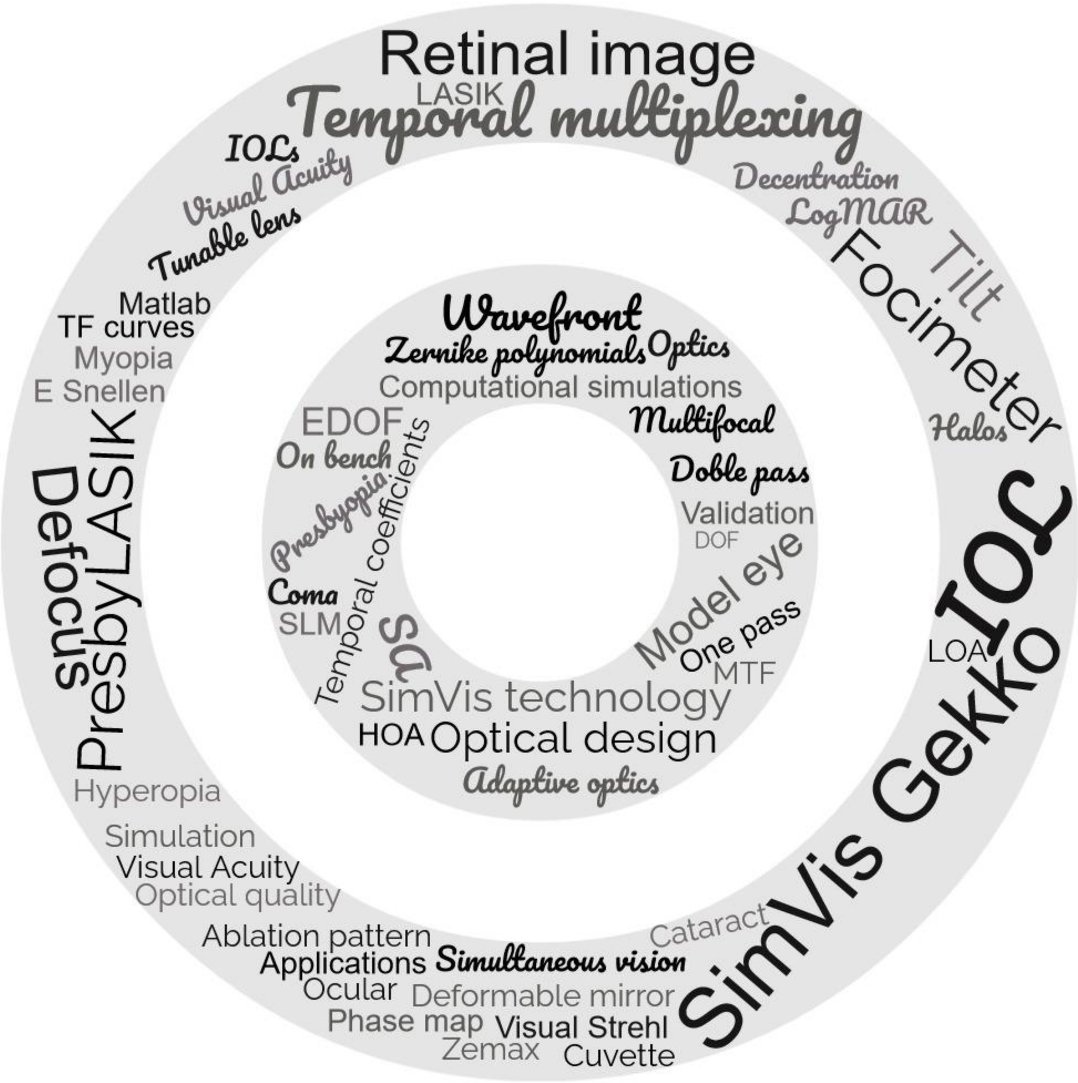
Retinal image
LASIK
Temporal multiplexing
IOLs
Visual Acuity
Tunable lens
Decentration
LogMAR
Tilt
Focimeter
Matlab
TF curves
Myopia
E Snellen
Halos
PresbyLASIK
Defocus
IOL
LOA
SimVis Gekko
Hyperopia
Simulation
Visual Acuity
Optical quality
Ablation pattern
Applications
Simultaneous vision
Cataract
Ocular
Deformable mirror
Phase map
Visual Strehl
Zemax
Cuvette
Wavefront
Zernike polynomials
Optics
Computational simulations
EDOF
On bench
Multifocal
Doble pass
Presbyopia
Temporal coefficients
Validation
DOF
Coma
SLM
SS
Model eye
One pass
MTF
SimVis technology
HOA
Optical design
Adaptive optics

List of contents

“La prueba final del conocimiento es tu capacidad de transmitirlo a otra persona”

Richard Feynman

1 Introduction

The natural ageing changes that occur in the crystalline lens include a progressive loss in its elasticity that results in an inability to increase its power to focus near objects on the retina. This process is called presbyopia and occurs in 100% of the population after an age of about 45 years old. Multiple optical solutions are available to provide vision at different distances after presbyopia onset in the form of glasses, contact lenses or surgery to reshape the cornea or to replace the crystalline lens with an intraocular lens. Over the years, the crystalline lens does not only loss its elasticity, but also its transparency with the appearance of opacifications, called cataracts, in 49% of the population between 60 and 70 years. Cataracts reduce both the amount of light on the retina and the quality of the image formed by the anterior segment, leading to blindness if the crystalline lens is not surgically removed and replaced by an intraocular lens. Cataract surgery is the most frequently performed surgical procedure in the world and there is an increasing number of IOL designs in the market. The evaluation and simulation of the different designs would allow a deeper understanding of the properties of the new designs when coupled to the eye and the individual fit when implanted in a subject. While the ultimate goal of new premium intraocular lenses is to improve visual quality and deliver spectacle-free vision, new technologies that are able to predict the post-operative visual quality prior to surgery, manage patient’s expectations by demonstrating vision with those lenses, and to adapt the choice to the patient’s needs and lifestyle are key to the adoption and success of new lens designs.

The SimVis Gekko (2EyesVision, SL) is a binocular wearable simultaneous vision IOL simulator that is designed to allow the pre-operative evaluation of the post-operative vision with different multifocal designs. The scientific interest of this thesis is the study of vision with premium corrections presbyopia correction, simulated with SimVis Gekko. The technical interest of this thesis is the validation of simulation strategies of different presbyopia corrections in the SimVis Gekko instrument. The industrial interest of this thesis is to expand the catalog of IOLs that can be simulated in the SimVis Gekko binocular visual simulator and to develop new applications for SimVis technology. In addition, through collaborations between the research group and two companies (PhysIOL and Alcon), the performance of two new IOL designs has been evaluated in a number of conditions to account for the impact of their design on vision.

In this chapter, we review the state-of-the-art and present the motivation for the thesis, the overarching hypothesis, and the open questions and goals targeted in the thesis.

1.1 The Visual system

1.1.1 The visual process

The human vision is a complex process that starts when light enters the eye, one of our most important and complex sensory organs. The visual process is divided into three essential stages (figure 1.1): (1) the optical stage that corresponds to the first step of vision, image formation, (2) the retinal stage where the image projected on the retina is sampled by the photoreceptors that convert the light into electrical impulses that is processed by a cascade of neurons and send through the optic nerve to the visual cortex, and (3) the cortical stage corresponding to the neural processing where the image is perceived and the information processed by the brain.

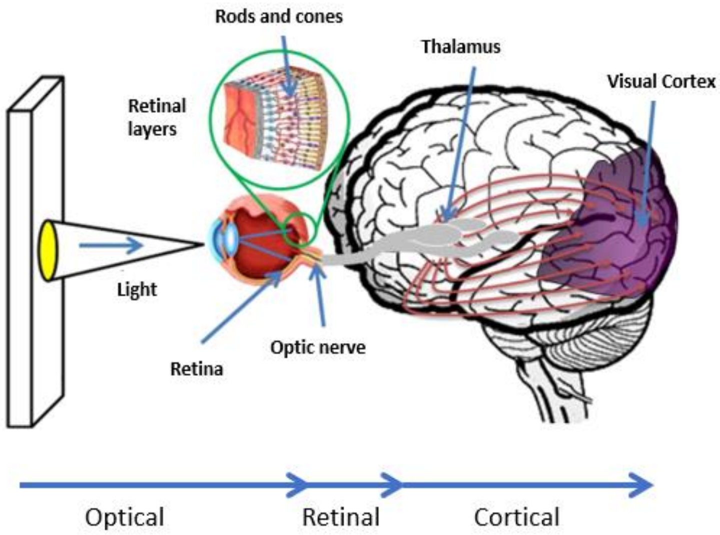

Fig. 1.1: *Visual system scheme. Adapted from Zabihian et al. 2012.*

The first step, i.e., the formation of images on the retinal plane, is a passive process. Despite the relative simplicity of the optical system formed by the cornea and the crystalline lens, or the intraocular lens in pseudophakic subjects, its importance is key and in fact it is one of the elements in the visual process that most limits the quality of vision (Artal 2014).

1.1.2 Optics of the eye

In adult humans, the eye is approximately a sphere with a diameter of around 24 mm in which the cornea and the crystalline lens project images of the outside on to the retina.

The light that reaches the eye enters through the cornea, the first ocular component. The *cornea* is an avascular transparent thin layer of about 12 mm of diameter and about 0.55 mm thickness in the central part. *The cornea* is approximately a spherical section with an average anterior and posterior radius of curvature of 7.8 mm and 6.5 mm respectively, and a refractive index of about 1.377. The cornea provides over the 70% of the optical power of the eye which correspond to about 40 D (Artal 2016). An aqueous tear film softens the first optical surface (anterior corneal surface) to provide the best image quality. The space immediately after the cornea is the anterior chamber filled with a transparent aqueous humor with an index of refraction of about 1.337.

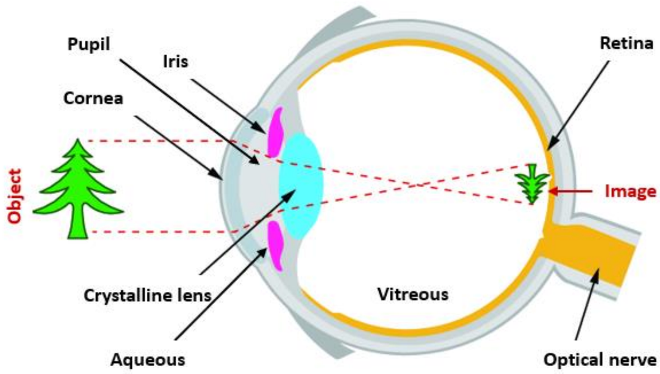

Fig 1.2: *Vertical cross section of the eye forming an image on the retina. Indicating the optical components of the eye. Illustration adapted from (da Costa 2019).*

The iris is formed by two set of muscles with a central hole whose size depends on its contraction and acts as a diaphragm limiting the amount of light passing through the eye and controlling the retinal illumination. The image of the iris through the cornea is the entrance pupil, and its image through the lens corresponds to the exit pupil. The ambient light changes the aperture size from less than 2.0 mm in bright light to more than 8.0 mm in the dark depending on the subject. Since eye is an aberrated optical system, the pupil size affects the image quality projected on to the retina, with small pupils producing an increase in the retinal image quality but with lower illumination.

The *crystalline lens* is located just behind the iris inside an elastic capsule held by ligaments called zonules to the ciliary body. The *crystalline lens* is a biconvex lens with an anterior and posterior curvature radius of about 10.2 and -6.0 mm respectively and with a non-homogeneous refractive index (gradient index). Its equivalent refractive index, the homogeneous refractive index of a lens with the same shape and dioptric power, is about 1.42. The crystalline lens is an active optical element that changes its shape modifying the optical power. When the ciliary muscles contracts and the tension of the zonules is relaxed the crystalline lens increase its thickness producing an increase in of the optical power of the crystalline lens. This mechanism is called accommodation and allows focused vision at different distances in young subjects. Filling the gap between the crystalline lens and the retina there is a transparent humor called vitreous, a gelatinous substance with a refractive index of about 1.336.

The retina is placed at the back of the eye and is a part of the central nervous system. It contains photoreceptors, rods and cones, that are neurons specialized in the detection of light. Rod photoreceptors are characterized by high sensitivity to light, detecting objects at extremely low lighting levels, allowing night vision. Cone photoreceptors respond to high levels of brightness and are responsible for daytime vision. There are three types of cones known as long- (L), medium-(M), and short-(S) wavelength-sensitive cones depending on which portion of the spectrum their photopigment absorbs the most (Dartnall et al. 1983). Normal trichromatic color vision utilizes all three cone photopigments (Figure 1.3). The central area of the retina is called fovea, and provides the highest visual resolution due to the high-density packed cone photoreceptors. The peripheral retina has highest density of rods, to detect movements in the visual field and its resolution is lower than the one at the fovea.

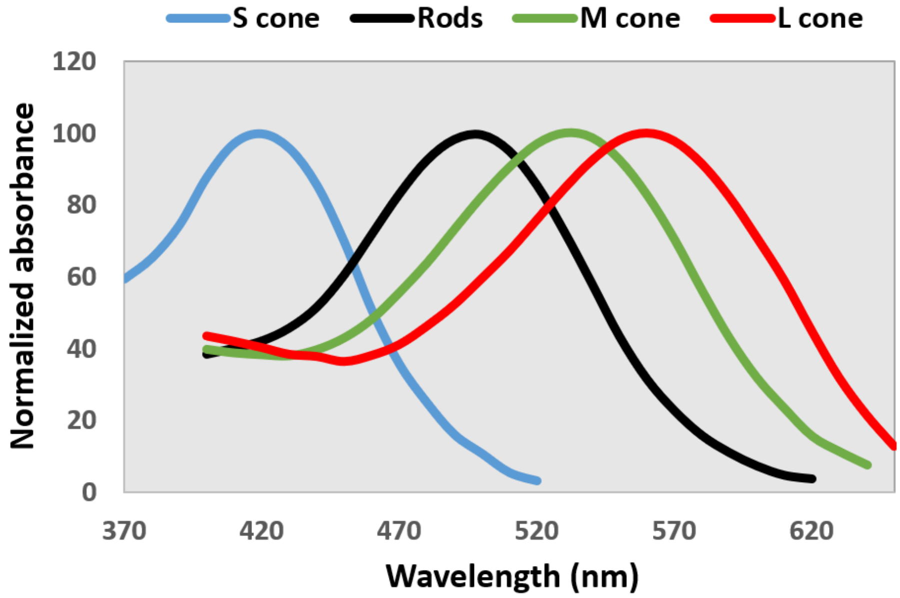

Fig. 1.3: *Normalized absorbance spectra for human visual pigments: rod and cones (S, M an L). Adapted from Dartnall et al. 1983.*

1.2 Optical quality of the eye

The eye is an aberrated optical system, suffering from low order aberrations (LOA) and high order aberrations (HOA). LOA are those typically measured in the optometry practice: defocus (myopia and hyperopia) and astigmatism. In addition, other optical phenomena such as diffraction and scattering contribute to the degradation of the retinal image optical quality (Marcos 2003).

Diffraction is an unavoidable physical effect that occurs when light waves pass through an aperture. In the eye, the effects of diffraction are notorious with low pupil sizes. An optical system is considered perfect when it the image quality is only limited by diffraction.

Scattering is produced when the light interacts with molecules or small particles that locally change the index refraction of intraocular media and is originated normally in the cornea and the crystalline lens (Hart et al. 1969, van den Berg et al. 1996). Scattering alters the light direction randomly, causing a blurring in the retinal image. In young eyes without pathologies the contribution of this factor is not important, but the scattering of the crystalline lens increases significantly with age (specially with cataract), and can also be originated in the cornea by disease or surgical procedures such as refractive surgery, resulting in a considerable degradation of the quality of the retinal image (Díaz-Douton et al. 2006).

Refractive error, a disorder of complex and multifactorial etiology, is characterized by a mismatch between the optical power provided by the cornea and the crystalline lens in the anterior segment of the eye, and the axial length that causes distant objects to be imaged in front (myopia) or behind the retina (hyperopia). In addition, in the presence of astigmatism the retinal image of a point source is focused at two perpendicular lines at two different focal positions. In the clinical practice, different corrections are applied to compensate these errors: (1) Ophthalmic lenses or spectacles, divergent for myopia, convergent for hyperopia and cylindrical (or sphero-cylindrical if astigmatism is combined with defocus) to compensate for astigmatism, (2) contact lenses that are worn on top of the cornea, (3) implantable collamer lens (ICL) that are placed during surgery in the anterior chamber of the eye before the iris and are mostly used in subjects with high ametropias, and (4) refractive surgery (such as PRK or LASIK) that consists of a corneal ablation that is central for myopia, peripherical for hyperopia and asymmetric to compensate astigmatism.

1.2.1 Ocular monochromatic aberrations

The eye's aberrations are generally measured in monochromatic light, and (unless otherwise noted) this thesis refers to monochromatic aberrations. Monochromatic aberrations arise from the shape of the different ocular surfaces, cornea and crystalline lens and their relative alignment (with tilts and decentrations), and depend on pupil diameter, accommodation, and other irregularities and asymmetries (Charman 1991, Unterhorst et al. 2015).

The wave aberration, i.e. the distortions of the wavefront (the surface of rays with the same phase) in the pupil plane is used to describe the optical quality of the eye. The wave aberration map, W(x,y), corresponds to the deviations of a wavefront exiting the pupil after progressing through the optics of the eye when compared to an aberration-free reference wavefront (sphere wavefront), illustrated in figure 1.4.

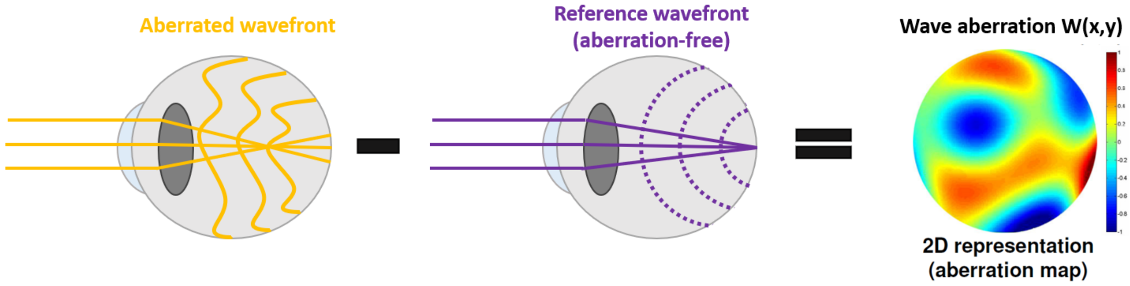

Fig. 1.4: *Schematic representation of wavefront aberration: aberrated wavefront (yellow), reference wavefront (purple) and wave aberration (color represents the distance between the aberrated and reference wavefront). Adapted from Sawides 2013.*

The ocular wave aberration is generally described mathematically by a Zernike polynomial expansion (Zernike 1934), which is a sum of Zernike polynomials weighted by the Zernike coefficients, as described in equation 1.1. Zernike polynomials consist of orthogonal basis of bidimensional functions that are defined in a circle normalized to unit. The Zernike basis is convenient in visual optics because of they are defined on circular pupil, such as the human eye's pupil, and because the low order aberrations represent well known refractive errors (defocus and astigmatism). The first Zernike polynomials are represented in figure 1.5.

$$W(x,y) = \sum_{n,m} c_n^m Z_n^m(x,y) \qquad \text{(eq. 1.1)}$$

W(x,y) is the wavefront aberration expressed in Cartesian coordinates, c_n^m represents the Zernike coefficient of order n and frequency m; Z_n^m (x,y) are the Zernike polynomials in Cartesian coordinates. Different order and sign convention are described for Zernike polynomials. In this thesis the OSA convention is used (Thibos et al. 2002).

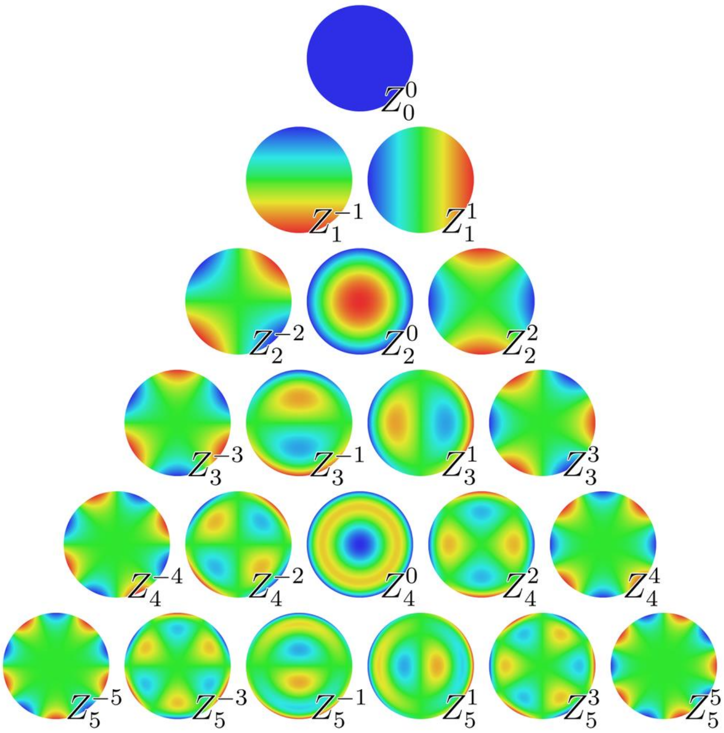

Fig. 1.5: *Zernike polynomials representation up to 6th order.*

The LOA Zernike coefficients c_2^0, c_2^2 and c_2^{-2} describe the curvature of the wavefront and its astigmatism and several authors have derived conversion formulas to derive the clinical refractive error and astigmatism from them. The formulation derived by Thibos et al. (Thibos et al. 1997, Thibos et al. 2004) for the positive-cylinder form is shown in eq 1.2.

$$M=\frac{-c_2^0\,4\sqrt{3}}{r^2}\;;\;\; J_0=\frac{-c_2^2\,2\sqrt{6}}{r^2}\;\;;\;J_{45}=\frac{-c_2^{-2}\,2\sqrt{6}}{r^2} \qquad \text{(eq. 1.2)}$$

$$S'=M+\sqrt{J_0^2+J_{45}^2}\;;C'=-2\sqrt{J_0^2+J_{45}^2}\;;\;\alpha=\frac{1}{2}\tan^{-1}(J_{45}/J_0)$$

Where M is the spherical equivalent, J_0 is the component of astigmatism that has a vertical or horizontal axis, J_{45} is the astigmatic component at oblique axis, and S, C and α would correspond to the clinical cylinder, astigmatism magnitude and astigmatism angle used in clinical settings.

HOA, although present in the eye, are not usually measured in clinical practice and their influence in retinal image quality is in general lower than for LOA. HOA can be measured with aberrometers and cannot be easily corrected with conventional ophthalmic lenses. In the current thesis two specific HOA (coma and spherical aberration) were studied to evaluate their influence on the optical quality of the eye and optical performance of multifocal corrections in chapters 3, 5 and 7.

Coma, a third-order aberration, is asymmetrical, rendering the images formed on the retina a comet-like appearance. Coma generally arises from misalignments of the optical elements, particular in presence of spherical aberration. In this thesis coma was induced to simulate as a secondary effect of the decentration of the corneal ablation in LASIK treatment (Moreno-Barriuso et al. 2001).

Spherical aberration is a fourth-order aberration, symmetrical aberration. It produces a wavefront with increasing or decreasing curvature from the center of the pupil towards the periphery and the image of a point created in the retina is a concentric ring pattern. Spherical aberration expands the depth of focus, but also decreases the optical quality (Yi et al. 2011, Benard et al. 2011), and correlates with pre-operative spherical error in post-LASIK eyes (Marcos et al. 2001, Llorente et al. 2004). In this thesis, the effects of inducing spherical aberration on vision with optical corrections were studied in chapters 3, 5 and 6.

1.2.2 Optical quality metrics

To evaluate the optical performance in terms of optical quality, different retinal image quality metrics derived from wave aberration functions have been used. In particular, in this thesis we used the Root Mean Square (RMS), the maximum of the Point Spread Function (PSF), the value of the Modulation Transfer Function (MTF) at a given spatial frequency, and the Visual Strehl ratio (VS). Definitions and details on the calculation of these metrics are described below.

The RMS wavefront error represents the amount of deviation between the perfect (ideal sphere) and a real wavefront. Lower values mean flatter wavefront aberration maps, generally associated to good optical quality. The RMS is derived directly from the Zernike coefficients using expression eq. 1.3:

$$RMS = \sqrt{\sum_{n,m} {c_n^m}^2} \qquad \text{(eq. 1.3)}$$

where C_n^m is the Zernike coefficient with order n and frequency m.

The PSF represents the intensity distribution of a point source as imaged through the optical system, and is calculated from the wave aberration (eq. 1.4), using Fourier Optics (eq. 1.5). Specifically, the PSF is the square magnitude of the Fourier transform of the Pupil Function P(x,y):

$$P(x,y) = A(x,y)\exp\big(ikW(x,y)\big) \qquad \text{(eq. 1.4)}$$

$$PSF(x,y) = \left|FT\left(P(x,y)\right)\right|^2 \qquad \text{(eq. 1.5)}$$

where A(x,y) is the amplitude of the light wave in the pupil, k is the wave number $k = 2\pi/\lambda$, W (x,y) is the wave aberration, and FT represents the Fourier Transform**.**

The PSF is influenced by blur, diffraction, pupil size, aberrations and scattering of light inside the eye. The PSF limited by diffraction (considered as a perfect optical system) is represented by the Airy disk.

The Optical Transfer Function is the autocorrelation of pupil function and the Fourier Transform of the PSF (eq. 1.6). The OTF is a complex function that defines the loss in contrast of a sinusoidal target and that is used in this thesis as an intermediate step to calculate the modulation transfer function, which is the modulus of the OTF.

$$OTF = FT\left(PSF(x,y)\right) \qquad \text{(eq. 1.6)}$$

The Modulation Transfer Function (MTF) is the contrast reduction of the different spatial frequencies when an image is formed by optical system. The eye is a low pass filter optical system, thus the contrast reduction is larger for high spatial frequencies, which represent the image fine details. ISO standards for the optical evaluation of the performance of intraocular lenses (11979-2) use the value of this function at different spatial frequencies as a threshold to determine IOL quality. In this thesis, the MTF is presented for two spatial frequencies (30 and 15 cpd) that are equivalent to 0 and 0.3 LogMAR visual acuity, respectively (Iyer et al. 2013).

$$MTF = |OTF| \qquad \text{(eq. 1.7)}$$

The Visual Strehl ratio is the volume under the MTF weighted by the neural contrast sensitivity function of the human eye, normalized by the diffraction limited value (Iskander 2006). In the current thesis, we used a neural CSF published in literature (Mannos & Sakrison 1974).

$$VSMTF = \frac{\int_{-\infty}^{\infty}\int_{-\infty}^{\infty} CSF_N(f_x,f_y)\cdot MTF(f_x,f_y)df_x df_y}{\int_{-\infty}^{\infty}\int_{-\infty}^{\infty} CSF_N(f_x,f_y)\cdot MTF_{DL}(f_x,f_y)df_x df_y}, \qquad \text{(eq. 1.8)}$$

Where CSF_N is the neural contrast sensitivity function, MTF is the modulation transfer function of the eye and MTF_{DL} is the modulation transfer function of a diffraction limited system with the same pupil size.

1.3 The aging eye

Two physiological age-related process affect the optical quality of the eye: presbyopia and cataract. Although several solutions are clinically prescribed to compensate their effects, none of them restore the lost capability of accommodation. The search of new treatments for presbyopia is one of the most intensive quests in ophthalmology today. Improving presbyopia and cataract treatments is a technological challenge in visual sciences.

1.3.1 Presbyopia and cataract

As described in section 1.1, the crystalline lens has the ability to modify its shape and size to change its optical power in a process that is known as accommodation. In an emmetropic eye, when the crystalline lens is relaxed the rays focus on the retina and with accommodation the lens increases its optical power to image on the retina near objects (figure 1.6). In the accommodation process the ciliary muscle is contracted producing an increase of the crystalline central thickness, of the lens radii of curvature and of its optical power. The eye accommodation is generally accompanied by a convergence movement of the two eyes towards the nasal side, and a constriction of the pupil. The combination of these three movements is known as near triad (Evans 2021).

The mechanism by which the eye can adjust the focus has been debated for more than 300 years and some of the greatest minds in science, including Young (Young 1801), Helmholtz (Helmholtz 1855) and Tscherning (Tscherning 1904), described its mechanisms using ingenious experiments.

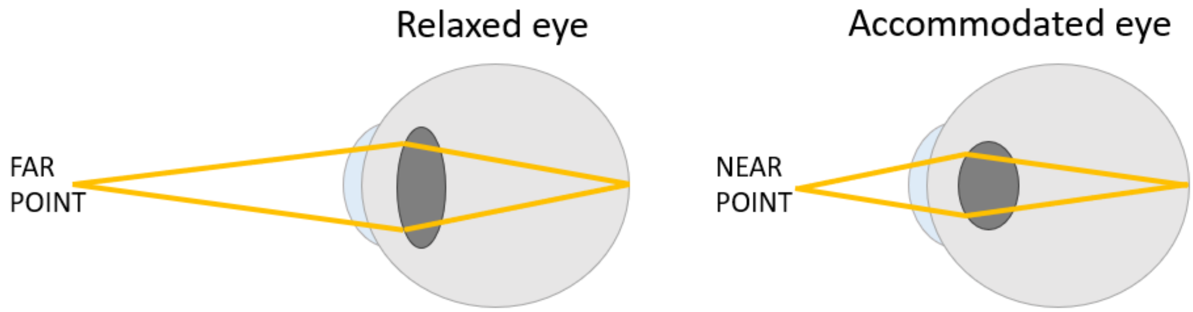

Fig 1.6: *Schematic drawing, left relaxed eye for far vision, right accommodated eye for near vision to focus the rays on retina crystalline lens increase curvature and thickness.*

The amplitude of accommodation is the difference in refractive power of the eye between the two states of complete relaxation and maximal accommodation. The amplitude of accommodation decreases with age (Duane 1922) at a rate of 0.3 D per year approximately between 10 and 55 years. With aging, the amplitude of accommodation decreases to the extent that near tasks are compromised, a condition that is called presbyopia (which means "old eye" in Greek). On average the onset age of presbyopia is around 45 years. With aging population, the estimated number of presbyopes around the world are expected to increase to 1.8 billion in 2050 (Grzybowski et al. 2020). There are different presbyopia treatments which can be adapted according to the patient's needs, although all have some disadvantages. Relevant corrections will be explained with detail in the next section 1.3.2

A cataract is an opacification of crystalline lens that can lead to blindness if it is not treated. Many circumstances such as exposure to UV light, disease (i.e. diabetes) and specific drugs can cause cataracts, but age is the most common factor (Petrash 2013). Cataract surgery is the only stablished method of treatment and is one of the oldest and most common surgical procedures worldwide. The technique had been improved constantly since the fifth century (Davis 2016) and today it consists of a replacement the crystalline lens by an intraocular lens (IOL).

1.3.2 Presbyopia and cataract treatments

Spectacles are the most accessible method to correct presbyopia. Monofocal near vision spectacles with a single power correct sight at one distance. Bifocal, trifocal or progressive addition spectacle lenses which incorporate designs with either two or three areas with different power, or a smooth transition between various optical powers respectively, allow vision at different distances (Charman 2014).

Contact lenses can also be used to compensate the effects of presbyopia. Monovision is a method in which a monofocal contact lens corrects one eye for distance vision and a different contact lens power is used in the contralateral eye so that the eye is corrected for near vision. Monovision is most frequently administered with contact lenses, although it is also practiced with intraocular lenses and LASIK. In modified monovision, a multifocal contact lens is fitted in one eye and a monofocal is fitted in the contralateral eye. Several contact lens manufacturers also offer multifocal contact lenses (MCLs) for presbyopia treatment. MCLs are generally refractive designs with are devoted for far and near, separated by smooth or more abrupt transition.

There are some surgical presbyopia treatment methods targeting the optics of the cornea by implanting a corneal inlay or removing tissue to change its shape (Moarefi et al. 2017). The latter is a form of LASIK, known as PresbyLASIK, uses a laser ablation procedure to reshape the anterior cornea such that Depth-of-Focus (DOF) is extended. Two different techniques are generally applied: peripheral and central PresbyLASIK. In central PresbyLASIK (which we will describe in more detail in chapter 8 of this thesis), the central ablation pattern corrects for near vision and peripheral for far, being the most used technique in patients (Vargas-Fragoso et al. 2017).

In Refractive exchange lens (REL) surgical procedures (Alió et al. 2014), the crystalline lens is removed (frequently still being transparent), and intraocular lenses are implanted to correct refraction and compensate presbyopia. The ideal implant would be a lens that could use the available forces of the ciliary muscle to change its optical power. Although several accommodating IOL (AIOL) have been proposed (Harman et al. 2008, de la Hoz et al. 2019) to date, there is little evidence of accommodation restoration in patients (Marcos et al. 2014). However, different strategies involving intraocular lenses are routinely used to compensate presbyopia on REL and cataract procedures: monofocal IOLs with spectacles for near vision, monovision correcting one eye for far and the contralateral for near, multifocal IOLs that superimpose in the retina images at different distances, and extended depth of focus (EDOF) IOLs.

Since the 1970s remarkable advances have occurred in IOL technology, material and design. In 1992 the first toric IOL was developed to compensate the astigmatism (Visser et al. 2013). The first multifocal IOLs for presbyopia correction were released 1990s, and, as mentioned above, different designs of accommodative IOLs are being proposed since late 2000's. Today, there are over 100 IOLs designs available in the market (Rampat et al. 2021), manufacturers tend to have a portfolio of lens designs to target different patient needs, and the IOL market size was valuated at USD 4.0 billion in 2021. With an aging population and the increase of surgeries in undeveloped countries; the expectation of annual growth rate is 4.8% from 2022 to 2030. IOLs can be classified according to its optical design (monofocal, multifocal, extended depth of focus), material (hydrophobic or hydrophilic) and technology (refractive or diffractive) as explained below.

Monofocal IOLs are those in which optical power compensate vision at far. The design of these lenses includes usually aspheric designs with negative spherical aberration to compensate the positive corneal spherical aberration.

Multifocal IOLs are designed to provide vision at different distances through the principle of simultaneous vision (more than one image is projected at the same time on retina). According with the optical principle used to create the multifocality, the IOLs can be classified as refractive or diffractive. In refractive lenses, the power profile is divided in zones with different optical powers (such as center near and periphery distance or alternative concentric rings) to provide simultaneous vision at two or more distances, or continuously change from the center to the periphery of the lens. These IOLs are normally pupil-dependent and sensitive to decentration. Diffractive lenses have concentric rings and multifocality is achieved by the different diffraction modes. These designs are less sensitive to decentration and less pupil-dependent than the refractive profiles, but they are known to produce more glares and halos and more loss of light due to scattering.

Extended depth of focus (EDOF) IOLs are a recent IOL classification (ANSI Z80.35-2018) that, in contrast with multifocal IOLs create an elongated focus, rather than several foci, to enhance the depth of focus. EDOF IOLs aim to provide good vision from far to intermediate distance reducing the photic effects (halos and glare) reported in multifocal IOLs.

The release of new IOL designs in the market brings to increase understanding of their optical properties and the impact of their design on visual quality. In particular, it is important to investigate how their optical design couples with the aberrations of the eye in normal and abnormal corneas, the effect of IOL tilt and decentration, and the possibility and accuracy of using Visual Simulators to simulate the lenses to study those questions non-invasively. In this thesis different studies address these questions with two commercial IOLs in particular, the Isopure IOL from PhysIOL-BVI and Acrysof IQ Vivity IOL from Alcon (chapters 3 -7).

1.4 Optical model eyes

Optical model eye quantitatively describes the eye as an imaging optical system. The first realistic schematic model eye was developed by Scheiner in the 17th century and since then, these models have been used to predict and explain the optical phenomena in vision.

Eye models of different complexity (in number of surfaces or in the description of refractive index) have been proposed in the literature (Atchinson 2016). In reduced eye models, only one refractive surface is used to describe the whole eye, such as in the Emsley model eye, figure 1.7 (A). Simplified eye models are composed of three refracting surfaces, one for cornea and two for crystalline lens, and example of which is the Gullstrand-Emsley eye, figure 1.7 (B). A model with four refracting surfaces, two for the corneal and two for the crystalline lens includes the Le Grand's full theorical eye, figure 1.7 (C). Some models include the internal structure of the crystalline lens, such as the Gullstrand's No 1. "exact" model eye, figure 1.7 (D). Eye models can also be paraxial, valid for small pupils and objects close to optical axis, or finite, which in some cases are adapted from paraxial models asphericing some of the surfaces or moving its fovea off axis. According to the origin of the data there are *population models*, in which a generic model eye is built with data obtained from a large population such as the Dubbelman eye model (Dubbelman et al. 2001, Norrby 2005), and *customized eye models*, where individual data is used to represent a particular eye.

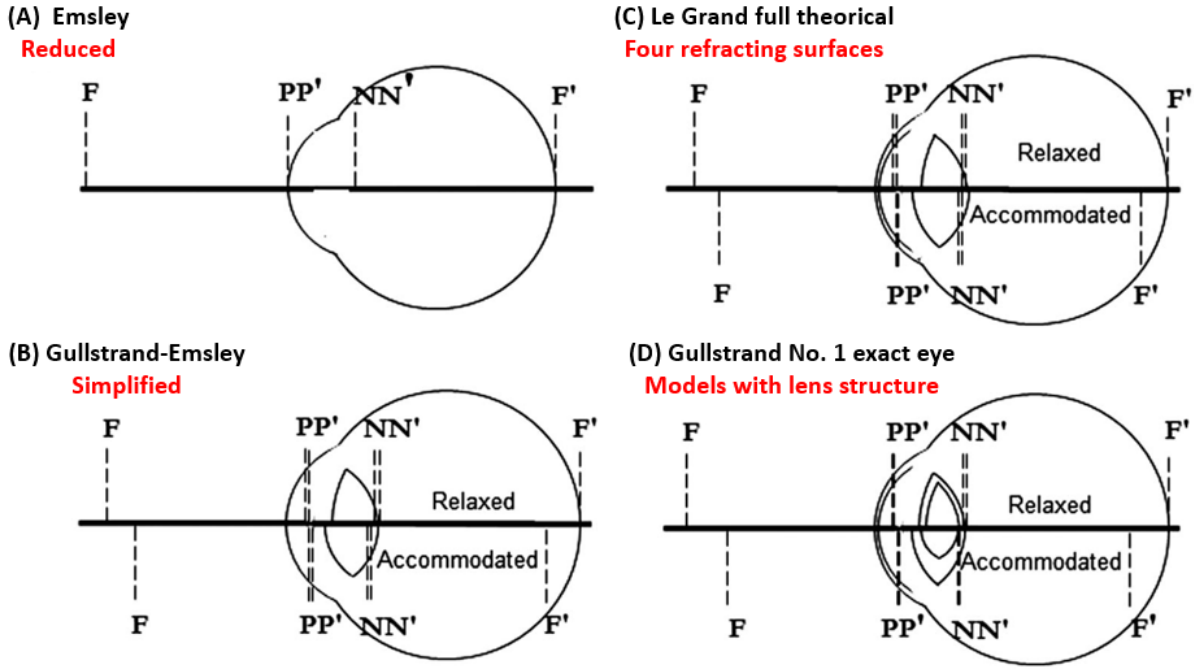

Fig 1.7: *Schematic model eyes representation. Adapted from Atchinson et al. 2016.*

Two Spanish groups presented customized pseudophakic model eyes in the early 2000s (Tabernero et al. 2006, Rosales and Marcos 2007) built with experimental data from different instruments. In those models, the topography of the anterior surface of the cornea was measured with a Placido ring topographer, the anterior chamber depth and the axial length was measured with an ultrasound biometer, and the tilt and decentration of the IOL was obtained studying the position of the Purkinje images originated at the cornea and at anterior and posterior surfaces of the crystalline lens. The studies showed that the aberrations calculated with the custom eye models were comparable to the ones measured with a wavefront sensor. A decade later, Sun et al. (Sun et al.2016) showed that Spectral Domain OCT could be used to generate full OCT-based pseudophakic eye models. Customized eye models allow to understand the relative contribution of geometrical and surgery-related factors to image quality.

In this thesis we will use different computer pseudophakic eye models to study the optical properties of four different intraocular lenses. Their characteristics will be explained more in detail at section 2.1. Essentially, a cornea with the average power and spherical aberration of the human cornea was built using optimization tools and combined with the studied intraocular lenses. Using those models, the through focus performance with the premium intraocular lenses was compared with the performance with standard monofocal IOLs. As will be detailed in section 2.1.2, computer eye models were also used to subtract the optics of the cornea and to calculate the IOL phase map.

Physical Model eyes for IOLs evaluation

On bench tests of IOL performance are typically conducted with physical model eyes, and international standards (for example ISO 11979-2) dictate the properties of these models, as well as the optical quality metrics that IOL design need to comply for commercialization. The physical eye models incorporate a lens (acting as cornea) in front of the IOL to be tested so that the rays converge onto the IOL mimicking the ray tracing in the human eye. There are two well-known ISO standards, ISO1, in which the "cornea" is a lens with zero spherical aberration, and the ISO2, in which the lens simulating the cornea has a 0.28 µm spherical aberration for a pupil radius of 6.0-mm. In both cases, the IOL tested is placed inside a cuvette whose dimensions are specified in the standard and the MTF values at different spatial frequencies (30 and 15 cpd) are reported.

In this thesis, as will be detailed in section 2.3.3, the IOL was evaluated on bench using an Adaptive Optics system in which the IOL was positioned in a plane optically conjugated with the entrance pupil of the eye. In addition, two wavefront shaping devices (a Deformable mirror and a Spatial Light Modulator) allowed us to obtain single and double pass images when inducing optical aberrations. While some of the methods parallel those described in the ISO standards, the aim of the model eyes used in this thesis is not to replicate the standards but rather to advance in the methods to simulate correctly vision after surgery by predicting the post-operative optics.

In this thesis, we have evaluated computationally four intraocular lenses using physiological eye models that were custom designed for each study performed (explained in section 2.1). By comparing the results with a monofocal, or a premium intraocular lens, we draw conclusions about the expected differences in real surgeries.

1.5 Visual simulators

Visual simulators allow patients to non-invasively experience new optical designs and techniques before surgery. This section presents the principles of operation of the visual simulators used in this thesis and review a state of the art of different commercial simulators.

1.5.1 Adaptive optics

Adaptive optics (AO) technology was first developed by the US military during the Cold War. In early 1990's, was declassified for use in astronomy for ground-based telescopes to compensate the blur-inducing optical aberrations caused by turbulence in earth's atmosphere. AO was first envisioned by Horace W. Babcock, in 1953 (Babcock 1953); but it came into common use in 1990s in several observatories. Today AO is applied are astronomy, microscopy (Booth 2007), and ophthalmology. Figure 1.8 shows an example of the use of Adaptive Optics in astronomy and in retinal imaging. Current applications in the eye are retinal imaging at high resolution (Godara et al. 2010), visual testing (Marcos et al. 2017) and visual simulators (Fernández 2012). Reviews of the use of Adaptive Optics in Ophthalmology can be found (Porter et al. 2006, Hampson 2008, Roorda 2011, Marcos et al. 2017, Marcos et al. 2020, Marcos et al. 2022).

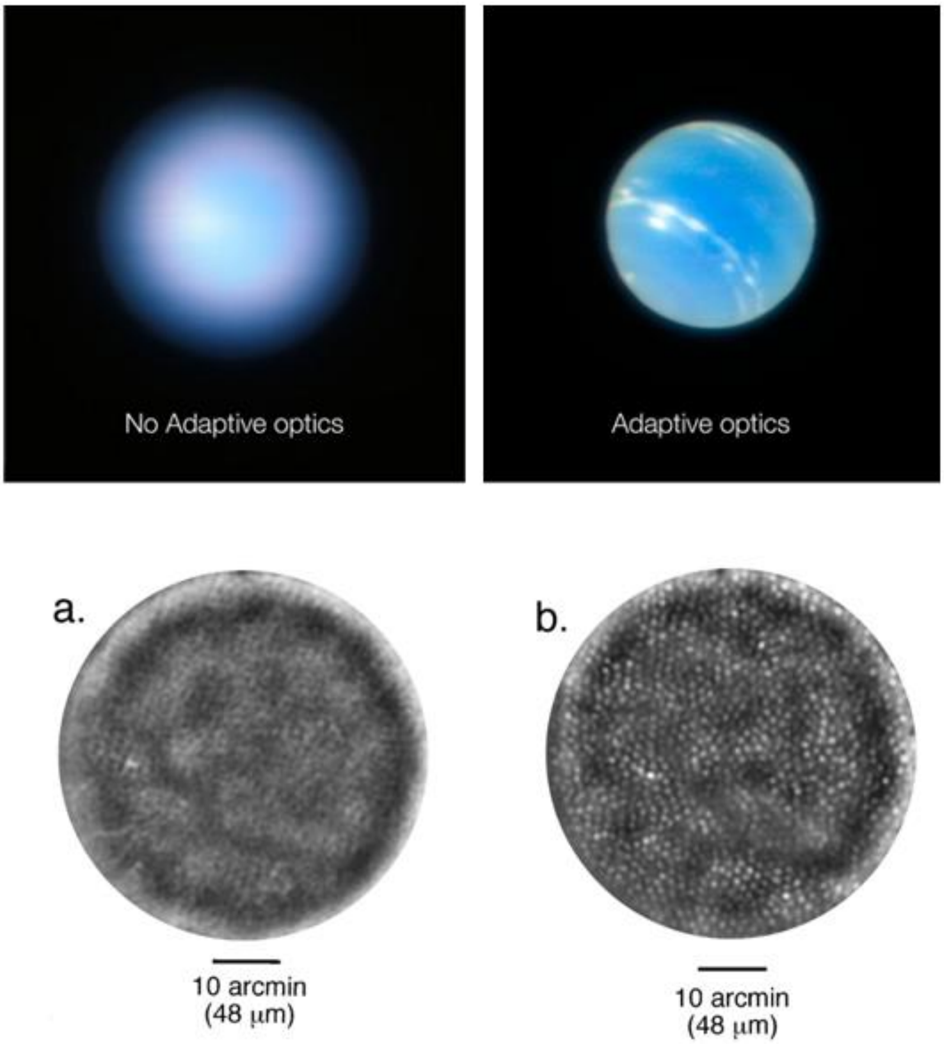

Fig 1.8: *Top: Neptune, imaged testing the Narrow-field adaptive optics mode of the MUSE/GALACSI instrument on ESO's very large telescope, without Adaptive Optics (left) and with (right) (credit: ESO/ P. Weilbacher). Bottom: Image of the retina at 4-des eccentricity without adaptive optics compensation (a) and with adaptive optics compensation (b) (Liang et al. 1997).*

Adaptive Optics principle

In adaptive optics the objective is to dynamically measure the optical aberrations that are present in an optical system using wavefront sensing technology and correct them using an active wavefront corrector. Adaptive Optics operates in a closed-loop process where the wavefront sensor measures the amount of aberrations and the control system modify the phase of the wavefront correcting component (either reshaping a deformable mirror or through local changes of phase) to correct the wavefront or to induce the desired aberration pattern. The AO principle is represented in figure 1.9.

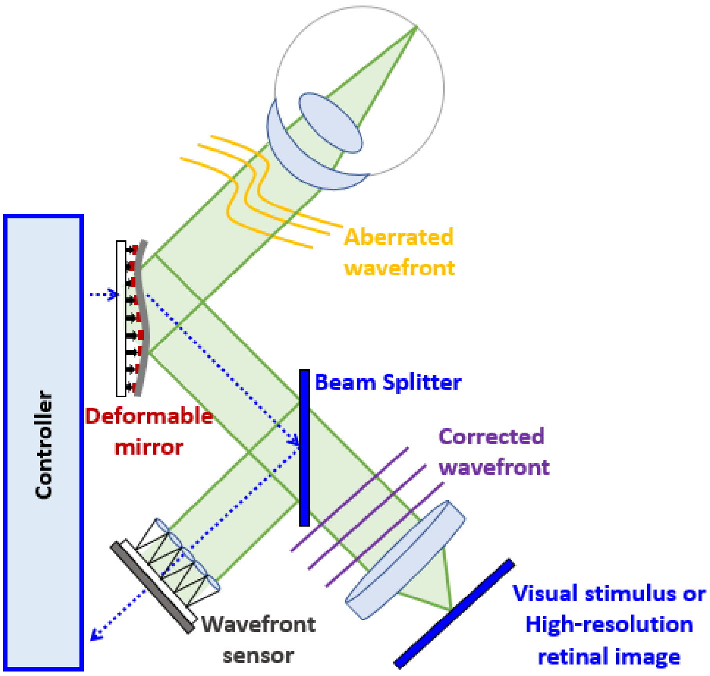

Fig 1.9: *Basic scheme of adaptive optics in vision*

Wavefront sensor and wavefront corrector

As shown in figure 1.9, in ophthalmic applications a beam of light is focused on the retina and the backscattered light that passes through the ocular media is sampled with the wavefront sensor. In this thesis the ocular wavefront used a near infrared beam for maximize subject's comfort, as well as the reflectivity properties of the retina and sensitivity of the wavefront sensor detection. The two main types of sensors that have been used for ophthalmic AO systems are Hartmann-Shack and pyramid sensors (Hampson 2008), being Hartmann-Shack the most common. The specifications of the Hartmann-Shack used in this thesis are described in section 2.3. Essentially, the sensor is composed of an array of lenslets (microlenses) conjugated with the entrance pupil of the eye and a detector (CCD camera) at the focal plane of the lenslets array. A flat wavefront would focus light behind each of the microlenses, on the detector, forming a regular array of spots. When an aberrated wavefront passes through the microlenses, the sampled portions of wavefront are focused by each lenslet on the detector. If the wavefront is flat and orthogonal to the optical axis, it will focus on the focal point of the lenslets. If the wavefront is tilted locally, the focus will be shifted with respect to reference (figure 1.10 (A)). The difference between the shifted spot and reference spot is the local slope of the wavefront. Wave aberrations are calculated form local slopes.

There are two main types of wavefront correctors: deformable mirrors (DM) and Spatial Light Modulators (SLM). Both systems work under the principle of phase conjugation, i.e. the corrector impose a reverse phase onto the beam to compensate the aberrations. DM in the AO system used in this thesis has a reflective membrane with a series of electromagnetic actuators to push or pull the membrane according to the applied voltage (figure 1.10 (B)). The DM works in a closed- loop with the sensor, and the algorithm calculates the amount of voltage that needs to be induced to correct and/or induce aberrations. In this thesis the Mirao52E DM from ImagineEyes was used in chapter 4, 5 and 7 to correct and induce aberrations. The most common SLM are based on LCoS (Liquid Cristal on Silicone). Different voltages are applied to each pixel producing a different change in the refractive index for each pixel, inducing phase local changes. In this thesis the Pluto SLM by HoloEye has been used to simulate the Isopure IOL (chapter 4 and 5) and Acrysof IQ Vivity IOL (chapter 7).

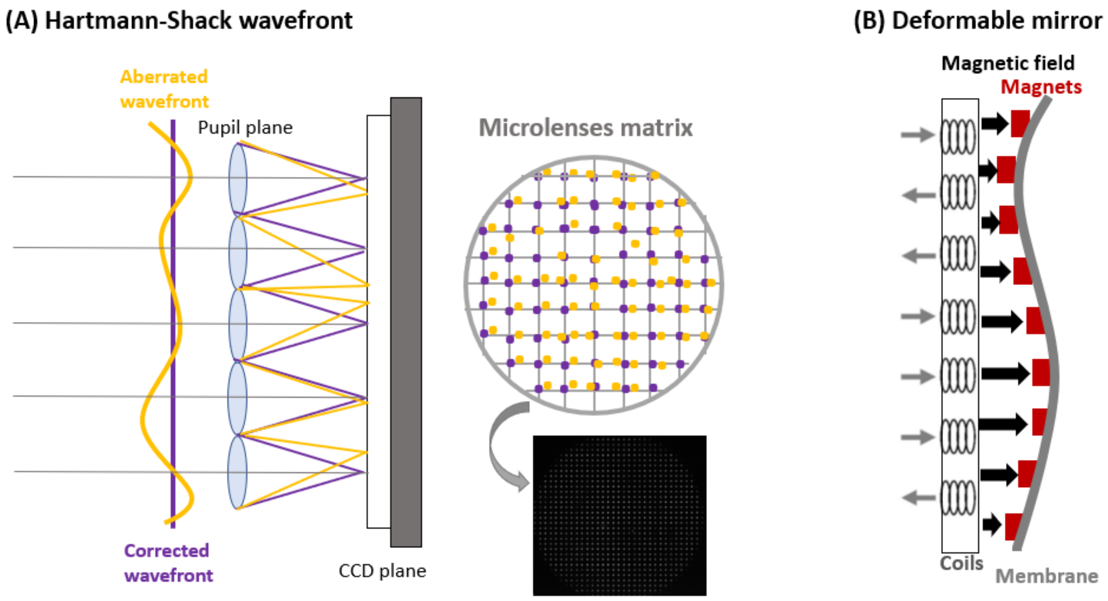

Fig 1.10: *(A) Illustration of an aberration-free wavefront (purple) and an aberrated wavefront (yellow) reaching the Hartmann Shack wavefront sensor. In microlenses matrix, purple the reference spots from the corrected wavefront (center) and yellow the aberrated spots shifted, an illustration of real microlenses matrix in AO system measured. (B) Schematic representation of a deformable mirror.*

1.5.2 Commercial visual simulators

Visual simulators use AO to correct the eye's aberrations and simulate vision with perfect optics, or (as in this thesis) to simulate prospective vision with a given correction or after a surgical procedure that modify the wave aberration. They allow a non-invasive way of testing different corrections in subjects and to evaluate their performance. Also, visual simulators allow to select the most suitable correction individually.

Most AO visual simulators are custom-developed laboratory prototypes (Marcos et al. 2017, Marcos et al. 2022), but there are also commercial simulators such as CRX1 by Imagine Eyes (France) was a monocular visual simulator based in a DM (Rocha et al. 2010) that is no longer in the market; VAO by Voptica (Spain) is a SLM-based monocular simulator (Hervella et al. 2019).

Also, there are commercial visual simulators that are not based on adaptive optics such as VirtIOL and ACMIT, that appear to be based on the projection of an IOL in the pupil plane of the eye using a cuvette (Studený et al. 2018, Brezna et al. 2016), and simultaneous vision simulators that target the simulation of corrections with the visual multiplexing principle. A commercial version, the SimVis Gekko by 2EyesVision (Spain) is a wearable, binocular, see-through and fully programmable simulator based on SimVis technology (Dorronsoro et al. 2016) and that is explained in more detail in the section 1.5.3.

1.5.3 SimVis technology

The SimVis technology was developed in the Visual Optics and Biophotonics Lab. The technology has evolved, from a two-channel optical bench system combining two badal optometers (de Gracia et al. 2013), to a monocular prototype based on spatial multiplexing in 2010 (Dorronsoro et al. 2010, figure 1.11) to a wearable binocular helmet based on temporal multiplexing (Barcala et al. 2022, Barcala et al. 2022).

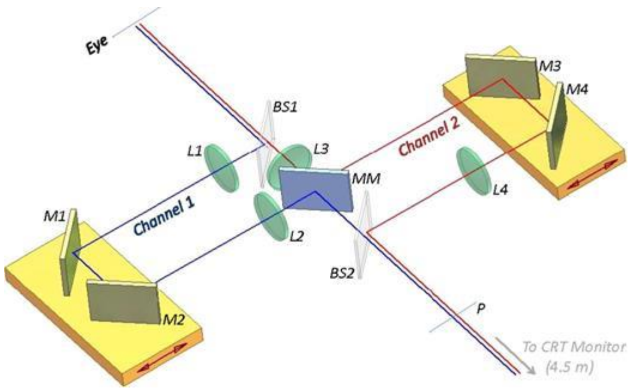

Fig 1.11: *Schematic representation of first SimVis technology prototype: monocular two-channel optical bench based on spatial multiplexing, using two badal systems. From de Gracia et al. 2013*

Temporal multiplexing of tunable lenses

Temporal multiplexing is a novel technique which allows simultaneous vision based on tunable lenses (TL) (Akondi et al. 2017). A TL is an optical active element that can change its optical power at high speed with an electrical signal and at a frequency that is higher than the eye's fusion flicker frequency (50 Hz) to produce a stimulus on the retina with static appearance that is equivalent to simultaneous vision. The use of TL allows new strategies to compact optical systems reducing the use of optomechanical elements and increasing the frequency response (Blum et al. 2011). The use of two TL (one per eye) allowed to develop a compact binocular wearable helmet as the commercial visual simulator SimVis Gekko (figure 1.12).

Fig. 1.12: *Wearable binocular commercial visual simulator, SimVis Gekko, from 2EyesVision, SL*

1.6 Motivation

At the beginning of this thesis, the SimVis technology had been demonstrated to be able to simulate IOL multifocal patterns in subjects. The main objective of this thesis was to demonstrate the simulation of new IOL designs and presbyopia correction patterns, streamlining the calculations of the parameters of the SimVis from the design using the geometrical design of the IOLs. The current thesis focuses in particular in the simulation of two new IOLs (Isopure by PhysIOL-BVI and Vivity by Alcon), classified as extended depth of focus (EDOF) IOLs, under a new IOL category classification released 2018 (ANSI Z.80.35-2018). In addition, the capability of SimVis to simulate PresbyLASIK patterns (corneal ablation patterns to correct presbyopia) was intended to study as new market application of the technology.

The overarching motivation of this thesis was to provide insights of the performance of new presbyopia corrections in the market, and in particular, the validation of the SimVis technology for new IOL and corneal refractive corrections.

1.7 Open questions

SimVis is a recent technology in the market and it is essential to investigate its possibilities and limitations when simulating new multifocal designs in the market.

In this thesis we have performed different computational and experimental studies to validate the application of SimVis technology to new IOL designs and PresbyLASIK ablation profiles.

The open questions are:

1. ***Is SimVis technology able to reproduce smooth designs such as the new EDOF IOL?*** In previous works of the group SimVis was demonstrated to simulate accurately multifocal diffractive and segmented designs, however, the applicability of the technology to simulate the smooth designs of EDOF IOLs was pending.

2. ***To what extent is the depth-of-focus extended with EDOF IOLs? Is the focus expansion maintained in presence of optical aberrations? What is the range of applicability of these lenses across eyes with different aberration profiles, including post-LASIK eyes?*** Visual simulators are extraordinarily well suited to answer this question, given the possibility to induce aberrations, and to test different lens designs on the same subject.

3. ***Is it possible to simulate PresbyLASIK with SimVis technology?*** PresbyLASIK profiles have never been simulated before in a visual simulator. SimVis technology is a powerful tool which has been demonstrated to accurately simulate multifocal intraocular lens and contact lens profiles and the technology can be used to attempt to simulate the outcome of laser refractive surgery patterns used for presbyopia correction.

1.8 Goals of this thesis

The goal of this thesis is to test and validate the ability of SimVis technology to simulate new multifocal patterns designs and techniques.

Specific goals:

- Simulation and validation of the use of SimVis technology for non-diffractive intraocular lenses with extended depth of focus.

- Increase understanding of the performance of this new IOL designs computationally and experimentally, evaluate the robustness of its performance against ocular aberrations and predict the suitability of these IOLs to specific challenging subjects, such as post-LASIK subjects.

- Increase the capabilities of simulation of SimVis technology with PresbyLASIK simulations.

1.9 Hypothesis

The overarching hypothesis of this thesis are:

- Visual simulators are an ideal tool to test new EDOF IOL performance, allowing subjects to experience vision with those new corrections before their implantation given an accurate representation.

- Interaction with the individual eye optics affects the performance of IOL in terms of Depth of Focus .

- Spherical aberration and subject’s pupil size change the depth of focus and affect the IOL performance.

- Increased corneal spherical aberration due to previous LASIK refractive surgery affects the performance of new EDOF IOL.

- Visual simulator based on SimVis technology can accurately simulate PresbyLASIK patterns.

1.10 Structure of the thesis

The thesis was structured as follows:

Chapter 1: Introduction*.* Summarizes of the state of the art of the different topics involved in this thesis, visual system, aberrations, optical quality, eye models, presbyopia and cataract and their corrections, and visual simulators. Also, the motivation and goals of this thesis.

Chapter 2: Methods**.** Describes the three common methods that were used for the studies: computational simulations, SimVis technology and adaptive optics visual simulator.

Chapter 3: Computational simulations as a predictor of the behavior of a new refractive IOL design: Isopure IOL. Presents computationally results to predict the optical performance of Isopure IOL in eye models as a function of corneal power, spherical aberration, tilt, decentration and IOL power in terms of optical quality and depth of focus.

Chapter 4: Evaluating the simulated performance of a new refractive IOL: Isopure IOL. *R*eports measurements with Isopure IOL in an adaptive optics system to evaluate the feasibility of its simulation with the optotunable lens and SLM, using the physical IOL in a cuvette as a reference.

Chapter 5: Evaluating the effect of corneal aberrations of Isopure IOL design using Adaptive Optics. Presents a study with the physical Isopure IOL and compares the results with the lens simulated with SimVis technology to study its interaction with ocular aberrations, on bench and with subjects.

Chapter 6: Computational simulations of the optical performance Acrysof IQ Vivity IOL in post-LASIK eyes. Shows the results of a computational study conducted with Acrysof IQ Vivity to evaluate the implantation of the IOL in subjects with LASIK surgery performed in 2000s in comparison with a monofocal IOL (Acrysof IQ) in terms of optical quality, depth of focus and halos.

Chapter 7: Computational and on bench visual simulation of Acrysof IQ Vivity. Describes the experimental measurements in an adaptive optics system on bench with Acrysof IQ Vivity to evaluate the IOL simulation with the optotunable lens and SLM.

Chapter 8**: SimVis simulation of PresbyLASIK corrections: Computational, on-bench and clinical validation of corneal ablation patterns for SimVis Gekko.** PresbyLASIK validation from its phase map to measurements with the wearable binocular SimVis Gekko in subjects.

Chapter 9**: Conclusions.** States the achievements and conclusions of this thesis.

List of scientific activities

Bibliography

“Un científico en su laboratorio no es sólo un técnico: es también un niño colocado ante fenómenos naturales que le impresionan como un cuento de hadas”

Marie Curie

2 Methods

In this chapter the experimental methodology used in this thesis is described. The chapter provides the assumptions and technical details of the computational simulations performed during the thesis, and optical layout, control and validations of the optical systems used in the thesis (the SimVis technology based on temporal multiplexing, and the adaptive optics based visual simulator, previously developed at VioBio Lab and implemented during the thesis) and some general computational and experimental protocols, both on bench and with patients.

The main research activity in the I+D department at 2EyesVision S.L. company involved Dra. Lucie Sawides (R+D engineer, specialized in the multifocal correction simulations and SimVis quality control, director of this thesis), Dr. Enrique Gambra (CTO), José Ramón Alonso-Sanz (mechanical engineer), Dr. Carlos Dorronsoro (CEO), Dra. Irene Sisó-fuertes and Dra. Xoana Barcala (clinical developers). In VioBio Lab (CSIC), the computer simulations were developed with Dr. Alberto de Castro (tenured scientist, specialized in computer simulations and IOLs, director of this thesis) and the adaptive optics experiments with, Dra. Clara Benedí-García, Dra. María Viñas and Dra. Sara El Aissati (adaptive optics specialists), all under the supervision of Professor Susana Marcos (VioBio Lab director, director of this thesis).

2.1 Computational simulations

Optical design is the process of estimating the parameters of a lens or an optical correction to solve a problem. In this thesis we used an optical design program, OpticStudio (Zemax, Kirkland, WA), which is a well-known ray tracing software that is often used to model the human eye. The software allows implementing complex optical systems and calculating rapidly optical properties such as the wavefront aberration or the modulation transfer function. We developed realistic pseudophakic model eyes with the objective of predicting the optics of the eye after cataract surgery. With these computational simulations our aim is to provide evidence about the properties of some of the intraocular lens (IOL) of the market. Also, we used the software to calculate the information needed to simulate an IOL profile in different visual simulators, (based on adaptive optics or temporal multiplexing).

In some of the works presented here, the idea was to study the performance of an IOL and make predictions on the IOL behavior in different conditions (e.g., in post-LASIK eyes, under different corneal spherical aberrations, or with tilt and decentration, among others).

2.1.1 Eye model

A standard average eye model was designed in OpticStudio (figure 2.2) to perform predictions in a general population. While some studies (Pérez-Gracia et al. 2020, Oltrup et al. 2021) used the cornea defined in the Navarro eye model (Navarro et al. 1985) (corneal power of 42.16 D and +0.139 µm SA, 6.0-mm pupil), we decided to optimize the conic constant so that our standard eye model corneal spherical aberration (SA) would follow *accepted* standards proposed in the literature (Norrby et al. 2007). In particular, we designed a cornea model with a power of 43 D and 0.28 µm of spherical aberration (SA) for 6.0-mm pupil diameter, which is the average SA found in the population as reported by different studies (Wang et al. 2003, Beiko et al. 2007).

Several standards were developed to evaluate intraocular lenses on bench. One of the most well-known, *ISO standard (*UNE EN ISO 11979-2, 2015) considers acceptable corneal designs those whose total effective power fall into the range of 41.5 and 43.5 D; and 2 types of model eye to evaluate the optical quality of IOLs described as ISO1 (corneal SA=0 µm) and ISO2 (corneal SA=0.28 µm). While there are some differences with the on-bench evaluation, that is performed with the intraocular lens in a cuvette and with the cornea simulated with a glass lens in air, the power and spherical aberration of our designed cornea fall within the range accepted by the ISO2 standard.

The aqueous and vitreous refractive indices were 1.376 and 1.336 respectively. The pupil was placed at a distance of 3.2-mm from the corneal posterior surface and limited the entrance pupil diameter.

Cornea Model

The standard eye model used a cornea model based on literature data and has an index of refraction of 1.376 (Marín 2006), a central thickness value of 0.55 mm (Liu et al. 1999), a spherical posterior corneal surface with a fixed radius of curvature of 6.5-mm (Rosales et al. 2010) and an aspheric anterior surface. A cornea of 43 D corneal power (Klyce 2000, Marín 2006) and 0.28 µm of corneal spherical aberration at 6.0-mm pupil diameter (Wang et al. 2003, Beiko et al. 2007) was designed. For a cornea of 43 D total power, the focal length calculated was 31.07 mm (f = (n'/43)*1000), 23.255 mm in air, and the anterior surface radius was modified and optimized in Zemax to fit the calculated focal length. Then, a merit function was programmed to calculate both the RMS focus and the spherical aberration, and the radius of curvature and conic constant of the anterior surface was optimized for the cornea to get the desired optical power and to have a specific spherical aberration for a 6.0 mm diameter aperture. Figure 2.1 shows the OpticStudio lens editor with the result of the optimization. The anterior corneal radius value calculated was 7.6681-mm, close to the average value of 7.7 mm found by Marín (Marín, 2006), and a conic of -0.0667. This cornea model was slightly modified for the different experiments when needed, as described in chapters 3, 6 and 7.

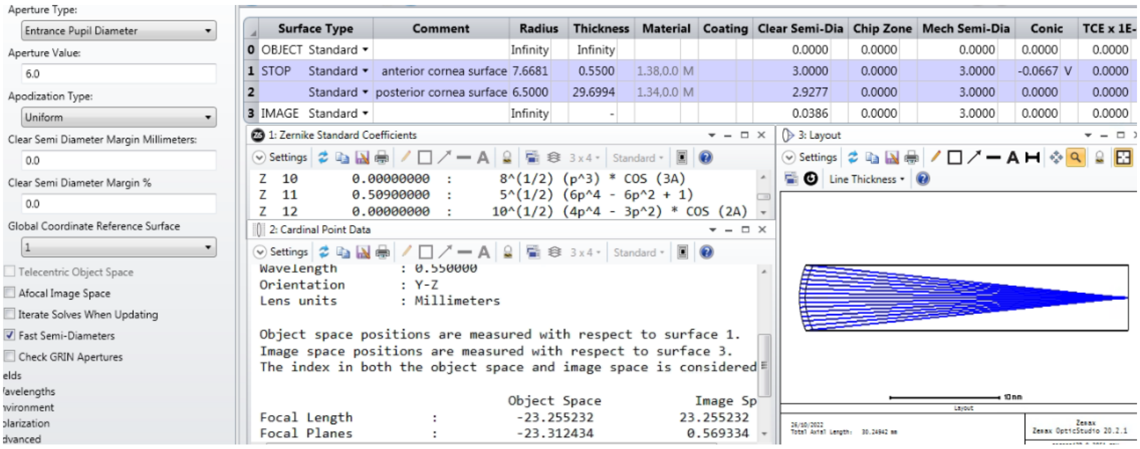

Fig. 2.1: *OpticStudio showing the cornea designed for the standard model eye. The different windows show, the properties where a 6 mm pupil diameter was selected, the Lens Data Editor with the two Standard surfaces defining the cornea, the Zernike Coefficients where the spherical aberration is the value desired (0.509 waves = 0.28 microns) and the cardinal point data with the focal length (calculated in air in OpticStudio).*

Pseudophakic eye model

In the pseudophakic eye model, the anterior chamber depth was set to 3.2 mm (Nemeth et al. 2006) and the intraocular lens was placed just behind the pupil. The IOL power depended on the study and the eye axial length was calculated using a monofocal IOL, with the same IOL power, material, and brand as the IOL under study, as the length for which the rays focused on the retina (maximum concentrations of rays, minimum spot size).

Two premium IOLs were studied and the corresponding monofocal IOL platforms used as a reference (and to calculate the axial length of the eye model, associated to a given IOL power). The optical designs of the lenses under study were provided by the manufacturer under confidentiality agreements. The premium IOLs were the Isopure IOL from PhysIOL-VBI (chapters 3 to 5) and the Acrysof IQ Vivity IOL from Alcon(chapters 6 and 7). The standard reference monofocal IOLs were the Micropure IOL and the monofocal Acrysof IQ SN60WF, respectively.

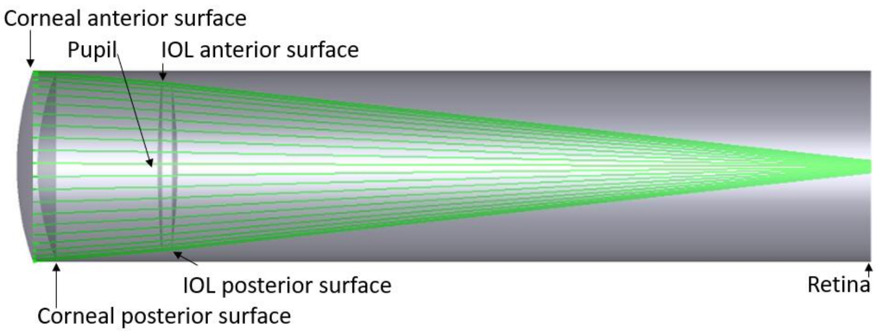

Fig. 2.2: *3D layout of a pseudophakic model eye in OpticStudio.*

2.1.2 Phase maps and IOL contribution

We used the term phase map to define the phase change produced when an intraocular lens is implanted in a subject. To calculate the phase map for a given IOL, we performed simulations and subtracted the aberrations of a pseudophakic model eye from those of a phakic model eye using a mesh of 256x256 pixels for a given pupil diameter. This methodology was described by Akondi et al. (Akondi et al. 2017) and is represented in figure 2.4 using a neutral lens to represent the crystalline lens.

The difference between pseudophakic and phakic model eyes arises from the presence of the crystalline lens. To investigate the potential effect of different crystalline lens parameters, we studied the phase map resulting when using three different crystalline lens models (placed at 3.2 mm from the posterior corneal surface): the neutral lens model, the young lens model and the old lens model. These models were built with knowledge on the change of spherical aberration with age (McLellan et al. 2001) and to confirm previous findings using a different visual simulation methodology (Villegas et al. 2019).

The *Neutral lens model* was designed using a paraxial lens that simulated the IOL power without introduction of aberrations.

The *Young lens model* was designed to simulate a 29-year-old crystalline lens. Its anterior radius of curvature was of 11.65-mm, its posterior radius -6.33-mm, and the lens thickness was 3.72 mm (Martinez-Enriquez et al. 2017). We used a constant refractive index of 1.41 (Uhlhorn et al. 2008) and optimized the conic constants in both crystalline surfaces (-4.9847 and -4.2392) to obtain a spherical aberration of 0.25 µm at 7.32-mm pupil diameter (McLellan et al. 2001).

The *Old lens model* was built to simulate a crystalline lens of a 79-year-old subject. Its anterior radius of curvature was 9.06-mm, its posterior radius -5.74 mm, and its lens thickness 4.759 mm (Martinez-Enriquez et al 2017). Its refractive index 1.40 (Uhlhorn et al.

2008) and conic constants in both surfaces was optimized (-1.3071 and -1.2951) to get a spherical aberration of 0.40 µm at 7.32-mm pupil diameter (McLellan et al. 2001).

We evaluated the effect of the crystalline lens aberration and ageing on the IOL simulations by calculating the phase map of the IOL contribution using the three different lens models, neutral, young and old lens and for a 3.0-mm pupil diameter. Figure 2.3 shows the through focus performance measured in a high-speed focimeter with the tunable lens (SimVis technology), in terms of TFVS, of an IOL phase map evaluated (Isopure 21 D) with the three lens models (neutral, young and old).

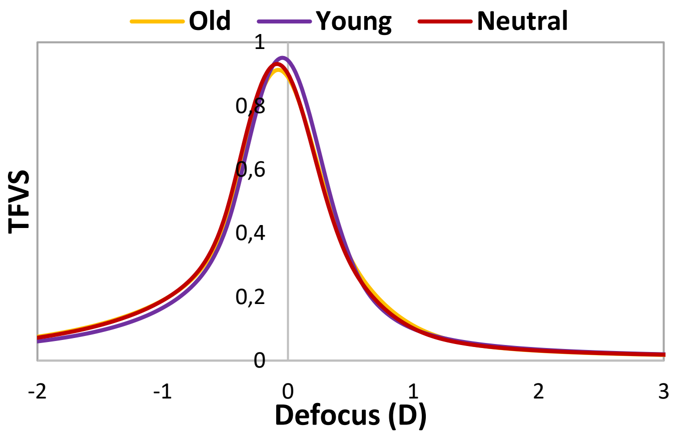

Fig. 2.3: *TFVS of IOL phase map (Isopure IOL), with three different cases of phakic eye: old, young, and neutral. 3.0-mm pupil diameter.*

Given the negligible differences on the TF performance of Isopure IOL 21 D obtained with different crystalline lens models, we performed all IOL phase map simulations in this thesis using the neutral lens model only (figure 2.4). The derived phase map was then either used in custom developed programs to calculate optical quality metrics that would represent the contribution of the intraocular lens without the cornea, or to simulate the contribution of the intraocular lens in a visual simulator.

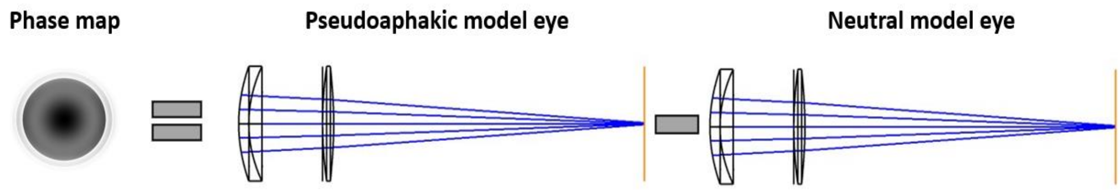

Fig. 2.4: *Schematic representation on how the phase map of the IOL was calculated.*

2.1.3 Optical quality metrics

To evaluate the optical performance of an IOL, the wavefront aberration map of the pseudophakic model eye was exported from OpticStudio into MATLAB (MathWorks, Natik, MA) and custom-built scripts were used to evaluate the through focus (TF) Modulation Transfer Function (MTF) and the TF Visual Strehl ratio (VS) (figure 2.5).

The *MTF* was calculated as the modulus of the OTF (Optical Transfer Function) as described in the introduction (eq. 1.7). We evaluated the contrast reduction as a function of the spatial frequency of an image, and specifically at two spatial frequencies, 50 lp/mm and 100 lp/mm (which correspond to about 15 and 30 cpd for the average human axial length). These are the frequencies that are indicated in the ISO normative 11979-2.

The Visual Strehl (VS) ratio, which quantifies the volume under the MTF at all frequencies weighted by the human contrast sensitivity function (CSF), as described in the introduction, (eq. 1.8). VS was chosen as quality metric, as it has been shown to correlate best with visual acuity in different studies (Marsack et al. 2004, Iskander 2006).

TF curves were calculated for MTF (30 and 15 cpd) and VS, as a function of defocus from -2 to 5 D (in 0.1 D steps) to evaluate the IOL optical performance at different distances. Depth of focus (DOF) was calculated from the TFVS curves as the defocus range for which the VS metric was above 0.12, as this value was determined to be the limit of normal visual function in subjects (Yi et al. 2011). The value corresponds to a visual acuity of about 0.2 LogMAR (Cheng et al. 2004, Iskander 2006, Yi et al. 2011).

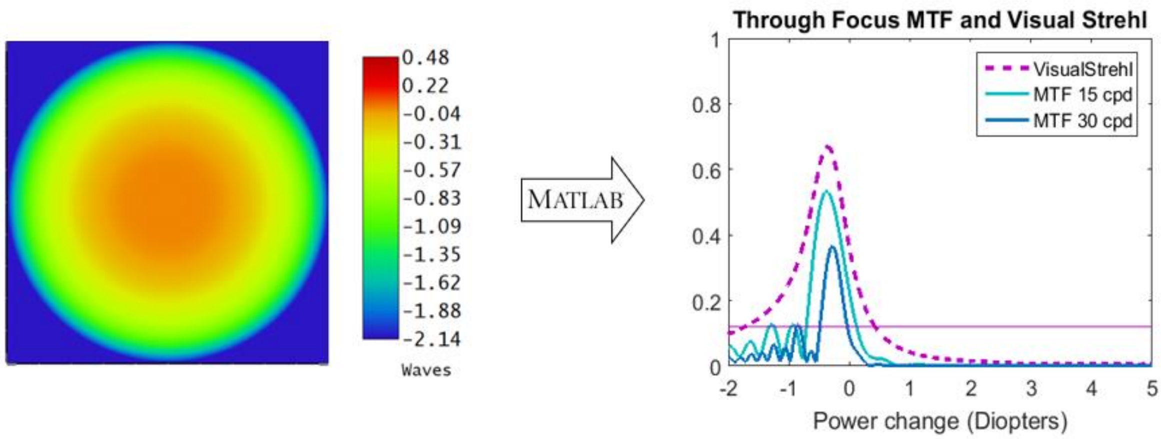

Fig. 2.5: *Left, 2D wavefront aberration of the pseudophakic model eye implanted with Isopure IOL, 21 D, obtained by ray tracing with OpticStudio. Right, the trough focus curve calculated with Matlab: Through focus Visual Strehl (pink dotted line), and through focus MTF at 15 and 30 cpd (blue lines) for a 4.5-mm pupil diameter. The pink horizontal line marks the value of VS equal at 0.12 to calculate the DOF.*

2.2 Sim+Vis Technology™

2.2.1 Temporal multiplexing

The Sim+Vis technology is the core of SimVis Gekko, a wearable, programmable, binocular and see-through simultaneous vision simulator to simulate any multifocal correction (Dorronsoro et al. 2016). It is based on temporal multiplexing. Subjects see through an optotunable lens that alternates between different foci at a speed higher than the fusion frequency of the human visual system (50Hz) (Watson A B 1986), creating a multifocal image of static appearance in the retina by superimposing a focus image with one or more defocused ones. Provided with a high-speed driver allowing a complete control of the tunable lens, Sim+Vis technology can replicate any through-focus power profile, and the corresponding image quality at each distance, provided that we correctly compensate for any dynamic effect that could affect the dynamic response of the optotunable lens (TL, EL-10-30, Optotune Inc., Switzerland) (Akondi et al. 2017; Dorronsoro et al. 2019).

Figure 2.6 shows an example of simulation by temporal multiplexing of a bifocal lens with the energy distributed equally (50%) in two foci, 0 and 3 D (far and near vision respectively). TL changes the optical power in a 20 ms period, so the power at far will be presented during 10 ms and at near during another 10 ms. The temporal pattern is repeated constantly in a loop, and the two temporal states of the lens are projected onto the retina that perceives a simultaneous bifocal image of static appearance due to the overlap of the focused and defocused images projected at high frequency. The possibility of choosing the energy balance of different optical powers allows to manipulate the simultaneous vision simulating different optical power profiles which reproduce different multifocal optical design (bifocal, trifocal, multifocal and EDOF).

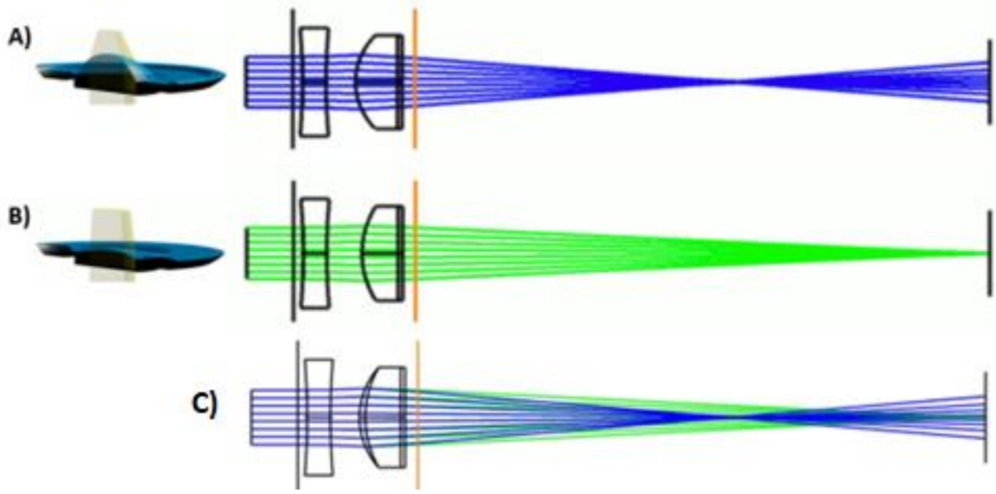

Fig. 2.6: *Representation of TL behavior. A) at left the graph representation of TL inducing a +3 D optical power and at right ray tracing representing a positive defocus. B) left graph representation of TL inducing an optical power of 0 D and right ray tracing representing the lens projecting the rays focused on the retina. C) superposition of the two foci on the retina.*

2.2.2 Characterization of the dynamic response of optotunable lens in a high-speed focimeter

The optotunable lenses (EL-10-30), manufactured by Optotune Inc., Switzerland, were dynamically characterized using a high speed focimeter that can calculate the power at 3.823 kHz (Dorronsoro et al. 2019). In brief, the high-speed focimeter comprises an incoherent source of polychromatic light to illuminate a tilted slit (25 µm wide and 3.0 mm long), a trial lens holder (those trial lenses are positive and negative thin lenses for an optometry trial used for set-up calibration) and an optotunable lens (EL-10-30, Optotune Inc., Switzerland) placed in conjugated pupil planes thanks to 4f systems, a high-speed camera (IL5S; Fastec Imaging USA), with a macro-objective (MO; 100-mm f/3.5; Cosina) and a prism, key component of the high speed focimeter. This prism covers half of the image of the slit and produces a displacement of the slit image that goes through the prism, proportional to the optical power induced by the TL, while the rest of the slit constitutes a reference image (not displaced when inducing an optical power to the TL). Figure 2.7 shows a diagram of the experimental set-up with and without the prism. This system provides direct and robust measurements of the TL optical power, and is insensitive to decentrations and misalignments.

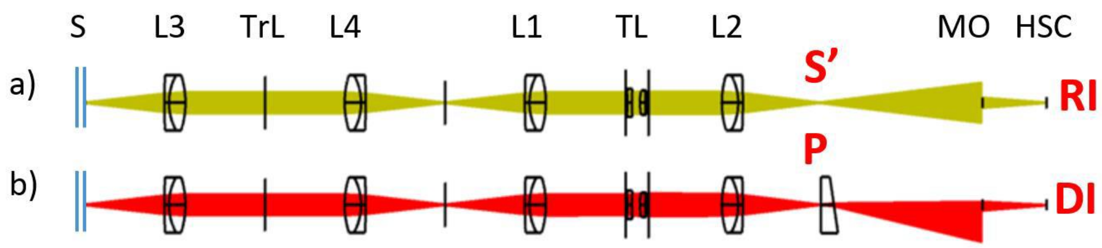

Fig. 2.7: *Optical set-up. S: Slit (an incoherent polychromatic light source and a diffuser are not shown); L3 and L4, and L1 and L2: 4F projection systems; TrL: Trial lenses; TL: Tunable lens; S': Intermediate slit image; P: (prism); MO: Macro objective; HSC: High-Speed camera. (**a**) Configuration without the prism providing a reference image RI. (**b**) Configuration with a prism in the region of the intermediate image S', providing a displaced image DI, with a displacement (concerning the reference) that changes with the axial position of the intermediate slit image S' and therefore changes with the optical power of the tunable lens TL. Both configurations co-exist in the same set-up, as the prism P only affects one-half of the intermediate image S' (Dorronsoro et al. 2019, Barcala 2021).*

The dynamic response of the optotunable lens was characterized by measuring the response to square electric input waves of different amplitudes with periodic temporal steps (20-ms period) (Akondi et al. 2018, Dorronsoro et al. 2019). The results showed similar normalized responses for different step heights and demonstrated a stable and time-invariant TL response. Nonetheless, the step responses showed over- and under -shoot that must be corrected to accurately simulate the multifocal patterns as shown in figure 2.8. To correct for the dynamic effect of the lens, the "impulse response" was calculated from the first derivative of the average normalized step response and convolved to the temporal profile of the pattern. The method has been explained in detail in previous publications (Akondi et al. 2018, Dorronsoro et al. 2019).

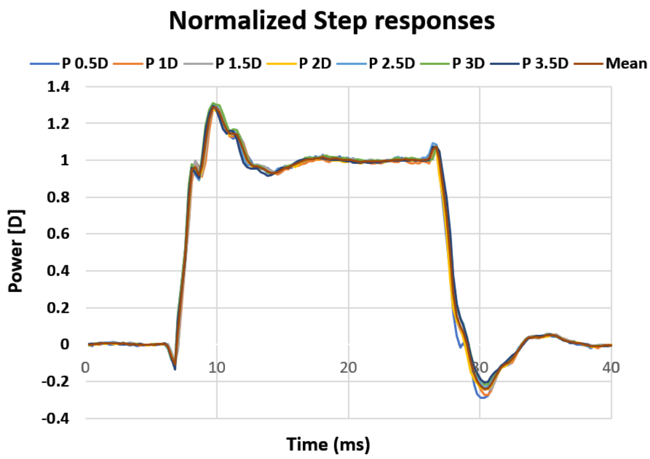

Figure 2.8: *Evaluation of the dynamic effects of an optoajustable lens (EL-10-30, Optotune Inc., Switzerland, AQAA1300). Normalized step responses of different amplitude and the average response (brown).*

2.2.3 Simulation of multifocal patterns with SimVis

Different multifocal patterns were simulated using the SimVis technology. The input data to simulate a pattern can be the IOL design provided by the manufacturer (where the phase map is calculated implementing the lens in OpticStudio as explained before in section 2.4), but also from on bench measurements or publicly available TF MTF curves at 15 cpd published in scientific articles or in regulatory documents that can be used to estimate the TFVS (Sawides et al. 2021).

In the current thesis, the designs of two IOLs, Isopure and Acrysof IQ Vivity, were provided by two manufacturers (Physiol-BVI S.A. and Alcon S.L. respectively) for collaborative projects under non-disclosure agreements. The phase map of the IOL contribution was extracted following the procedure detailed above (section 2.1.2) from the pseudophakic eye model and the neutral lens eye model. Then, the MTF was estimated from the phase map with the pupil function using Fourier Optics. TFVS curves were used to evaluate the real performance of the multifocal pattern and simulate the IOL through temporal multiplexing. Custom routines in Matlab were used to calculate a series of SimVis temporal coefficients, based on the equation previously described by Akondi and colleagues (2017). These temporal coefficients stand for the weighting factors of a series of defocused monofocal PSFs, adjusted to match the TF optical quality of the IOL (real lens TFVS) in an iterative optimization procedure to obtain the SimVis temporal profile of the multifocal IOL (SimVis lens).

In parallel, as said in the previous section, the dynamic behavior of the optotunable lens, AQAA 1300, was evaluated in order to accurately compensate for the dynamic effects, if any. To correct for the dynamic effects, the TL impulse response function (Akondi et al. 2018) was used and applied to the SimVis temporal profile of the lens to calculate the temporal “corrected wave” in an iterative optimization of the electrical input signal driving the lens where some constraints were taken into account (20ms period, temporal coefficients of at least 0.1 ms and no more than 150 temporal coefficients to simulate the design).

To validate the SimVis lens simulation, we used the high-speed focimeter previously described in section 2.2.2 to evaluate experimentally the TFVS ratio of the SimVis programmed lens with and without the dynamic effects correction. The SimVis-programmed Lens is validated by comparison of the real and experimental TFVS curves (on average error in the Visual Strehl ratio height at peaks was less than 3%), and the peaks of the design are not shifted more than 1/8 D from the real multifocal design. The number of temporal coefficients varies according to the real lens design and to the TL used to simulate the specific design.

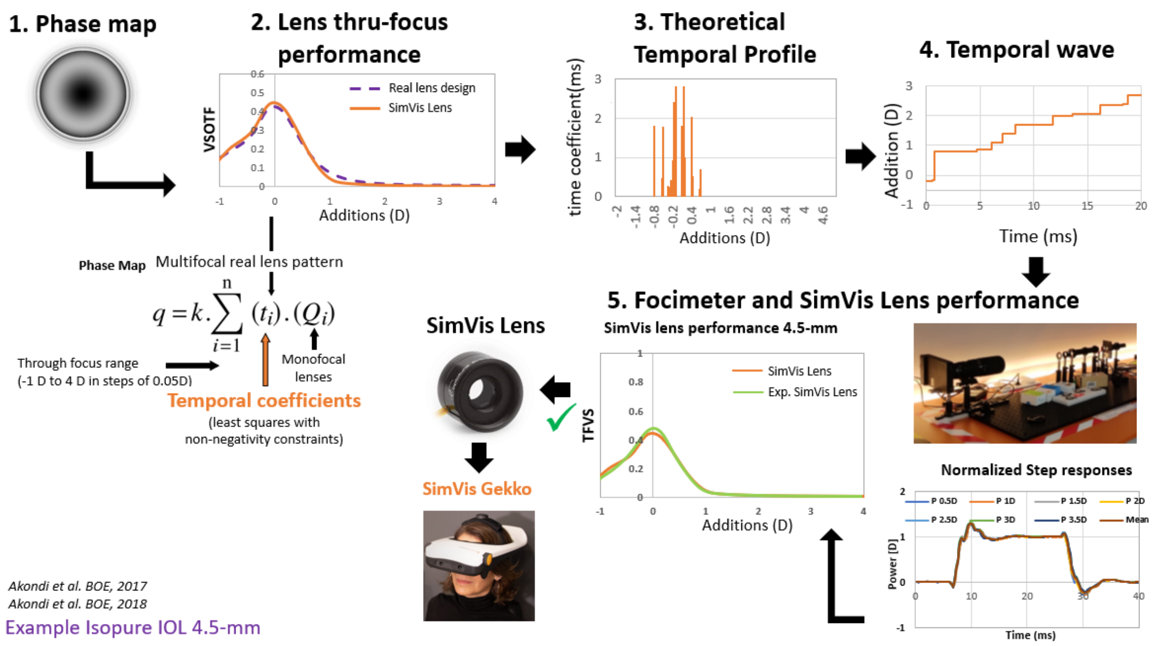

Figure 2.9: *Overview of the pipeline to simulate and validate the simulation of an intraocular lens (in the sample Isopure IOL from PhysIOL/BVI for a 4.5mm pupil diameter) with SimVis technology.*

Once the SimVis simulation performance is validated on the high-speed focimeter, the multifocal pattern is ready to be used with the SimVis technology (either with the SimVis Gekko binocular visual simulator (as in chapter 8) or with the optotunable lens alone in an adaptive optics system described below).

2.3 Adaptive Optics System

The Adaptive Optics System (AO) used was developed in VioBio Lab (CSIC) and incorporated different wavefront modulators (deformable mirror and spatial light modulator) as well as a channel where an optotunable lens could be implanted to simulate an IOL using SimVis. The system allowed the selection of a wide range of illumination wavelengths selected from a supercontinuum laser source. The system configuration and applications of the VioBio Lab AO simulator are described in an ample number of publications from the group (Viñas 2015, Vinas et al. 2015, Vinas et al. 2017, Vinas et al. 2019, Marcos et al. 2020, Aissati et al. 2020, Benedi-Garcia et al. 2021)

2.3.1 General description

Figure 2.10 shows a diagram of the experimental AO system that was described in detail in previous publications (Vinas et al. 2017, Benedi-Garcia et al. 2021).

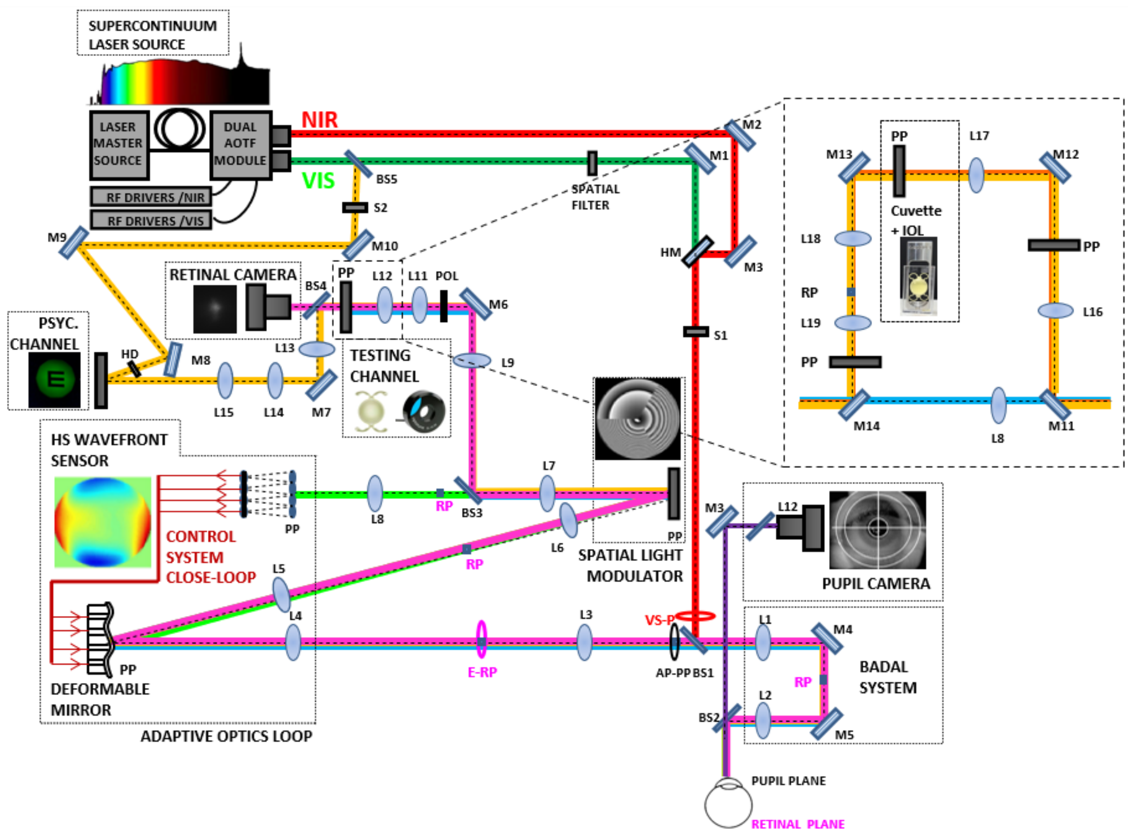

Fig. 2.10: *VioBio Lab AOII scheme: near infrared (NIR) path (red line); Visible (VIS) path (green line); Adaptive optics channel (green line); SLM and testing channel (blue line); cuvette (orange line); retinal camera channel (pink line); psychophysical channel (yellow line) and pupil camera (purple line) (Viñas 2015; Benedi-Garcia 2021).*

The AO system comprises eight different channels described below:

1) ***Illumination channel:*** A supercontinuum laser source (SCLS, SC400 femtopower 1060 supercontinuum laser source, Fianium Ltd, United Kingdom), provides the light of the system in a wide range of wavelengths from 450 nm to 1020 nm. A dual Acousto-optic Tuneable filter (AOTF) module (Gooch & Housego, United Kingdom) is coupled to the SCLS and controlled by Radio Frequency (RF) drivers to select the desired wavelength and intensity (from 450 to 1020 nm) and allows two different outputs with collimated beams coupled to two different multimode fibres: one for visible light (VIS) and the other for infrared light (IR). The spectral bandwidth is 2-4 nm for VIS light and 3-6 nm for NIR light. VIS and NIR illuminate the AO channel path; always after any realignment, implementation and/or before measurements on eye for experiments, the laser power is measured with a power meter in the corneal plane to ensure that laser safety standards are maintained for each wavelength on a range from 0.5 to 50 µW (at least one order below ANSI standards) to avoid ocular damages (Delori et al. 2017, White et al. 2007, Morgan et al. 2008). VIS light was splitted to illuminate the stimulus in the psychophysical channel and to perform AO measurements/corrections. In this thesis SCLS light at 555 nm was used to obtain retinal images in an artificial eye and illuminate the stimulus to measure the Visual Acuity in subjects. IR light to measure the ocular aberrations in subjects.

2) ***Adaptive optics (AO) channel****:* the main components are a Hartmann-Shack wavefront sensor (HS) and an electromagnetic deformable mirror (DM), placed in conjugated pupil planes through a relay of lenses (is possible to use the SLM instead the DM to AO loop, in this thesis only DM was used). The HS (HASO 32 OEM, Imagine Eyes, France) is formed by a matrix of 40 x 32 microlenses, an effective diameter of 3.6-mm and centered at 1062 nm. The DM (MIRAO52, Imagine Eyes, France) consists of a high quality reflecting membrane (silver coated>98% for 830 nm wavelength) with 52 actuators located behind, an effective diameter of 15 mm and a maximum generated wavefront amplitude (stroke) of ±50 µm. HS and DM have a magnification in the system x0.5 and x2 respectively, considering as reference the pupil of the system that is x1. HS and DM work in close-loop, HS measure the aberrations and DM correct and/or induce desire aberrations. With the artificial pupil of the system (AP), also placed in a conjugate pupil plane, it's possible to select and set the pupil diameter in the measurements to the desired value. AO system has many optical elements (figure 2.10), the AO channel correct the system aberrations along calibration before measurements, reducing the RMS from 0.45 µm to 0.018 µm at 7.0-mm pupil diameter. AO closed-loop allows to induce positive and negative spherical aberration with the DM in measurements, and measure and correct the ocular aberrations in subjects.

3) ***Spatial light modulator (SLM) channel:*** The SLM (PLUTO-VIS; Holoeye Photonics AG, Germany) controls a liquid crystal on silicon (LCoS) active-matrix reflective mode phase-only liquid crystal display. Its resolution was 1920 x1080 pixels; 0.7" diagonal; pixel pitch: 8.0 µm, the image frame rate was 60 Hz; and the maximum resolution was 62.5 lines/mm; 8 bits. The device was placed in a conjugated pupil plane with x1 magnification. The SLM was calibrated to be used with a wide range of wavelengths in the VIS spectrum (420-700 nm) and a linear polarizer was placed in front of the SLM with a specific angle to ensure the optimum output. Applying different voltages to the different pixels the phase of the wavefront is modified between 0 and 2π allowing to simulate multifocal designs. The SLM can reproduce 256 gray scale levels in an image which contains the wrapped phase map that we send through a computer from a software package developed in the lab. The IOLs (Isopure and Acrysof IQ Vivity) phase maps at different pupil sizes, were mapped into the SLM to simulate them.

4) ***Testing channel:*** allows to place an active element in a conjugated pupil plane with x1 magnification, either placing an optotunable lens to simulate the IOL via temporal multiplexing, or placing the IOL in a cuvette or using phase plates for system calibration (Vinas et al. 2017).

   The ***optotunable lens*** (Optotune, AQAA 1300) is aligned in the system with a x-y-z stage through a flip mount (implemented by the author of this thesis to validate the SimVis simulations in the same session and conditions) and connected to a set of drivers and controlled by Bluetooth from the AO computer.

   A ***cuvette*** was designed and implemented to compensate 20 D of the optical power of the IOL (the "old" cuvette only could be used for 0 D IOLs which normally are not manufactured) and published in the co-authored publication Benedi et al. 2021. Due to the limited space on the system, a second floor was built over the testing channel pupil plane using mirrors, flips and a relay of lenses (figure 2.10). In combination with the Badal system, it is possible to correct a range of IOL powers from 16 to 24 D. The IOL is fixed in a metal mount and immersed in the cuvette filled with distilled water (similar eye index refraction).

5) ***Badal system:*** consists in two flat mirrors (M4 & M5) and two lenses (L1 & L2, focal lengths = 125 mm), mounted on a motorized system to manipulate the focal distance to the eye in a range from -8 to 8 D allowing to compensate the defocus of the eye in subjects (in myopic and hyperopic eyes), to induce the defocus to perform the through focus curves measurements and to compensate the IOL defocus when the IOL is measured physically in a cuvette. The Badal system can be controlled automatically with a custom-made software or by the subject with a numerical keyboard.

6) ***Psychophysical channel:*** formed by a Digital Micro Mirrors device (DMD, DLP® DiscoveryTM 4100 0.7 XGA, Texas Instruments Incorporated, USA) placed in a conjugated retinal plane and controlled by a programable computer graphics system for psychophysical visual stimulus generation (ViSaGe, Cambridge research system). The DMD is a rectangular array of moving micro-mirrors and allows the presentation of high-resolution gray-scale images, illuminated monochromatically by the SCLS, combined with a rotatory holographic diffuser (HD) that breaks the coherence of the laser to obtain a uniform stimulus illumination. The visual stimulus is a letter of 45

pixels, 0.15 degrees angular subtend, equivalent to a VA of 0.3 LogMAR. The luminance of the stimulus was 20-25 cd/m2 across the spectral range tested psychophysically (450-700 nm). When the measurements are with polychromatic light, the DMD is illuminated with a white light source placed in the system with a flip-mounted mirror.

7) ***Retinal imaging channel:*** images of the beam spot are projected into a CCD camera (ORCA-R2, Digital CCD camera, C10600-10B, Hamamatsu Photonics K.K., Japan, 12 or 16 bit, 1344x1024 pixels, 6.45x6.45 µm pixel size) through a collimated lens (L9, 63 mm focal length) and a camera lens (L16, 135 mm focal length). The laser beam is filtered by a spatial filter (microscope objective (x20), 25 µm pinhole and 50 mm focal length) before entering in the eye. This channel is an "one-and-a-half-pass", conjugated in a retinal plane, with the aerial image being the autocorrelation of the image of the laser spot with a 2-mm entry beam and 1-mm exit beam. This channel is used to get doble pass images of the IOL TF curves.

8) ***Pupil monitoring channel:*** A pupil camera (DCC1545M, High Resolution USB2.0 CMOS Camera, Thorlabs GmbH, Germany) is used to align (and monitor) the subject's natural pupil and the artificial eye onto the adaptive optics system with an x-y-z stage, taking the line of sight as reference and using a ring of infrared diodes (λ = 900 nm) placed in front of the eye to provide suitable illumination for alignment.

To control the different components of the adaptive optics system, two computers (PC1 and PC2) with commercial and custom-built programs are used. PC1 controls the AO channel (DM and HS), the pupil monitoring, the Badal system and the illumination channel (power and wavelength). PC2 controls retinal imaging Channel, psychophysical channel (DMD and ViSaGe), SLM and the CMOS of the artificial eye.

2.3.2 AO calibration

Different experiments were performed with the AO system to study the optical quality of IOLs, to validate on-bench the simulation of the IOL and to perform psychophysical measurements on patients. Common procedures are described in this section and specific protocol will be described in the corresponding chapter.

Before each measurement, the system was aligned, the power of the illumination sources was measured with a power meter, and a new interaction matrix was built for MIRAO and SLM using controller programs (HASO and CASAO).

The alignment of the cuvette was doublechecked using a 20D IOL to ensure the right position of the Rassow lens doublechecking that the result of the through focus optical quality of a known trifocal IOL that served as reference was the expected one (no movement in the stimulus when projected on the retina of the model eye, absence of astigmatic effects, correct location of the three IOL foci with the Badal and best image quality at 0 D).

The SLM was first aligned using the linear polarizer that provides an optimal output, and checked using different known patterns mapped into the SLM. Defocus patterns which were compensated with the Badal system and bifocal patterns which were evaluated performing through focus curves. The phase map calculated for IOLs simulations (explained in section 2.1.2) with custom algorithms in Matlab, were evaluated from the multifocal phase maps by performing 2π-wrapping such that, $\Phi = X$ [mod 2π], where X represents the unwrapped phase map and Φ is the wrapped phase map. The generated phase pattern is a grey-scale image, where each level of grey corresponds to a certain phase difference in the interval [0 2π] that is mapped into SLM (figure 2.11).

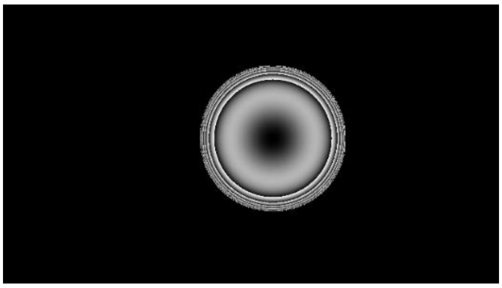

Fig. 2.11: *SLM 2π-wrapping phase map pattern for Isopure IOL 4.5-mm. The phase map was projected at the position of the optical beam.*

SimVis optotunable lens driver uses digital counts to change the power of the lens. First, the TL was calibrated to have the relationship between diopters and digital counts using the Badal system to induce a defocus in a range from 0 to 5 D in 0.5 D steps and compensating it by increasing the digital counts. After the calibration, different IOL patterns (using the SimVis lens pattern with the temporal coefficients that define a given IOL) can be correctly simulated with the optotunable lens previously validated on the high-speed focimeter (TL AQAA 1300).

To calibrate the **retinal camera** before measurements, a bifocal multifocal phase plate with 2 radial zones was placed in the testing channel pupil plane. The bifocal phase plate performance was evaluated in the image retinal camera program (figure 2.12) to ensure the spot centration in x and y axis, the intensity in the TF images and the absence of saturation or irregular spot size, and the position of the focus.

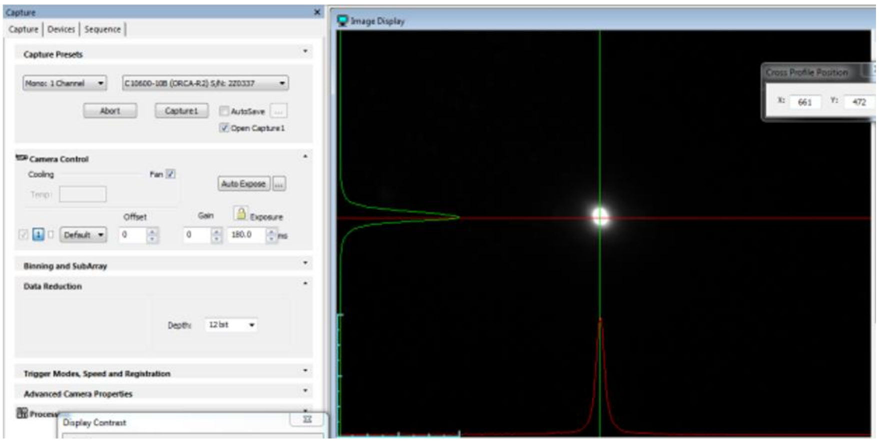

Figure 2.12: *Image Retinal camera program. Camera always was calibrated with a phase plate to ensure the alignment with the x and y axis program diagram, intensity with the laser beam diagram and a through focus had been made in the bifocal pattern to evaluate that camera objective was on focus.*

2.3.3 On-bench measurements in AO system with an artificial eye

We evaluated the optical performance of the IOL on-bench (simulating the lens with the SLM or the SimVis optotunable lens or with the IOL in cuvette) using an artificial eye aligned in the AO system (as it was a subject's eye) with a 3-D translational stage. The artificial eye consisted of a 50 mm focal length achromatic doublet with either a rotating diffuser as retina for double pass retinal image quality measurement, or a CCD camera (DCC1240C - High-Sensitivity USB 2.0 CMOS Camera, 1280 × 1024, Global Shutter, Color Sensor; Thorlabs GmbH, Munich, Germany) that acted as retina to capture images of the projected visual stimuli in the single pass experiment.

For the ***single pass (1P)*** experiment, through focus retinal image quality was evaluated. A Snellen E letter was displayed in the DMD (letter size of 45 pixels, 0.15 degrees angular subtend, equivalent to a VA of 0.3 LogMAR) with a black background and projected onto the retina of the artificial eye (i.e. the CCD camera). DMD was illuminated with the supercontinuum laser source at 555 nm for green light experiment or with white light. Series of images were collected through focus in a range between -4.0 to +1.0 D, in steps of 0.25 D changing the vergence with the Badal system.

The optical quality of the IOL design was analyzed in terms of the correlation metric (eq. 2.3) that compare the similarity between two images. The through focus images of the degraded E letter, seen with the IOL in the cuvette or through the simulated IOL with the SLM or the optotunable lens, was compared to a reference image, different according to the three different channels used. For Cuvette channel, the reference image corresponds to the image in focus on the system without any IOL; for the SLM channel, the reference image was taken without any SLM simulation and with the polarizer and on focus image in the system; and for the SimVis channel, the reference image was taken with the optotunable lens inducing a static 0D optical power.

$$corr = \frac{\sum_n (X_n - \overline{X_n})(Y_n - \overline{Y_n})}{\sqrt{\sum_n (X_n - \overline{X_n})^2 \sum_n (Y_n - \overline{Y_n})^2}} \qquad \text{(eq. 2.3)}$$

For the ***double pass (2P)*** experiment, through-focus double-pass retinal images were collected illuminating the eye with a collimated beam changing the vergence of the rays with the Badal system between -3.0 and +1.0 D, in steps of 0.25 D, and images of the beam spot "in a half past" were collected in the CCD camera of the retinal imaging channel. Wavelength illuminating the stimulus was 555 nm, constant laser power and camera properties, and ensuring that none of the images were saturated.

The optical quality was calculated as the average Full Width at Half Maximum (FWHM) of the intensity profile of four meridians (0, 45, 90 and 135 degrees) passing through the center of PSF images, estimating the lateral extend (in pixels) for which the intensity was above half of the maximum intensity of the image.

The Depth-of-Focus (DOF) on-bench was defined as the range of diopters for which the metric (correlation metric and the normalized FWHM,) was above 0.8 (Marcos et al. 1999).

Additionally, two new metrics were defined: (1) the optical degradation at far, defined as ratio between the optical quality at 0D and the optical quality with no IOL (AO system without lens nor simulation), (2) the optical benefit at intermediate distance, defined as the ratio between the average optical quality with the IOL under study and the optical quality with no IOL at intermediate distance (1.5 D).

2.3.4 Experimental measurements on subjects in the AO system

All the subjects that participated in the different studies signed a consent form approved by the CSIC institutional review boards after they had been informed on the nature of the study. All protocols met the tenets of the Declaration of Helsinki.

In all the measurements, the subject's pupil was dilated, and the accommodation paralyzed with tropicamide (1%): 3 drops were instilled at the beginning of the session (spaced every 10 minutes) and re-instilled every hour. The pupil size in the experiment was always limited by the artificial pupil in the system to have the same pupil diameter in all subjects across measurements. Measurements were made monocularly, and subjects wear a patch in the opposite eye along the measurements. A dental impression was made for each subject and mounted in the x-y-z linear stage to align the subject into the AO system and the subject's pupil was monitored during the experiment, controlling pupil centration.

Subject's spherical error was measured and corrected with the Badal system before each TF curve measurement (astigmatism always was lower than 0.75 D and wasn't compensated in the measurements). Subjects viewed the psychophysical stimuli projected on the DMD, illuminated with the SCLS 555 nm or the white light. The subjects had to select their best focus (repeated 3 times) by moving the badal optometer with a numerical keyboard while looking at a Maltese cross. Spherical refraction was known before measurements, the search for the best focus was initiated with 2 D myopic defocus over their spherical refraction using a step size of 0.05 D.

Visual Acuity (VA) was measured using a high contrast tumbling Snellen E letter with 8-Alternative Forced Choice procedure (8AFC: pointing up, down, left, right, oblique up-right, oblique up-left, oblique down-right, oblique down-left) and a QUEST (Quick Estimation by Sequential Testing) algorithm was used to estimate the threshold of the minimum recognizable letter size (Watson et al. 1983, Brainard et al. 1997, Borgo et al. 2012, Lu et al. 2013). Subjects indicated the orientation of the E letter (presented for 0.5 seconds) with a numerical keyboard, 32 trials were used for each VA measurement (figure 2.12 shows one measurement of VA). The VA was calculated as the mean of the last 5 reversals and the variability as the standard deviation of those 5 values.

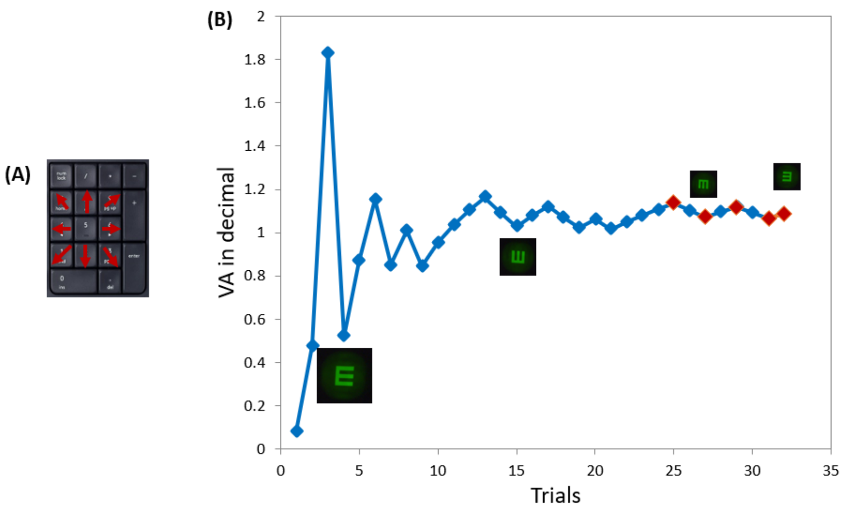

Fig. 2.13: *(A) keyboard used in the VA measurement with the 8 directions that subjects must press according with E letter stimulus orientation. (B) Example of QUEST obtained for subject S#8 (chapter 4 and 5) with 32 trials, the red points show the reversals, the VA in decimal was calculated as on average of these last reversals. The E stimulus images are a visual representation to show how size decreases with high score in VA.*

Through focus visual acuities were measured in decimal units and converted to logMAR. The visual DOF was calculated as the range of defocus for which VA was 0.2 LogMAR or better in the near region (negative defocus) (Yi et al. 2011).

The visual degradation at far and the visual benefit at intermediate distance for subjects were calculated using differences visual acuities with respect to a monofocal/no lens condition: (1) the visual degradation at far was defined as the difference in VA LogMAR with IOL under study at 0 D relative to the no IOL condition, and (2) visual benefit at intermediate, as the difference in LogMAR between IOL under study and the no IOL condition VA at an intermediate distance of 1.25 D (Vedhakrishnan et al. 2022).

“Music is the arithmetic of sound as

Optics is the geometry of light”

Claude Debussy

3 Computational simulations as a predictor of the performance of a new refractive IOL design: Isopure IOL

Computational simulations were conducted to understand and predict the behavior of a new Intraocular lens in the market, Isopure IOL by PhysIOL (Liege, Belgium), a premium monofocal IOL design to improve intermediate vision to provide an extended depth of focus (EDOF). A series of different studies were designed in order get a better understanding of the optical coupling of IOL and different corneas (in terms of corneal powers and spherical aberrations), the impact of tilt and lens decentration on IOL performance and to demonstrate the IOL consistency across different IOL base powers.

The studies were performed as part of a research collaborative agreement with PhysIOL/BVI (Liège, Belgium/Waltham, MA, USA), and the IOL design was obtained under an NDA-protected agreement between PhysIOL and CSIC.

Preliminary results were presented in IONS Barcelona 2019 as an oral contribution by C. Lago under the title **"Optical design: Extended depth of focus intraocular lens and corneal shape influence"**, who was awarded with IONS travel grant, and at ESCRS 2019 as an e-poster presented by S. Marcos and entitled **"Pseudophakic IOLs: Enlarged-Depth-of-Focus". In addition, part of this study was presented at two invited presentations by C. Lago: FacoElche 2021 "Principios ópticos Isopure 1,2,3", and FacOptom 2021 "Extendiendo el foco, Isopure 1,2,3" "**. Also, a manuscript entitled "**Computational simulations as a predictor of the performance of a new refractive IOL design: Isopure IOL"** is in preparation**.**

The contribution of the author of this thesis was, with the help of co-authors, the design of model eye used in the simulations, the development of the methodology to extract different metrics to analyze the Isopure IOL optical quality and to analyze the results.

3.1 Introduction

The category of extended depth of focus (EDOF) applied to an intraocular lens (IOL) is a recent classification described in the ANSI Z80.35-2018 standard. EDOF IOLs aim at extending the depth of focus (DOF) of the eye implanted with the IOL, to preserve excellent optical quality at far vision (i.e. comparable to a monofocal IOL) while providing similarly good intermediate vision. Also, the refractive profile of these IOLs minimizes the photic effects that have been described with diffractive multifocal IOLs. According to the ANSI standard, the optical performance characterization for an IOL to qualify as EDOF must be measured and compared to the optical performance of a monofocal IOL that has the same dioptric power for far vision and the optical performance parameters evaluated with: (a) the modulation transfer function (MTF) over an optical defocus range that includes the clinical function of IOL; (b) the depth of focus range; (c) the MTF characterization at far (0D) with decentration and tilt; (d) Unwanted optical / visual effects compared to monofocal and multifocal IOL; (e) expected visual acuity at specified defocus values. The *Imaging quality of* EDOF IOLs by measuring its MTF in a model eye (ISO 11979-2, Annex C) for 3.0-mm-diameter aperture and the manufacturer shall have the option of setting the minimum MTF specification based on either the area under the curve between two spatial frequencies or the MTF value found at 50 cycles/mm (15 cpd) or greater.

Typically, IOLs are designed and tested on generic computational and physical eye models, where the cornea represents the corneal average power and spherical aberration. In most cases, the IOL is simulated or placed in the optical axis. Extrapolating the performance of IOLs, particularly EDOF IOLs, to eyes with different amounts of corneal spherical aberration, or in the presence of IOL tilt and decentration is not straightforward, in part because many of these lenses are based on the induction of spherical aberration. In the current chapter, we study with the aid of computational simulations the optical performance of the Isopure IOL when combined with corneas of different power and spherical aberration and in presence of different values of tilt and decentration.

Previous work in our lab has resorted to customized eye models, where anatomical information of corneal elevation data, measured IOL tilt and decentration and eye rotation, axial distances, etc… is incorporated in the eye models. Corneal topographies were obtained either from videokeratoscopy (Rosales et al. 2007, 2008) or OCT (Sun et al. 2014). IOL tilt and decentrations were obtained from Purkinje imaging (Rosales et al. 2010), Scheimpflug imaging (de Castro et al. 2007) or OCT (Sun et al. 2014). Wave aberrations from ray tracing on these eye models matched experimental wavefront measurements from aberrometry, and allowed deeper understanding on the individual contributions of geometrical/anatomical feature to optical degradation.

Unlike standard model eyes that used fixed amounts of SA and are rotational symmetry, custom model eyes use experimental anatomical data to capture the individual's complexity and variability. Testing the Isopure IOL in realistic pseudophakic eye models will anticipate optical performance of the new IOL in different eyes and assess the relative impact of the different factors contributing to image quality. The general purpose of the current chapter is the evaluation of the performance of the Isopure IOL computationally in realistic eyes.

The calculations of the through focus performance with the Isopure IOL entailed the design of a model eye in which the performance (optical quality and DOF) was studied for: (1) different corneal powers, (2) different corneal spherical aberrations, (3) realistic values of IOL tilt and decentration, and (4) different IOL powers ranging from 10 to 35 D. Optical simulations were also conducted to generate the wavefront map to represent the Isopure IOL in a Spatial Light Modulator (SLM) (Vinas et al. 2017), and following proprietary protocols at 2EyeVision, to generate the specific temporal coefficients that represent the Isopure IOL by temporal multiplexing using an optotunable lens (SimVis Technology, Dorronsoro et al. 2016). Part of the results generated in this study will be used in the on-bench evaluation of the Isopure IOL and on patients below in chapters 4 and 5.

3.2 Methods

3.2.1 The Isopure and Micropure intraocular lenses

Isopure IOL is a bi-aspheric refractive optics lens, with a specific surface design to provide a good optical quality at far vision, and an intermediate visual improvement with respect to monofocal IOLs without inducing photic effects. This lens works under the Isofocal technology^{TM}, patented by VioBio Lab (CSIC) and developed by Physiol-BVI. Anterior and posterior surfaces are aspheres with aspheric coefficients optimized up to the 10th order in each surface, represented in figure 3.1 (Fernández et al. 2013, Marcos 2019). The IOL had been designed using a multiconfiguration approach, optimizing a retinal image quality metric (spread of spots in the retinal spot diagram) for both far and intermediate distances, while keeping performance relatively independent of the pupil size (Fernández et al. 2013). The optimization was individually performed for each IOL power, on computer eye models with variable axial lengths. IOL material is a G-free (glistening-free), hydrophobic acrylic material patented by Physiol-BVI. According to the manufacturer, the IOL has a diameter of 11 mm, UV and blue light filter, its refractive index is 1.53 and its Abbe number 42.

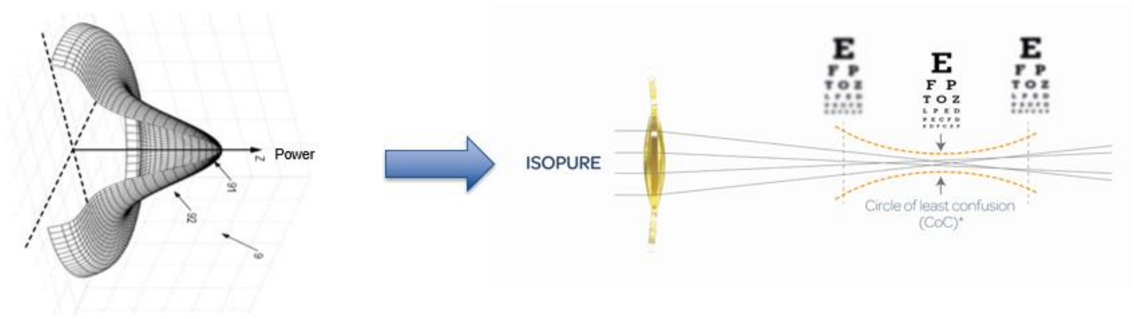

Fig. 3.1: Left, optical design of Isopure IOL based on conics of high order in both surfaces. Right, ray tracing of elongation of focus; central rays focus on a single point but peripheral rays convergence around this central focus (Courtesy of Christophe Pagnoulle).

Micropure IOL is a biconvex aspheric monofocal IOL manufactured by Physiol-BVI. It has the same material; hydrophobic acrylic material (G-free), index of refraction 1.53 and Abbe number 42, as Isopure IOL and its diameter is 11 mm. Hence, the difference with the Isopure IOL is only the optical design of its surfaces. The optical performance with both IOLs was compared in the situations described below.

3.2.2 Eye model

Pseudophakic computer model eyes were designed with the ray tracing optical design program OpticStudio (Zemax, Kirkland, WA), as explained in chapter 2 (section 1). In each eye model the axial length was adjusted so that the retinal spot size was minimum (maximum concentrations of rays). The IOL power used for the computational simulations was 21 D (unless otherwise specified, section 3.3.4).

The starting point of our eye model was detailed in Chapter 2 (section 1). Basically, a standard model of the cornea of the human eye with 43 D and 0.28 µm of SA (for a 6-mm pupil diameter) was used. However, in the current chapter, we used different parameters and conditions:

Corneal power

IOL studies usually determine the optical quality of an eye model as a function of the entrance pupil. However, as the corneal radius is more convex, the optical power of the anterior surface of the cornea increases and refracted rays are more convergent illuminating less area of the IOL, which could influence the IOL performance. Three model corneas with three different corneal powers, 39, 43 and 47 D, were constructed to assess the performance of Isopure IOL. The power values were selected based on literature (Marín. 2006). As in previous studies by the group (Rosales et al. 2006, Rosales et al. 2007) we kept the posterior radius of curvature constant (6.5 mm) and optimized the anterior radius of curvature to find the desired power. The radius of curvature of the anterior surface of the cornea found remained within physiological values, i.e., between 7 and 8.6 mm (Dubbelman et al. 2002), and the anterior corneal asphericity was optimized in each model to keep the corneal spherical aberration equal to 0.28 µm for a 6.0 mm entrance pupil diameter (Wang et al. 2003, Beiko et al. 2006). The radii of curvature and conic constants found are shown in Table 1.

Corneal power	39D	43D	47D
Anterior radius	8.3476-mm	7.6681-mm	7.0912-mm
Conic	0.0763	-0.0667	-0.1688

Table 1: *Optical design parameters on anterior corneal surface for the three different corneal powers of 39, 43, and 47 D.*

Spherical aberration and pupil size

It is well known that the pupil diameter and the spherical aberration influence the depth of focus (DOF) value (Metcalf 1965, Campbell 1957, Charman et al. 1977, Marcos et al. 1999, Rocha et al. 2009, Benard et al 2010, Yi et al. 2011, Xu et al. 2015). We studied the influence of spherical aberration and pupil size using the 43 D cornea model and a nominal corneal spherical aberration of 0.28 µm for a 6.0-mm pupil diameter (Wang et al. 2003, Beiko et al. 2006) which would correspond to 0.08 µm for a 4.5-mm pupil diameter using Zernike polynomial scaling formulas (Schwiegerling 2002). To evaluate the influence of SA on the IOL performance, 10 different values of spherical aberration were added to the cornea model ranging from -0.50 µm to +0.50 µm in a 0.1 µm step for a 4.5-mm pupil diameter, and the corneal SA was evaluated at two pupil diameters (3.0 and 4.5-mm). The range of values was selected to exceed the range of expected corneal spherical aberrations. For example, the range of spherical aberrations found in normals was from 0.28 µm (Wang et al. 2003, Beiko et al. 2006) and the range of induced with LASIK surgery (Marcos et al. 2001, Llorente et al. 2004), when converted to 4.5 mm pupil, is from 0.14 to -0.18 µm.

IOL Tilt and decentration in comparison with Micropure IOL

IOL tilt and decentration impact, to some extent, the optical quality in the pseudophakic eye, Although the surgical technique is in constant evolution IOL centration, tilt and decentration still occurs as reported in literature (Rosales et al. 2006, de Castro et al. 2007, Rosales et al. 2007, Rosales et al. 2010, Ale et al. 2011, Wang et al. 2013, Perez-Merino et al. 2018). While tilt and decentration appear to be primarily driven by the pre-operative crystalline lens centration, some designs appear to be more susceptible to tilt and decentration than others (Marcos et al 2014).

The tilt of an IOL was simulated in the pseudophakic model eye with either the Isopure IOL (21 D) or the Micropure IOL (21 D) with cornea model of 43 D corneal power and 0.28 µm of SA at 6.0-mm pupil diameter. Based on literature data (de Castro et al. 2007), the average tilt found after cataract surgery is about 2.5 degrees. We evaluated the optics when the IOL was centered and at 2.5- and 5-degrees tilt, corresponding to the average and twice the average value, as shown in figure 3.2 (A). The mean decentration found was 0.5 mm and we evaluated 0.5 and 1.0 mm, see figure 3.2 (B). The optics of the model was studied for two different pupil diameters, 3.0 and 4.5 mm, and the effect of tilt and decentration evaluated in terms of optical quality (MTF at 15 cpd) and depth of focus.

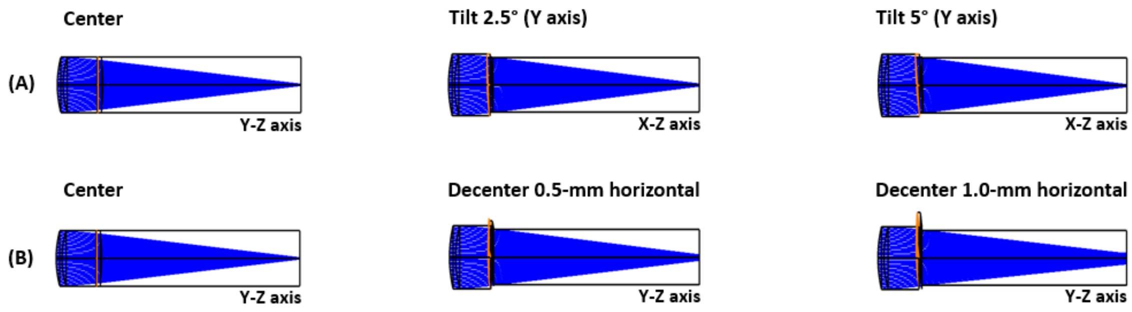

Fig. 3.2: *Three layouts from OpticSudio of the model eye inducing tilt (A) and decentration (B). On the left the centered IOL, in the middle the IOL with a mean value of tilt (2.5 degrees) or decentration (0.5-mm), and on the right the IOL with twice the mean value of tilt (5 degrees) and decentration (1.0-mm).*

IOL power

In clinical practice, the IOL power that fits each patient to compensate defocus, is calculated when planning the cataract surgery with formulas that use eye parameters such as the corneal radius of curvature, its axial length or, in the most advanced formulas, the thickness of the crystalline lens (Olsen 2007, Xia et al. 2020, Marcos et al. 2021). For this reason, all the IOLs designed by manufacturers include a catalog with a wide range of IOL powers and the same optical performance. The Isopure IOL designed by PhysIOL is available with optical powers ranging from 10 to 35 D. In this study, we evaluated the optical performance of the Isopure IOL for four different powers: 10, 15, 21 and 35 D, when they were combined with different corneal spherical aberration (0, 0.14 and 0.28 μm).

3.2.3 Metrics

We used the optical metrics mentioned in chapter 2, to evaluate the optical performance of Isopure IOL. The wavefront map of each model eye was exported from OpticStudio into MATLAB (MathWorks, Natik, MA). Custom-built scripts were used to calculate the through focus (TF) Modulation Transfer Function (MTF) at two spatial frequencies: 30 and 15 cpd. These specific frequencies were selected because they are the spatial frequencies used to evaluate IOLs following the ISO standard (ISO 11979-2, also in ANSI Z80.35-2018). The TF Visual Strehl (VS) was also calculated to evaluate the optical performance. VS quantifies the volume under the MTF at all frequencies weighted by the human contrast sensitivity function (CSF) and has been shown to correlate well with visual acuity in different studies (Marsack et al. 2004, Iskander 2006).

The TF MTF (30 and 15 cpd) and VS were calculated from -2 to 5 D (in 0.1 D steps) to evaluate the IOL optical performance at different distances. DOF was estimated from the TF VS curve by calculating the defocus range in which the VS metric was above 0.12 (Yi et al. 2011). As said before, this value was selected because it was found to be a limit for a correct visual function in subjects and correlates with 0.2 LogMAR in Visual Acuity (Cheng et al. 2004, Iskander 2006).

3.3 Results

3.3.1 Isopure IOL performance across corneal powers

Figure 3.3 shows the phase maps of the model eyes implanted with the 21 D Isopure IOL for three different corneal powers (39, 43, and 47D) and two pupil diameters (3.0 and 4.5-mm). As expected, for the smaller pupil diameter, the phase map is a cropped version of the central phase map for 4.5 mm.

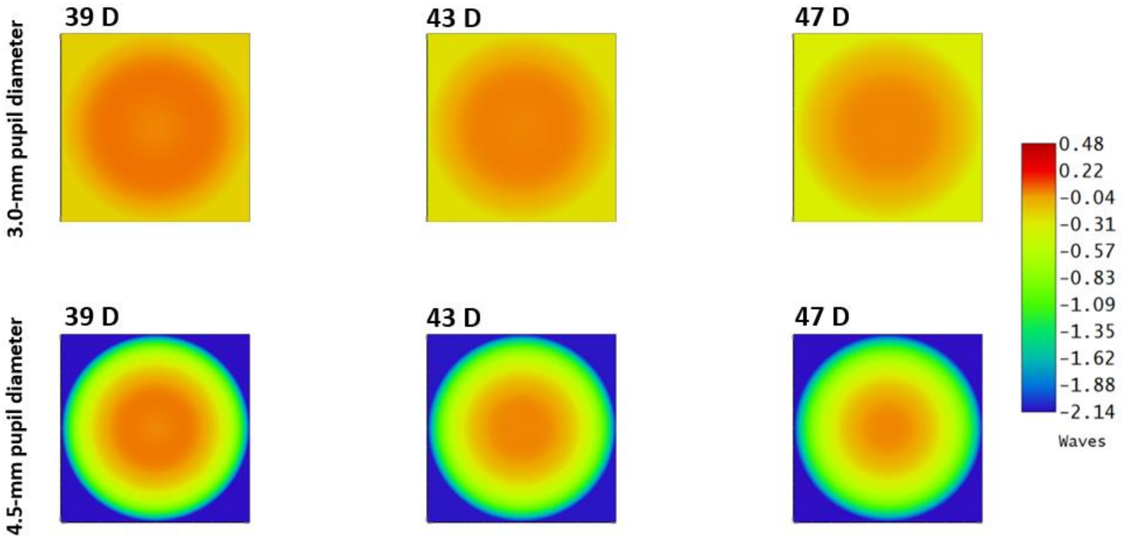

Fig 3.3: *Phase maps extracted directly from OpticStudio with different corneal power of 39 D (left), 43D (middle) and 47 D (right), and two pupil diameters of 3.0-mm (upper row) and 4.5-mm (lower row). All the wavefront maps are in the same scale and expressed in waves.*

Figure 3.4 shows the TF MTFs (30 and 15 cpd) and the TFVS in model eyes implanted with the Isopure IOL (21 D), for the three different corneal powers (39, 43 and 47 D), and the two pupil diameters (3.0 and 4.5-mm).

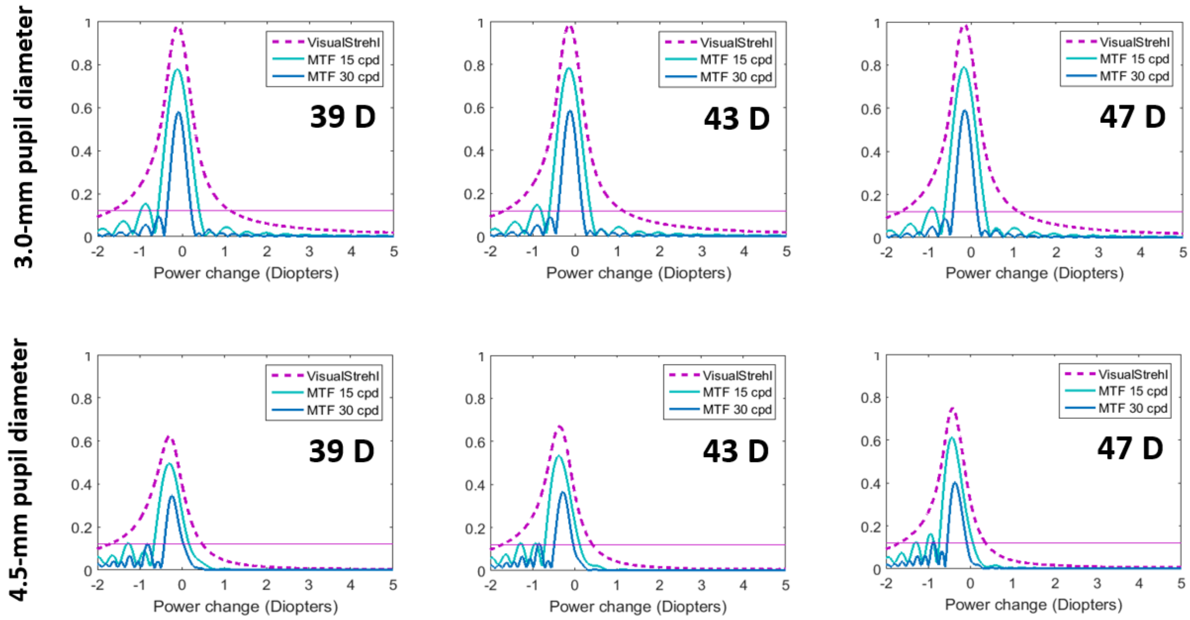

Fig. 3.4: *Through focus curves of the MTFs at 30 cpd (dark blue) and 15 cpd (light blue) and the VS (dotted pink), with increasing corneal power from left to right (39, 43 and 47 D) and two pupil diameters, 3.0-mm (upper row) and 4.5-mm (lower row). The pink horizontal line marks the value of a VS = 0.12, used to calculate the IOL DOF.*

Figure 3.5 shows the maximum MTFs at 30 cpd (A), at 15 cpd (B), maximum VS (C) at far and DOF in diopters (D) for the different corneal powers and pupil diameters studied. For 3.0-mm pupil diameter, all the metrics evaluated (maximum values of MTF and VS, and DOF) are higher than for 4.5-mm and remain relatively constant with corneal power, whereas for 4.5-mm pupil diameter, the maximum values of MTFs at 30 and 15 cpd and VS slightly increased with corneal power (from 0.34, 0.49 and 0.62 (39D) to 0.40, 0.61 and 0.75 (47D) for MTF at 30cpd, MTF at 15 cpd and VS respectively) and the DOF decreases with increasing corneal powers from 2.23 D (39D) to 2.02 D(47D).

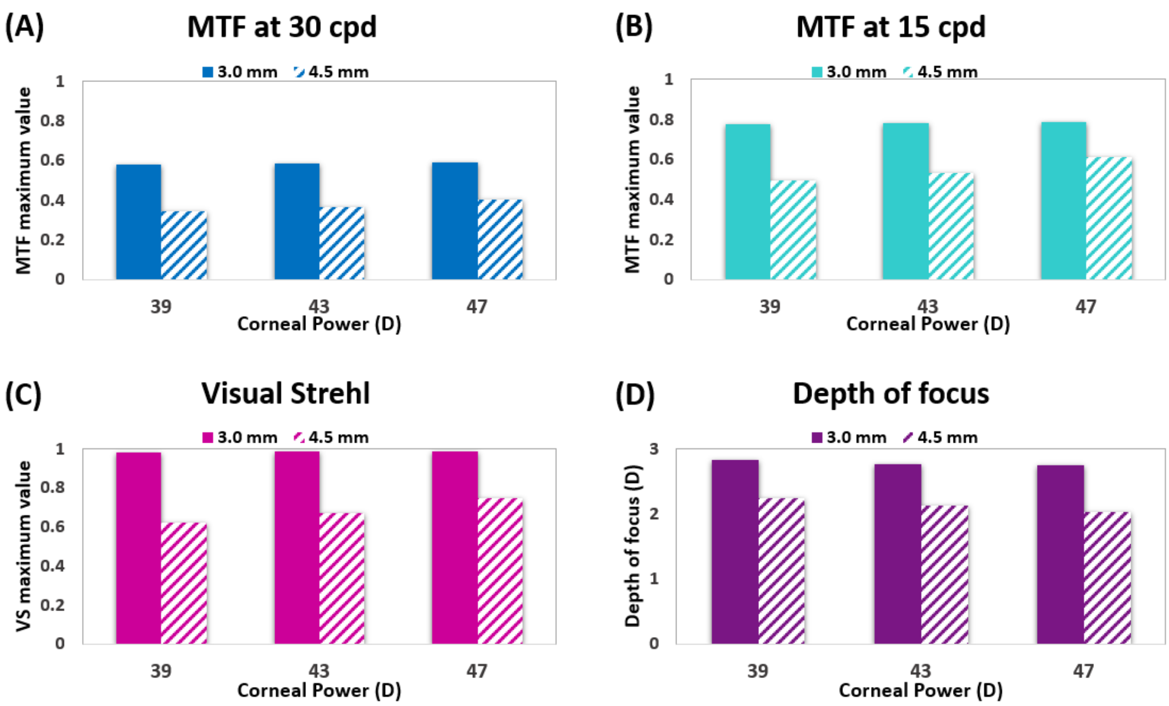

Fig. 3.5: *Maximum MTF at 30 cpd (A), at 15 cpd (B), maximum VS at far (C) and DOF (D). The solid bar represents the results for 3.0-mm pupil diameter and the streaky bar for 4.5-mm pupil diameter.*

3.3.2 Corneal spherical aberration and pupil diameter

In total, eleven different model corneas were used, with induced corneal spherical aberration ranging from -0.5 to 0.5 µm in 0.1 µm step (added to the mean cornea model and calculated for a 4.5-mm diameter) and corresponding to asphericities ranging from -2.81 to 1.91. Figure 3.6 shows the TFVS curves for the eleven SA conditions (the "0" value stands for the mean cornea with 0.28 µm of SA at 6.0-mm pupil diameter, 0.08 µm at 4.5-mm) and the two pupil diameters of 3.0 and 4.5mm. Overall, the induction of positive spherical aberration produced a shift of the highest VS peak toward negative defocus, and negative spherical aberration shifts the peak toward positive defocus.

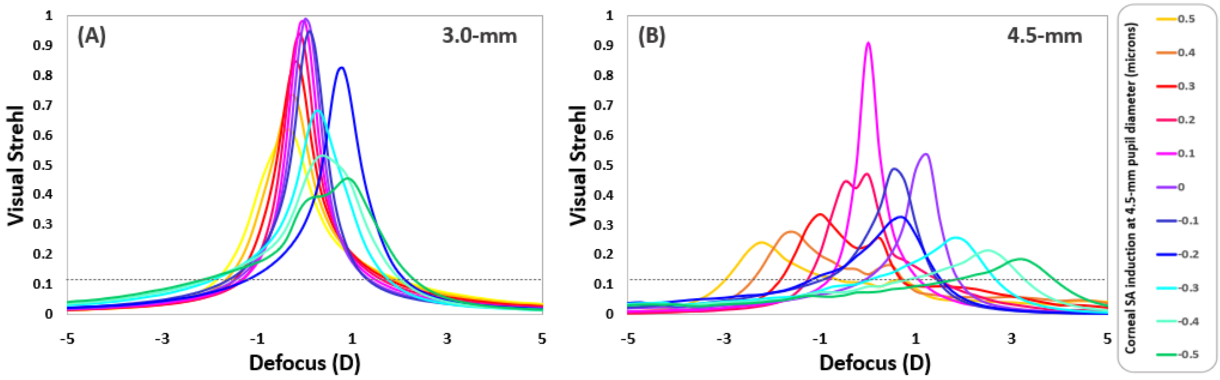

Fig. 3.6: *TFVS curves at 3.0-mm pupil diameter (A) and 4.5-mm (B) for the 11 induced SA ranging from -0.5 µm to 0.5 µm in 0.1 µm step (values of SA induction were calculated for 4.5-mm; 0µm SA induction correspond to the mean model cornea). Grey dotted line shows VS=0.12 to calculate the DOF.*

To evaluate the performance of the IOL with the different amounts of induced SA, the maximum value of VS and DOF were calculated in all conditions, as shown in figure 3.7. The figure also shows the range of values found in patients after LASIK surgery to correct preoperative spherical error between -4.5D (medium myopic eye) and 4.5D (medium hyperopic eye), 0.14 to -0.18 µm (Marcos et al. 2001, Llorente et al. 2004), plotted as red vertical lines.

VS decreased with SA induction. As expected, this effect was higher at 4.5-mm pupil diameter because the amount of SA is larger. VS ranged from 0.46 to 0.99 and 0.19 to 0.91 for 3.0 and 4.5-mm respectively. DOF increased with the induction of SA, ranging from 2.7 to 4.2 D and from 1.8 to 3.7 D for 3.0 and 4.5-mm pupil diameters respectively. For 4.5mm pupil diameter and a +0.1 µm induced SA, the maximum VS was higher than for 0 SA induction, probably because the induced SA compensated the negative IOL SA.

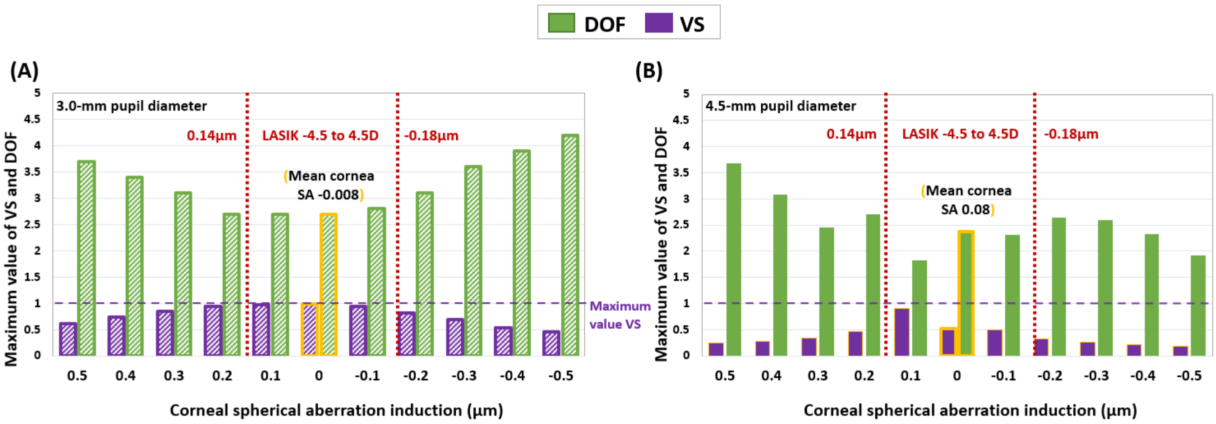

Fig. 3.7: *Representation of the maximum value of VS (purple bars) and DOF (green bars) for different induced corneal SA and two pupil diameters, (A) 3.0-mm (dashed bars) and (B) 4.5-mm (solid bars). Yellow lines show the cornea with no SA induction (represent a mean cornea of 0.28 µm calculated at 6.0-mm pupil diameter, corresponding to 0.08 µm at 4.5-mm and -0.008 µm at 3.0-mm). The SA induction was made in a range of 1.0 µm (from -0.5 to 0.5 µm, in 0.1µm step). Dotted horizontal purple line shows the maximum value of VS (1.0). Vertical red dotted lines show the values of SA in post LASIK corneas with preoperative spherical error from -4.5D to +4.5 D (from medium myopic to medium hyperopic refractive error).*

3.3.3 IOL tilt and decentration - Isopure and Micropure IOLs

Figure 3.8 shows the phase maps extracted from OpticStudio (Zemax) with the Isopure (upper row) and Micropure (lower row) IOLs, centered (on axis) and with different levels of decentration (0.5 and 1.0-mm in horizontal axis) and tilt (2.5 and 5 degrees in y axis). All analysis as a function of tilt were performed for 3 and 4.5-mm pupil diameters. For the IOL decentration, 3 and 3.5 instead of 4.5 mm diameters were used to avoid tracing rays outside of the optical zone of Isopure IOL, 4.6-mm.

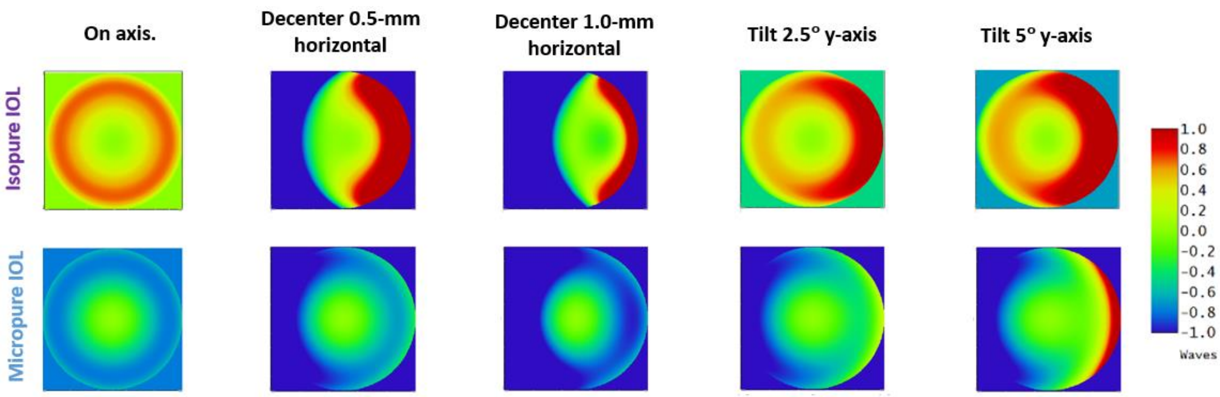

Fig. 3.8: *Representation of the phase maps extracted directly from OpticStudio (Zemax) of pseudophakic model eye with Isopure and Micropure IOLs implanted, IOL on axis, with a decentration of 0.5 and 1.0-mm in horizontal axis, and with a tilt of 2.5 and 5 degrees in y axis. All wavefront maps are in same scale, expressed in waves, for 4.5-mm for centered and tilted IOL and 3.5-mm for IOL decentration.*

Figure 3.9 shows the variation of the DOF and the maximum value of the MTF (15 cpd) when inducing a 2.5- and 5-degree tilt in the Isopure and Micropure IOL position, for two pupil diameters (3.0-mm and 4.5-mm). The Isopure IOL showed to be less sensitive to tilt than the monofocal Micropure IOL and the effect of tilt was mainly visible for 4.5-mm pupil diameter. The DOF of the Isopure was mainly maintained at 2.3D with maximum differences below 0.1 D, whereas for the Micropure, the DOF changed between 1.7 and 2.1 D at the expense of a decrease in the maximum optical quality (as seen in the MTF decrease in Fig 3.9 right).

At 3.0-mm pupil diameter, the DOF difference between IOLs was below 0.05 D, and slightly increased from 2.8 to 2.95 D. In terms of optical quality, the MTF at 3.0-mm was similar for both IOLs (0.76 for Isopure IOL and 0.79 for Micropure) and decreased when tilted about the same amount (0.07 and 0.06 for Isopure and Micropure IOL respectively). As before, we found that Isopure IOL was less affected by tilt (with tilt MTF decreased 0.05, from 0.43 to 0.38, with Isopure and 0.24, from 0.81 to 0.57, with Micropure IOL).

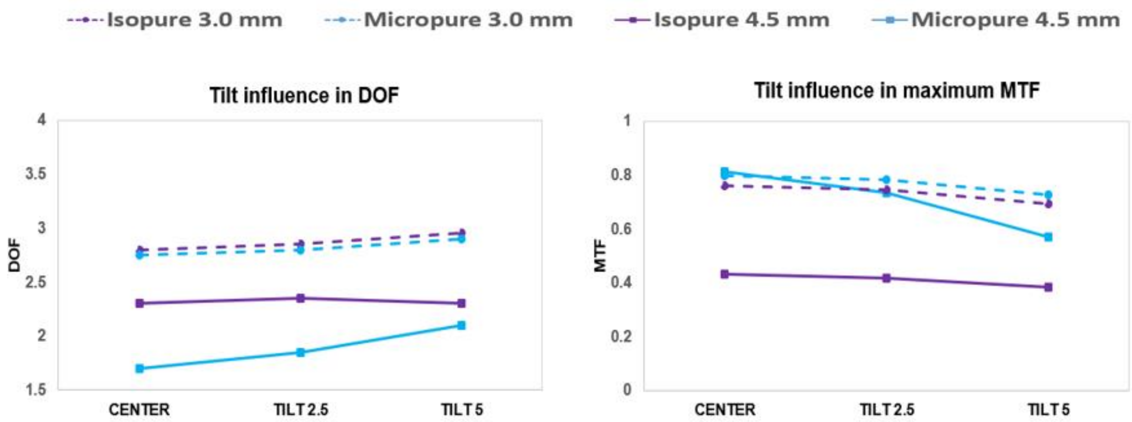

***Fig. 3.9**: Effect of tilt on the Isopure (purple) and the Micropure (blue) IOLs in terms of DOF (left) and maximum value of MTF 15cpd (right), for two pupil diameters, 3.0mm (dashed line) and 4.5-mm (continuous line). Two values of tilts were evaluated: 2.5- and 5-degrees in y-axis.*

Figure 3.10 shows the effect of IOL decentration. Unlike the results found with tilt, decentration affects more the performance of Isopure IOL when compared with the monofocal Micropure lens. DOF increased from 2.75 and 2.5 D (on axis) to 3.45 and 3.05 D (for 0.5mm decentration) to 3.7 and 2.9 (1.0 mm decentration) on average for 3.0 and 3.5 mm respectively. The maximum MTF value decreased from 0.79 and 0.76 on axis to 0.29 and 0.23 for 1.0 mm decentration for 3.0 and 3.5-mm pupil respectively.

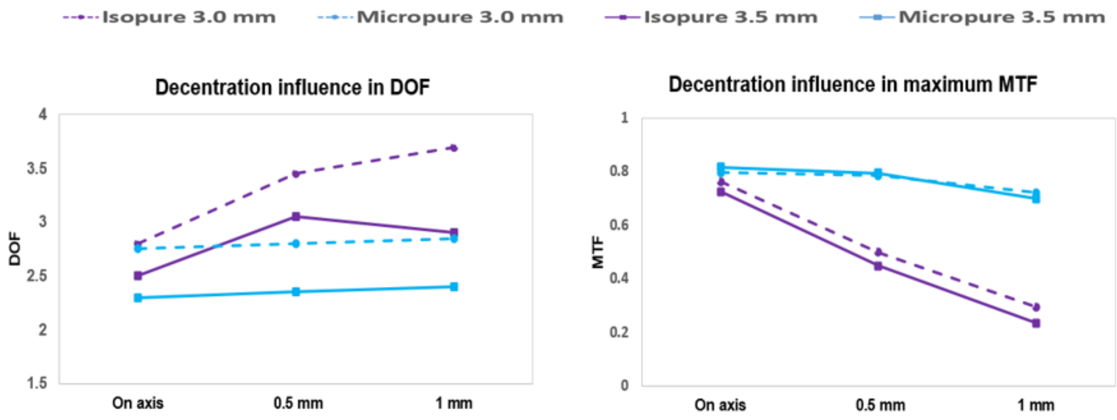

Fig. 3.10: *Effect of decentration on the Isopure (purple) and the Micropure (blue) IOLs in terms of DOF (left) and maximum value of MTF 15cpd (right), for two pupil diameters, 3.0mm (dashed line) and 3.5-mm (continuous line).Two values of decentration were evaluated: 0.5 and 1.0-mm horizontally.*

3.3.4 Performance of different IOL powers

The performance of the Isopure IOL was evaluated in terms of the DOF and the maximum TFMTF at 15 cpd, for four different IOL powers (10, 15, 21, and 35 D), for three different model corneas with corneal SA of 0 µm, 0.14 µm and 0.28 µm (calculated for a 6.0-mm pupil diameter) and for two pupil diameters (3.0-mm and 4.5-mm). Figure 3.11 summarizes the results. In general, for 3.0-mm pupil diameter, there were no changes when different IOL powers or corneal SA were simulated. In contrast, for 4.5-mm, the DOF decreased, on average 0.4 D (from 2.4 D to 2.0 D) with increasing corneal SA; the largest decrease was found for the 10D (0.5 D) and 15 D (0.65 D) IOL power. The maximum MTF increased by 0.25 on average (from 0.34 to 0.60) whith corneas with increasing SA, with the largest change found for the 15 D IOL (0.39). This results agreed with the ones presented in section 3.3.2 in figure 3.7, because DOF increased with induced negative SA and TFMTF peak value was maximum for the average cornea of 0.28 µm SA.

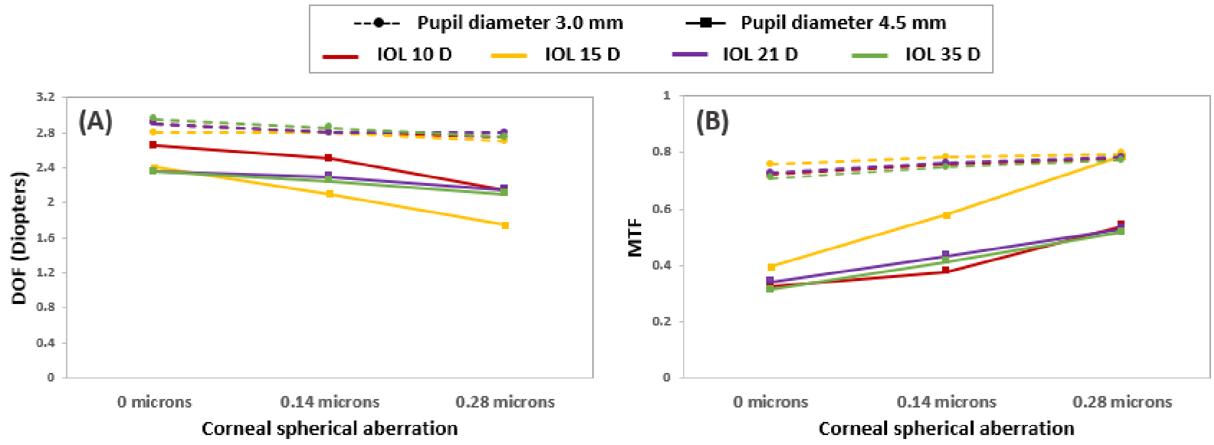

Fig. 3.11: *DOF (A) and maximum MTF value at 15 cpd (B) for the Isopure IOL of four different powers: 10 D (red), 15 D (yellow), 21 D (purple) and 35 D (green), and for three different corneal spherical aberration of 0, 0.14 and 0.28 µm (represented on the x-axis). Two pupil diameters were analyzed: 3.0-mm (dashed line) and 4.5-mm (continuous line).*

3.4 Discussion

The optical performance of a new refractive IOL, Isopure IOL from Physiol-BVI, was evaluated using pseudophakic eye models designed with OpticsStudio in Zemax, in a wide range of conditions, using different model corneas, with different corneal powers and corneal spherical aberration. The effect of tilt and decentration was also estimated using realistic post-operative values, and the optical performance through different IOL powers was evaluated for different pupil diameters and amounts of spherical aberration.

The studied corneal powers ranged from 39 to 47 D to analyze the whole range of corneal power found in the literature (Marín 2006) and have found to have a low influence in the IOL behavior. In terms of optical quality, at 4.5-mm pupil diameter, the trend in all metrics is to increase the optical quality when the corneal power increased, with an average increase of 0.10 in MTF when the cornea power changed from 39 to 47 D, which could be explained by the smaller axial length of the models with higher cornea power. In terms of DOF, higher values were found with lower corneal power (39 D). This could be expected because DOF increases with the effective focal length of the system. However, the differences were small and at 4.5-mm, DOF difference between the models with 39 and 47 D corneas was only 0.21 D. In all cases, DOF was higher than 2.0 D.

We illustrated in the graphs the range of spherical aberration values that could be expected in subjects that had undergone LASIK surgery two decades ago. There is a tendency to use EDOF IOLs for those patients with abnormal corneal SA due to the IOL negative spherical aberration which could compensate the excess of ocular spherical aberration produced by LASIK surgery. In a range of spherical aberrations expected for subjects that had undergone LASIK surgery to correct from -4.5 D to +4.5 D of spherical error, +0.14 to -0.18 µm for a 4.5-

mm pupil diameter (Llorente et al. 2004), we found that the IOL maintains a good performance with a DOF ranging from 1.82 to 2.8 D and a VS ranging from 0.33 to 0.99 across the conditions studied.

As said before, in ISO standards to evaluate the performance of IOLs two model corneas are defined: ISO 1 in which the cornea spherical aberration is zero, and ISO 2 with a corneal spherical aberration of 0.28 µm. Those value for ISO2 is equivalent to the one of the average corneas that we designed and the value for ISO1 cornea could be reproduced studying the situation when -0.1 µm of SA at 4.5 mm, which would compensate the corneal aberration, was induced. In both situations the IOL holds a good balance of DOF and optical quality: DOF values are 2.7/2.37 D for ISO 2 and 2.8/2.32 for ISO 1 (3.0 and 4.5-mm pupil diameter respectively); and VS values are 0.99/0.52 for ISO 2 and 0.95/0.50 for ISO 1 (3.0 and 4.5-mm respectively).

We evaluated computationally the optical performance of the Isopure IOL for the average literature value of 2.5 degrees of tilt, 0.5-mm of decentration, and twice the amounts and found that the Isopure is more stable to tilt than the monofocal IOL. However, decentration strongly affected both the optical quality and DOF of the Isopure IOL. In a study of IOLs decentration and tilt by computer simulations (Eppig et al. 2009) concluded that image quality sensitivity depended on the IOL design. The findings of Eppig et al. and the ones reported on a study by Perez-Gracia et al. 2020, where on bench monofocal IOLs with different amount of spherical aberration were analyzed inducing different amounts of tilt and decentration, are that decentration affect more the MTF value than tilt, and that misalignment affect more IOLs with higher values of SA, in agreement with our results since Isopure IOL SA is higher (more negative) than Micropure IOL and is less affected by tilt.

We did not find differences between the optical quality of eye models with different IOL powers or different amounts of SA for 3.0-mm pupil diameters. However, for 4.5-mm pupil size, DOF and optical quality (in terms of MTF at 15cpd) resulted in a decrease in DOF and increasing MTF value with induction of SA that was more pronounced in the low power IOLs. The change in DOF and MTF could be explained because of the compensation between the corneal and IOL spherical aberration.

Isopure IOL was studied at two pupil diameters, trying to simulate photopic conditions with the 3.0-mm pupil and mesopic with 4.5-mm. Pupil diameter is affected by light and by age (Guillon et al. 2016) and 4.5-mm is a reasonable maximum pupil size for the typical cataract surgery patients. An on-bench study performed by Physiol (personal communication), show an increase of DOF with the ISO 2 cornea, which agreeing with our findings.

Part of the computational studies has been performed experimentally to validate the computational predictions with the physical IOL provided by Physiol-BVI and the simulated Isopure IOL, in next chapters: 4 and 5.

3.5 Conclusion

The Isopure IOL was studied through computational simulations to evaluate the optical performance of the lens. Four complementary studies were performed to predict the behavior of this new IOL design: (1) corneal power influence; (2) spherical aberration induction to know its influence on IOL performance and the suitability implantation for post-LASIK subjects; (3) tilt and decentration impact of Isopure IOL in the pseudophakic eye; (4) evaluation of lens optical performance in a power range from 10 to 35 D. In these studies different eyes were models were built according with the optical parameters to study. As a conclusion of the computational evaluation of Isopure IOL:

- Isopure IOL holds a good balance between optical quality and DOF. For 4.5-mm pupil diameters, MTF was higher than 0.5 and DOF larger than 2.0 D.
- A change in corneal power has low influence in Isopure IOL behavior.
- An increase of MTF and a reduction of DOF was found for some values of corneal spherical aberration.
- Isopure IOL keeps a good performance with corneas with SA expected in post-LASIK subjects, showing that more than spherical aberration rules the IOL behavior. However, experimental and clinical studies should be done in this direction to confirm the suitability of this IOL for post-LASIK subjects.
- Isopure IOL performance is affected by decentration but is stable against tilt.
- A stable IOL behavior was found across a range of Isopure IOL powers studied.

In this chapter Isopure IOL was evaluated computationally to predict it behavior in different clinically relevant conditions. The next chapter will present the simulation of the IOL in an Adaptive Optics system and the feasibility to experimentally simulate Isopure IOL with SimVis technology.

4 Evaluating the simulated performance of a new refractive IOL: Isopure IOL

The Adaptive Optics system was used in this chapter as a tool to experimentally validate the feasibility to simulate the Isopure IOL with different visual simulator components: the spatial light modulator and the optotunable lens for simultaneous vision simulation (SimVis technology). Different measurements were performed to experimentally validate the simulation of the Isopure IOL on bench and in 10 young subjects.

Part of this study was presented in FacoElche 2021 as an invited presentation entitled **“Principios ópticos Isopure 1,2,3”** and in FacOptom 2021 as invited speaker in a round table entitled **“Extendiendo el foco, Isopure 1,2,3”** by C. Lago.

The contribution of the author of this thesis includes literature search, to set up the new cuvette channel, white light source and SimVis driver’s implementation on the Adaptive Optics system, to calibrate and align the AO system, to design the protocols, perform the measurements, analyze the data and write the article.

4.1 Introduction

The increase in IOL designs in the market is paralleled with the interest in testing the optical performance of the new designs. The simulation of the post-operative vision with visual simulators is a non-invasive technique, ideal to study the perception with new designs even before the manufacturing process. Most visual simulators are laboratory prototypes based on AO (Fernandez et al. 2009, Sawides et al. 2011, Vinas et al. 20217), and some are commercially available such as VAO (Hervella et al. 2020) by Voptica, based on SLM, and SimVis Gekko (Dorronsoro et al. 2016) by 2EyesVision, a simulator that is not based on Adaptive Optics but use the concept of temporal multiplexing at high speed to simulate multifocality (Akondi et al. 2017). Visual simulators allow subjects to experiment with vision before the physical correction is implanted or adapted, and to select the design which result in the best optical performance before adaptation or surgery (Vinas et al. 2019, Barcala et al. 2022).

Previous works of the group have shown the accuracy of the representation of diffractive and segmented lenses with a spatial light modulator or with temporal multiplexing using an optotunable lens with SimVis, the technology behind SimVis Gekko from 2EyesVision. In those works, the through-focus visual acuity (TFVA) in subjects with the simulated IOLs pre-operatively matched with the post-operatively TFVA with the corresponding implanted IOL (Vinas et al. 2017, Marcos et al. 2020). Comparisons were performed on the same phakic subjects with IOLs of zero-based power inserted in a cuvette (Vinas et al. 2019) and projected onto the subject's eye and the simulated IOL (with SimVis and with SLM). In a recent publication, we presented a new simulation channel where subjects could see through an IOL that was placed in a cuvette and projected on the eye with a modification of the Rassow lens-based system to eliminate the IOL base power taking into account the magnification of the entrance pupil with respect to the pupil (Benedí-García et al. 2021). A good correspondence was found between the on-bench evaluation and the subject's visual performance with 3 different physical IOLs in the cuvette (monofocal Podeye IOL, diffractive trifocal FineVision IOL and refractive extended depth of focus Isopure IOL, all by BVI-PhysIOL).

The study of Benedí-García et al. was the starting point of this experimental chapter, where the performance of Isopure IOL (21D IOL power) immersed in the cuvette was studied with the AO system. The measurements performed with the physical intraocular lens placed in the cuvette were considered as a reference to compare with the simulations performed with the SLM or the optotunable lens using SimVis technology.

Computational simulations were performed to calculate the IOL phase map to simulate the Isopure IOL on the SLM, and to calculate the temporal coefficients to simulate the IOL with optotunable lens. In this chapter, the temporal coefficients calculated to describe the IOL performance with the optotunable lens, and the procedure to correct the dynamic effects of the optotunable lens were experimentally validated with the high speed-focimeter described in chapter 2. On bench through focus (TF) measurements in an artificial eye and on subjects were obtained with (1) the IOL physically immersed in a cuvette, (2) the phase map of the Isopure IOL mapped onto a SLM, and (3) the temporal multiplexing IOL simulation applied to the optotunable lens. The effect of pupil diameter on the IOL performance was tested in all conditions, for two pupil diameters of 3.0 and 4.5-mm.

4.2 Methods

Adaptive Optics System

We used the custom developed AO Visual Simulator described in section 2.3. In brief, the following channels have been used: (1) Illumination channel with a Super Continuum Laser Source (SCLS) with selectable emission wavelength to illuminate with green light of 550 nm; (2) the AO-loop channel that comprises the Hartmann-Shack wavefront sensor and the deformable mirror (DM) to compensate for the aberrations of the optical system; (3) the SLM channel to simulate the IOL mapping its phase map; (4) the testing channel with either the physical IOL placed in the cuvette, or the optotunable lens (SimVis technology) simulating the IOL; (5) the Badal system to induce defocus to either compensate the defocus in subjects or study their through focus performance; (6) the psychophysical channel using the Digital Micromirror Device (DMD) to present a visual stimulus that was illuminated with the supercontinuum laser source through a diffuser filter; (7) the double-pass retinal imaging capture, to register the images of a circular object projected onto the retina and imaged back onto a CCD camera; and (8) the pupil monitoring channel to align the eye into the system.

Intraocular lens and cuvette

All measurements were performed with the Isopure IOL (PhysIOL-BVI, 21D) (Fernández et al. 2013, Marcos 2019), whose optical design has already been described in chapter 3. In essence its surfaces were described by high order conic coefficients with the objective to provide good far vision and enlarge the depth of focus to improve intermediate vision with respect to a monofocal IOL.

The cuvette had a metallic support where the IOL was mounted and immersed in distilled water. The Rassow lens was placed at an optical distance twice its focal length (120-mm) from the IOL plane and was designed to compensate a 20 D IOL power in a conjugated pupil p lane. In this study the Isopure IOL power was 21 D and the Badal optometer was combined with the Rassow system to compensate the IOL residual defocus of 1 D. The Isopure IOL was projected on the entrance pupil of an artificial eye (on bench measurements) and on the subject's eye pupil.

Fig 4.1: *Illustration of IOL mounted in the metallic support inside the cuvette.*

Spatial Light Modulator (SLM)

The SLM was placed in a conjugated pupil plane to project the IOL simulation in the entrance pupil plane of the subject or the model eye. For the Isopure IOL simulation in the SLM, the phase map representation of Isopure IOL profile were calculated at two pupil diameters, (3.0 and 4.5-mm) presented in figure 4.2. These phase maps were used for mapping into the SLM and to simulate the IOL.

SimVis channel

The temporal coefficients of Isopure IOL were calculated to simulate the lens with the optotunable lens at two pupil diameters (3.0-mm and 4.5-mm). The simulation mimics the Through Focus Visual Strehl ratio (TFVS) of the real IOL calculated from the IOL phase map. An optotunable lens (Optotune AQAA, reference number 1300) was first characterized in the high-speed focimeter (measuring its dynamic response), to compensate the dynamic effects of that particular optotunable lens. The IOL SimVis simulation with the compensation of the dynamic effects was experimentally validated with the high-speed focimeter described before (Akondi et al. 2017, Dorronsoro et al. 2019). Finally, the optotunable lens (AQAA 1300) was inserted in the testing SimVis channel of the AO system in a conjugated pupil plane to project the simulation in eye.

No IOL condition

In order to study the extension of focus with and without Isopure IOL design, the through focus curve was obtained without an intraocular lens. In the cuvette channels, flip mirrors were set up to bypass the cuvette when desired.

On bench measurements with an artificial eye

Through focus one pass (1P) and double pass (2P) measurements were performed with an artificial eye to evaluate the IOL optical performance with the different active elements (SLM and optotunable lens) in comparison with the IOL immersed in the cuvette that was used as a reference. For 1P measurements, the retinal image quality was studied obtaining images of E Snellen as stimulus, projected on the DMD, with the CCD camera of the eye model. A series of TF images ranging from -4.0 to +1.0 D, in steps of 0.25 D were collected changing the vergence with the Badal system. For 2P measurements the retinal images were collected in a retinal plane conjugated with the eye, using as illumination source a collimated beam to project a point onto the retina, and changing the vergence of the beam between -3.0 and +1.0 D. in steps of 0.25 D. All measurements were performed at 3.0-mm and 4.5-mm pupil diameter illuminating the stimulus with 555 nm light and with constant laser power and camera properties ensuring that none of the images were not saturated.

The data was analyzed as follows: for 1P on bench measurements, the optical quality was measured in terms of the correlation metric, defined as the cross correlation between the image obtained with the condition studied and the reference image. For 2P retinal images, the optical quality metric used was the Full Width at Half-Maximum (FWHM) of the retinal spot. To evaluate the optical behavior in comparison with the no IOL condition, optical degradation at far and the optical benefit at intermediate, defined as the ration between the optical quality with the lens and the one in the no IOL condition, was calculated. The Depth-of-Focus (DOF) was calculated for the normalized FWHM on bench as the range of diopters for which the metric was above 0.8 (Marcos et al. 1999). An ANOVA test was used to evaluate statistical differences across conditions.

Subjects and measurement protocol

The study was performed on ten 10 young subjects (9 females and 1 male, average age 29.8 ± 3.4 years, and average spherical error of -0.17 ± 1.10 D). Astigmatism was less than 0.75 D in all subjects. Measurements were obtained under cycloplegia (tropicamide 1%). All protocols met the tenets of the Declaration of Helsinki. Subjects consented after they had been informed on the nature of the study, protocols and implications of their participation.

Subjects viewed the psychophysical stimuli projected on the DMD, illuminated at 555 nm, through the selected active element which simulate the IOL: (1) real IOL immersed in the cuvette, (2) SLM with the IOL phase map, (3) the optotunable lens to simulate the IOL with SimVis technology or (4) no IOL condition. The aberrations of the system were corrected with the deformable mirror. The subject's eye pupil center was aligned with the optical axis of the system with an x-y-z stage and stabilized with a dental impression on a bite bar and monitored with the pupil camera. The subjects selected their best focus (repeated 3 times) by moving the mirrors of the Badal optometer with a numerical keyboard while looking at a Maltese cross (as stimulus). The search for the best focus was started inducing 2 D of myopic defocus over their spherical refraction using a step size of 0.05 D. The search for best focus was repeated before each TF VA measurements with the conditions of the measurement.

The Visual Acuity (VA) was measured using a tumbling E letter with an 8-Alternative Forced Choice (8AFC). Subjects indicated the orientation of the E letter (presented for 0.5 seconds) with a numerical keyboard. The orientation and size of E letter was calculated according to the subject's response with a QUEST (Quick Estimation by Sequential Testing) algorithm (Lu et al. 2013, Watson et al. 1983, Borgo et al. 2012, Brainard et al. 1997). In this study 32 trials and 20 reversals were used for each VA measurement. The result was calculated as the mean of the last 5 reversals and the variability as the standard deviation of those 5 values. The data for these studies (presented in chapter 4 and 5) were collected in three sessions that lasted 210 minutes each.

The accuracy of the simulations was assessed with the RMS difference between the through focus curves obtained with the model eye between different simulation devices. The DOF was calculated from the TF curves as the range in which the defocus (in the near region, i.e.

negative defocus) for which VA was 0.2 LogMAR or better (Yi et al. 2011). The Visual degradation at far and optical benefit at intermediate (Vedhakrishnan et al. 2022) were compared across simulators and to the IOL in comparison with no IOL condition. An ANOVA test was used to evaluate statistical differences across conditions.

4.3 Results

4.3.1 Isopure phase map

The Isopure (21 D) phase map is represented in Fig 4.2 for two pupil diameters (3.0 and 4.5-mm). These phase maps were mapped in the SLM for IOL simulation.

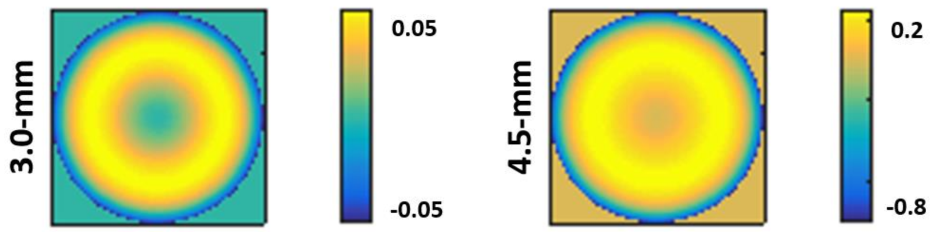

Fig. 4.2: *Phase maps representing of Isopure IOL profile for 21 D, at two pupil diameters (3.0 and 4.5-mm). Units of the phase map are waves (0.55 nm).*

4.3.2 Isopure IOL simulation with SimVis technology and validation with the high-speed focimeter

The temporal coefficients that best mimic the Isopure IOL visual performance, in terms of visual Strehl ratio, were calculated for two pupil diameters (3.0 and 4.5-mm) using the procedure described in chapter 2 where the TFVS of the IOL ("real lens TFVS") was assessed from the phase map of the IOL contribution. The SimVis simulation was first computationally validated (comparing the "real lens TFVS" and the "SimVis TFVS") with custom Matlab programs and experimentally validated using the high-speed focimeter ("experimental SimVis TFVS"). As shown in figure 4.3, the experimental SimVis TFVS (orange) matches the SimVis TFVS (red) and the real lens TFVS (blue), for the two pupil diameters.

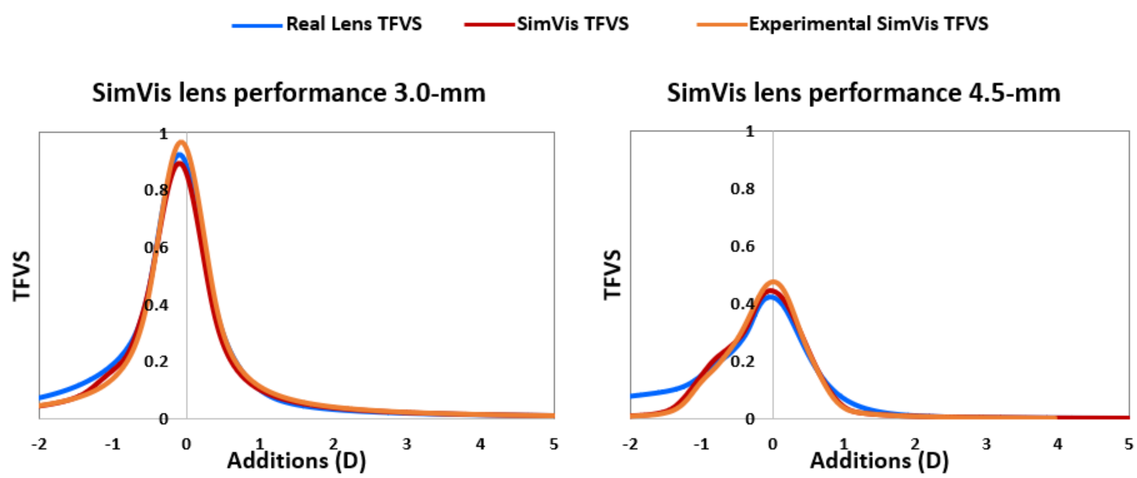

Fig 4.3: *TFVS for Isopure IOL 21 D at two pupil diameters, 3.0 and 4.5-mm. Blue represent the real lens TFVS; Red the SimVis TFVS of Isopure IOL that mimics the real lens, and orange is the experimental TFVS of Isopure IOL validated in the high-speed focimeter with the optotunable lens dynamic effects compensated.*

4.3.3 Experimental through focus retinal images (E-stimulus and double pass)

Through focus images (4 D range, every 0.25 D steps) were collected in the single pass (1P) double-pass (2P) configuration. Examples of the image series are shown in figure 4.4 for 3.0-mm (A) and 4.5-mm pupils (B); the no IOL condition and the three simulators: Cuvette, SLM and SimVis; are represented.

(A)-Through-Focus one pass (1P) and double pass (2P) images series Isopure IOL for 3.0-mm pupil diameter:

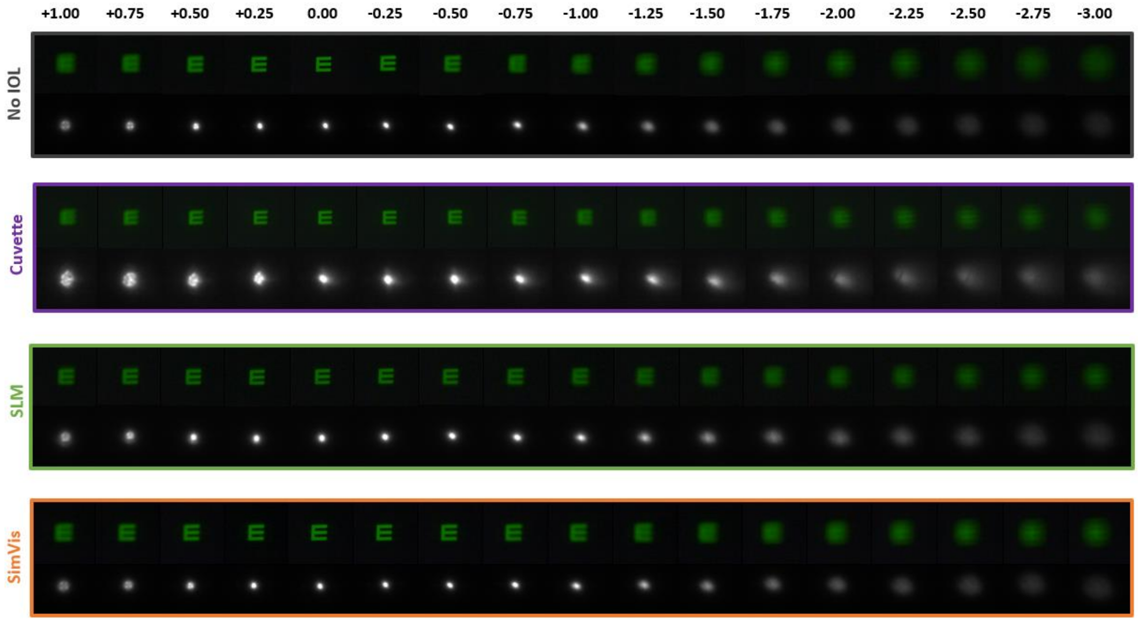

(B)-Through-Focus one pass (1P) and double pass (2P) images series Isopure IOL for 4.5-mm pupil diameter:

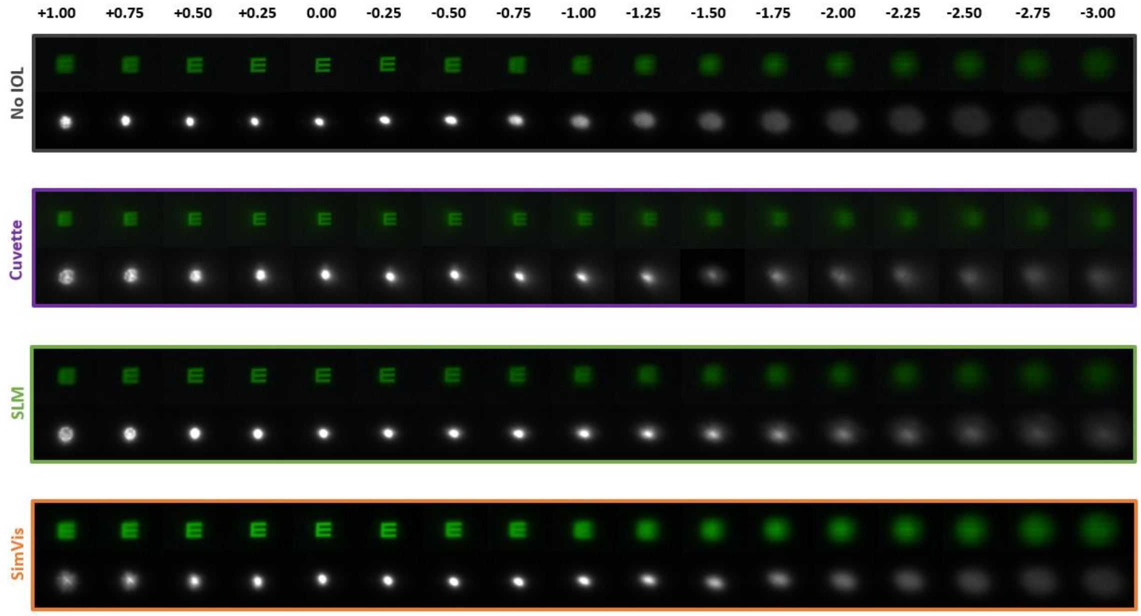

Fig. 4.4: *TF series of single-pass images of an E-letter stimulus (top images) and double-pass images of a spot (bottom images) in an artificial eye, through the no IOL condition (upper, black box) and Isopure IOL in the cuvette (purple), Isopure IOL simulated with the SLM (green) and in Isopure IOL simulated with the optotunable lens (SimVis channel) (orange). (A) for 3.0-mm pupils; (B) for 4.5-mm pupils. All data are for monochromatic green light 555 nm.*

These TF images are a sample of the optical bench measurements (E letter-stimulus and retinal imaging) taken in the AO system. The figure (A) represents measurements at 3.0-mm of Isopure IOL simulations using the cuvette, the SLM and the SimVis channel (purple, green and orange respectively), and no IOL condition (black). In the images, it is visible that the range in which image quality is enough to identify the E stimulus, i.e. the DOF, is larger for Isopure (around 1.50 D larger) than for the no lens condition (around 1.00D) for 3.0-mm pupil diameter. In the image (B) the results for 4.5-mm pupil diameter are shown. The DOF is visibly higher for 3.0-mm than for 4.5-mm pupil diameter where a slight reduction in DOF to around 1.5 and 0.75 D for Isopure and no IOL respectively can be observed.

Figure 4.5 shows the evaluation of the performance of the simulated Isopure IOL. IOL on cuvette (purple), SLM (green), and SimVis (orange) simulations were compared to the no IOL condition (grey) using the correlation metric (single pass configuration, left), the FWHM metric (double pass configuration, middle) and the RMS differences between simulators (right) for 3.0 and 4.5-mm pupil diameters. The three simulators (cuvette, SLM and SimVis) were in good agreement with an average RMS difference between simulators lower than

0.10 and a maximum RMS difference value for 1P images of 0.037. The metrics through focus curves show a similar tendency between simulators and the DOF of the simulated Isopure is higher than for the no IOL condition. As expected, at far the Isopure IOL simulations have slightly less optical quality in comparison with no IOL condition, as predicted by computer simulations in chapter 3.

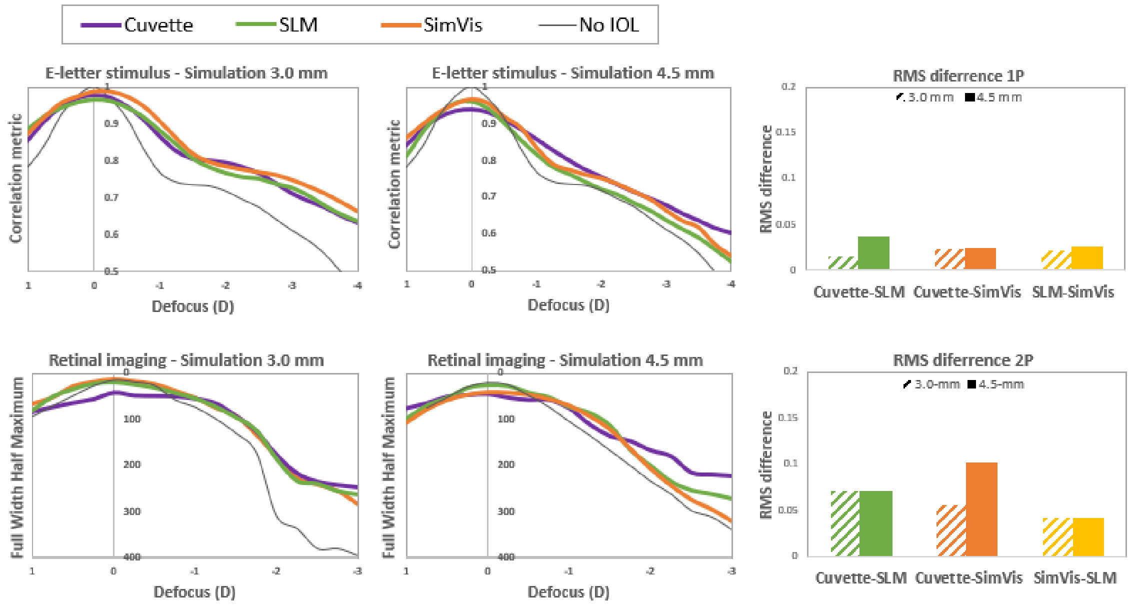

Fig. 4.5: *TF correlation metric for 1 pass E-letter stimulus (left) and FWHM for double-pass retinal imaging of a point (middle) for the different simulating platforms (Cuvette (purple line), SLM (green line) and SimVis (orange line)) in comparison with no lens condition (gray line). Right, RMS difference between simulators. All the results are presented in two pupil diameters for 3.0 (top) and 4.5 mm (bottom).*

The DOF was calculated from the TF 2P curves (fig 4.6) and, as said before, was defined as the range in negative diopters from the maximum value (which was placed at 0 D, corresponding far vision) to 0.8 (Marcos et al. 1999); with FWHM normalized values.

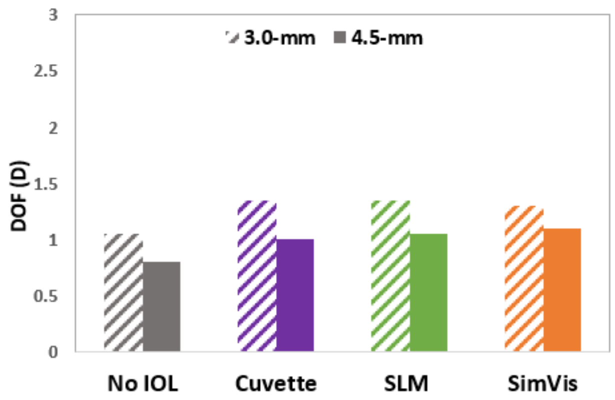

Fig. 4.6: *DOF value of retinal imaging TF, calculated as the range of diopters from peak in the curve located at 0D (far vision) to values in the negative part above or equal to 0.8. DOF was calculated for two different pupil sizes: 3.0-mm (dotted bars) and 4.5-mm (solid bars) and for the No lens condition (grey) and IOL simulations: Cuvette (purple), SimVis (orange) and SLM (green).*

Figure 4.6 shows the DOF calculated for the 2P image series for the four conditions (no IOL, Physical IOL in cuvette; IOL simulated with SLM and IOL simulated with SimVis) for the two pupil diameters. On average across simulators, the DOF was higher for 3.0-mm pupil diameter (1.33±0.03 D) than for 4.5mm (1.05±0.05 D), and in comparison with the no IOL condition, increases by 0.28 and 0.25 D for 3.0-mm and 4.5-mm respectively.

4.3.4 Experimental measurements on subjects

Figure 4.7 shows the through focus visual acuity in a range of +1 to -2 D, on average across the ten young subjects that participated in the study, using either the IOL in cuvette (purple), the IOL simulated with the SLM (green) or the SimVis technology (orange), or no IOL in the system (grey), for two different pupil diameters. The RMS difference was calculated and used to evaluate the simulation accuracy between simulators.

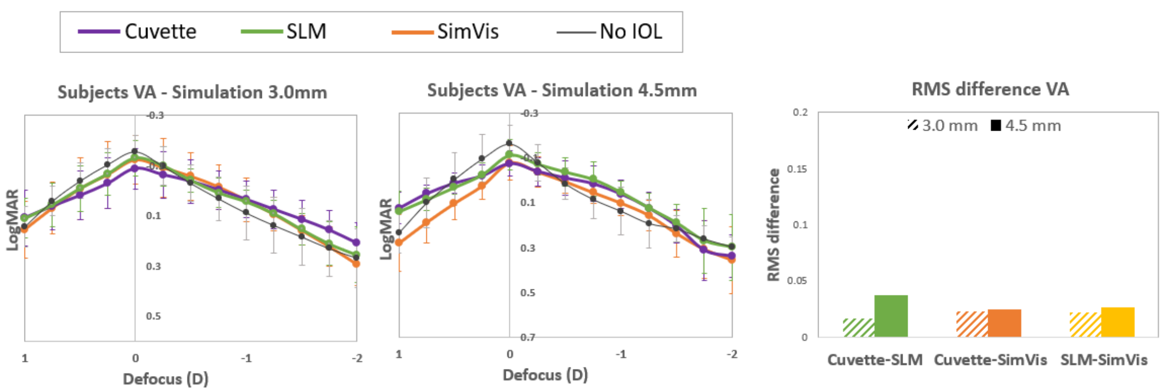

Fig. 4.7:*TFVA curves, on average across 10 subjects, for the four different conditions (Cuvette, purple; SLM, green; SimVis, orange line and no lens, grey) for 3.0-mm (left) and 4.5-mm (middle) pupil diameter. Right: RMS difference between simulators.*

VA at far decreased in comparison with the no IOL condition although LogMAR values were always negative. On average for all simulators, VA at far was -0.12±0.10 and -0.09±0.02 LogMAR; for 3.0 and 4.5-mm pupil diameters and the difference with the no-IOL condition was 0.03 and 0.07 LogMAR. The accuracy of the simulation, that was assessed by the RMS difference of the TF curves between simulators for the entire focus range, was always below 0.05, indicating a good agreement between simulators.

To evaluate the IOL performance the Visual Degradation at far and Visual Benefit at intermediate distance (80-cm) were calculated. The results are as show in figure 4.7 (A). Visual degradation at far was calculated subtracting the LogMAR VA at far with the Isopure IOL simulation from the LogMAR VA at far for the No IOL condition, and Visual Benefit at intermediate subtracting the LogMAR VA at intermediate distanced with the Isopure IOL simulation from the LogMAR VA at intermediate for the No-IOL condition. DOF was calculated as the range of diopters above 0.2 LogMAR VA (Yi et al 2011) form far (0 D) to negative values and compared across and no IOL condition at two pupil diameters (figure 4.8 (B)).

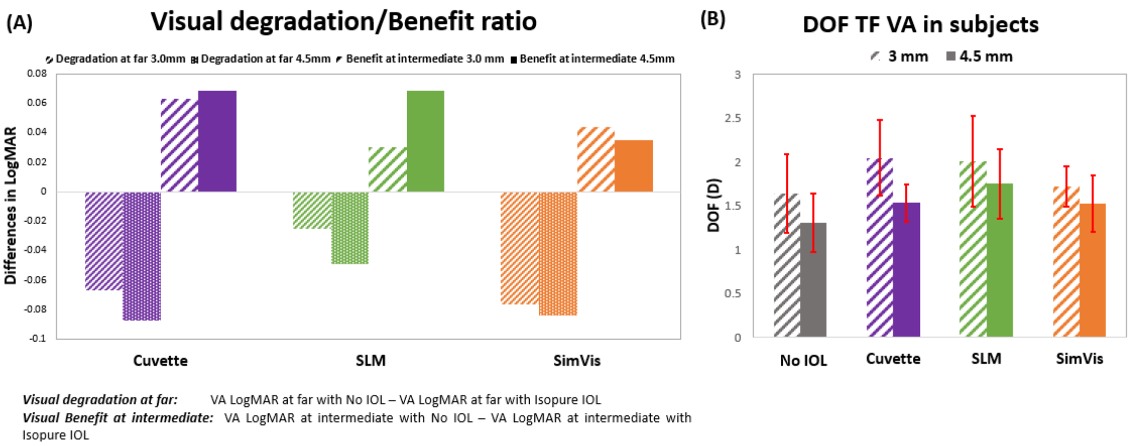

Fig 4.8: *(A), Results of Visual degradation at far (negative values) and Visual benefit at intermediate (1.25D, positive values) which describes the performance of Isopure IOL physically in a Cuvette (purple) and simulated with SLM (green) and SimVis (SimVis). (B) DOF calculated from TF VA curves as range of diopters above LogMAR 0.2, for Isopure (cuvette, SLM and SimVis) and no IOL condition. These metrics were calculated for two pupil diameters: 3.0 mm (dotted bar) and 4.5 mm (solid bar).*

The Isopure lens was designed to provide an extension of DOF, but consequently, as it's shown in figure 4.8 (A), it produces a slight degradation of optical quality at far distance, always lower than 0.10 LogMAR (in the cuvette, SLM and SimVis technology). The results show that Isopure IOL would reduce visual performance at far (negative values of visual degradation at far, meaning that VA at far should be lower than the one obtained with a monofocal lens); but improving performance at intermediate distance (positive values of visual benefit at intermediate, meaning that VA at intermediate distance is higher with Isopure lens).

In figure 4.8 (B) the DOF is largest for 3.0-mm pupils; on average across simulators 1.92 D ± 0.32D and 1.63±0.45 D for VA in subjects (Isopure IOL and No IOL respectively). DOF decreases for Isopure IOL at 4.5-mm pupils 0.32 D on average across simulators (1.60 D ± 0.21D) although always present higher DOF than No IOL condition.

4.4 Discussion

In this study, we explored the simulation feasibility on the optical and visual performance with a commercial Extended depth-of-focus (also known as premium monofocal IOLs), the Isopure IOL (BVI-PhysIOL) using three active elements in an AO system: the physical IOL immersed in a cuvette, IOL phase map mapped in an SLM, and IOL simulated with a SimVis with temporal multiplexing. Visual simulators are excellent tools to investigate new IOLs design visual performance as they allow non-invasive direct measurement of visual performance and comparing different conditions in the eye of a subject.

Monofocal and multifocal IOLs with different materials were simulated with visual simulators and a good agreement was observed between the predicted visual performance before surgery and the post-operative measured visual performance (Fernandez et al. 2009, Vinas et al. 2019). In addition, other studies had shown the good correspondence in TF visual performance among physical phase plates with multifocal designs and physical IOLs immersed in a cuvette and SLM or SimVis technology simulating those IOLs (Vinas et al. 2017, Vinas et al. 2017). Recently, we have proved the similarity between IOLs computer simulations and projected IOLs with standard power (20-22 D) immersed in cuvette removing the optical base power using a modified Rassow telescope (Benedi-Garcia et al. 2021). In this chapter we present the results of the simulation of Isopure IOL with a SLM and SimVis technology, and compare them with the results immersing a 21 D IOL in a cuvette projected in the pupil plane of an artificial or on the subject´s pupil. The cuvette IOL TF performance was considered as a reference and compared the TF performance found with simulators: SLM and optotunable lens. An additional no IOL condition had been measured in phakic eyes with paralyzed accommodation to mimic a monofocal IOL, although some variability with respect to a true monofocal IOL might be expected associated to intersubject differences in the crystalline lens aberration. In addition, we evaluated the effect of pupil diameter on Isopure IOL performance at 3.0 and 4.5-mm. All measurements were performed in an artificial eye and subjects.

As expected from its EDOF design, the Isopure IOL expanded depth of focus with respect to the no IOL condition, as shown both on-bench and in subjects (figures 4.5 and 4.7). We found an increase of DOF by 0.28 D on average across simulators in comparison with no IOL condition (0.28 and 0.29 D for 3.0-mm; 0.25 and 0.30 D for 4.5-mm; for 2P and VA respectively). In a on bench study by Physiol available the brochure in BVI medical, on bench measurements at 3.0-mm of the Isopure IOL in comparison with a monofocal IOL (Micropure) show an extension of 0.26 D DOF of Isopure over the monofocal, which fits with our finds of 0.28 D DOF extension at 3.0-mm for on bench 2P measurements in comparison with no IOL condition. In a study by Bova et al. 2022, reported 0.25 D increase DOF of Isopure over a monofocal IOL; in a study on 84 subjects implanted binocularly with the Isopure IOL and a monofocal IOL (12 months post-op), from binocular photopic VA defocus curves, and the reported 1.5 D DOF. The similarity is remarkable, despite some differences between our study and that of Bova et al, including our younger cohort (mean age in their study was 71.33 ± 7.91 and 29.8 ± 3.4 years in our study), pupil diameter (natural pupil on their study), a comparison with an aspheric monofocal IOL (TECNIS PCB00 IOL (Johnson and Johnson Vision, AMO Groningen BV).

Our visual performance results also agree well with those in 18 pseudophakic subjects implanted with the Isopure IOL from a recent study by Stodulka et al. 2021. The reported post-op VA in that study was -0.02 LogMAR binocular at far, and 0.14 LogMAR binocular at 1.25 D (80 cm), to be compared with our results on average across simulators -0.11±0.01 and -0.09±0.07 LogMAR at far, and 0.08±0.01 and 0.13±0.0 at 1.25 D for 3.0 and 4.5-mm respectively (figure 4.6). Our results at intermediate distance for 3.0-mm, fit well with a study by Morris et al. 2022, 0.07±0.12 LogMAR at 70 cm. The slightly better performance in our group may be associated to our use of monochromatic light (in a previous study we showed a comparable gain from using monochromatic instead of white light illumination for targets viewed monocularly than from binocular summation for targets viewed binocularly (Vinas et al. 2019) or our younger group, compared to a post-cataract surgery population (69.4 ± 6.9 years in Stodulka et al). The slight decrease of performance at far (less than 10% on bench and 0.1 LogMAR, figure 4.6 and 4.7) is compensated by a gain at intermediate distances (figure 4.4 and 4.7, for on bench and subjects).

The effect of IOL performance with two pupil diameters was studied, DOF increase at lower pupil diameter around 0.30 D on average across simulators, 1.33 D and 1.92±0.15 D LogMAR at 3.0-mm and 1.05 D and 1.60±0.09 D LogMAR at 4.5-mm, for on bench measurements (2P) and subjects respectively (figure 4.5 and 4.7). This is in agreement with the BVI medical Isopure IOL brochure that also show on bench measurements where the DOF with Isopure IOL is enlarged 0.22 D from 4.5 to 3.0-mm pupil diameters.

The study further demonstrates the use of the AO visual simulators to understand prospective performance with IOLs prior to intraocular lens implantation. Also, we assessed the quality of the IOL simulation, the multi-channel nature of the system allows simulating the IOL in SLM and SimVis lens. The results of our study indicate a good accuracy of the tested EDOF IOL simulations suggesting that this IOL can be used in visual simulators as SimVis Gekko without significant differences in performance.

A potential limitation of the study is the fact that it was conducted in a relatively younger population than the intended target for this lens. Since crystalline accommodation was paralyzed pharmacologically and the pupil limited by a 3.0 and 4.5-mm artificial pupil, two major properties of aging (presbyopia and pupillary miosis were mimicked). An older population may have shown a decline in VA from neural aspects (Baloh et al. 1993) as well as shifts in the crystalline lens spherical aberration towards more positive values (Glasser et al. 1998). Since all conditions were tested in the same subject, the reported relative effects (i.e. no IOL vs EDOF IOL) should not be influenced by neural resolution. Regarding the measurements performed in phakic eyes, Villegas et al. 2019 showed that, in general, the spherical aberration of the crystalline lens (present in pre-op visual simulations but removed in cataract surgery) plays a minor role in the simulated performance with IOLs conducted pre-operatively. The trend for larger benefit at intermediate found (and lower degradation at far) in all conditions with Isopure IOL simulators (cuvette, SLM and SimVis), shows a good accuracy of EDOF IOL simulated.

4.5 Conclusion

Experimental simulation (cuvette, SLM and SimVis) of Isopure IOL has been performed in an adaptive optics visual simulator, to evaluate the optical performance of the IOL and the accuracy of the simulations to validate its implementation in the lens catalog of SimVis Gekko. Measurements were performed on bench and with 10 young subjects. The conclusion of the experiment is:

- AO simulators are a suitable tool to assess new IOL designs, EDOF IOLs, and predict the behavior in pseudophakic eyes before surgery.
- Isopure EDOF IOL show a good balance between DOF, 1.92±0.15 and 1.60±0.09 D, and visual acuity at far, -0.11±0.01 and -0.09±0.07 LogMAR, for 3.0 and 4.5-mm pupil diameters, respectively (average across simulators). All conditions tested with Isopure IOL, on bench and in subjects, across simulators and pupil diameters, show on average, higher values of DOF than no IOL condition.
- The influence of DOF in pupil diameter tested in Isopure IOL, shows an increase of DOF with lower pupil diameter in all conditions tested, increasing on average 0.28 D.

This chapter shows a good correspondence of the results found on bench and with subjects with literature validation the Isopure IOL simulation. In the next chapter will be presented the Isopure IOL results of ocular aberration influence experimentally to evaluate its design and consider its implantation in post-LASIK subjects.

5 Evaluating the effect of corneal aberrations of Isopure IOL using Adaptive Optics

In this chapter, we show our work on the evaluation of the performance of Isopure IOL in presence of positive and negative spherical aberration, and when correcting the ocular aberrations with the deformable mirror of the adaptive optics system. Experimental measurements were performed both on the model eye and on patients.

Part of this study have been published in Biomedical Optics Express (BOE) by C Lago et al.: **“Evaluating the effect of ocular aberrations on the simulated performance of a new refractive IOL design using Adaptive Optics”**, Biomed. Opt. Express 13(12), 6682-6694 (2022).

The contribution of the author of this thesis was to perform a complete literature search for studies on Isopure IOL and on computational simulations with EDOF IOLs, to implement the white light source on the adaptive optics system; to calibrate and align the Adaptive Optics system, to design the measurement protocols, to perform the measurements, to analyze the data obtained and to write the article.

5.1 Introduction

Experimental visual simulation of the IOLs in human subjects allows non-invasive testing of the lens design in combination with the optics of eye. Our visual simulators contains active elements to simulate the IOL under study (a Spatial Light Modulator (SLM) to represent the IOL phase map, and an optotunable lens using the SimVis technology based on temporal multiplexing (Dorronsoro et al. 2016; Akondi et al. 2017)), and a Deformable Mirror (DM) to manipulate the optics of the eye or to correct for the subject's ocular aberration and/or induce different combination of aberrations. Several studies have used AO Visual Simulators to investigate the impact of inducing spherical aberration on visual performance (Piers et al. 2007), on accommodation (Fernandez et al. 2005) and on the eye's depth-of-focus in normal eyes (Rocha et al. 2009). New IOL designs aim at providing multiple focus or expanding depth-of-focus to improve vision at near and intermediate distances in subjects that do not have the capability to accommodate. Therefore, a question that arises is to what extent the optical performance and the nominal functionality of these IOLs (i.e. depth-of-focus) is affected by the magnitude of corneal aberrations, and preserved upon differences in the underlying spherical aberration.

In this chapter, we further investigated the interaction of the eye's aberrations with the Isopure IOL performance under different conditions. The IOL was: (1) immersed in a cuvette in the testing channel of the AO Visual Simulator and projected onto the subject's pupil or artificial eye, (2) Mapped into the SLM, and (3) simulated using the optotunable lens (under SimVis technology). Then, the adaptive optics deformable mirror was used to (A) induce positive and negative spherical aberration (0.2µm) and (B) correct subject's ocular aberrations (simulating an aberration-free eye). Additionally, the IOL performance was evaluated with monochromatic light (555 nm) in comparison with white light while the physical IOL was inserted in the cuvette.

5.2 Methods

Adaptive Optics System

Measurements were obtained using the AO Visual Simulator described in chapter 2. The main components were used in the current chapter are: (1) the Super Continuum Laser Source (SCLS) to select emission wavelength (monochromatic (555nm) or polychromatic (white) light); (2) the Hartmann-Shack wavefront sensor to measure the subjects aberrations and calibrate the DM for aberrations induction; (3) the DM to compensate for the aberrations of subjects and induce spherical aberration; (4) the SLM to introduce the IOL phase map; (5) the cuvette where the physical IOL was inserted; (6) the optotunable lens to simulate the IOL with SimVis technology; (7) the Badal system to correct subject's refractive error and induce defocus in the through focus curves measurements.

DM spherical aberration mapping

Vision was studied in four configurations of the adaptive optics deformable mirror: (1) without correcting the aberrations of the eye, i.e. natural aberrations with the IOL projected onto the subject eye; (2) correcting the eye's aberrations, i.e. mimicking an ideal condition of "implanting" the IOL in an aberration-free eye, (3) inducing positive SA (+0.2 µm at 4.5-mm pupil diameter) on top of the subject's natural aberrations or artificial eye, (4) inducing negative spherical aberration (-0.2 µm at 4.5-mm pupil diameter) on top of the subject's natural aberrations or artificial eye. All conditions were evaluated using monochromatic light (555nm unless otherwise specified).

We chose to induce +0.2µm SA for 4.5mm, equivalent to inducing 0.87 µm at a 6.5-mm pupil diameter calculated using scaling formulas derived elsewhere (Schwiegerling 2002) as it was close to previously reported values of spherical aberration induced by a high myope, 5 D, corneal refractive surgery with the ablation profiles used 20 years ago (Marcos et al. 2001, Moreno-Barriuso et al. 2001).

In NoAO condition (with natural ocular aberrations) and with spherical aberration induction conditions; the defocus was compensated with the Badal but the astigmatism was not corrected (always lower than 0.75 D).

Physical Intraocular lens in cuvette

Measurements were performed with an Isopure IOL (PhysIOL-BVI) of 21D inserted in the cuvette. As already described in chapter 2 and 4, the cuvette has a metallic support where the IOL is mounted and immersed in distilled water to simulate ocular media. The Rassow lens was designed to compensate a 20 D IOL power and the remaining 1D was compensated using the Badal system.

IOL simulation with SLM or optotunable lens

The Isopure IOL was simulated for a 4.5 mm pupil diameter using either the SLM (with the phase map describing the Isopure IOL mapped into it) or the optotunable lens (working under the SimVis technology) as described in chapter 4.

On bench measurements

Through focus one pass (1P) and double pass (2P) measurements were performed with the artificial eye mounted in the 3-D translational stage as explained in chapter 2, under the different experimental conditions. For 1P measurements, the E Snellen stimulus was presented on the DMD and projected to the CCD camera of the artificial eye. The retinal image quality was studied through focus collecting a series of images ranging from -4.0 to +1.0 D, in 0.25 D steps, for each condition. In the 2P experiment, through retinal images were collected with the double pass CCD camera, from -3.0 to +1.0 D in 0.25 D steps. In both, the vergence of the beam was changed moving the mirrors of the Badal system. The

IOL performance (either mounted in the cuvette or simulated with the SLM and optotunable lens) were performed for the four conditions of the AO deformable mirror, for a 4.5-mm pupil diameter and monochromatic light (555 nm).

Additionally, polychromatic (white) light was used and measurements performed under natural aberration condition, for 3.0-mm and 4.5-mm pupil diameters. The camera properties and laser power were constant along the measurements; and ensuring that none of images were saturated.

For 1P on bench measurements, the optical quality was measured in terms of the correlation metric and for double-pass retinal images, the Full Width at Half-Maximum (FWHM) was calculated as the average FWHM of four intensity profile at different orientations passing through the center of the spot. The obtained optical quality for the different simulators (cuvette, SLM, optotunable lens) was compared to the no IOL condition. Additionally, the optical degradation at far and the optical benefit at intermediate (1.50 D range) metrics were used and the DOF calculated as the range of diopters for which the correlation and the normalized FWHM metrics were above 0.8 (Marcos et al 1999).

Measurements on *Subjects*

The same subjects that performed the previous experiments, ten 10 young subjects (9 females, 1 male), participated in the study. Their average age was 29.8 ± 3.4 years, and their average spherical error of -0.17 ± 1.10 D. Inclusion criteria was an astigmatism lower than 0.75 D. Measurements were obtained under cycloplegia (tropicamide 1%). As before, all protocols met the tenets of the Declaration of Helsinki. Subject's consented after they had been informed on the nature of the study, protocols and implications of their participation.

Subject were aligned into the AO system and viewed the psychophysical stimuli projected on the DMD, illuminated at 555 nm or with white light, through the selected visual simulator (real IOL immersed in the cuvette, or the optotunable lens simulating the Isopure IOL) or through the system without any IOL (no IOL condition). The AO deformable mirror was either correcting or inducing different amounts of SA. The Badal system was used to correct the subject defocus and performed before each though focus visual acuity measurements, as the induction of SA shifted the subject's best focus. Visual Acuity (VA) was measured using a tumbling E letter with 8-Alternative Forced Choice (8AFC) procedure and QUEST (Quick Estimation by Sequential Testing) algorithm (Lu et al. 2013, Watson et al. 1983, Borgo et al. 2012, Brainard et al. 1997).

The impact of aberration correction and spherical aberration induction was assessed in terms DOF estimated from the TF curves as the defocus range (in the near region, i.e. negative defocus) for which VA was 0.2 LogMAR or better (Yi et al. 2011). Additionally, the visual degradation at far (difference in VA LogMAR at 0 D relative to the no IOL condition (on average)) and the optical benefit at intermediate (average optical quality in the intermediate distance (1.25 D) for Isopure IOL relative to the no IOL condition) (Vedhakrishnan et al. 2022) were calculated. ANOVA tests were conducted to evaluate statistical differences across conditions.

5.3 Results

Experimental Through Focus optical quality (on bench)

Figure 5.1 shows the through-focus (TF) 1P and 2P retinal images for the AO system without any IOL, and for the Isopure IOL immersed in the cuvette and with induction of +0.2 µm (B), 0 µm (C) and -0.2 µm (D) spherical aberration on top of fully corrected aberration state, all for a 4.5mm pupil diameter. Images reveal a qualitatively higher DOF for Isopure (around 1.50 D) than for the no IOL condition (around 1.00 D).

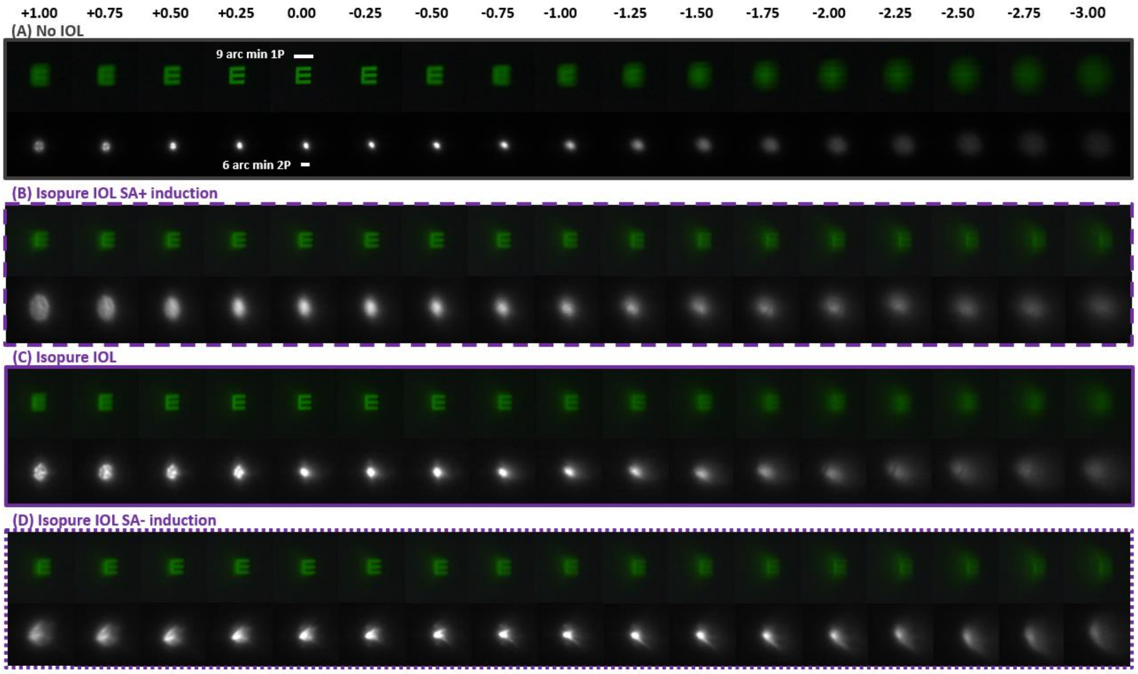

Fig. 5.1: TF series, in a range of 4 D in 0.25 D steps; of single-pass images of an E-letter stimulus (top images) and double-pass images of a spot (bottom images) in an artificial eye, through (A) no-IOL condition; (B) Isopure in a cuvette in combination with +0.2 µm spherical aberration induced in DM (C) Isopure IOL in the cuvette and an aberration-free eye and (D) Isopure lens in a cuvette in combination with -0.2 µm spherical aberration induced on the DM. All measurements of Isopure IOL illustrated are with IOL immersed in a cuvette. Pupil diameter 4.5-mm.

Figure 5.2 compares optical metrics (correlation for 1P and normalized FWHM for 2P) that define the IOL optical performance across Cuvette, SLM and SimVis, when an additional spherical aberration of ±0.2 µm for a 4.5-mm pupil diameter was induced.

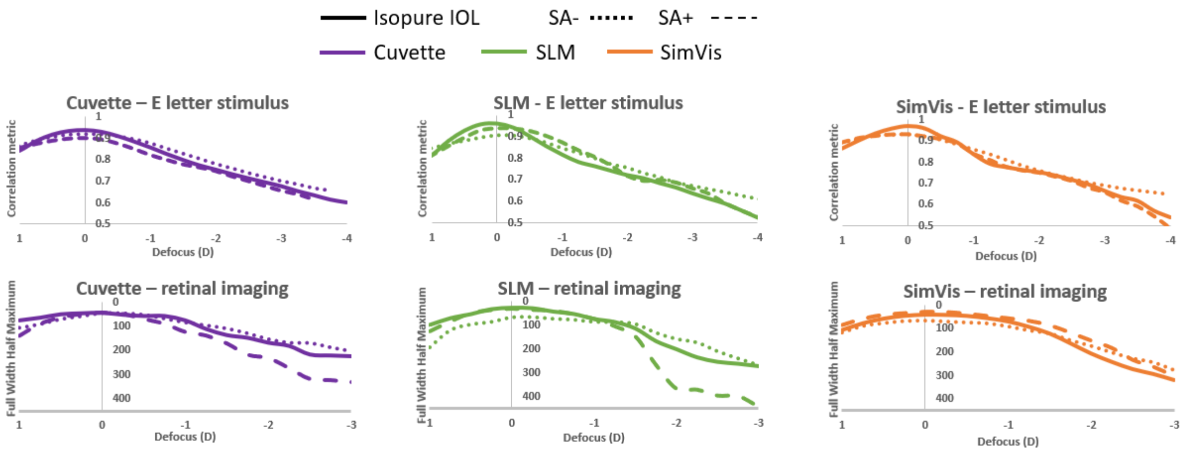

Fig. 5.2: *Top, TF for E-letter stimulus projected on the artificial retina (CCD) of an artificial eye (correlation metric). Bottom, TF for double-pass retinal imaging of a point (FWHM in pixels, 0.16 arcmin per pixel). All the TF curves were measured in the three simulating platforms: Cuvette in purple (left), SLM in green (middle) and SimVis in orange (right). In all condition were induced +/- 0.2 microns (at 4.5-mm pupil diameter) of spherical aberration in a DM and compared with the normal condition. All measurements were made at 4.5-mm pupil diameter.*

We expected an increase of the optical quality at far and a narrower TF curve when positive spherical aberration was induced, that partly compensated the negative spherical aberration induced by the IOL, and a decrease in optical quality and widening of DOF with the induction of negative SA. While there aren't large differences between the conditions (SA+, SA- and natural aberrations) in the measurements performed with E letter stimulus, this trend is visible in the results (Figure 5.2).

In the TF 2P metric with the IOL in cuvette and SLM measurements, the differences between conditions are more evident, especially in the reduction of DOF when inducing positive SA. However, with SimVis simulations these differences between conditions are minimum. We think that these can be due to the way in which SimVis simulates the IOL. SimVis works under temporal multiplexing, and the interaction with additional aberrations is not possible. When the lens is placed in the cuvette or simulated in the SLM the aberrations of the subject (particularly the spherical aberration) could be compensated by the simulated lens but this is not possible with SimVis because the phase of the wavefront is not changed locally.

Experimental Through-Focus visual acuity (in subjects)

Figure 5.3 (A) shows the wave aberrations maps of all subjects participating in the study: natural aberrations (No IOL condition, top row); and the quality of the AO-correction (bottom row). The subjects have been ordered by increasing Root Mean Square wavefront error under natural aberrations (as shown in Fig. 5.3(B)). Natural aberrations (NoAO, No Adaptive Optics aberrations correction) RMS ranged from 0.13 to 0.5 µm and decreased below 0.1 µm in all AO (ocular aberrations corrected with AO) cases; 0.07 on average for

4.5-mm pupils. Figure 5.3 (C) shows the amount of native spherical aberration in all subjects.

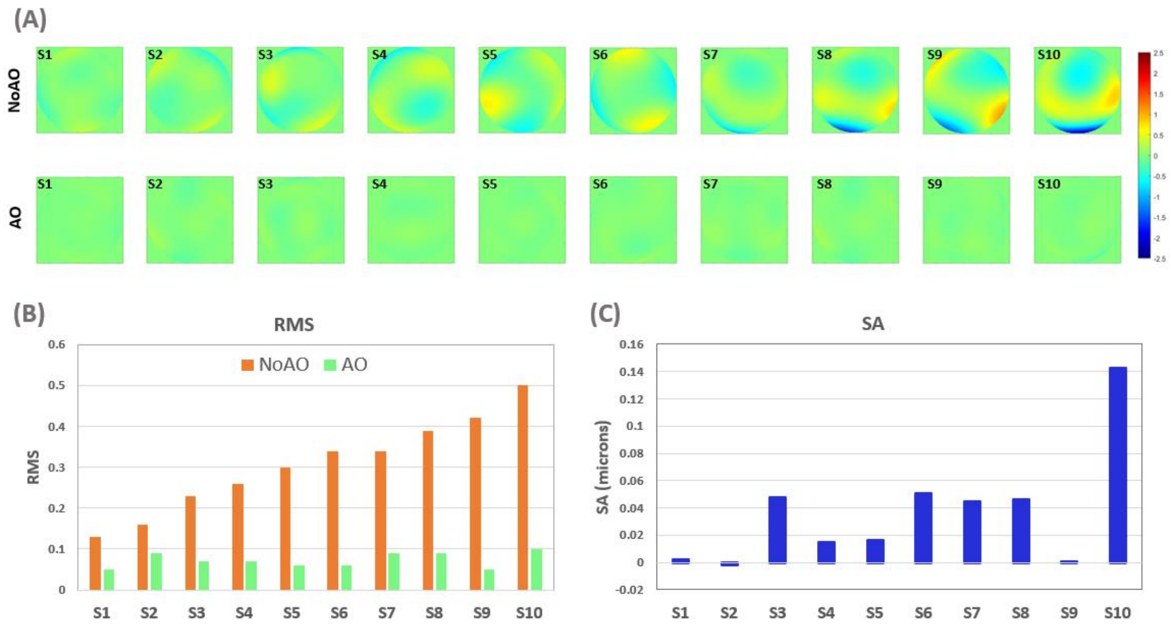

Fig. 5.3: *(A) Wave aberration maps for Natural aberrations (top panels) and AO-corrected aberrations (bottom panels) for all 10 subjects (scale bar in µm) (B) Root Mean Square Wavefront error (RMS) with (AO) and without corrections (NoAO) of the natural aberrations of the eye. (C) Natural Spherical Aberration. Data are for 4.5-mm pupil diameter.*

Figure 5.4 shows the TF VA curves for all subjects and conditions (thin lines) and the average behavior (thick lines) when the IOL is simulated with the cuvette (top row) and the SimVis technology (lower row). The TF VA with the natural aberrations of the subjects is shown in Figure 5.4 (A) and (C) in grey and compared with the TF VA when seeing through the simulation of the IOL. In both subfigures, it is clear that the presence of the Isopure IOL (purple lines IOL in a cuvette and orange lines simulated IOL with SimVis) decreases the quality at far with respect to the no IOL (grey lines), although on average across subjects, the decrease is not statistically significant, and that the lens expands the DOF (average DOF is 1.30 D with the natural aberrations, and 1.53 and 1.52 D for IOL in cuvette and IOL simulated with SimVis technology respectively. With natural aberrations and seeing through the IOL in the cuvette, the largest DOF expansion with the IOL occurred for subjects S6 and S7 (from 1.10 D to 1.65 D, and from 0.9 D to 1.65 D, respectively). When the measurements were performed with natural aberrations and IOL simulated with SimVis technology, the largest DOF expansion with IOL occurred for subjects S6 and S10 (from 1.10 D to 2.15 D, and from 0.8 D to 1.95D, respectively).

In figure 5.4 (B), the comparison between the behavior with the IOL and natural (purple lines) or corrected (red lines) aberrations is shown. On average, the performance of the IOL does not change when the aberrations of the subjects are corrected.

Figure 5.4 (D) compares the TFVA between AO-correction aberrations (red lines) with natural aberrations (orange line) when the IOL is simulated with SimVis (optotunable lens), in this case on average, the optical performance of the lens is better with the natural aberrations: VA at far and DOF increase 0.05 and 0.36 D, respectively. As said before, we interpret this different behavior because of the lack of compensation between aberrations when the lens is simulated with SimVis.

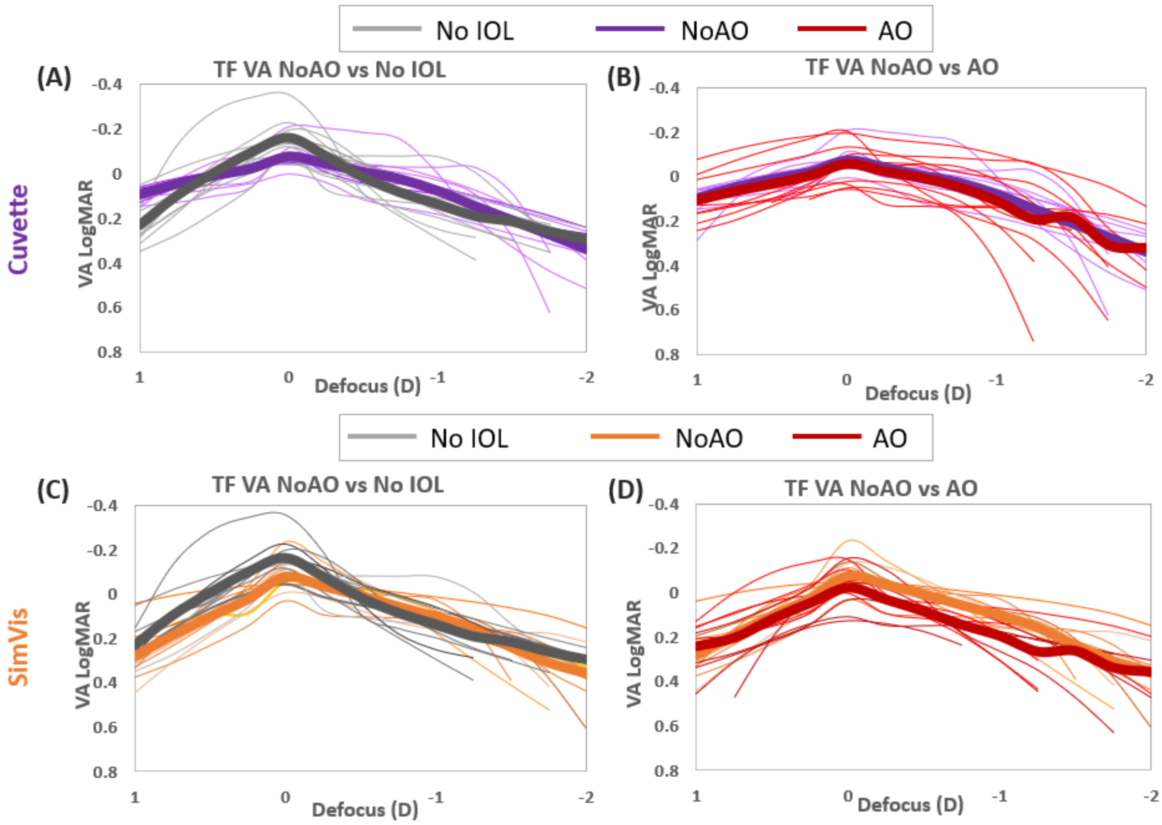

Fig. 5.4 *TF VA in subjects. (A) compares the Isopure IOL immersed in a cuvette with natural aberrations (purple lines) and no IOL condition (grey lines). (B) illustrate the optical performance of Isopure IOL in the cuvette, when is measure with natural aberration (purple) and ocular aberrations corrected with AO (red lines). (C) compares the optical performance of Isopure IOL simulated with SimVis technology (orange) with no IOL condition (grey line). (D) Represents the optical performance of the lens simulated with SimVis technology when is measured with natural aberrations (orange) and ocular aberrations corrected with AO (red lines). The thin lines represent the TF curve measured to each subject while the thick line represent the results on average across subjects in each condition. All measurements were performed at 4.5-mm pupil diameter.*

The individual TF VA curves for each subject are shown in figure 5.5. Panel (A) shows the TFVA when the IOL was simulated using the cuvette channel and panel (B) the TFVA when the IOL was simulated with SimVis technology (optotunable lens). Individually (Fig. 5.5 (A)), AO-correction only improved peak performance over the natural conditions with the IOL in S8 (by 0.19 LogMAR), while in subjects S2, S4 and S7 performance with the IOL was actually better with the natural aberrations than with AO-correction (by -0.08, -0.04 and -0.11 LogMAR). In figure 5.5 (B), the subjects with best peak performance in AO correction are S3, S5 and S9 (0.06, 0.02 and 0.03 LogMAR respectively) in comparison with NoAO; but the differences are lower in comparison with cuvette measurements. The performance with the IOL with SimVis was better for the rest of the subjects as exception of S4, where the peak performance is better with negative SA induction.

Analyzing the DOF behavior, in Fig.5.5 (A) in S4 and S8 the presence of additional positive spherical aberration (SA+) reduces the DOF with the IOL. In S8, S9, and S10 the induction of negative spherical aberration (SA-) produces the widest DOF. With SimVis lens, Fig.5.5 (B), in half of the subjects the DOF expansion is widest with subject's ocular aberrations; but there are some differences in S8 and S9, where the widest DOF it's produced by negative spherical aberration (SA-) induction; and S1, S3 and S7 by positive spherical aberration (SA+); never in AO condition.

However, in general the TF performance with the IOL appears to be primarily driven by the IOL design, and it seems like the role of the individual (and corrected/induced) aberrations is secondary. The intersubject variability of the TF curves (averaged across defocus positions) is similar for AO and NoAO condition (-0.06 and -0.07 LogMAR for AO and NoAO respectively).

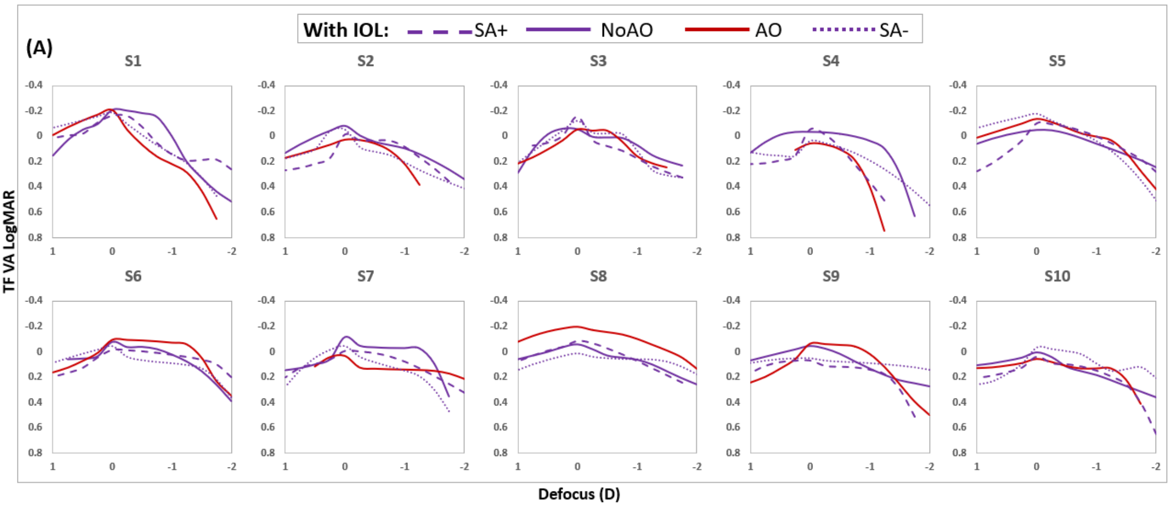

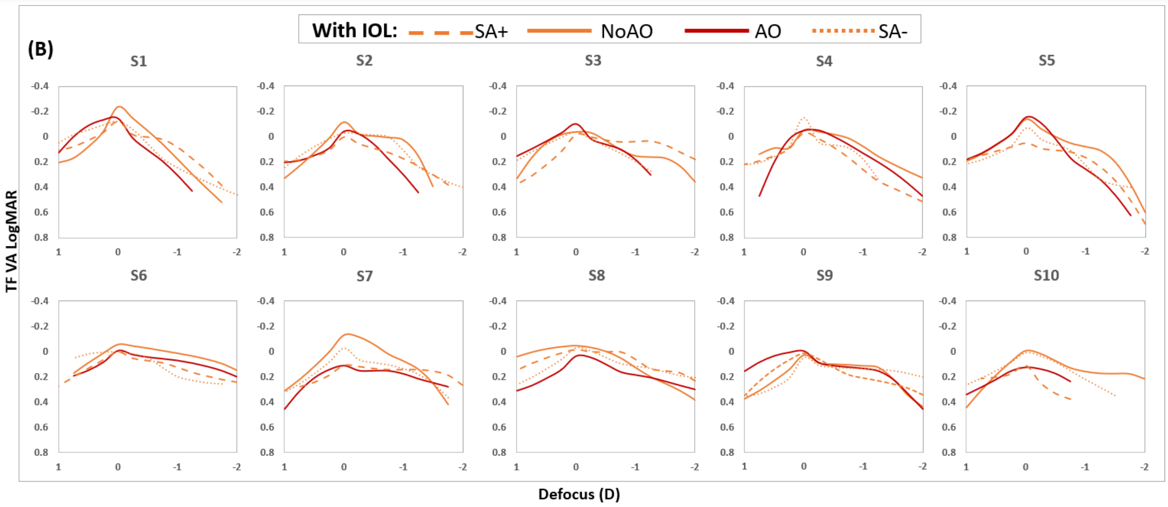

Fig. 5.5: *All 10 eyes, in each panel, and 4 conditions: natural aberrations (solid line), corrected aberrations (red line), induced positive spherical aberration (SA+, dashed line), induced negative spherical aberration (SA-, dotted line). (A) for measurements with Isopure IOL physically immersed in a cuvette and (B) for Isopure simulated with SimVis technology.*

The TFVA measured when SA was induced over the subject's natural aberrations is shown in Figure 5.6 when the IOL was simulated with the cuvette channel or with SimVis. Three conditions were evaluated: Isopure IOL with subject's ocular aberrations (natural aberrations), inducing -0.2 µm of SA and inducing +0.2 µm of SA in a DM.

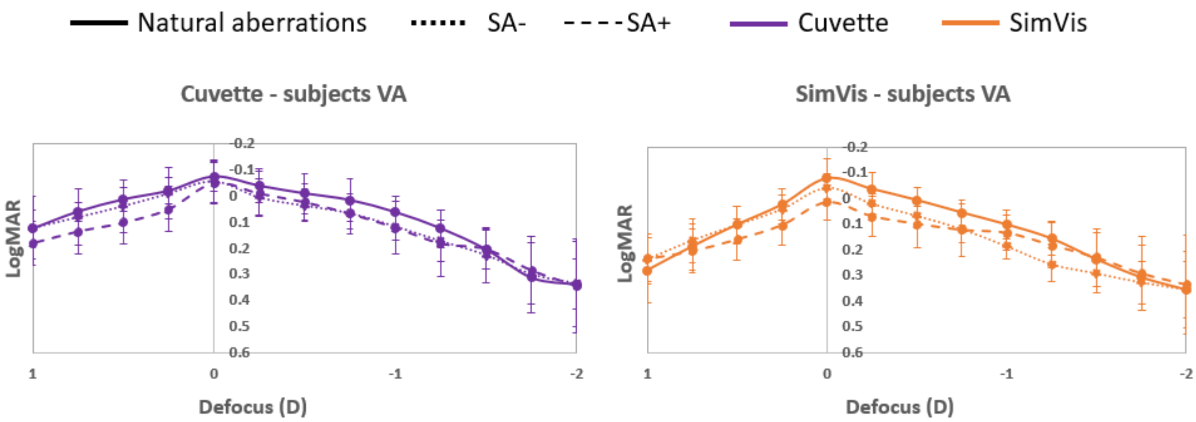

Fig. 5.6: *Left, TF VA with IOL immersed in a cuvette. Right, TF VA with IOL simulated with SimVis lens. In all condition were induced +/- 0.2 µm of spherical aberration in a DM and compared with the normal condition. All measurements were made at 4.5-mm pupil diameter.*

The condition without inducing aberrations (natural aberrations) it’s always the best performance for the Isopure IOL as the induction of SA (positive or negative) reduced the optical quality.

Fig. 5.7 (A) shows the average DOF across subjects, for all conditions when aberrations are manipulated (positive or negative SA induced and correction of ocular aberrations, AO), in comparison with natural ocular aberrations (NoAO) and no-IOL condition. The measurements had been performed with Isopure IOL in a cuvette (purple bars) and simulated in SimVis technology (orange bars) in comparison with no IOL condition (grey bars). The presence of the Isopure IOL produced an increase in DOF by 0.23 D on average. The expansion of DOF was largely independent on the presence or correction of high order aberrations, and of the induction of positive or negative spherical aberration: 0.23 D/0.23 D no AO, 0.19 D/0.11 D with positive SA, 0.15 D/-0.13 D with AO, and 0.24 D/ -0.19 D with negative SA, for IOL immersed in a cuvette and IOL simulated with SimVis respectively.

Visual Acuity at far (Fig. 5.7 (B)) was significantly better with no IOL, although it was on average above 0 in all conditions as exception with IOL simulated by SimVis when SA+ is induced. Values on average were lower for SimVis simulations and differences across conditions were lower for IOL in a cuvette: -0.03±0.04 and -0.06±0.01 LogMAR for SimVis and Cuvette respectively. Figure 5.7 (C) shows visual degradation at far and visual benefit at intermediate (1.25 D), in terms of LogMAR difference from the No IOL condition. Visual Degradation at far was always negative because VA at no IOL condition was always better and visual benefit at intermediate was positive when positive SA was induced (SA+) and with subject’s natural aberrations (NoAO); and negative when the aberrations were corrected (AO). Wen negative SA was induced (SA-) visual degradation was positive when the lens was simulated with the cuvette channel and negative when the simulation was done with SimVis technology. As before, we guess that the differences found when simulating the lens with the cuvette or the SimVis could be due the different interaction with the aberrations imposed.

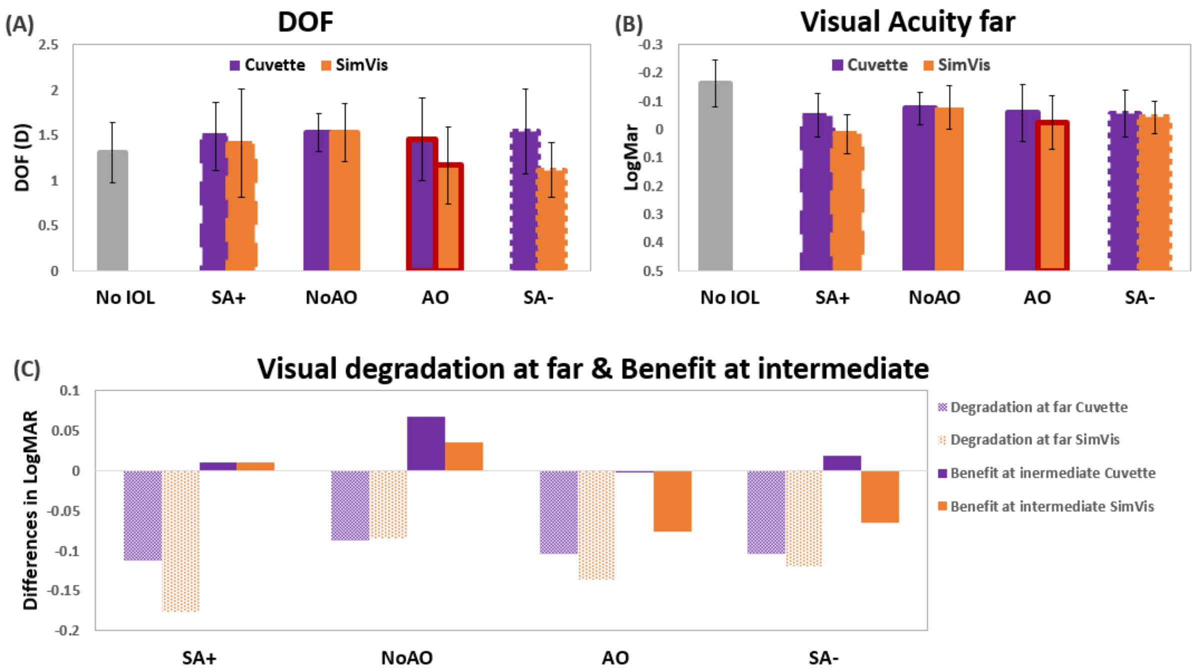

Fig. 5.7: *(A) DOF estimated from the TF VA curves of Fig. 5.5, as the negative dioptric range above which LogMAR is better than 0.2. Results are average of the DOFs calculated across subjects for each condition (B) LogMAR VA at far, averaged across subjects for each condition (C) Visual degradation at far (light color) and visual benefit at intermediate (1.25 D, dark color) as LogMAR differences with respect to the No IOL condition, averaged across subjects for each condition.*

The measurement simulating the Isopure IOL with the cuvette channel was performed using monochromatic light (555 nm) and polychromatic light (white light) at 4.5-mm and 3.0-mm pupil diameters. The results are shown in figure 5.8. The measurements had been performed in optical bench (1P) imaging a E letter in the retina of the model eye, and on subjects by measuring the TF VA. DOF (range of diopters from far with VA above 0.2 LogMAR) and maximum visual acuity at far was calculated in TF VA subjects on average to evaluate the influence of polychromatic and monochromatic light in the optical performance of the Isopure lens.

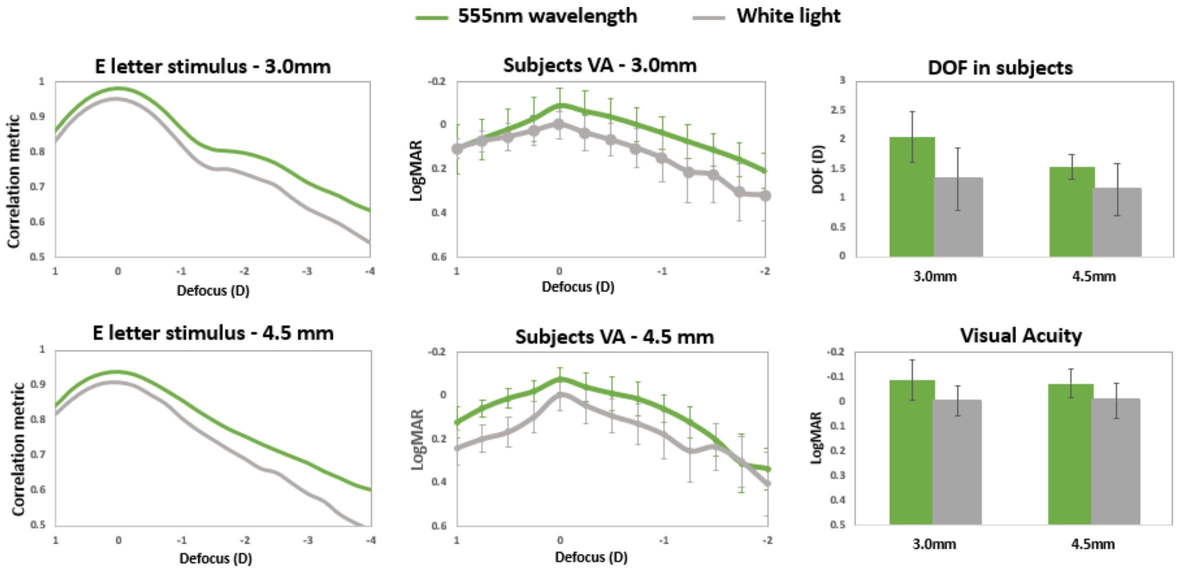

Fig. 5.8 *Left, TF E letter stimulus, in the middle TF VA in subjects, and right valued of DOF and Visual Acuity at far on average for subject's measurements. All the measurements were made with the Isopure IOL immersed in a cuvette. The measurements were performed at two pupil diameters: 3.0-mm (top) and 4.5-mm (bottom). The green line/bar represents the monochromatic light at 555 nm, and the grey line/bar represents the polychromatic light (white light).*

The use of white light always decreased the optical performance of Isopure IOL, but the shape of the curve was preserved. At right, the graphs of DOF and Visual Acuity, quantify the optical performance of the Isopure lens (on average) when is measured with different illumination (monochromatic and polychromatic). DOF decrease with white light 35% and 25% in comparison with green light at 3.0 and 4.5-mm pupil diameter respectively but we didn't obtain a no-IOL condition with white light to study the difference in DOF with and without the IOL with a polychromatic stimulus while. VA decreased for white light in comparison with green light, with the two pupil diameters, about 0.1 LogMAR.

5.4 Discussion

In this study, we explored the effect of combining high order aberrations (natural, corrected or induced positive or negative spherical aberrations) and chromatic effect on the optical and visual performance with a commercial Extended depth-of-focus (a.k.a premium monofocal IOL), the Isopure IOL (BVI-PhysIOL). Visual simulators are a non-invasive technique, excellent to investigate visual performance with manipulated aberrations. Unlike computer eye models where, even if they customized to the subject's anatomy and 3-D biometry, can only predict retinal image quality, visual simulations allow direct measurement of visual performance under manipulated aberrations. Also, unlike measurements on pseudophakic subjects implanted with the IOL under investigation, visual simulators allow comparing different conditions in the eye of a subject. A standard clinical study would involve various groups of subjects classified, for example, by the magnitude of their corneal aberrations, although differences may be confounded by intersubject variability in the neural response, which is minimized by intra-subject testing of different aberration conditions, achieved with a DM in an AO visual simulator.

In this study, we compared the simulation with the cuvette channel, with the ones using the SLM and SimVis, and to correct the natural aberrations of the eye to study how induce SA (Piers et al. 2004, Fernández et al. 2021) would change the TF performance. The results with Isopure IOL simulation were compared with the results found in the natural eye condition (i.e. in the no IOL condition). This no-IOL condition in phakic eyes with paralyzed accommodation mimicked an eye with a monofocal IOL, although some variability with respect to a true monofocal IOL might be expected associated to intersubject differences in the crystalline lens aberration.

As expected from its EDOF design, the Isopure IOL expanded depth of focus with respect to the no IOL condition, as shown both on-bench (Fig. 5.1) and in subjects (Fig. 5.7). In subjects, we found an increase of DOF by 0.23 D and 0.22 D (No IOL: 1.30±0.33 D; NoAO+IOL in a cuvette: 1.53±0.21 and NoAO+IOL in SimVis technology: 1.52±032 D), which compares with the 0.25 D increase reported by Bova et al. 2022 in a study on 84 subjects implanted binocularly with the Isopure IOL and a monofocal IOL (12 months post-op), from binocular photopic VA defocus curves, and the reported 1.5 D DOF. The similarity is remarkable, despite some differences between our study and that of Bova et al. 2022, including our younger cohort (mean age in their study was 71.33 ± 7.91 and 29.8 ± 3.4 years in our study), pupil diameter (natural pupil on their study and dilated in this study), a comparison with an aspheric monofocal IOL (TECNIS PCB00 IOL (Johnson and Johnson Vision, AMO Groningen BV). and their results after 12 months post-operative and binocular.

Our visual performance results also agree well with those in 18 pseudophakic subjects implanted with the Isopure IOL from a recent study by Stodulka et al. 2021. The reported post-op VA in that study was -0.02 LogMAR binocular at far, and 0.14 LogMAR binocular at 1.25 D (80 cm), to be compared with our -0.07±0.05 and -0.08±0.08 at far and 0.12±0.07 and 0.15±0.06 LogMAR at 1.25 D (NoAO+IOL condition, Cuvette and SimVis technology respectively). The slightly better performance in our group could be associated to our use of monochromatic light, in figure 5.8 the values of VA at far for white light are 0±0.07 and 0±0.06 LogMAR for 3.0 and 4.5-mm respectively. The use of AO allowed us to test the impact of aberrations on the performance of the Isopure IOL. On bench data (on an artificial eye with no aberrations) showed a relatively minor impact of the induced aberrations over the lens design (Fig. 5.2). The IOL produced an expansion of DOF regardless the absence of aberrations or presence of positive or negative spherical aberration. Although this IOL design is not particularly driven by 4th order spherical aberration (the high order aspheric coefficients introduce also high order spherical term and a smooth alternation of far and intermediate zones across the pupil), some induction of negative spherical aberration is expected. While this potential interaction does not appear to be captured in the correlation metric (induction of positive spherical aberration, SA+, does not seem to counteract the negative spherical aberration of the lens and improve optical quality over the AO or the SA-condition), it may be behind the slightly narrower DOF with SA+ captured by the FWHM metric, for IOL immersed in a cuvette and simulated with SLM, in SimVis simulations with the optotunable lens, there are minor differences between conditions, this could be explained due the interaction of aberrations could be different with temporal multiplexing.

The intersubject variability (in natural aberrations and neural response) appears to dissipate those trends, and on average, there is no difference in DOF, and at far or near performance in absence or presence of positive or negative SA (Fig. 5.6 and 5.7). The tolerance of the Isopure IOL to high order aberrations and to spherical aberration expands previous findings in subjects that show that the performance of this lens is tolerant to the induction of astigmatism (Rocha et al. 2007). An on-bench study (Zheleznyak et al. 2012) showed that the reduction in DOF with corneal astigmatism and high order aberrations was higher for multifocal than for monofocal intraocular lenses, and that the benefit of the increase in DOF with multifocal IOLs diminished when more than 0.75 D astigmatism remained uncorrected. The lens evaluated in this study was designed to augment the DOF with respect to a monofocal IOL but only to intermediate distances, maintaining optical quality for far and cannot be consider a multifocal intraocular lens. We think that this could be an explanation for the observed constancy in the DOF when spherical aberration was induced. Our subject data indicate a higher prevalence of the IOL design over the individual's aberrations on both visual acuity at far and DOF. Also, multiple studies have found a degradation of VA and an expansion of DOF when spherical aberration is induced (Rocha et al. 2007, Yi et al. 2011). However, while those effects are expected when aberrations are corrected or induced on virgin eyes, they do not appear to occur in combination with the Isopure IOL. As found on bench (5.2), correcting or inducing aberrations have little impact on performance in combination with the IOL. On average, while there is a significant reduction in Visual Acuity at far in presence of the IOL with respect to the no-IOL condition (Fig. 5.4 (A) and (C)). The differences in VA and DOF across different aberration conditions are not statistically significant when the IOL is immersed in a cuvette (-0.06±0.01 LogMAR and 1.50±0.04 D, on average across conditions, purple bars in Fig. 5.7 (A) and (B)) although differences increase slightly when IOL is simulated with SimVis lens (-0.03±0.04 LogMAR and 1.30±0.20 D on average across conditions, orange bars in Fig. 5.7 (A) and (B)). Individually, however, there were some subjects where performance was more influenced by induction of positive or negative spherical aberration or correction of high order aberrations as shown in figure 5.6. However, we did not find a straightforward relation of this effect with the natural amount of spherical aberration, or overall optical quality in these subjects (Fig. 5.3).

The use of white light decreased about 0.1 logMAR the VA peak found in the TF curves and about 25% the DOF. The lower VA was expected because of the broadening on the PSF produced when all frequencies are taken into account (Aissati et al. 2022) and this could also explain the reduction in DOF. Regretfully, we couldn't study the DOF change with Isofocal when polychromatic light was used because we didn´t capture a no-IOL condition in the experimental session. However, with white light we expect this to be in the order of the one found with monochromatic light (0.23 D).

The study further demonstrates the use of AO visual simulators to understand prospective performance with IOLs prior to intraocular lens implantation. While in this study the IOL was, inserted in the Cuvette and simulated with SimVis technology, and projected on the subject's eye, as it was designed to evaluate the impact of aberrations on the lens performance, and not the quality of the IOL simulation (as shown in chapter 4). The results of our study indicate that the tested EDOF IOL is tolerant to the induction and correction of aberrations, suggesting that this IOL could be used in a large proportion of the population (from almost perfect eyes to relatively large amounts of spherical aberrations) without significant differences in performance. More studies with a larger sample size and including subjects in the age range of the average cataract surgery subjects should be conducted to clarify the findings of the study. The simulated spherical aberration induction is consistent with that found in post-myopic LASIK (positive SA) and post-hyperopic LASIK subjects (negative SA) (Marcos et al. 2001, Llorente et al. 2004), indicating that the evaluated IOL could also be suitable (provided that the IOL power is adequately selected) in post-LASIK subjects.

A potential limitation of the study is the fact that it was conducted in a relatively younger population than the intended target for this lens. Since crystalline accommodation was paralyzed pharmacologically and the pupil limited by a 4.5-mm artificial pupil (in addition, 3.0-mm for white light measurements), two major properties of aging (presbyopia and pupillary miosis were mimicked). An older population may have shown a decline in VA from neural aspects (Baloh et al. 1993) as well as shifts in the crystalline lens spherical aberration towards more positive values (Glasser et al. 1998). Since all conditions were tested in the same subject, the reported relative effects (i.e. monofocal No IOL vs EDOF IOL) should not be influenced by neural resolution. On the other hand, given the little impact of relatively large amounts of spherical aberration, it is unlikely that age-related changes or individual differences in spherical aberration play a significant role in the described effects. Villegas et al. 2019 show that, in general, the spherical aberration of the crystalline lens (present in pre-op visual simulations but removing in cataract surgery) plays a minor role in the simulated performance with IOLs conducted pre-operatively. In any case, the described AO visual simulator has the capacity to remove the spherical aberration (although not the scattering) of the natural crystalline lens using the DM, for simulations in cases where that may play a role (i.e. monofocal aspheric IOLs aiming at correcting the aberrations of the cornea). While with strong scattering media, the fidelity of the simulation can be compromised, in a recent study by Barcala et al. (Barcala et al. 2022) we studied the perceptual response with four binocular presbyopic corrections, and found that the individual perceptual scores before and after cataract surgery were correlated for all distances. Finally, the study did not consider the effect of potential adaptation to the natural high order aberrations of the eye (Sawides et al. 2011). Previous studies have shown that visual performance with naturally high order aberrations (i.e. keratoconus) surpasses that of normal subjects through the same aberrations as the keratoconus subjects induced with AO (Chen et al. 2008) suggesting neural adaptation or perceptual learning to the long-term optical degradation. While potential differences in performance with the IOLs associated to natural or induced aberration (of the same amount) can only be tested in groups with naturally high positive or negative spherical aberration (i.e. the mentioned post-LASIK eyes) it is unlikely that our results are biased by this effect, as we did not find performance trends associated to the magnitude of the natural aberrations, and the measured effects appear dominated by the IOL design. The trend for larger benefit at near found (and lower degradation at far) found for the Isopure IOL in combination with the natural aberrations of the eye, in comparison with other conditions, including fully corrected optics, could reflect some adaptation to the natural optics, or simply a result of the IOL design for eyes with normal amounts of aberrations. On the other hand, the fact that TF visual acuity curves in eyes with all aberrations corrected and through the same IOL show large differences in TF VA curves (even if the retinal image quality is identical in the entire dioptric range) suggest that neural factors are critical and further emphasize the importance of the visual simulation, beyond optical expectations.

5.5 Conclusion

Isopure IOL was experimentally simulated in an AO visual simulator with the cuvette channel and SimVis (simulations previous validated in chapter 4), to evaluate the influence of aberrations of its performance, using a deformable mirror to correct and/or induce aberrations in the eye (artificial and subjects). 4 configurations were evaluated: (1) Isopure IOL with ocular aberrations; (2) inducing +0.2 µm of spherical aberration on top the ocular aberrations; (3) inducing -0.2 µm of spherical aberration on top the ocular aberrations and (4) correcting the ocular aberrations with IOL simulated. In addition, IOL physically in the cuvette was measured with monochromatic (555 nm) and white light. As a conclusion:

- Isopure EDOF IOL experimentally measured DOF was 1.53 ± 0.21D and 1.52±0.21 D and visual acuity at far was -0.07 ± 0.05 and -0.08±0.08 LogMAR, on average, when the lens was simulated with the cuvette channel and with SimVis technology, respectively.
- All conditions tested with Isopure IOL (correcting ocular aberrations and inducing spherical aberration) show on average, higher values of DOF than no IOL condition, when the lens was simulated with the cuvette. With the SimVis simulation, the behavior of the lens was similar with natural aberrations, however, when aberrations were corrected or spherical aberration was induced DOF and VA decreased, which could be explained due to the lack of compensation of aberrations with temporal multiplexing.
- With white light the performance of Isopure IOL is preserved, but lower values of VA around 0.1 LogMAR lower for both pupil diameters, and DOF 35% and 25% lower for 3.0 and 4.5-mm pupil diameter, respectively, were found.
- Isopure IOL always presents a good balance between DOF and optical quality at different conditions tested, it’s a robust IOL which seems to be effective in a high range of subjects, including post-LASIK subjects.

6 Computational simulation of the optical performance of Acrysof IQ Vivity IOL in post-LASIK eyes.

Acrysof IQ Vivity IOL was launched in January 2021 in the US as the first and only non-diffractive extended depth of focus lens. The lens was designed and manufactured by Alcon Healthcare S.A. Through a collaborative agreement with the company, we had access to the simulation of this lens with the software OpticStudio to evaluate its optical performance in post-LASIK eyes.

Part of this study was presented in ARVO 2021 as oral presentation entitled **“Simulated assessment of presbyopia correction IOLs in post-LASIK patients”** by C. Lago who was awarded an ARVO Travel Grant. Results were also presented on ESCRS 2021 with a poster entitled **“Predicted optical quality and halos with the Vivity EDOF IOL in post-LASIK patients”** that was presented by S. Marcos and is being reviewed for publication in an article in the Journal of Cataract and Refractive Surgery with the title **“Computational simulation of the optical performance of an extended depth of focus intraocular lens in post-LASIK eyes”**

The contributions of the author of this thesis, with the help of the directors, was to design the different computational model eyes, to extract the wavefront maps, to calculate the halos metric, and to analyze the results.

6.1 Introduction

LASIK (laser-assisted in-situ keratomileusis), which is a well-known ocular treatment, with more than 30 years of evolution (Reinstein et al. 2012), reshapes the cornea for the correction of refractive errors. Typically, an excimer laser is used to ablate the cornea, following an ablation profile such that the central cornea is flattened in myopic LASIK or steepened with respect to the periphery in hyperopic LASIK. While the theoretical Munnerlyn algorithm does not necessarily induce high order aberrations (Munnerlyn et al. 1988), approximations of this algorithm, and discrepancies due to laser efficiency losses on a curved surface, and ablation plume shielding caused induction of spherical aberration and coma, especially with larger corrections (Marcos et al. 2001, Moreno-Barriuso et al. 2001, Llorente et al 2004, Cano et al. 2004 and Dorronsoro et al. 2006).

Several studies in the early 2000s (Chen et al. 2002, Anera et al. 2003, Pop et al. 2004, Kohnen et al. 2005), reported a change in corneal asphericity, and an associated increase in the magnitude of spherical aberration (SA) following LASIK. In particular, two works by our group reported induction of positive spherical aberration following myopic LASIK (Marcos et al. 2001) and induction of negative SA following hyperopic LASIK (Llorente et al. 2004). The induction of corneal SA was proportional to the magnitude of the spherical correction, with slopes of 0.17 µm/D for myopic LASIK and -0.28 µm/D for hyperopic LASIK, in patients operated with the Bausch and Lomb, Technolas 217-C laser (wavelength 193 nm; pulse repetition rate 50 Hz and a peak radiant exposure 120 mJ/cm^2). The studies also showed increased coma, although its magnitude was not statistically significantly correlated with the pre-operative spherical error (Moreno-Barriuso et al. 2001). In later studies, we showed through both computational simulations of the ablation process and experimental measurements (Dorronsoro et al. 2006) that a large percentage of the induction of SA could be explained by the ablation efficiency loss in the periphery due to the non-normal incidence.

Many patients that had undergone LASIK surgery in the 2000's are in need of cataract surgery today. The presence of an early LASIK surgery has posed challenges in the application of the standard formulas of calculation of the IOL power calculation, due to the unusual corneal shape (Aramberri 2003). Furthermore, with an increasing number of IOL designs now available for cataract and presbyopia correction, the selection is even more complex (Alió et al. 2017). Among the new IOLs, EDOF IOLs (Kohnen et al. 2020), which generally exhibit refractive profiles, appear to be less prompt to image degradation and artifacts than diffractive IOLs, while they are designed to expand visual functionality at intermediate distances. A question of clinical value is to investigate whether these lenses may be well-suited to patients with unusually high amounts of high order aberrations, such as those following LASIK surgery.

In this study were performed computational simulations in pseudophakic post-LASIK eye models virtually implanted with the EDOF Acrysof IQ Vivity IOL (Alcon), and the monofocal Acrysof IQ IOL (Alcon) as a control. The Acrysof IQ Vivity is a wavefront shaping lens, designed with a patented X-Wave technology (McCabe et al. 2021); which, according to the manufacturer, consists of a 2.20-mm wavefront shaping optics in the central part of the anterior surface to stretch and shift the wavefront avoiding light splitting. The aim of the design is to extend the depth of focus to enhance intermediate vision without compromising far vision.

6.2 Methods

6.2.1 Pseudophakic computer eye models

Acrysof IQ Vivity IOL (EDOF IOL) and Acrysof IQ IOL (monofocal IOL) of 22D, both from Alcon healthcare S.A. were studied computationally to assess the validation of Acrysof IQ Vivity IOL in post-LASIK eyes. The virtually "implanted" IOLs was either the Acrysof IQ Vivity (EDOF IOL) or the Acrysof IQ (control monofocal IOL), with 22 D labeled power. According to the technical product information by Alcon (Alcon 2020); both IOLs (made of the same material, acrylate/methacrylate copolymer) exhibit anterior aspheric biconvex shape, have the same optical zone diameter, 6.0 mm, overall length 13 mm, haptic angle 0 degrees and UV blue light filtering. IOL geometry and refractive index at 555 nm were provided by the manufacturer.

Pseudophakic computer eye models were designed in OpticStudio (Zemax, Kirkland, WA) with a model cornea with an aspheric anterior corneal surface, a spherical posterior corneal surface (6.5 mm radius of curvature) and 0.55 mm central corneal thickness. IOLs were placed at 4.5 mm behind the posterior corneal surface and the aqueous and vitreous refractive indices were 1.336. For the non-LASIK cornea, the radius of curvature (7.668 mm) and the asphericity (-0.066) of the anterior surface were optimized such that the corneal power was 43 D and the corneal SA was +0.28 µm for a 6.0-mm pupil diameter (Beiko et al. 2007). The axial length of the computer model eye was adjusted such that far images projected on the retina were in focus, with minimum spot radial size.

Three different post-myopic LASIK corneas were simulated with low, medium, and high negative refractive corrections (-2.5, -4.5 and -7.5 D) and two post-hyperopic LASIK corneas with low and medium positive refractive corrections (+2.5 and +4.5 D). The SA induced by these corrections was obtained from the experimental data previously reported (Marcos et al. 2001, Llorente et al. 2004) on the corneal (and total) high order aberrations induced by LASIK surgery with a B&L, Chiron Technolas 217-C, equipped with the PlanoScan software. The SA and coma induced were simulated using a Zernike Standard Phase surface type placed at the cornea. Table 6.1 shows the SA induced in the different post-myopic and post-hyperopic LASIK tested conditions. Induction of coma (0.5 µm a 6.5-mm pupil diameter, consistent with the reported amount in literature by Moreno-Barriuso et al. 2001) was also studied.

Pre-op spherical error (Diopters)	Induced spherical aberration (µm) (6.5-mm pupil diameter)
High myopia, -7.5	1.05
Mid myopia, -4.5	0.54
Low myopia, -2.5	0.20
Low hyperopia, +2.5	-0.74
Mid hyperopia, +4.5	-1.30

Table 6.1: *Corneal SA induced with LASIK surgery for different pre-operative spherical error at 6.5-mm pupil diameter.*

6.2.2 *Optical quality and Depth of focus.*

The eye's wavefront aberrations were obtained by ray tracing with OpticStudio as explained in chapter 2, for 3.0 and 5.0-mm pupil diameters. The Point Spread Function (PSF) and Modulation Transfer Function (MTF) were calculated, in an 8 D focus range, in 0.1 D steps. Retinal image quality was described in terms of Visual Strehl (VS). The following metrics were analyzed as a function of LASIK induced SA and coma: VS at far (0 D), VS at an intermediate distance (1.50 D) and the depth of focus (DOF), defined as the usable defocus range for which VS>0.12 (Yi et al. 2010). These metrics were calculated in all conditions and used to compare the performance of eyes (virgin and post-LASIK) virtually implanted with either the EDOF or the monofocal IOL.

6.2.3 *Computational simulation of halos.*

The presence of halos was estimated with a method similar to that described by Alba-Bueno et al. 2014. Retinal images of a 2-arcmin pinhole stimulus were simulated by convolution with the PSF of the eye, and the diameter that encircles the 50% of the intensity was calculated (illustration in figure 6.1). Higher values of this metric mean more spread halos in the image.

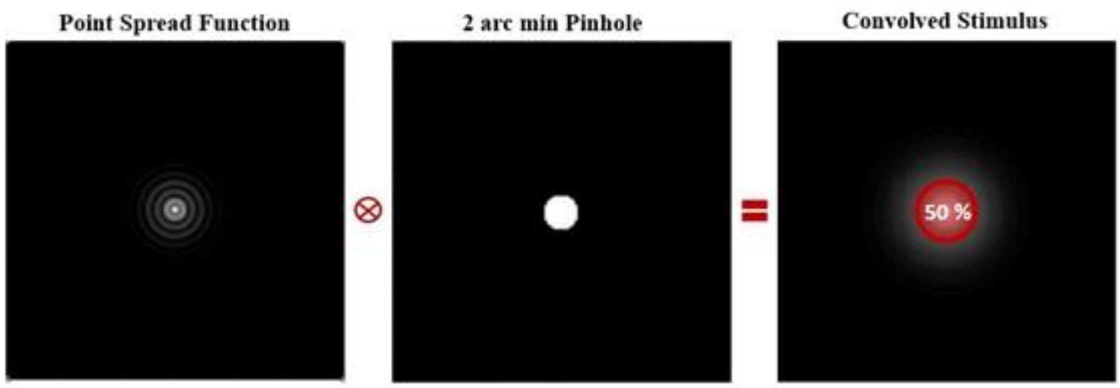

Fig.6.1: *Methodology used to simulate halos: The retinal image was simulated by convolving the PSF with a 2-arcmin pinhole and the diameter that encircles the 50% of the energy was calculated.*

6.3 Results

Figure 6.2 shows the estimated VS for far at 5.0-mm (left) and 3.0-mm pupil diameter (center) and the associated depth-of-focus for 3.0-mm pupil diameter (right) in the pseudophakic eye models, as a function of induced SA, for eyes implanted with the EDOF IOL (orange circles), the monofocal IOL (purple circles) and the value for virgin eyes without LASIK treatment (orange and purple crosses).

The VS for far in the eye model with EDOF and monofocal IOL for 5.0-mm pupils, in virgin eyes is 0.67 and 0.61 for monofocal and EDOF IOL respectively; and differed by 0.05, on average across SA (Fig. 6.2-A). The presence of SA induced by LASIK produced a sharp decrease in VS at far from values >0.60 in non-LASIK eyes to <0.3 in eyes with ±1 µm (over 6.5-mm pupil) induced SA for both IOLs.

Figure 6.2-B shows the VS for far with both lenses for 3.0-mm, exhibiting a very different performance from that of 5.0-mm. 0.98 and 0.52 for virgin eyes with monofocal and EDOF IOL respectively. The average VS was on average 0.43 higher with the monofocal than the EDOF IOL. Also, VS was rather constant across eyes with different amounts of SA, decreased by 9% on average in both IOLs respect to virgin eyes.

DOF for 3.0-mm pupils (Fig 6.2-C) with the EDOF IOL was higher in corneas with induced negative SA (post-hyperopic LASIK) while DOF with the monofocal IOLs DOF was higher in corneas with induced positive SA (post-myopic LASIK). The rate of change of the DOF with the EDOF IOL was slower than with the monofocal (-0.20D/micron for EDOF IOL and 0.34D/micron for monofocal IOL). In virgin eyes, DOF was 2.5 D with the EDOF IOL and 1.40 D with the monofocal. On average across conditions, DOF (mean±STD) was 2.52±0.18 and 1.50±0.31 D in post-LASIK eyes for 3.0-mm pupils, with EDOF and monofocal IOL, respectively and the difference between distributions was significant ($p<0.05$).

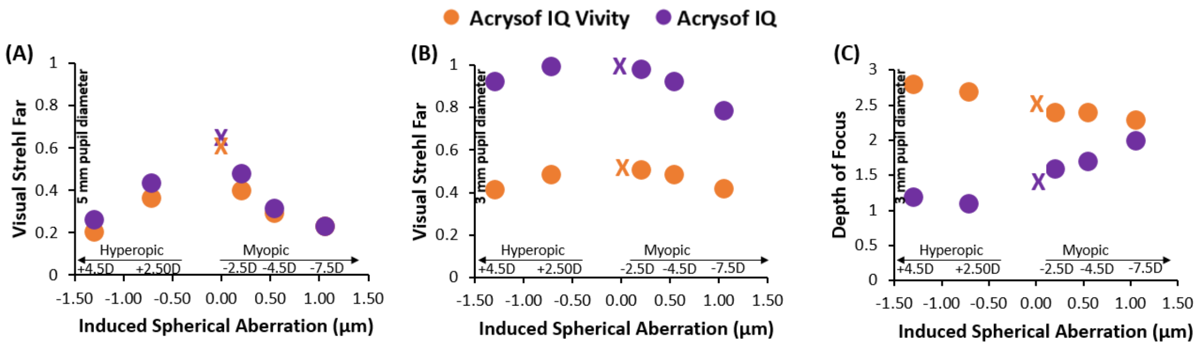

Fig 6.2: (A) *VS for 5.0-mm pupil diameter; (B) VS for 3.0-mm pupil diameter; and (C) DOF for 3.0-mm pupil diameter as a function of induced SA for the eye model (values for 6.5-mm pupil diameter) with the eye "implanted" with Acrysof IQ Vivity IOL (orange) and Acrysof IQ IOL (purple). The cross-shaped marker represents the VS value of a pseudophakic eye with an average virgin (non-surgical) cornea implanted with the Acrysof IQ Vivity IOL (orange) and with Acrysof IQ IOL (purple).*

Figure 6.3 shows similar analysis as figure 6.2 but simulating SA in combination with 0.5 µm of coma induced by LASIK (at 6.5-mm pupil diameter). The results parallel those of the condition where only SA was induced, although the VS (for 5.0-mm pupils) is further decrease by 0.35 and 0.33 on average, for the EDOF and the monofocal IOL respectively. At 3.0-mm pupil diameter the VS decreased on average by 22% and 19% for EDOF and monofocal IOL respectively, respect to virgin eyes when SA is induced.

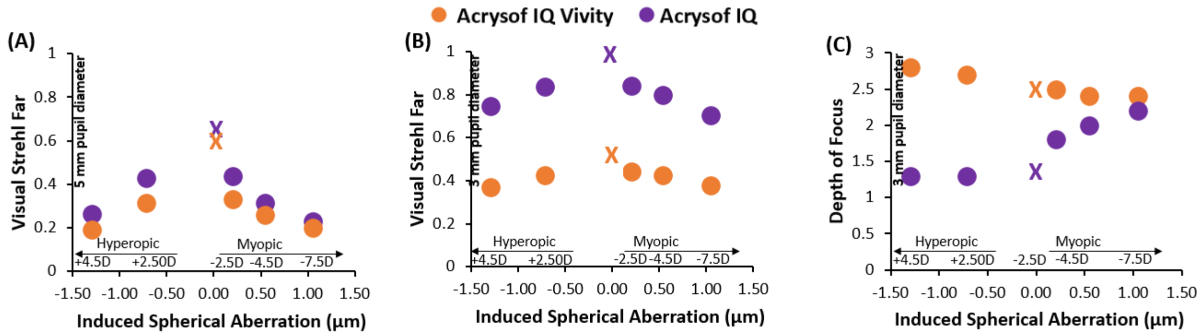

Fig 6.3: (A) *VS metric for 5.0-mm pupil diameter; (B) VS for 3.0-mm pupil diameter; and (C) DOF for 3.0-mm pupil diameter as a function of induced SA for the eye model with Acrysof IQ Vivity IOL (orange) and Acrysof IQ IOL (purple) when both SA and coma are induced by LASIK. The cross-shaped marker shows the VS value of a pseudophakic eye with an average virgin (non-surgical) cornea implanted with the Acrysof IQ Vivity IOL (orange) and with Acrysof IQ IOL (purple).*

Figure 6.4 shows the halo metric which accounts for the spatial size of halos (angular diameter in arcmin that encircles the 50% of the energy), for 5.0 (Fig. 6.4-A) and 3.0-mm (Fig. 6.4-B) pupil diameters, for the EDOF IOL (orange) and the monofocal IOL (purple), for virgin corneas (red cross marker), LASIK-induced SA (solid line), and LASIK-induced SA in combination with coma (dashed line).

With non-LASIK corneas, the halo metric was 2.22 arcmin for the monofocal IOL, and 1.82 arcmin for the EDOF IOL, for 5.0-mm pupils respectively. While the halo metric was fairly constant for 3.0-mm pupils (except for hyperopic cases with EDOF IOL), there was a sharp increase when increasing the magnitude of the SA for 5.0-mm pupils.

Noticeably, for 5.0-mm pupils, the minimum halo size was obtained in non-surgical corneas, lower for EDOF IOL than monofocal IOL, also with EDOF IOLs the minimum halos size occurred in corneas with induced positive SA. The halo metric with EDOF IOLs exceeded that obtained with monofocal IOLs when negative SA was induced (6.56 vs 5.95 arcmin on average for the EDOF and monofocal IOLs respectively when only negative SA was induced). However, with positive SA induced (myopic LASIK) resulted in reduced halos with the EDOF when compared with the monofocal IOLs, by 1.62 (SA) and 1.71 (SA+coma*).* For 3.0-mm pupil diameters, the presence of coma had a minimal impact with an average increase across conditions of 0.25 and 0.28 arcmin for EDOF and monofocal IOL respectively without mid hyperopic condition where differences are noticeable for EDOF IOL, 3.91.

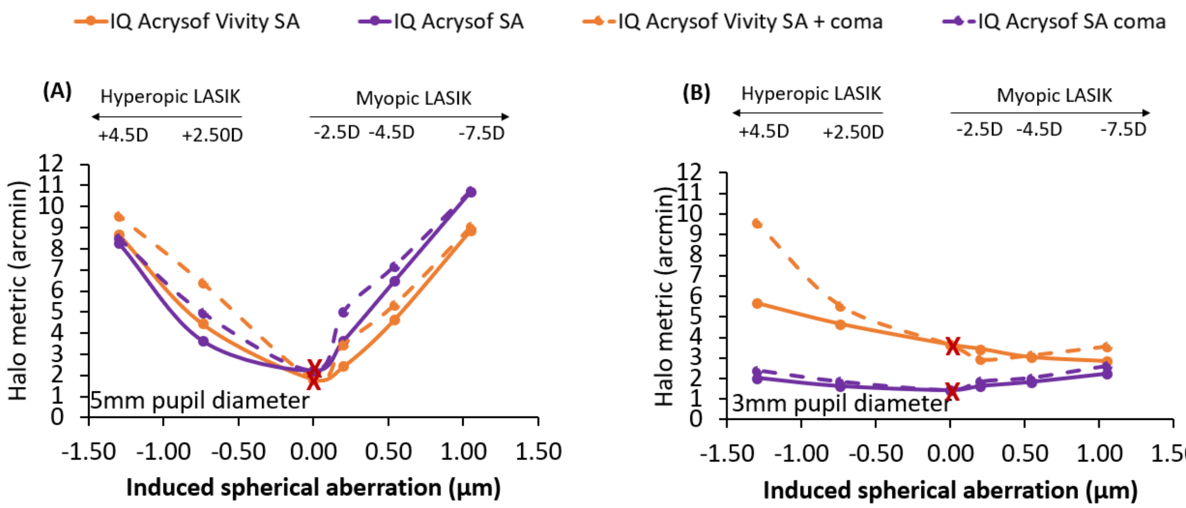

Fig. 6.4: *Halo metric for EDOF and monofocal IOL as a function of LASIK-induced SA for a 5.0-mm pupil diameter (A) and 3.0-mm pupil diameter (B). The no treated cornea case is represented with 0-µm induction of SA (red cross maker). The continuous line represents the cases where only SA is induced, and the dotted line represents the combination of induced SA and coma. Results are shown for 5.0 and 3.0-mm pupil diameters.*

6.4 Discussion

The performance of two intraocular lenses were evaluated using computer model eyes with post-LASIK corneas, simulated adding the SA or SA and 0.5 µm of coma (Marcos et al. 2001, Moreno-Barriuso et al. 2001, Llorente et al. 2004). The studied IOLs were a monofocal aspheric IOL, Acrysof IQ, and the EDOF IOL Acrysof Vivity IQ, by Alcon.

Our computer eye model follows standards proposed in the literature (Norrby et al. 2007). In particular, we used a (non-surgical) corneal model that mimics the ISO standard, both in power (43 D) and magnitude of SA (0.28 µm, for a 6.0-mm diameter pupil) (Wang et al. 2003). While this choice is slightly different to that followed by other studies in the literature (Perez-García et al. 2020, Perez-García et al. 2020, Oltrup et al. 2021) that use the cornea defined in the Navarro eye model (Navarro et al. 1985) (42.16 D and +0.139 µm SA, 6.0-mm pupil), it is closer to the average population (Wang et al. 2003)' and to on-bench testing parameters.

An on-bench study (Borkenstein et al. 2021) compared the performance of Acrysof IQ Vivity with a trifocal IOL in terms of the MTF at 50 lp/mm and Strehl ratio for far objects using the ISO standard with corneal SA. These experimental results with Vivity IOL show a higher image quality for larger pupils than for smaller pupils at far, in good agreement with the results of our simulation. The study did not report DOF. A clinical study on 40 patients (Gundersen et al. 2021), and another on 16 patients (Kohnen et al. 2022) who were implanted binocularly with the Acrysof IQ Vivity IOL showed good far and intermediate vision and low reports of patients bothered by glare, halos or starburst.

Our comparisons between the simulated performance with the Acrysof IQ and Acrysof IQ Vivity IOLs in non-LASIK eyes can be contrasted with two studies that compared the clinical outcomes of these two lenses (McCabe et al. 2021, McCabe et al. 2022). After 6 months of implantation, in photopic conditions, McCabe et al. 2021, McCabe et al. 2022 found that the DOF was higher in the eyes implanted with the EDOF IOLs than the ones implanted with the monofocal. In addition, VA at 66 cm was higher for the EDOF IOL, in agreement with our findings for 3.0-mm pupil diameters. Additionally, data on the influence of pupil diameter in the performance of the Vivity Acrysof IQ IOL described in an FDA report (FDA PMA P930014) showed an increase in DOF in patients when the pupil diameter decreased, matching the increase in DOF (from 1.00 to 2.57 D) that was shown in our computer simulations when pupil diameter decreased from 5.0 to 3.0-mm (1.20 to 2.50 D). Furthermore, a study by Pastor-Pascual et al. 2022 presented aberrometry measurements on normal patients implanted with the monofocal IOL and with the EDOF IOL. Their reported DOF estimates are based on VS calculations, and therefore directly comparable with our simulations which use the same metric. They show a high degree of correspondence with the current study: DOF with the EDOF IOL in the clinical study was 2.50 D, 1.25 D broader than with the monofocal IOL, (in our simulations 2.5 D, 1.40 D broader than with the monofocal, for 3.0-mm pupil diameters). These VS-based DOF values are also in close agreement with Gundersen et al. 2021, who reported a DOF obtained from binocular VA defocus curves of 2.50 D in 40 patients implanted with EDOF IOL in a modified monovision strategy.

While to our knowledge there are no reports of clinical performance of the Vivity IOL in LASIK patients, the good correspondence between our computer simulations with clinical performance suggests that we can extrapolate a similar methodology to predict performance in post-LASIK patients. To describe post-operative corneas, we used aberrometry data in pre- and post- myopic and hyperopic patients obtained in our laboratory in the early 2000's (Marcos et al. 2001, Moreno-Barriuso et al. 2001, Llorente et al. 2004). While conclusions are limited to the aberrations induced by the particular laser used in these surgeries (B&L Technolas 217-C), and on the laser parameters such as the programmed algorithm and laser fluence (Dorronsoro et al. 2006), the timeline appears realistic, as a number of patients who had LASIK 20 years ago are approaching presbyopic/cataract surgery today and it is still challenging today to choose a multifocal IOL in patients with reshaped corneas (Perez et al. 2009, Naseri et al. 2010, Iijima et al. 2015, Fisher et al. 2018). A simplification of our approach is to treat the aberrations induced by surgery as an additive phase map, instead of replacing the pre-op anterior corneal shape by the post-operative topography. However, we implemented both options and observed that differences were minimal, and opted for the additive phase map because of the ease to implement an induction of SA and coma without impacting higher order aberrations.

Our simulations show significant degradation of the optical quality in post-LASIK eyes (circles in Figures 6.2 and 6.3) in comparison to non-surgical eyes (cross-markers in those figures), particularly for 5.0-mm pupil diameters, as higher amounts of aberrations with larger pupils degrade retinal image quality further. For small amounts of induced SA, the impact of LASIK on performance with implanted IOLs is markedly different in myopic and hyperopic LASIK (see asymmetries in the VS curves in Fig 6.2 (A), for induced -0.72 or +0.20

μm). This may be explained by the fact that negative SA induced by hyperopic LASIK cooperates with the negative SA of the aspheric IOL to compensate the positive corneal SA. For 5.0-mm pupil diameters this results in lower DOF with induced negative SA, with both the monofocal and EDOF IOLs.

While for 5.0-mm pupils both the monofocal and EDOF IOLs appear to be similarly impacted by the LASIK-induced aberrations, the performance of the EDOF and monofocal IOLs is drastically different at 3.0-mm pupil diameters: visual degradation at far, visual benefit at near and DOF is consistently higher with EDOF IOLs in all conditions. Furthermore, at 3.0-mm pupils, the presbyopic-correction profile of the EDOF IOL appears to prevail above the LASIK-induced aberrations, such that the DOF is much higher with the EDOF than with the monofocal IOL for the same cornea and remains relatively constant regardless the magnitude of corneal aberrations. For 5.0-mm both lenses produce similar DOF, 1.22±0.40D and 1.20±0.39D on average for monofocal and EDOF IOL respectively, as VS results, for this reason it was not represented in the graphs.

Halos were quantified by the diameter encircling 50% of the energy. Computational and on bench studies on the halos produced by multifocal IOLs (Alba-Bueno et al. 2014), showed that halos depend on IOL addition, design, and pupil diameter. In post-LASIK eyes, halos are a direct consequence of the induced SA and coma. Unlike other EDOF IOLs, the principles of operation of the EDOF IOL under study do not rely on manipulating the spherical aberration, and therefore spherical aberration and halos do not appear to be coupled when implanted in post-LASIK corneas. Our simulations on non-surgical corneas show lower halos with the EDOF IOL than the monofocal IOL (cross markers in Fig 6.4 (A)), and a small impact of pupil diameter on halo size (cross markers in Fig 6.4-(A) vs Fig 6.4(B)); although these differences do not appear to be clinically relevant as recently published questionnaire-based reports (Bala et al. 2022). The larger halos in post-LASIK eyes for 5.0-mm than for 3.0-mm pupils indicates the large contribution of the LASIK-induced aberrations on halos. Post-hyperopic LASIK eyes with monofocal IOLs exhibit smaller halos than Post-myopic LASIK eyes (5.0-mm pupils), presumably because of the above-mentioned compensatory effect of SA. In the presence of coma, the value of the halo metric increased more asymmetrically with positive and negative SA in EDOF IOL.

Interestingly, the EDOF IOL appears to protect against the halos produced by myopic LASIK, resulting (for the same post-LASIK cornea) in significantly smaller halos than with monofocal IOL when positive SA is induced. While the nature of this favorable interaction between the EDOF IOL profile and SA needs further investigation, the finding is reminiscent of prior reports of favorable interaction between scattering and SA (Perez et al. 2009). That study reported on bench and in vivo contrast sensitivity (CSF) measurements through diffusers, positive SA and various amounts of defocus, and found that, under several conditions, the combination resulted in higher contrast, concluding that the effect was of optical origin.

6.5 Conclusion

We have built pseudophakic post-LASIK models using published data on the LASIK-induced SA and coma, and geometrical information of the IOLs (monofocal and EDOF IOLs). Our simulations show that the Acrysof IQ Vivity IOL produces a significant benefit at intermediate distance at the expense of some degradation at far, although those differences are unlikely clinically relevant (Bala et al. 2022). For large pupils the Vivity IOL behaves similarly to a monofocal IOL, but significantly enlarges the DOF for smaller pupils. In post-LASIK eyes we found that the performance of the Acrysof IQ Vivity was rather immune to the presence of high order aberrations, and exhibited a quite constant DOF for a large range of corneal positive or SA. The Vivity IOL appears particularly suitable in post-myopic LASIK surgery eyes, given the larger DOF expected compared to that produced by the monofocal IOL for smaller pupils, and the smaller halo for larger pupils. While our computer eye models capture corneal shape and the IOL geometry, several aspects could make them rather realistic. For example, computer eye models can incorporate patient-specific geometrical and biometric data of the cornea and lens, IOL tilt and decentrations, or the off-axis location of the fovea, which have shown to reproduce the eye's wave aberration. Also, previous studies from our group have reported on the effect of manufacturing variability and centration experimentally with another IOL, which could be the object of a future study. Further support to these recommendations could be achieved through visual simulations in real post-LASIK patients. On bench Adaptive Optics Visual Simulators or wearable visual simulators (SimVis) are capable of simulating IOLs by mapping a phase map representing the lenses or by temporal multiplexing (Akondi et al. 2017, Vinas et al. 2017, Vinas et al. 2017, Akondi et al. 2018, Vinas et al. 2019, Radhakrishnan et al. 2019, Vinas et al. 2019). Understanding the coupling of the IOL design with the corneal aberrations and pupil size through computer and visual simulations is a valuable avenue to improve lens design and customized IOL selection.

- When compared with a monofocal IOL, the Acrysof IQ Vivity IOL enlarges the DOF, from 1.2 to 2.5 D, at the expense of some degradation at far, VS from 0.61 to 0.52 and 0.67 to 0.98, for monofocal and EDOF IOL, 5.0 and 3.0 mm, respectively.
- In post-LASIK eyes, performance of the Acrysof IQ Vivity is rather immune to the presence of high order aberrations and exhibits a quite constant DOF (less than 0.5 D change) for a large range of corneal SA.
- The Vivity IOL appears particularly suitable in post-myopic LASIK surgery eyes, given the larger DOF expected compared to that produced by the monofocal IOL for smaller pupils, and the smaller halo for larger pupils.

This chapter showed results of the Acrysof IQ Vivity computer simulations and the prediction of the suitability of this IOL for post-LASIK subjects, according with literature results in clinics our findings are in agreement. Next chapter will show the results of Acrysof IQ Vivity simulation accuracy experimentally with SimVis technology.

7 Computational and on bench visual simulation of Acrysof IQ Vivity

The Acrysof IQ Vivity IOL by Alcon Research Labs was evaluated computationally in the previous chapter was simulated on bench using the Spatial Light Modulator of the AO system and implemented for its use with SimVis technology. Experimental tests were performed to study the through focus optical performance both in a model eye and on subjects with paralyzed accommodation.

Part of the on-bench validation was presented in an oral communication in the XIII Reunión Nacional de Óptica (RNO) held in 2021 entitled "**Validation of EDOF IOL simulations in an adaptive optics visual simulator"** and the final results were presented in a poster n the Optics and Photonics for Scientific Progress 2021 (OPSP) entitled **"From real lens design to simulation in SimVis Gekko"** by C. Lago.

The contributions of the author of this thesis, with the help the directors and Sara El Aissati, was to design the computational model eyes, to extract the wavefront maps, to calculate the phase maps and temporal coefficients to simulate the IOL with SimVis, to simulate Vivity IOL with an EO lens correcting the dynamic effects measured in a high speed focimeter, to implement and calibrate an adaptive optics system, to perform the measurements on bench and to analyze the results.

7.1 Introduction

The comparison of the outcomes of computational simulations and experimental studies simulating vision with a particular IOL design are key to clarify the different assumptions on which each of the simulations method rely and to study the limitations of the simulation technologies, such as resolution of abrupt changes in the deformable mirror (DM) or chromatic aberration in the spatial light modulator (SLM).

As stated before, the AO system used in this thesis, allows the comparison between three different simulators that uses different physical principles. While with the SLM, the phase map, extracted from the IOL design, is mapped on the liquid crystal display, with the cuvette channel, the physical IOL is conjugated with the entrance pupil plane of the eye and with the optotunable lens (SimVis technology), the principle of temporal multiplexing creates the appearance of a multifocality on the retina. In addition, the supercontinuum laser source of the system allows performing measurements at different wavelengths and single and double pass measurements allow an independent measurement of the retinal image quality.

We conduced experimental tests on model eyes and on subjects to study the fidelity of the different simulating options (SLM and SimVis) when compared to the cuvette channel.

7.2 Methods

7.2.1 Computational model eyes

The model eye described in chapter 2 was used with the IOL Acrysof IQ Vivity. Two IOL powers were studied (20 and 22 D) with the same corneal power 43 D and a corneal spherical aberration (SA) of 0.28 µm at 6.0-mm pupil diameter, which corresponds to the average SA found in the population (Wang et al. 2003, Beiko et al. 2007). The anterior chamber depth was set to 3.20 mm and axial length was calculated to minimize the RMS spot size using OpticStudio. We studied the optical quality at 3 different pupil sizes (3.0, 4.0 and 5.0-mm diameter) to assess the IOL performance with different light conditions.

The metrics calculated to assess the optical quality were: the Modulation Transfer Function (MTF) at 30 and 15 cycles per degree (cpd), the Visual Strehl ratio (VS). The TF value of the metric was calculated for the three different pupil diameters (3.0, 4.0 and 5.0-mm) in a range of 7 D (from -2 D to 5 D). As before, the DOF was defined as the range of diopters for which the VS was equal or above 0.12 (Yi et al. 2011). All these metrics were calculated with custom scripts written in Matlab that used as input the wavefront maps extracted from the model eyes in OpticStudio.

7.2.2 IOL simulation with the SLM

The procedure to simulate an IOL in the SLM of the AO system was detailed in chapter 2. Essentially a phase map that represents the aberrations of the lens was calculated by subtracting the wavefront aberrations of the computational pseudophakic eye model eye with the IOL implanted described previously, with the wavefront aberrations of the same model eye with a neutral IOL, simulated with a paraxial surface in OpticStudio.

The phase map was mapped in the SLM and projected onto the pupil of the subject with the AO system so that the optical characteristics of the intraocular lens, i.e. multifocality, additional spherical aberration or other aberrations, could be experienced by the subject that viewed the stimulus projected in the display of the AO system through those particular optics.

7.2.3 IOL simulation with the SimVis

The procedure to simulate a lens design with the SimVis channel was also described in detail in chapter 2. Basically, the optical power of an optotunable lens was changed at high speed to mimic the TF VS ratio of the lens, trough temporal multiplexing.

First the through focus VS of the phase map described in the previous section was calculated with Fourier Optics by calculating the MTF and then multiplying by the average of the human eye (Mannos et al. 1974) divided by the diffraction limited MTF for the same pupil size weighted with the human CSF. Then the temporal coefficients that needed to be applied to a tunable lens were calculated using custom programs developed by 2EyesVision (Akondi et al., 2017, 2018) and the simulation was validated using a high-speed focimeter, where the time spent at each optical power was calculated. The methods used for this simulation accounted for the dynamic effects that appear when driving the tunable lenses at high speed (Akondi et al. 2018, Dorronsoro et al. 2019).

7.2.4 IOL simulation using the cuvette channel

The cuvette channel was described Chapter 2 and in a recent publication (Benedi-Garcia et al. 2021). A physical IOL was inserted in a cuvette and projected onto the eyes pupil by using a Rassow telescope, that consisted of a 4-focal system formed by the IOL and a 20 D achromatic lens, to compensate 20 D of the optical power of the IOL (the cuvette is placed in a conjugated pupil plane with the artificial eye). The subject viewed the stimulus through the cuvette channel that formed an afocal system. When a lens with a base power different than 20 D was inserted on the cuvette, in this study 22 D, the 2 D residual defocus was compensated with the Badal system.

7.2.5 Experimental measurements on the artificial eye

Through focus single (1P) and double pass (2P) images were obtained using the model eye. Essentially, a Snellen E letter (letter size 45 pixels, 0.15 degrees angular subtend, equivalent to a VA of 0.3 LogMAR) was shown in the DMD and illuminated with the super continuum

LASER and the image projected on the artificial eye retina was obtained with a CCD, and by substituting the CCD with a diffuser, the spot projected on the retina was captured with the double pass retinal image camera. Optical quality was estimated from the images using the metrics described before. In essence, the quality of 1P images was estimated by cross correlating them with an image captured by correcting all optical aberrations in the system, and the 2P image quality was estimated with the full width at half maximum (FWHM) of the double pass PSF captured by the camera.

Both, 1P and 2P TF optical quality curves were studied when the 22 D Acrysof IQ Vivity IOL was simulated with the three simulators described before (SLM, IOL on cuvette and SimVis technology) with 3 different pupil diameters (3.0, 4.0 and 5.0-mm). In addition, the measurements were performed using a monochromatic stimulus (green, 555 nm) and polychromatic light (white light).The differences between the three optical simulations of the lens (SLM, SimVis and cuvette) were evaluated using the root mean square (RMS) of the difference between TF optical quality curves.

7.3 Results

7.3.1 Optical quality and DOF of the computational model eyes

Figure 7.1 shows the OpticStudio wavefront aberrations obtained from the pseudophakic model eyes implanted with the 20 D and 22 D Acrysof IQ Vivity IOL respectively. Data are shown for different pupil diameters and as expected, the smaller pupil diameters are cropped and magnified versions of the maps for larger pupil diameters. Phase in this figure is expressed in waves (0.55 µm). As can be observed there are no differences in the phase map between the two powers.

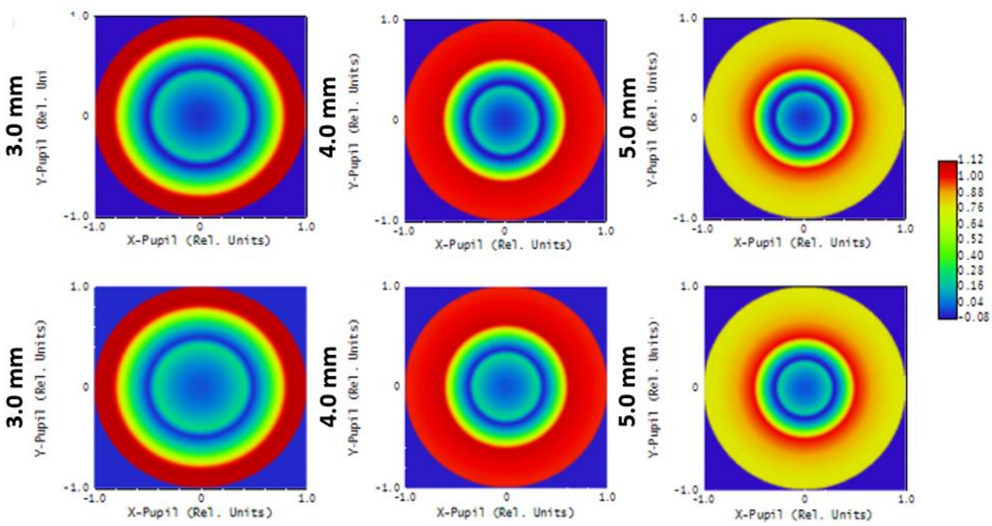

Fig. 7.1: *Wavefront aberrations of the model eye implanted with the Acrysof IQ Vivity IOL 20 D (top) and 22 D (bottom), for 3 different pupil diameters (3.0, 4.0 and 5.0-mm).*

Figure 7.2 shows the TF MTFs at two different frequencies (30 and 15 cpd, according with the ANSI Z80.35-2018) and the TF VS in eyes implanted with the Vivity IOL with 22 D as well as the 0.12 threshold value used to calculate the DOF (Yi et al. 2011). As expected, we obtained the same TF curve when the 20 D IOL was simulated. For 20 D similar results were found (not shown here).

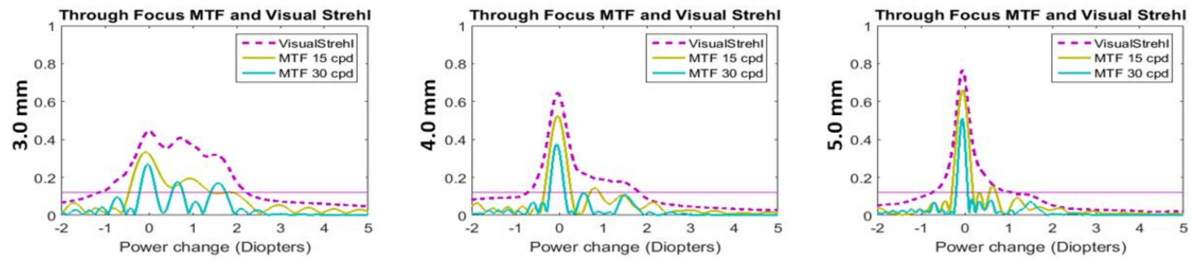

Fig. 7.2: *TF image quality for the 22 D Acrysof IQ Vivity IOL, for 3 different pupil diameters (3.0, 4.0 and 5.0-mm), in model eye. Image quality metrics: MTF at 15 and 30 cpd and VS. The horizontal line indicates 0.12 value (used in DOF metric).*

The difference in metric value at best focus changed considerably with pupil size from 3.0 and 5.0-mm pupil diameter the metric increased from 0.27 to 0.5, from 0.33 to 0.66 and from 0.44 to 0.76 for MTF at 30 cpd, MTF at 15 cpd and VS, respectively, with most of the change occurring below 4.0-mm pupil diameter.

The change in DOF with pupil size was gradual (see Figure 7.2) and decreased when the pupil diameter increased from 3.29 D for 3.0-mm, to 2.57 D at 4.0-mm, and 1.89 D at 5.0-mm pupil diameter.

7.3.2 Phase map representation of the Acrysof IQ Vivity IOL.

Figure 7.3 shows the phase map representation of the 22 D Acrysof IQ Vivity IOL at 3 different pupil diameters (3.0, 4.0 and 5.0-mm). These phase maps were represented in the SLM for IOL simulation.

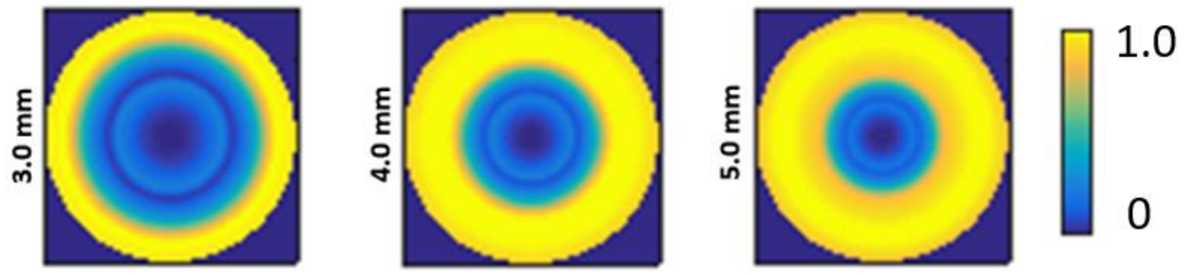

Fig. 7.3: Phase maps representing the Acrysof IQ Vivity IOL profile for 22 D, and three pupil diameters (3.0, 4.0 and 5.0-mm). Units of the phase map are waves (0.55 nm).

7.3.3 SimVis representation of the Acrysof IQ Vivity IOL

The phase maps with the information of the phase added by the IOL shown in Figure 7.3 were used to calculate the TF performance of the IOL in a range of 7 D (from -2 to 5 D). The SimVis temporal coefficients were adjusted so that the SimVis simulation pattern replicated the TF optical performance of the real lens and the results of the simulations are shown in figure 7.4 for three different pupil diameters (3.0, 4.0 and 5.0-mm). The graphs represent the nominal TF optical performance obtained computationally from the lens phase map (violet lines), and the expected TF performance of SimVis simulation when applying the temporal coefficients to a tunable lens (orange lines). The differences between the Acrysof IQ Vivity TFVS and the SimVis simulated TFVS were always below 0.1 and the mean RMS of the difference between curve was 0.016, 0.013 and 0.019 for 3.0, 4.0 and 5.0-mm respectively. Similar results (not shown here) were obtained with the 20 D IOL.

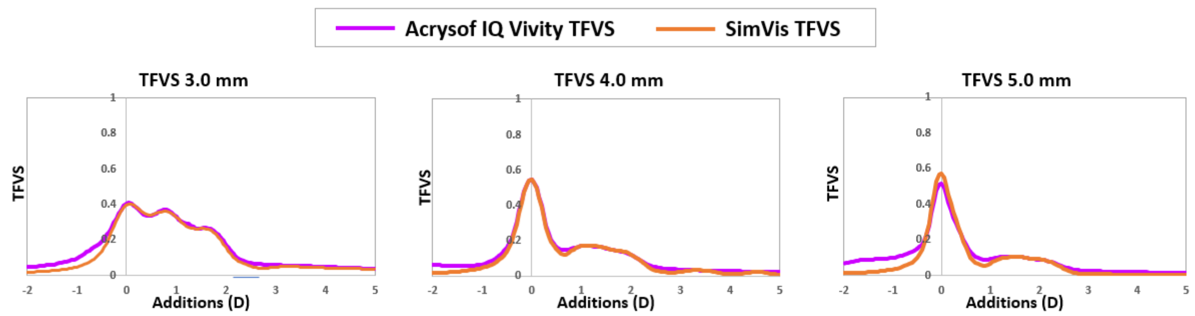

***Fig. 7.4:** TFVS performance of the Acrysof IQ Vivity IOL (magenta) and the SimVis simulation of this lens (orange). Data are for the 22D Acrysof IQ Vivity IOL and 3 pupil diameters (3.0, 4.0 and 5.0-mm).*

The physical IOL provided by Alcon healthcare S.A. had a power of 22 D and the SimVis simulation for this study was performed using the phase map of the IOL with this power. In the figure 7.5, the upper graphs show the set of SimVis temporal coefficients used to represent the IOL for the three pupil diameters (3.0, 4.0 and 5.0-mm). The simulation using these coefficients was validated experimentally using the high-speed focimeter described in chapter 2. Essentially the dynamic change of focus of the tunable lens was obtained and the VS was estimated from the change of focus to evaluate the TFVS of the IOL simulation with the correction of the dynamic effects of the optotunable lens. The TF performance of IOL (computational SimVis TFVS, orange) and the performance of the SimVis simulation (Experimental SimVis TFVS, grey) are represented in figure 7.5. The differences were always lower than 0.05 and the mean RMS of the difference between curves was 0.015, 0.027 and 0.020 for 3.0, 4.0 and 5.0-mm respectively.

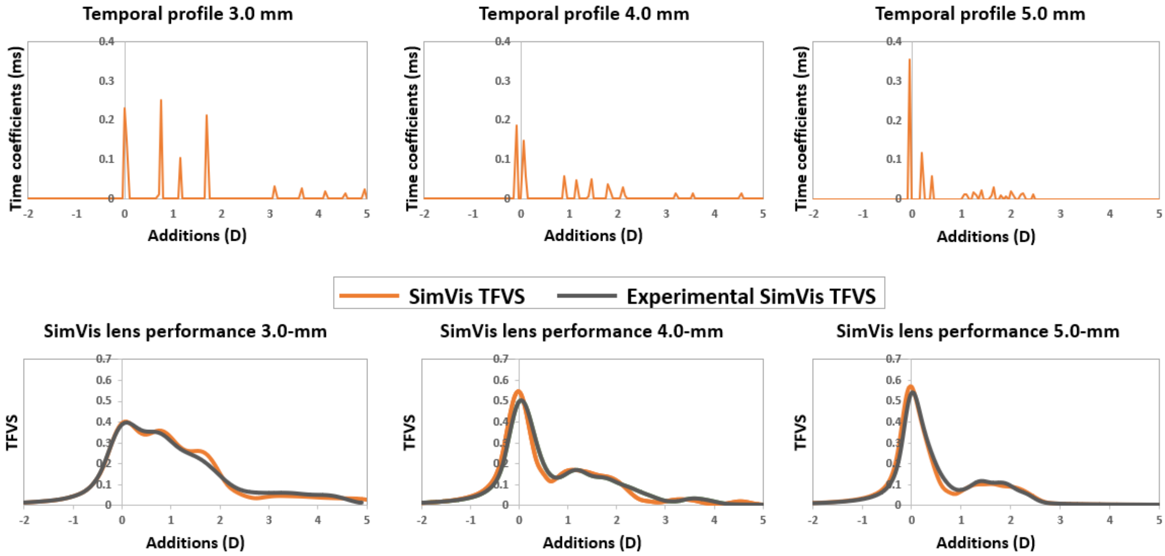

Fig. 7.5: *Temporal coefficients representing the lens on SimVis (top) and TF SimVis VS performance (bottom) of the Acrysof IQ Vivity IOL 22D (orange) and the experimental SimVis TFVS simulation of the lens (grey). Data are for the 3 pupil diameters (3.0, 4.0 and 5.0-mm).*

7.3.4 Through Focus optical quality when simulating the lens with SLM, SimVis and the cuvette channel.

On-bench through focus single and double pass optical quality

Examples of the 1P and 2P image series are shown for 3.0-mm (figure 7.6) and 5.0-mm pupils (figure 7.7), for the three simulation modalities: SLM, SimVis and Cuvette.

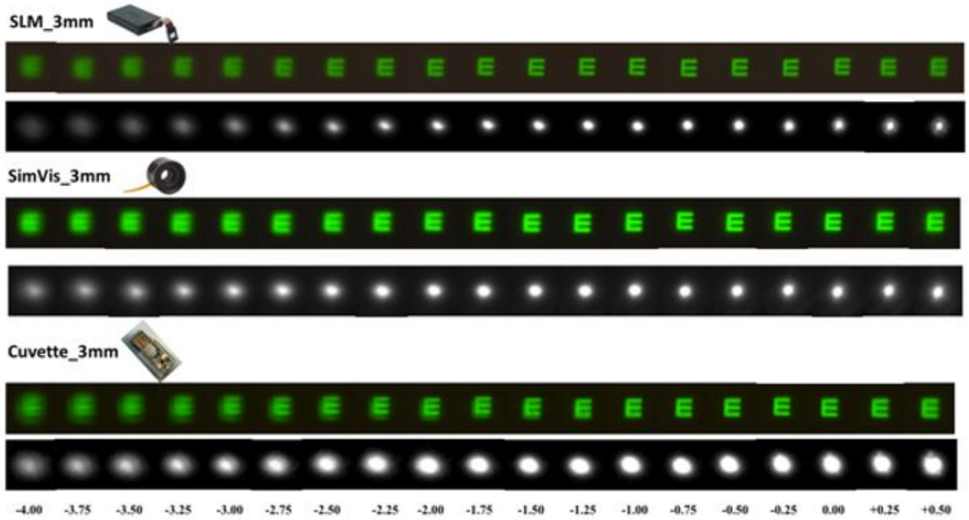

Fig. 7.6: *TF series of single-pass images of an E-letter stimulus (top images) and double-pass images of a spot (bottom images) in an artificial eye, through the Acrysof IQ Vivity Lens (22 D) simulated in the SLM (upper), in the SimVis (middle) and the physical lens immersed in the cuvette (bottom) for 3.0-mm pupils. Double pass images were captured with a 12-bit camera and seem to be saturated in the image. All data are for monochromatic green light.*

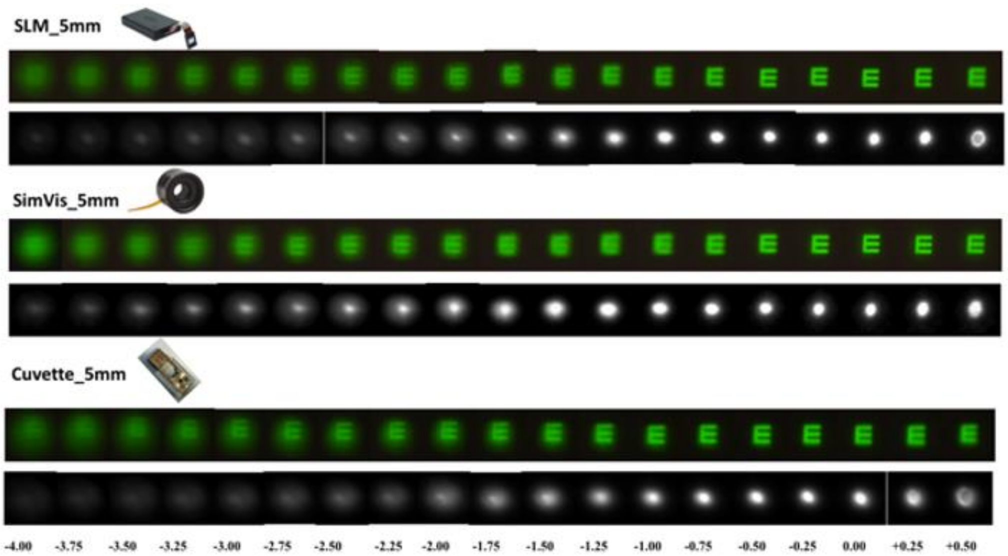

Fig. 7.7: *TF series of single-pass images of an E-letter stimulus (top images) and double-pass images of a spot (bottom images) in an artificial eye, through the Acrysof IQ Vivity Lens (22 D) simulated in the SLM (upper), in the SimVis (middle) and the physical lens immersed in the cuvette (bottom) for 5.0-mm pupils. All data are for monochromatic green light.*

Figure 7.8 shows the image quality calculated using cross correlation in the 1P images (upper row) and FWHM of the obtained spot in 2P images (bottom row). The results of the three different pupil diameters are shown for the three simulating channels: SLM (green), SimVis (orange) and cuvette (purple).

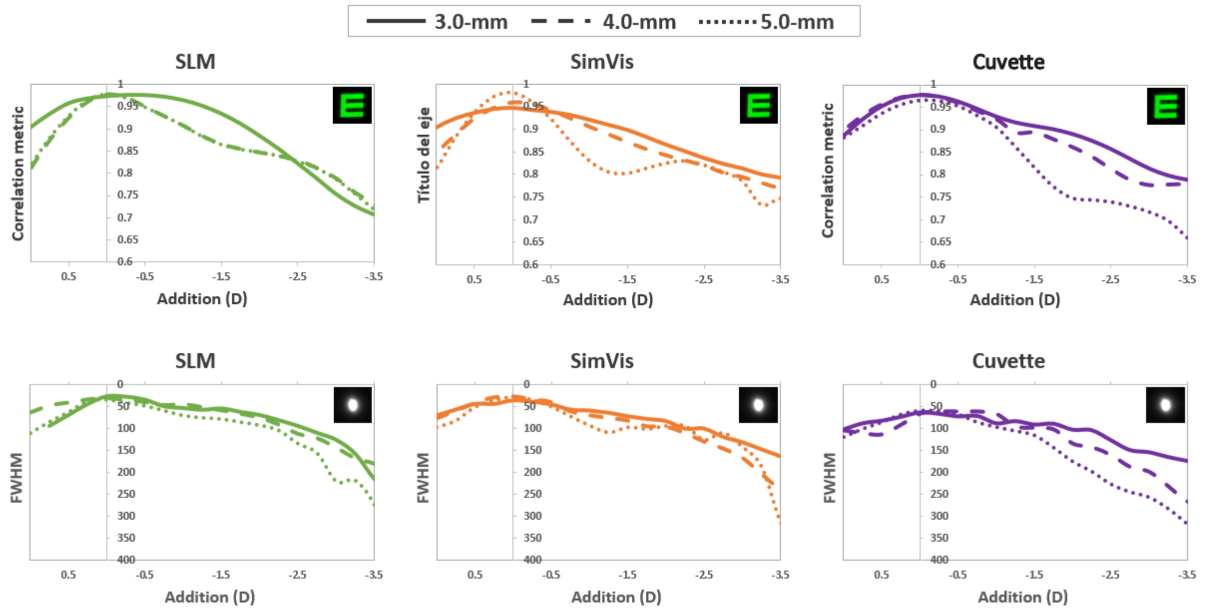

Fig. 7.8: *Top. TF for E-letter stimulus projected on the artificial retina (CCD) of an artificial eye (correlation metric). Bottom, for double-pass retinal imaging of a point (FWHM), for three different pupil diameters (3.0, 4.0 and 5.0-mm) and the three simulating platforms: SLM (green), SimVis (orange) and Cuvette (purple).*

From the above curves it is evident that the DOF decreases when the pupil diameter increases with the three simulations. However, the change in the peak metric value is more subtle and seems to be higher for 5.0-mm pupil diameter when the lens was simulated with SimVis, about the same value with SLM and with the cuvette.

The comparison between the three simulating platforms (SLM, SimVis and Cuvette) for the three pupil diameters (3.0, 4.0 and 5.0-mm) is presented in figure 7.9.

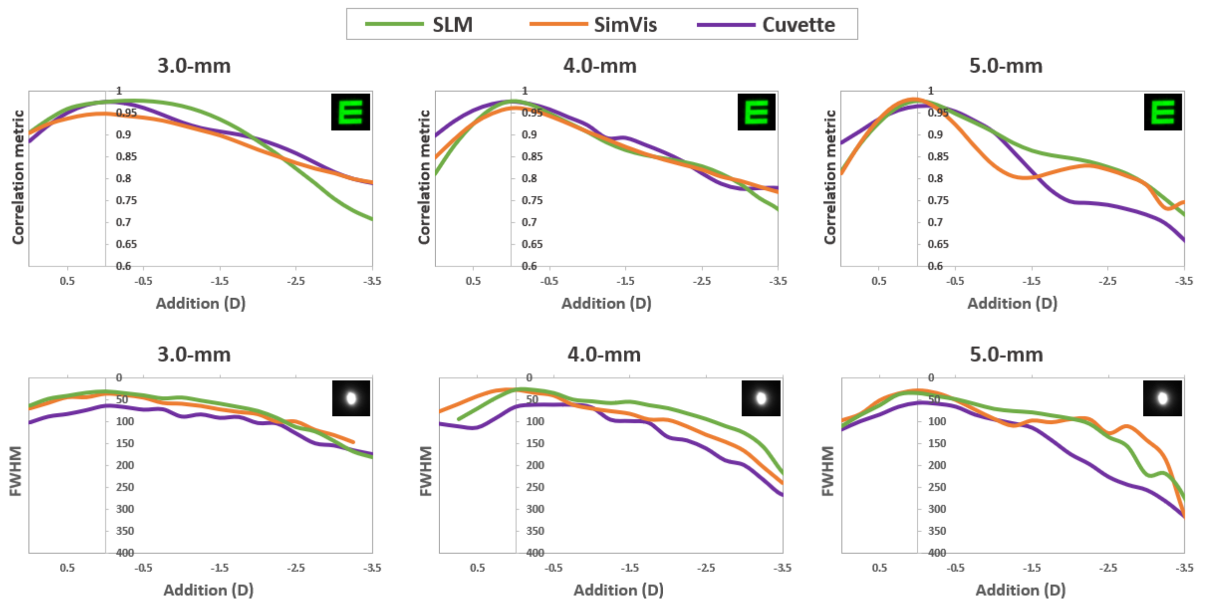

Fig. 7.9: *Top. TF for E-letter stimulus projected on the artificial retina (CCD) of an artificial eye (correlation metric). Bottom, for double-pass retinal imaging of a point (FWHM), for different pupil diameters (3.0, 4.0 and 5.0-mm) in the three simulating platforms: SLM (green), SimVis (orange) and Cuvette (purple).*

The TF curves in Fig 7.9 show a good correspondence between the three simulation methods: SLM, SimVis and cuvette channels. The fit between simulations was assessed using the cuvette channel with the physical IOL as reference and calculating the RMS difference of the TF curves for a given simulation (SLM or SimVis) for the entire focus range. Figure 7.10 shows the RMS difference for the TF of the single pass E-stimulus images (top), and for the TF of the double-pass images (bottom). Differences between the physical lens and simulations tend to be higher for larger pupils, but they are generally small (less than 10% of the metric range).

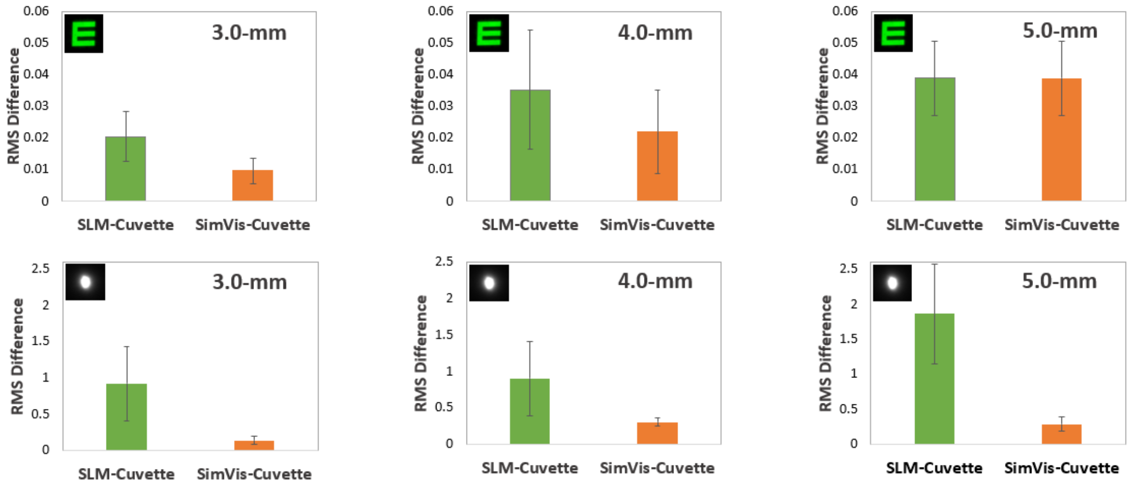

Fig. 7.10: *RMS difference of the TF curves between the SLM (green) or SimVis (orange) simulated lens with the cuvette, for single pass E-stimulus images (top) and double-pass images (bottom) for three pupil diameters (3.0, 4.0 and 5.0-mm).*

Figure 7.11 shows the performance with green light (555nm) and white light illumination of the stimulus, when the IOL was immersed in the cuvette at 5.0-mm pupil diameter. As can be observed, with white light the correlation metric decay is slower than with green light.

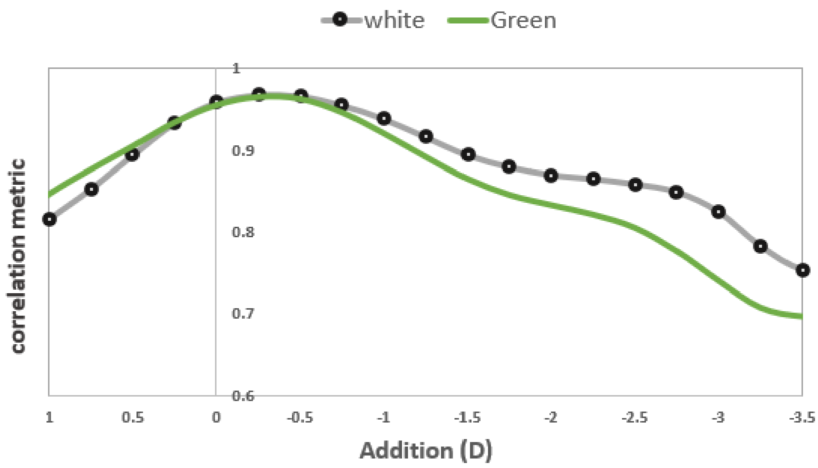

Fig. 7.11:*TF curves (for E-letters stimulus) in green (green solid line) and white (solid dots). Data are for 5.0-mm pupils and correspond the Acrysof IQ Vivity lens (22 D) immersed in the cuvette.*

7.4 Discussion

The Acrysof IQ Vivity IOL was evaluated computationally in pseudophakic model eyes and on-bench with physical eye models, in a cuvette and simulated as a phase map and temporal. Multiplexing with different visual simulators (in different channels in an AO visual simulator platform). As discussed in the previous chapters, we designed a custom model of the cornea with a spherical aberration equal to the average spherical aberration found in the population (Want et al. 2003, Beiko et al. 2007). In the previous chapter we demonstrated little influence of corneal spherical aberration, therefore our tests did not include varying spherical aberration.

The results of the computational simulations performed with the Acrysof IQ Vivity IOL show that the performance is similar between the 20 and 22 D IOL power lenses (Figure 7.2). Also, the simulations performed to calculate the time coefficients needed to simulate this lens with SimVis show a good agreement between the nominal and the theoretically calculated TFVS with SimVis (Fig 7.4 and 7.5), confirming the optical similarity through focus of both lens powers. Studying different powers can be important since in some cases, there can be slight differences of performance between IOLs in the same catalog across powers (chapter 3).

We found that the optical quality increased when increasing the pupil diameter from 0.33 at 3.0-mm pupil diameter to 0.76 at 5.0-mm pupil diameter (VS metric) and that the DOF increased with small pupil diameter: from 1.8 D at 5.0-mm to 3.35D at 3.0-mm. These results are in agreement with those presented by Fernández-Vega-Cueto et al. 2022, who reported the TF MTFs curves of Acrysof IQ Vivity in optical bench at two pupil diameters 3.0 and 4.5-mm and found that MTF peak value at distance increased with larger pupil (28.9 and

38.9 for 3.0 and 4.5-mm respectively). In another study by Pieh et al. 2022, reported TF MTFs with different IOLs, at 3.0 and 4.5-mm pupil diameter at 546 nm, and showed an increase of energy at far when the pupil increased, and an extension of DOF when pupil decreased.

Despite the change in IOL performance with pupil diameter, the DOF was always above 1.5 D and the peak VS above 0.3. As discussed in the previous chapter, our results agree with those performed by Pastor-Pascual et al. 2022 that used aberrometry measurements on normal patients implanted with Vivity IOL and estimated that DOF was 2.50D, and with those by Gundersen et al. 2021, who measured binocular Visual Acuity in 40 patients and reported an average DOF of 2.5 D.

In the on-bench measurements data. shown in Fig 7.8, EDOF expansion is observed qualitatively for 3.0-mm pupils in 1P E-stimulus TF curves, and 2P TF curves across the 3 active elements evaluated (SLM, SimVis and cuvette) when compared with the results for 5.0-mm pupil diameters. These results agree with the data on the influence of pupil diameter in the performance of the Vivity IQ IOL described in an FDA report (Schallhorn 2021) that showed an increase in DOF (from 1.00 to 2.10D) in patients when the pupil diameter decreased (from more than 4.0-mm to less than 3.0-mm)

The quality of simulation was assessed by the RMS difference of the TF curves for a given simulation (SLM or SimVis) when compared with data in the cuvette, which were taken as reference. Although differences between simulators with the cuvette increased at larger pupil diameters (5.0-mm) they are generally small (less than 10% of the metric range). Differences can arise from different factors. The phase presented in the SLM is limited between 0 and 2π and was wrapped for presentation. Since with larger pupils the aberration values are larger, more wrapping is needed to simulate the IOL than for small pupils. The wrapping process could increase the scattering of light in the SLM surface and decrease image quality when compared with other simulator techniques. SimVis also deviated from the simulations using the cuvette. With SimVis, different simulations were performed for the different pupil sizes and the three were validated using the focimeter and the largest differences are found for the largest pupil sizes. During the experiment the lens was carefully centered, all the measurements were performed in the same day to avoid possible differences arising from IOL misalignments. We ensured that there were not bubbles in the cuvette that could increase the scattering, nonetheless, micrometric decentration could results in small deviations of the TFVS.

The IOL performance at 5.0-mm was measured using the cuvette channel with white light to compare with the results obtained in monochromatic light (green, 555-nm) and the results show an increase of the DOF with the IOL performance when is measured with polychromatic light. This was also observed in an on-bench study by Pieh et al. 2022 with Acrysof IQ Vivity measured at 546 nm and white light.

7.5 Conclusions

In this study, we conclude from our computational analysis on Acrysof IQ Vivity IOLs optical performance that the behavior is not different for the IOL powers 20 and 22 D, and that this EDOF IOL offers high optical performance in a range of pupil diameters 3.0 to 5.0 mm at best focus with a higher optical quality for 5.0-mm pupil diameters and a widest DOF for 3.0-mm pupil diameters. These results agree with previous reports found in the literature with measurements on ISO approved model eyes or on patients after cataract surgery.

The phase maps to simulate the lens in an SLM and to calculate the temporal coefficients needed to simulate the lens with SimVis technology were estimated and the lens was simulated in the AO system with a good correspondence (RMS difference less than 10%) with the simulation based on introducing the lens on a cuvette and projecting it on the eye's pupil with a Rassow telescope, confirming the ability to simulate the Acrysof IQ Vivity IOL with high fidelity.

- Acrysof IQ Vivity is a pupil dependent intraocular lens with high optical performance at 5.0-mm pupil diameters, and a maximum DOF with 3.0-mm pupil diameters.
- The lens can be simulated in the SLM and with SimVis technology and a good correspondence was found (RMS difference less than 10%) between the simulations when compared to the cuvette channel.
- SimVis technology can be used to simulate this intraocular lens with temporal multiplexing.

8 SimVis simulation of PresbyLASIK corrections: Computational, on-bench and clinical validation of corneal ablation patterns for SimVis Gekko

This study validates a new application for the SimVis Gekko, the binocular simultaneous visual simulator, that used the SimVis technology based on temporal multiplexing to simulate, for first time, corneal ablation multifocal patterns before PresbyLASIK refractive surgery. It was performed in collaboration with the company Schwind eye-tech-solutions GmbH, Kleinostheim, Germany.

The preliminary results were presented as a poster presentation at The European Society of Cataract and Refractive Surgery congress 2022 under the title **“SimVis simulation of Lasik corneal ablation patterns for presbyopia correction- Computational, on-bench and clinical validations”** and the corresponding article is in preparation.

The contributions of the author of this thesis, with the help of co-authors, were the extraction of power profiles, computational and on-bench validations with a high-speed focimeter of the SimVis simulations for different pupil diameters, and clinical protocol design for clinical validation in subjects wearing the SimVis Gekko.

8.1 Introduction

As described in the introductory chapter, there are different presbyopia corrections strategies such as glasses, multifocal contact lenses, monovision, IOLs, corneal inlays, corneal shrinking techniques (conductive keratoplasty) and corneal ablation for presbyopia (Titiyal et al. 2021). Laser in situ keratomileusis for presbyopia correction (PresbyLASIK) (Shetty et al. 2020) is a surgical technique that combines the LASIK ablation pattern, to correct for the subject’s refractive distance error, and the correction for near/intermediate distances to reduce the dependency of spectacle in subjects with presbyopia. Two different techniques can be performed: peripheral or central PresbyLASIK technique, central being the most used in clinics (Vargas et al. 2017). In central PresbyLASIK technique, the central ablation pattern corrects for near vision and the peripheral pattern corrects for far vision. The PresbyLASIK market is increasing with different kinds of corneal ablation patterns that are available such as CustomVue™ VISX (AMO Development LLC, Milpitas, California, USA) (Jung et al. 2008), Supracor (Technolas Perfect Vision GmbH, München, Germany) (Ryan et al. 2013) or PresbyMax (SCHWIND eye-tech-solutions GmbH, Kleinostheim, Germany) (Baudu et al. 2013). Therefore, the need to develop techniques to simulate accurately what the subjects would experience after PresbyLASIK surgery is crucial. As far as we know, there is no visual simulator able to simulate PresbyLASIK surgery beforehand. Nonetheless, being able to simulate these patterns before surgery will avoid discontent after PresbyLASIK treatment and/or a new intervention with "presby reversal” surgery (Luger et al. 2014).

SimVis Gekko, a binocular simultaneous visual simulator based on liquid membrane optotunable lenses (TLs) (Dorronsoro et al. 2019) working under temporal multiplexing (Akondi et al. 2017) proves to simulate accurately multifocal intraocular lens (IOLs) designs (Akondi et al. 2018, Vinas et al. 2019, Vinas et al. 2019, Sawides et al. 2021) and multifocal contact lens (MCLs) designs (Vinas et al. 2020, Barcala et al. 2020) demonstrating that the SimVis simulations mimic the real lens performance. With this study, we go beyond and demonstrate that the SimVis technology can accurately simulate corneal ablation patterns for presbyopia corrections and make the SimVis Gekko visual simulator more versatile. In collaboration with Schwind eye-tech solutions GmbH (Kleinostheim, Germany), we simulated PresbyLASIK corrections – PresbyMAX – for different additions and validated the simulation in three phases: computationally using custom Matlab routines, on-bench using a high-speed focimeter (Dorronsoro et al. 2019) and clinically on subjects wearing the SimVis Gekko.

8.2 Methods

8.2.1 Corneal ablation profiles

SCHWIND eye-tech-solutions GmbH (Kleinostheim, Germany) is a company that produces refractive surgery lasers and develops Corneal Ablations patterns for PresbyLASIK (ablation of the stroma with an excimer laser to create a multifocal pattern in the cornea to treat presbyopia), LASIK (to correct defocus and astigmatism), and TransPRK (laser ablates the cornea directly over the epithelium until the stroma with a pattern designed to correct defocus and astigmatism). The PresbyMAX is a central PresbyLASIK with bi-aspheric ablation profile that multifocally corrects both eyes (Luger et al. 2012, Uthoff et al. 2012). Three different patterns were designed to correct presbyopia with PresbyMAX, all the patterns are designed to correct far vision for the dominant eye (DE); and to provide good intermediate/near vision for the non-dominant eye (NDE). Among the different designs for presbyopia corrections, there are:

(1) µ-monovision pattern: both eyes are treated symmetrically with the same multifocal pattern. The non-dominant eye (NDE) pattern has the distance target shifted with slight myopic defocus spreading the DOF until near vision; while DE has the far target at 0D and near target covers intermediate distance.

(2) hybrid pattern: The ablation pattern is asymmetric between eyes, in NDE is used the same multifocal pattern than in µ-monovision while DE is treated with half of the multifocality, with a half of DOF.

(3) Monocular pattern: the multifocal ablation pattern is only applied to the NDE (designed for intermediate and near vision), and the DE is corrected with a 0D monofocal.

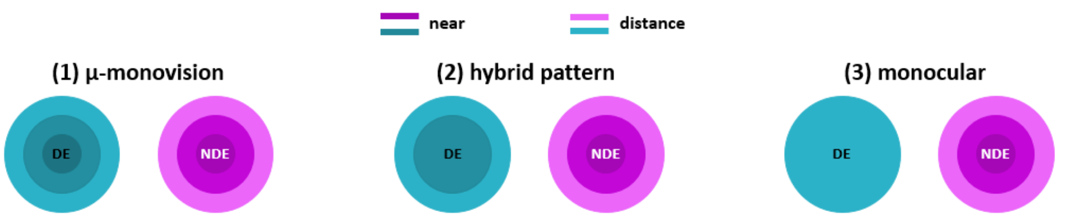

Fig. 8.1: *Classification of the 3 types of ablation pattern. Pink line represents the non-dominant eye (NDE) and the blue line the dominant eye (DE). (1) is the µ-monovision pattern, (2) hybrid pattern and (3) monovision pattern. All of them are represented for a refraction at far 0D and Addition of 2 D.*

Power profiles of the local refractive corrections applied to the cornea for the Hybrid design were provided by Schwind eye-tech-solutions company for a 0D refraction (emmetropic eye correction) and five different additions ranging from 1.50 to 2.50 D in 0.25D steps, for both dominant (DE) and non-dominant (NDE) eye patterns, in the same format as published by Luger et al. 2012 and Uthoff et al. 2012. As an example, figure 8.2 shows the local corneal refraction profiles for NDE (pink) and DE (blue) patterns for a 1.75D addition.

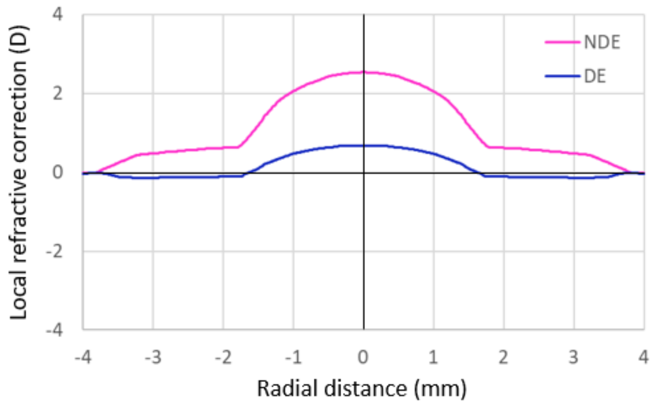

Figure 8.2: *Example of data provided by Schwind eye-tech-solutions: Hybrid local refractive correction profiles (0D refraction and 1.75D addition) applied to the cornea as a function of radial distance for the dominant eye (DE, blue) and non-dominant eye (NDE, pink) patterns.*

8.2.2 General pipeline to include the SimVis lens into the SimVis Gekko

Figure 8.3 shows the overview of the pipeline to validate a SimVis lens from the local refractive correction profile (showed in the methods chapter for Isopure IOL) for the NDE hybrid profile at 4.0-mm pupil diameter with a 1.75D, provided by SCHWIND-eye-tech-solutions. The SimVis temporal profile of the corneal ablation pattern was estimated from calculations of the corresponding through focus optical quality in terms of through Focus Visual Strehl ratio (TFVS).

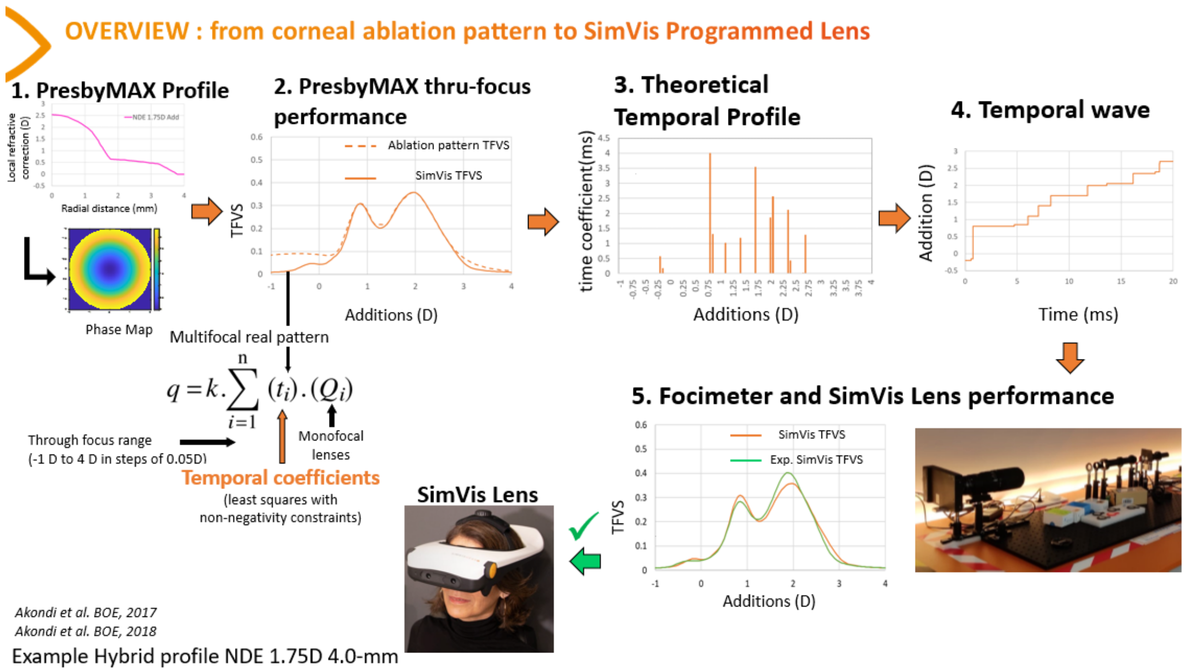

Fig.8.3: *Characterization and validation of a corneal ablation pattern: example for hybrid NDE with addition of 1.75D for 4.0-mm pupil diameter. (1) Calculation of the wave aberration (phase map) from the local refractive correction profile of the design. (2) Calculation of the through focus performance (Visual Strehl optical metric, TFVS ratio) for the PresbyMAX design and from the SimVis Lens calculated. (3) the SimVis temporal coefficients obtained through an iterative optimization procedure and (4) obtention of the SimVis temporal profile. (5) On bench validation of the SimVis lens, measuring the Experimental SimVis Lens using the high-speed dynamic focimeter provided with a high-speed camera (3823 fps). Then the SimVis Lens can be used in the SimVis Gekko, on subjects.*

First, the wave aberration map (phase map) of each PresbyMAX pattern was calculated from the corresponding local refractive correction profile provided by SCHWIND-eye-tech-solutions. Then, the MTF was estimated from the wave aberration and pupil function using Fourier Optics. The Visual Strehl ratio (VS) was used as an optical quality metric, estimated as the neural contrast sensitivity weighted Modulation Transfer Function (MTF) of the system (Marshack et al. 2004, Iskander et al. 2006). The through-focus performance (TFVS ratio) of the design was evaluated, Figure 8.3(2), and SimVis temporal coefficients, Figure 8.3(3), describing a lens from the theoretical through focus calculation described before (Akondi et al. 2018, Akondi et al. 2017) were calculated. These temporal coefficients stand for the weighting factors of a series of defocused monofocal PSFs, tuned to match the through focus optical quality of the corneal ablation pattern design in an iterative optimization procedure to obtain the temporal profile of the SimVis Lens, Figure 8.3(4). Then, the SimVis lens was validated on-bench with a high-speed dynamic focimeter [1], provided with a high-speed camera (3823 fps), where the through focus visual Strehl ratio of the Experimental SimVis Lens is evaluated with specific Matlab custom routines. The SimVis

Lens was validated when it mimics the real lens design in terms of TF Visual Strehl ratio, where the peaks of the design are not shifted more than 1/8 diopter from the real lens design. The number of temporal coefficients will vary according to the pattern design.

8.2.3 Computational validation

First, phase maps were calculated using custom Matlab programs from the local refractive correction profiles of the corneal ablation patterns. In total, 30 phase maps were generated corresponding to DE and NDE profiles, 5 different additions (1.5 to 2.5 in 0.25D step) and 3 different pupil diameters of 3.0, 4.0 and 5.0-mm. Figure 8.4 shows, as an example, the phase Maps for the Hybrid design for 1.75D add, the DE and NDE patterns for 3.0, 4.0 and 5.0-mm pupil diameters.

Then, the through focus visual performance (in terms of Visual Strehl ratio) for each PresbyMAX pattern were calculated using custom Matlab routines (Estimated TFVS) and the SimVis temporal profiles evaluated according to the temporal coefficients that best represents the corneal ablation profile for temporal multiplexing and the SimVis lens TFVS calculated.

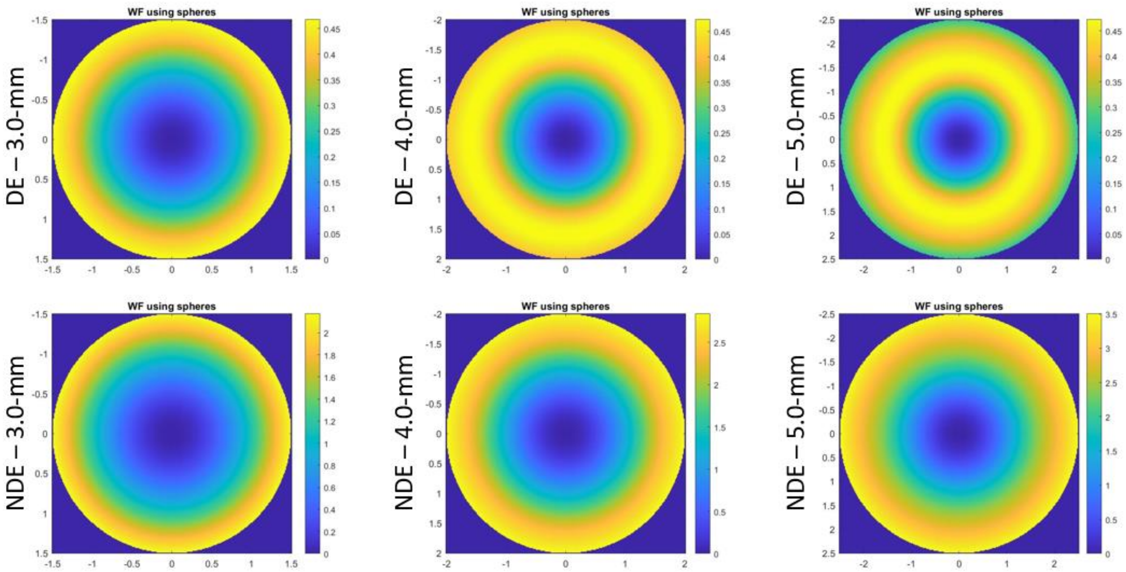

Fig. 8.4: *6 Phase map representation of hybrid pattern with addition of 1.75D, up the Dominant eye (DE) for 3.0, 4.0 and 5.0 -mm pupil diameter (from left to right), below the Non-Dominant Eye (NDE) representation for the 3 pupil diameters.*

8.2.4 On Bench validation of the SimVis PresbyMAX ablation patterns

A high-speed focimeter provided with a high-speed camera (3823 fps) explained in detail in chapter 2 section 2, (Dorronsoro et al. 2019) was used to validate on-bench the SimVis simulations of the 30 hybrid corneal ablation profiles. An optotunable lens EL-3-10 (Optotune, Switzerland, reference ARAA2311) was placed in a conjugated pupil plane and the tunable lens was characterized to check for dynamic effects that should be corrected.

Then, the optical quality of the SimVis simulations (experimental SimVis TFVS) were evaluated using custom programs in Matlab and compared to the TFVS of each PresbyMAX patterns.

8.2.5 Clinical measurement on subjects wearing the SimVis Gekko visual simulator while simulating SimVis PresbyMAX ablation patterns

Local refractive correction profiles

To clinically validate the SimVis simulations of corneal ablation patterns, visual acuities measured in subjects wearing SimVis Gekko in a clinical environment were compared to visual acuities measured in subjects that underwent PresbyLASIK (PresbyMAX) surgery, based on literature one year after surgery (Luger et al. 2020). Luger and colleagues measured Through Focus Visual Acuities (TFVA) in 19 subjects (51±3 years old, range from 45 to 55 years; SEQ=-0.57D±1.98D) with a mean addition of 1.76±0.36D and measured in photopic condition with a pupil diameter in photopic condition smaller than 3.0-mm. Therefore, to compare the TFVA measured with the SimVis Gekko simulating PresbyMAX pattern to the published data form Luger and colleagues, the SimVis simulations of a hybrid profile at 3.0-mm pupil diameter and 1.75D add for dominant (DE) and non-dominant (NDE) eyes were used in the clinical validations.

Subjects

A total of 20 healthy presbyopic subjects (54±5 years old, range from 46 to 62 years) participated in the study. The refraction was measured with a mean SEQ = RE 0.60±1.93D (right eye, RE) and 0.55±1.99D (left eye, LE). Table 8.1 summarized subject's information in terms of ages and refractions.

Motor dominance was assessed, as it is of relevance to decide which simulation (DE or NDE) was projected in the subject's eyes before measuring the though focus visual acuity (TFVA) curves. Subject's refraction was corrected for far in both eyes with trial lenses in a dedicated slot of the SimVis Gekko for all TFVA curve measurements.

Through focus visual acuity measurements

Three TFVA curves were measured in binocular conditions in a range from -4 to 1D, in steps of 0.50D:

(1) TFVA curve measured with a monofocal lens simulated in both eyes in the SimVis Gekko
(2) TFVA curve measured with the SimVis Gekko simulating the hybrid 1.75D 3.0-mm DE (in the dominant eye of the subject) and NDE (in the non-dominant eye of the subject) patterns. In this case, the myopic defocus designed in the hybrid profile was kept and only the refraction of the subject is corrected, providing information of natural vision after PresbyLASIK surgery.

(3) TFVA curve measured with the SimVis Gekko simulating the hybrid 1.75D 3.0-mm DE (in the dominant eye of the subject) and NDE (in the non-dominant eye of the subject) patterns, but correcting for the µ-monovision, i.e. with an over-refraction in both DE and NDE (so that the hybrid pattern is shifted to have best vision at far). In this case, the subject's natural refraction was corrected as well as the µ-monovision of the hybrid profile (mean µ-monovision compensation: DE -0.24±0.23D / NDE -2.06±0.34D, see table 6.1) to compare the data to the TFVA measurements published data (Luger et. al. 2020) where TFVA curves were measured one-year postoperatively in subjects with PresbyMAX surgery and compensating for µ-monovision. Table 8.1 also summarizes the over-refraction applied for each subject in their dominant and non-dominant eyes.

	RE (D)	LE(D)	Age	Over-Rx DE (D)	Over-Rx NDE (D)
S1	+2.00	+2.00	49	-0.25	-2.00
S2	-0.25	0.00	48	-0.50	-2.50
S3	+1.25	+2.00	52	-0.50	-1.50
S4	+0.25	+0.25	56	-0.25	-2.25
S5	-2.50	-2.50	47	-0.25	-2.50
S6	+1.75	+1.75	58	0	-1.50
S7	+0.75	+1.00	60	0.25	-2.50
S8	-1.25	-2.75	48	-0.25	-2.00
S9	+2.50	+2.50	53	0.25	-1.75
S10	-0.25	0.00	53	-0.25	-2.50
S11	+0.75	-1.50	60	-0.25	-2.25
S12	-0.50	0.00	58	-0.25	-2.00
S13	-0.75	-0.50	46	-0.50	-2.25
S14	+7.00	+6.00	62	-0.25	-1.25
S15	+0.25	+0.25	47	-0.25	-2.00
S16	-0.50	0.00	61	-0.25	-2.00
S17	-1.00	-1.25	46	-0.50	-2.00
S18	+1.25	+1.5	56	-0.50	-2.00
S19	+0.25	+0.25	57	-0.50	-2.25
S20	+1.00	+1.50	57	-0.25	-2.00

Table 8.1*: Subject's information, refractions in diopters for right eye (RE) and left eye (LE), ages and refraction compensating the µ-monovision induced by PresbyMAX pattern (Hybrid 1.75D add and 3.0-mm simulation) in Dominant eye (Over-Rx DE(D)) and Non-Dominant eye (over-Rx NDE(D)) in diopters.*

8.3 Results

8.3.1 Computational validation

Through focus performance of PresbyMAX design

Figure 8.5 shows the estimated through focus visual Strehl ratio curves calculated from the phase maps of the hybrid profiles, for the 5 different additions (from 1.50 to 2.50 in 0.25D steps), 3 pupil diameters of 3.0, 4.0 and 5.0-mm and calculated for the DE and NDE patterns. All TFVS curves were calculated in a range of 5D (from -1 to 4D).

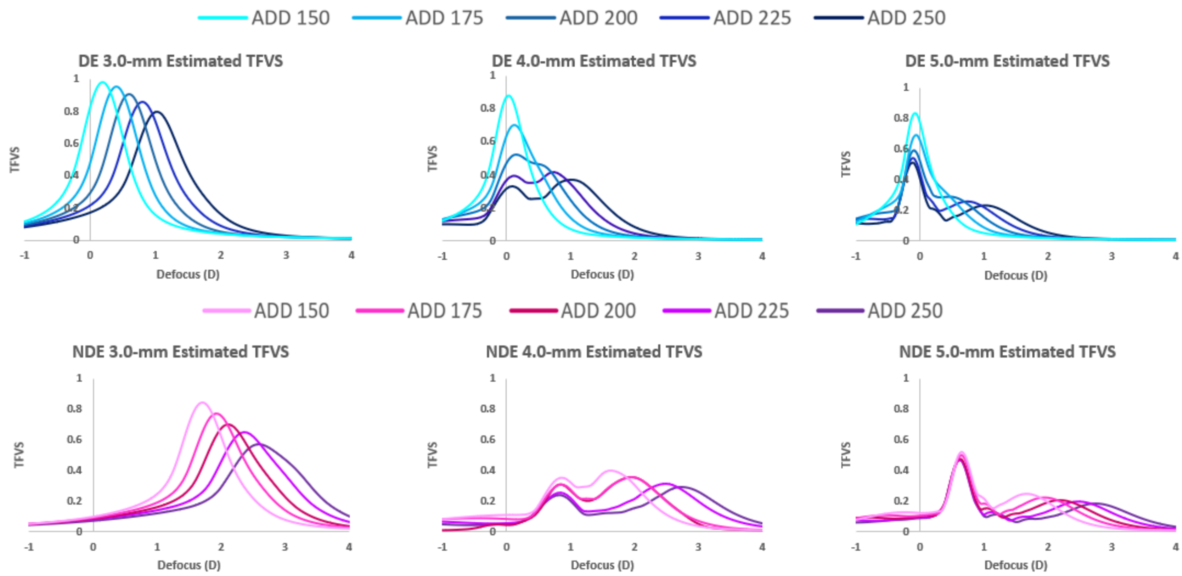

Fig. 8.5: *Estimated TFVS curves for hybrid pattern for 5 additions (from 1.50D to 2.50D in 0.25D steps), three pupil diameters (3.0, 4.0, 5.0-mm) and calculated for DE (blue) and NDE (pink).*

SimVis programmed Lens

a. Temporal Coefficients TCs

From the PresbyMAX Estimated TFVS ratio, we calculated the best combinations of Temporal Coefficients to accurately simulate the multifocal pattern. Figure 8.6 shows, as an example with Design Hybrid 1.75D Add, for NDE and DE, how the pattern spreaded through additions as we increased the pupil diameter.

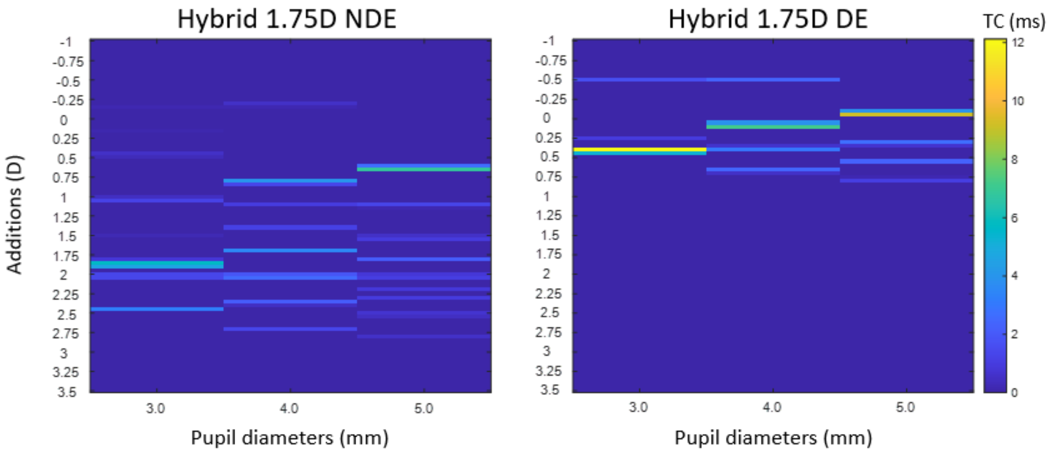

Fig 8.6: *Temporal Coefficients (TC) in milliseconds, spread through additions with increasing pupil diameters. Hybrid PresbyLASIK design for 1.75D Add and both NDE and DE eye patterns.*

b. SimVis through focus performance

Figures 8.7 and 8.8 show the comparison between the TFVS ratio for the PresbyLASIK designs (Estimated TFVS) and the SimVis lens (SimVis TFVS) simulated with the set of temporal coefficients for the PresbyLASIK designs (Hybrid NDE and Hybrid DE) for the five additions and three pupil diameters. In all conditions, the SimVis programmed lenses mimic the performance of the PresbyLASIK designs and the cross correlation were above >0.99 in all conditions.

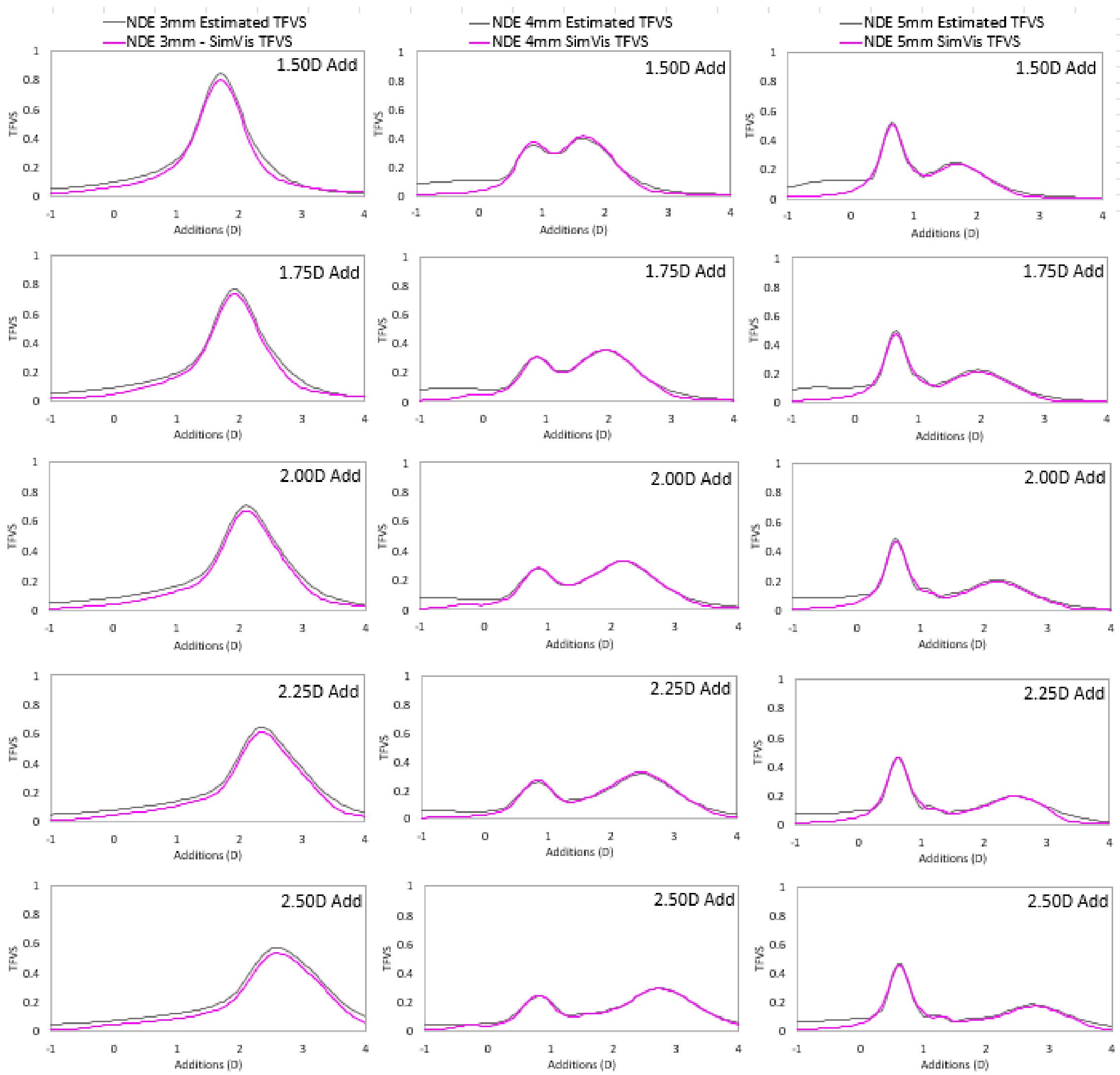

Fig 8.7: *Hybrid Design, NDE pattern - Computational validation: PresbyMAX designs and SimVis through focus performance. Through focus visual Strehl ratio for the PresbyLASIK designs (Estimated TFVS in gray) and for the SimVis lens (SimVis TFVS in dashed pink) for the three different pupil diameters (3.0-mm left column, 4.0-mm middle column and 5.0-mm right column) and five different additions (from 1.5 D to 2.5 D in a 0.25 D step).*

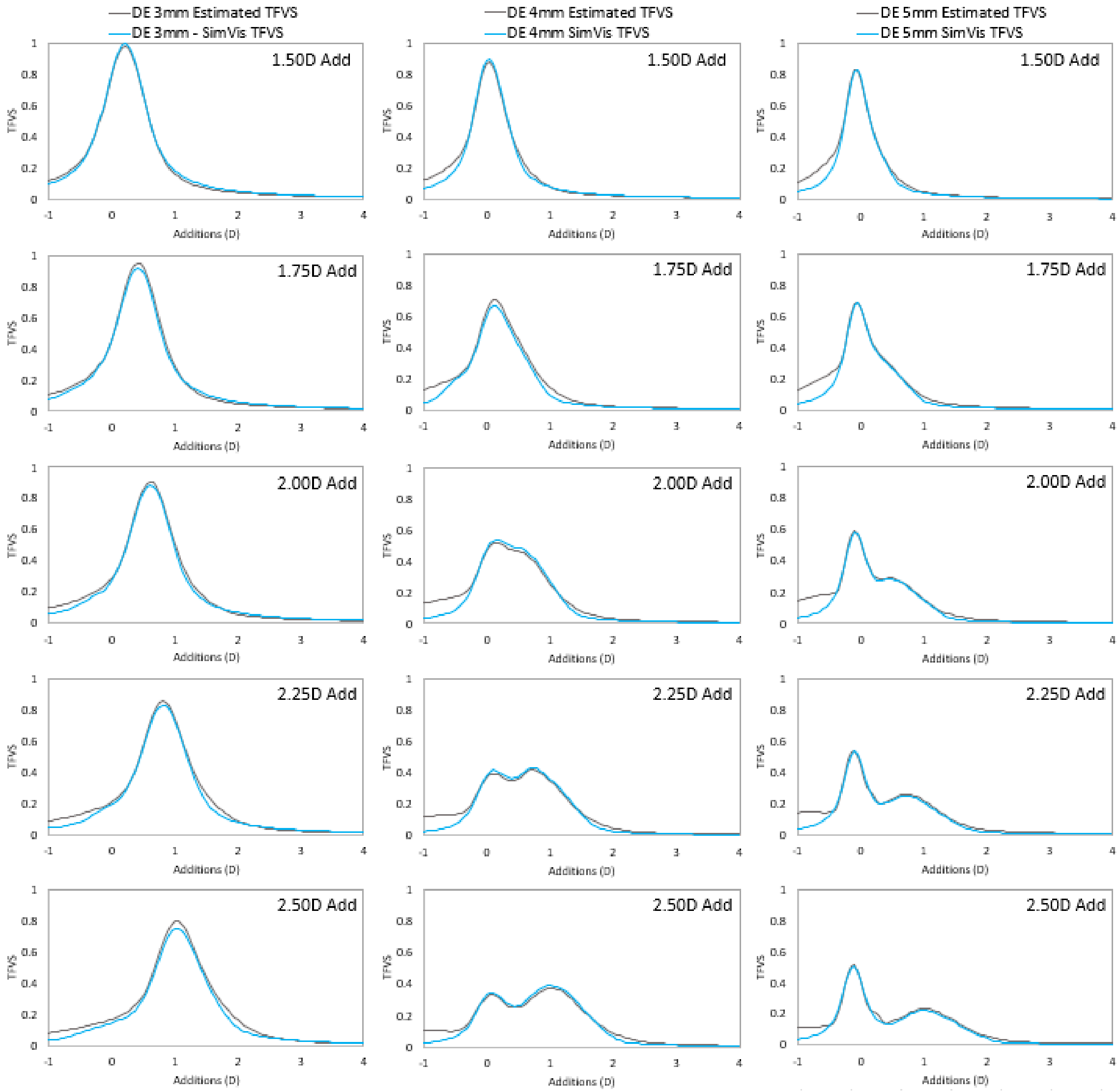

Fig 8.8: *Hybrid Design, DE pattern - Computational validation: PresbyMAX designs and SimVis through focus performance. Through focus visual Strehl ratio for the PresbyLASIK designs (Estimated TFVS in gray) and for the SimVis lens (SimVis TFVS in blue) for the three different pupil diameters (3.0-mm left column, 4.0-mm middle column and 5.0- mm right column) and five different additions (from 1.5 D to 2.5 D in a 0.25 D step).*

8.3.2 On Bench validation of the SimVis PresbyMAX ablation patterns

To test the SimVis simulated multifocal lenses, we used the custom high speed focimeter provided with the high-speed camera (3823fps). Optotunable lens of model EL-3-10 (reference ARAA2311) was mounted in the tunable lens support and the SimVis Lens simulation tested using specific custom developed algorithms that estimates the TFVS of the Experimental SimVis lenses. All the SimVis lens simulations were tested in the high speed focimeter (Hybrid NDE and Hybrid DE x five additions x three pupil diameters) on the same day. Calibration of the focimeter was done for a room temperature of 25ºC. Commonly, the working tunable lens increase its internal temperature by typically around 2-3ºC along the measurements. It is known that an increase in temperature could induce a shift of the multifocal design and we registered shifts below 0.1D during the course of the measurements.

Figures 8.9 and 8.10 show the TFVS ratio for the SimVis lens (computationally validated in fig 8.7 and 8.8) and the experimental SimVis Lens (measured in the high-speed focimeter, in green) for the different PresbyLASIK designs for the five additions, both DE and NDE eye patterns and the 3 pupil diameters. In all conditions, the Experimental SimVis Through focus optical quality replicated the optical quality of the corneal ablation patterns with a curve shape similarity metric (cross-correlation) >0.99. Therefore, all the PresbyMAX hybrid designs for additions from 1.5D to 2.5D and the three different pupil diameters are validated and ready to be used in the SimVis Gekko for clinical trials on subjects.

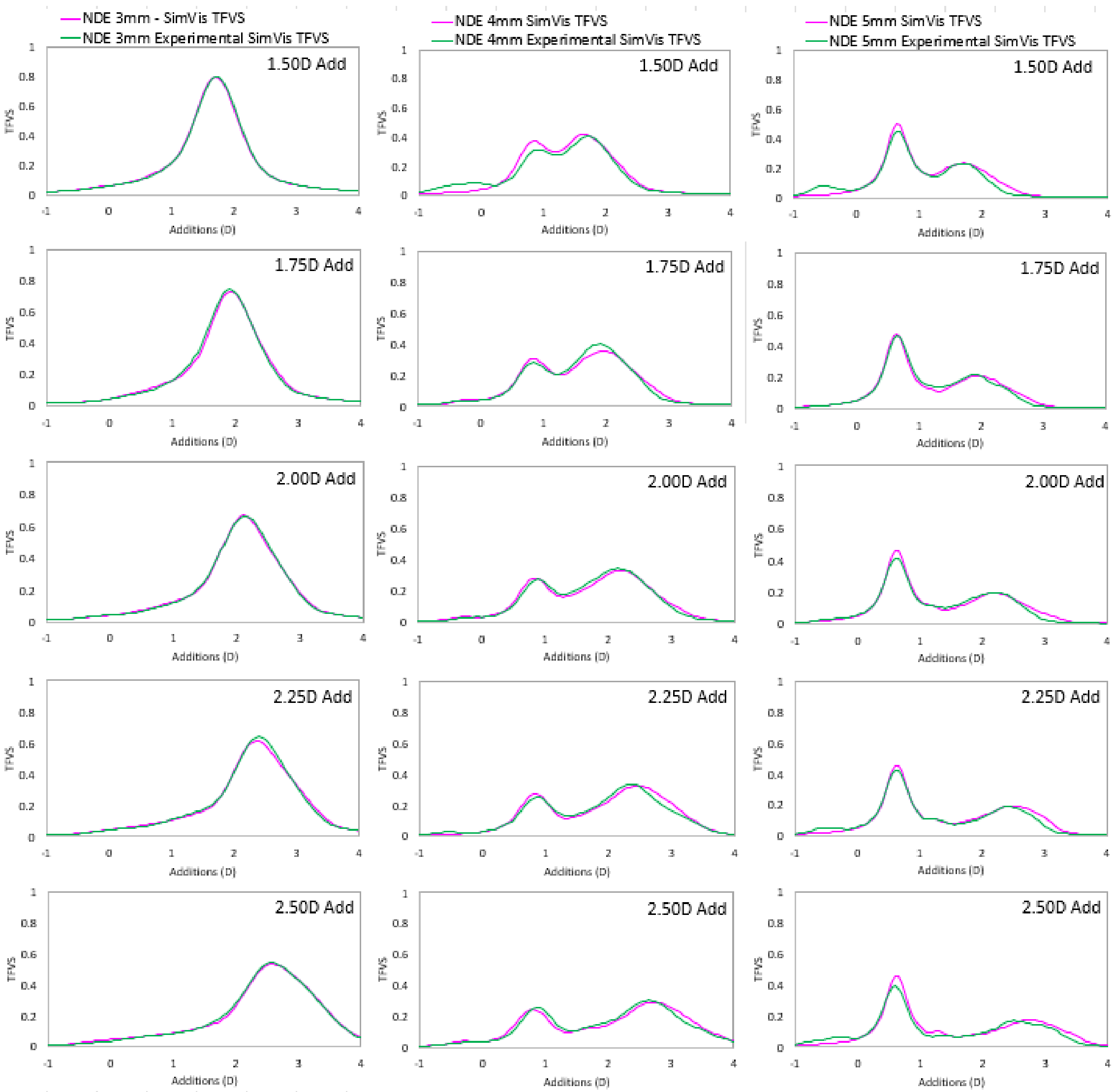

Fig 8.9: *Hybrid Design, NDE pattern - On-bench validation: SimVis lens (computationally validated, pink) and Experimental SimVis lens through focus performance (green). Through focus visual Strehl ratio for the PresbyMAX design HYBRID NDE and for the three different pupil diameters (3.0-mm left column, 4.0-mm middle column and 5.0- mm right column) and five different additions (1.50D to 2.5D), evaluated in the high speed focimeter with an optotunable lens EL-3-10 (ARAA2311)*

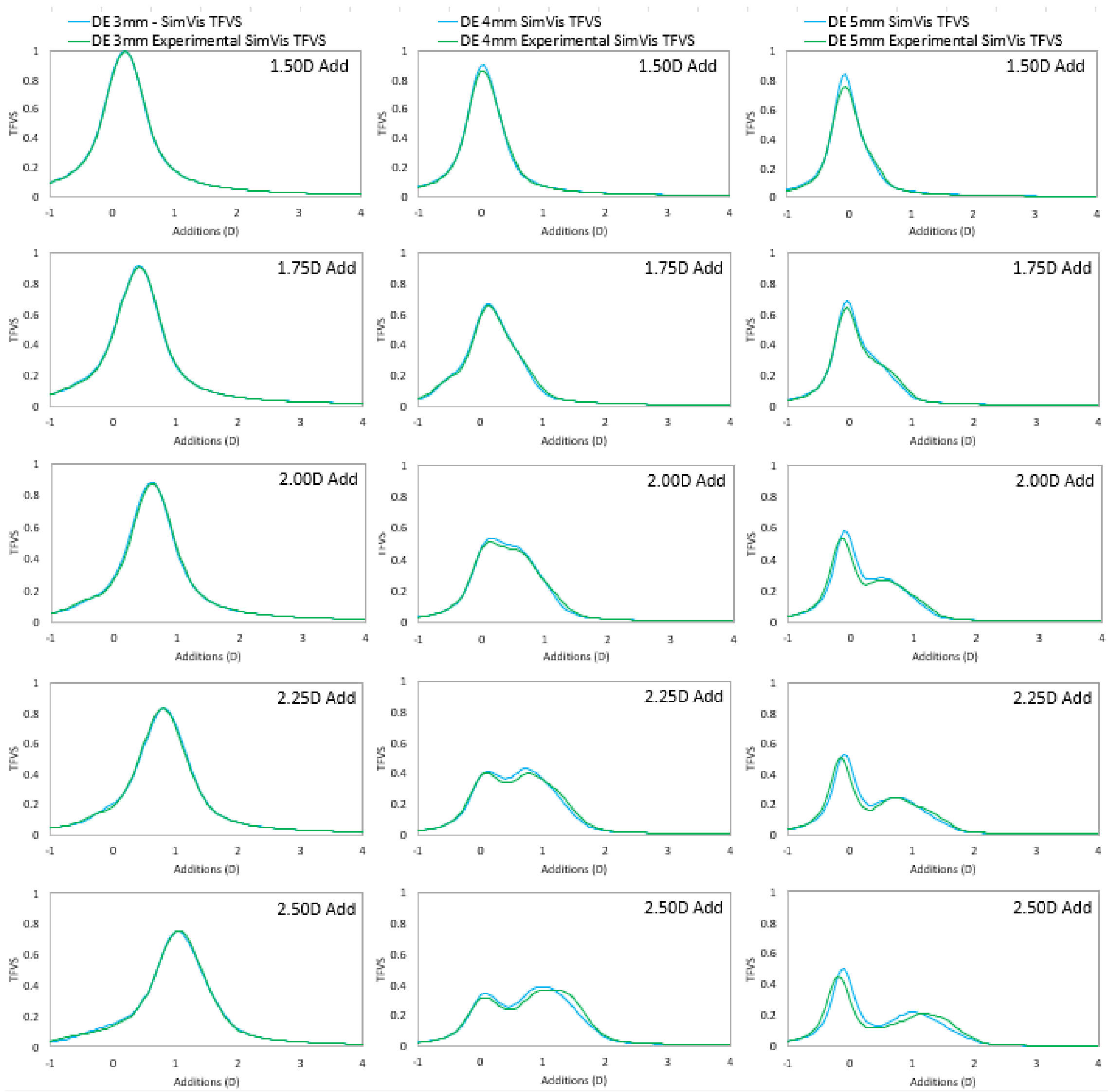

***Fig 8.10**: Hybrid Design, DE pattern - On-bench validation: SimVis lens (computationally validated, blue) and Experimental SimVis lens through focus performance (green). Through focus visual Strehl ratio for the PresbyMAX design HYBRID NDE and for the three different pupil diameters (3.0-mm left column, 4.0-mm middle column and 5.0-mm right column) and five different additions (1.50D to 2.5D), evaluated in the high speed focimeter with an optotunable lens EL-3-10 (ARAA2311)*

8.3.3 Clinical results on subjects wearing the SimVis Gekko binocular visual simulator while simulating SimVis PresbyMAX ablation patterns

For the clinical validation, we used the SimVis Simulation of the PresbyMAX Hybrid pattern 1.75D Add and a 3.0-mm pupil diameter. Twenty presbyopes subjects participated in the study and binocular TFVA curves (-4.0 to +1.5 D), with and without compensation for µ-monovision, were measured through SimVis simulated PresbyMAX patterns and compared to (1) binocular TF-VA curve through SimVis Gekko simulated monofocal-FAR in both eyes and (2) published binocular 1-year postoperative TF-VA curves of subjects that underwent PresbyMAX surgery (Luger et al. 2020). Figure 8.11 shows the TFVA curves for the bilateral monofocal (0D), the binocular TFVA curves for the PresbyMAX pattern (DE and NDE for 1.75D and 3.0-mm simulations) and the binocular TFVA curves with PresbyMAX pattern with compensation of µ-monovision, compared to the TFVA for Luger et al. 2020 measured in subjects 1-year after PresbyLASIK surgery. The mean binocular LogMAR VA at far was -0.10±0.02 (bilateral monofocal), -0.05±0.06 (hybrid with µmonovision), -0.07±0.04 (µmonovision compensated) and -0.10±0.03 (Luger et al. 2020). As shown in the figure, the Hybrid simulation (with the µmonovision component) extends the depth of focus by around 1.75D compared to bilateral monofocal maintaining a binocular VA above 0.2LogMAR.

On average, the binocular TF-VA curve through SimVis Gekko compensating for micro-monovision slightly over-estimates those reported in literature from subjects that underwent PresbyLASIK, with an RMS error between curves of 0.15µm and a shape similarity metric of 0.9877 in the range of -3.5D to 0.5D, but it can be explained by the different pupil sizes of the subjects wearing the SimVis Gekko and patients with presbyLasik surgery, as detailed in the discussion.

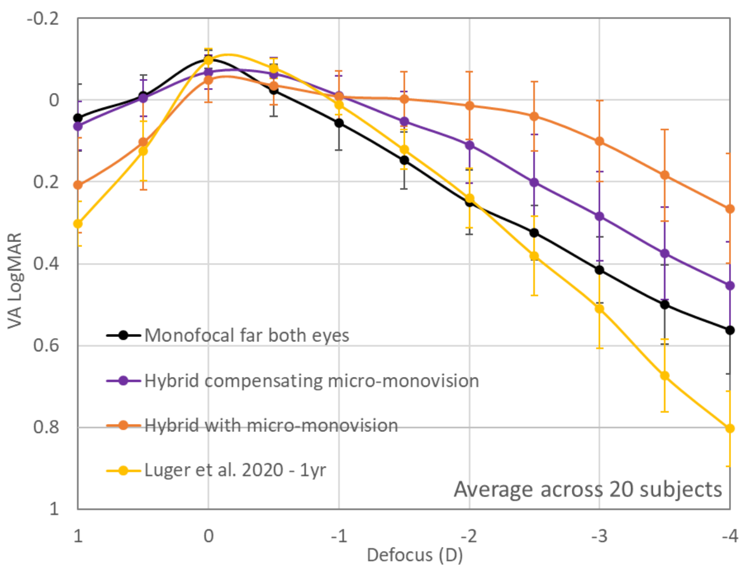

***Fig 8.11**: Clinical Validation of PresbyMAX Hybrid 1.75D Add and 3.0-mm pupil diameter: Through Focus Visual Acuity defocus curves (from +1 to -4 D in steps of 0.50D). Orange and purple lines are the TFVA curves measured in subjects wearing the SimVis Gekko with the PresbyMAX simulation (hybrid 1.75D add and 3.0-mm pupil diameter) with the µ-monovision component (orange) and compensating for the µ-monovision (purple); grey line is the TFVA curve measured wearing the SimVis Gekko simulating a monofocal FAR (0D) in both eyes and yellow line is the TFVA curve measured 1-year postoperatively on subjects after PresbyMAX surgery (Luger at al. 2020)*

8.4 Discussion

In this study have been calculated PresbyMAX hybrid ablation patterns with 5 additions (from 1.50 D to 2.50 D in steps of 0.25 D) to demonstrate that SimVis technology is able to reproduce different additions in 0.25 D steps of a same pattern of PresbyMAX. Currently, before surgery in clinics, the protocol is measuring the refraction at far, intermediate and near distance, depending on the results, the distance correction and the addition is calculated for the ablation profile. The possibility of being able to simulate different ablation patterns (µ-monovision, monocular and hybrid) and different additions before surgery, helps to select the best pattern and addition for each subject, helping to obtain the optimum visual comfort and minimizing errors in the selection of refractive parameters.

The TFVS curves measured experimentally in a high speed focimeter shown a very accurate reproducibility of TFVS SimVis curves (curve shape similarity metric (cross-correlation) >0.99) of hybrid ablation patterns measured at three different pupil diameters (3.0, 4.0 and 5.0-mm) and with five different additions (from 1.50D to 2.50D in steps of 0.25 D).

Clinical study was designed trying to match and validate SimVis simulations with Luger et al. 2020 results, to have the most similar conditions in our measurements were simulated ablations patterns with 1.75 D addition at 3.0-mm pupil diameter. The results with hybrid pattern with µ-monovision compensated matches on average those reported in literature from subjects that underwent PresbyLASIK allowing to validate the PresbyLASIK simulations with SimVis Gekko.

In Luger et al. 2020 study the pupil diameter was in photopic conditions with certain variability between subjects lower than 3.0-mm, while in this study was fixed at 3.0-mm, the pupil diameter variability from literature results could influence in the TF-VA performance as shown in figure 8.12 where we show the performance of the hybrid pattern for DE and DNE changes while increasing the pupil diameter of the ablation pattern. Therefore, it is of interest to be able to simulate each PresbyMAX pattern for different pupil diameters.

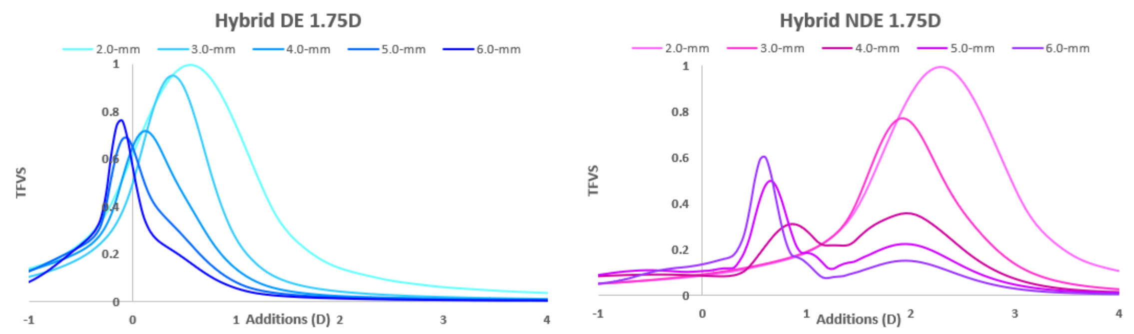

Fig. 8.12*: Estimated TFVS curves for hybrid pattern 1.75D addition, 5 pupil diameters from 2.0 to 6.0-mm in 1.0-mm steps, for DE (left, blues) and NDE (right, pinks)*

8.5 Conclusion

In this chapter a new application of SimVis Gekko binocular visual simulator was presented. The TFVS of the hybrid corneal ablation power profile was extracted for 3 different pupil diameters (3.0, 4.0 and 5.0-mm) and 5 additions (from 1.50 to 2.50 in steps of 0.25D); the time coefficients were calculated to mimic the TFVS ablation profile performance, the 5 different additions and 3 pupil diameters were measured in the high-speed focimeter with an optotunable lens (DE and NDE), and finally clinical validation was performed for the hybrid profile of 1.75D of addition at 3.0-mm pupil diameter in 20 presbyopic subjects binocularly in comparison with the study of Luger et al. 2020. According with the outcomes of the study, we concluded that:

- We demonstrated that SimVis Gekko is able to accurately simulate corneal ablation patterns, using the local corneal refractive correction information of the ablation profile. To date, there is no clinical device able to simulate those PresbyLASIK refractive corrections. The excellent match between the estimated optical quality of the ablation pattern in terms of through focus visual Strehl TFVS, and the experimental SimVis TFVS suggests that SimVis Gekko is a reliable simulator to capture vision through simulated corneal ablation patterns before surgery.
- Subjects can try (as far as we know, for the first time in a visual simulator), their particular visual experience prior refractive surgery as we found that binocular TF-VA curves measured in subjects that underwent PresbyLASIK match TF-VA curves in subjects through SimVis Gekko PresbyMAX simulations measured in similar experimental conditions. The results of hybrid pattern keeping the µ-monovision offers more realistic values of depth of focus after PresbyMAX treatment.

9 Conclusions

In this thesis computational simulations results and data obtained with an adaptive optics visual simulator and with SimVis Gekko simultaneous visual simulator have been used to develop new applications of SimVis Gekko visual simulator: (1) evaluating two new IOLs in the market and validating the accuracy of simulations; and (2) validating the SimVis Gekko for PresbyLASIK simulations before surgery.

The main accomplishments of this thesis are:

- First implementation of two extended depth of focus, Isopure IOL by Physiol-BVI and Vivity IQ IOL by Alcon, in a visual simulator with the SimVis technology.
- First demonstration of the accuracy of the simulation of Isopure IOL. Phase maps and temporal coefficients were calculated and measured in an adaptive optics visual simulator on bench and with 10 young subjects.
- First characterization of the optical properties of Isopure IOL. The larger DOF calculated in eye models and measured on subjects with the IOL when compared to the results obtained with a standard monofocal IOL was key to understand the optical properties of this lens.
- First study on the change in DOF and maximum VS ratio with different powers and spherical aberration corneas with Isopure IOL.
- First experimental study on the influence of ocular aberrations on Isopure IOL performance. Optical quality, depth of focus and Visual acuity were measured and calculated on bench and with subjects in an adaptive optics system with Isopure IOL physically in the cuvette and simulated in SimVis inducing and/or correcting ocular aberrations with a deformable mirror. First characterization of the difference performance with white light and monochromatic light (555 nm).
- New EDOF IOL, Acrysof IQ Vivity by Alcon. Optical performance computationally for post-LASIK subjects. Comparisons of optical quality, depth of focus and halos has been made with a monofocal IOL and EDOF IOL. New model eyes were developed and halo metrics to evaluate them.
- Experimental validation of EDOF IOLs and experimental validation of the simulation with SimVis and SLM in an adaptive optics visual simulator. Phase maps and temporal coefficients were calculated and measured on bench in an adaptive optics system at different pupil size (3.0, 4.0 and 5.0-mm) and compared with the physical IOL (Acrysof IQ Vivity) in a cuvette. Also, the chromatic effect was evaluated wit polychromatic and monochromatic light.

- Optical validation of a new SimVis Gekko application, PresbyLASIK. From PresbyLASIK power maps profiles, temporal coefficients were calculated and measured in a high-speed focimeter for a range of additions from 1.25 D to 2.50 D. Measurements in a binocular wearable SimVis Gekko visual simulator, binocularly has been made to compare with real data on literature and validate PresbyLASIK simulation (1.75 D addition) with SimVis technology.

The conclusions of this thesis are:

1. It is possible to simulate extended depth of focus intraocular lenses such as Isopure IOL from Physiol-BVI or Acrysof IQ Vivity from Alcon with a tunable lens using SimVis technology when the design of the IOL is known. In this thesis, we developed a procedure to calculate the phase map of the IOL and described the protocol to implement it in a calibrated tunable lens.

2. Isopure IOL from Physiol-BVI was studied computationally using corneas of different power and spherical aberration and IOL tilts and decentrations. While power had little influence in Isopure IOL performance, a reduction of DOF was found for some values of spherical aberration. For 4.5 mm pupil diameter, MTF was higher than 0.5 and DOF was always above 2 D and both the optical quality and DOF were more affected by decentration than by tilt.

3. The average DOF and VA found for Isopure IOL when evaluated in a visual simulator in a group of subjects was, on average, 1.60 D and -0.09 LogMAR for 4.5-mm pupil diameters. All conditions tested with Isopure IOL, on bench and in subjects, across simulators and pupil diameters, show on average, higher values of DOF than no IOL condition that increased on average 0.28 D.

4. When correcting ocular aberrations and inducing positive or negative spherical aberration the increase in the DOF with respect to the no-IOL condition was maintained. The performance of IOL simulation with SimVis technology is similar to those found with physical lens in the cuvette channel in terms of peak VA and DOF. Small differences may arise from the lack of compensation of cornea-IOL aberrations when the IOL is simulated with temporal multiplexing.

5. When compared with a monofocal IOL, the Acrysof IQ Vivity IOL expands the DOF (from 1.2 to 2.6 D for monofocal and Vivity IOLs, respectively) at the expense of some degradation at far (VS 0.95 and 0.5 for monofocal and EDOF IOL, respectively). The performance of the Acrysof IQ Vivity is rather immune to the presence of the high order aberrations expected in LASIK subjects and exhibits a quite constant DOF (less than 0.5 D change) for a large range of corneal SA.

6. The Acrysof IQ Vivity IOL can be simulated in the SLM and with SimVis technology and a good correspondence was found with the TF results found using the cuvette channel (RMS difference less than 10%). SimVis technology can be used to simulate the Acrysof IQ Vivity IOL intraocular lens with temporal multiplexing.

7. SimVis Gekko is able to accurately simulate corneal ablation patterns, using the local corneal refractive correction information of the ablation profile. The excellent match between the estimated optical quality of the ablation pattern in terms of through focus visual Strehl TFVS, and the experimental SimVis TFVS suggests that SimVis Gekko is a reliable simulator to capture vision through simulated corneal ablation patterns before surgery.

These conclusions relate with the motivation of the thesis stated in section 1.6 as follows:

1. SimVis technology can be used to accurately simulate EDOF IOLs such as Isopure IOL from Physiol-BVI or Acrysof IQ Vivity by Alcon.

2. Both EDOF IOLs studied computational and experimentally, has shown the robustness of their designs, holding a good balance of depth of focus and optical quality with optical aberrations inductions, both IOLs show good optical performance to be implanted in some cases of post-LASIK surgery subjects, a challenge in clinics.

3. A new application was validated, PresbyLASIK, for SimVis Gekko binocular visual simulator. Increasing the competitivity of the visual simulator in the market.

10 List of scientific activities

Publications on this thesis

1. **Lago CM**, de Castro A, Benedí-García C, Aissati S, Marcos S. Evaluating the effect of ocular aberrations on the simulated performance of a new refractive IOL design using Adaptive Optics. Biomedical Optics Express 2022; 13: 6682

2. Benedi-Garcia C, Vinas M, **Lago CM**, Aissati S, De Castro A, Dorronsoro C, Marcos S. Optical and visual quality of real intraocular lenses physically projected on the patient's eye. Biomedical Optics Express 2021; 12: 6360-6374

3. Marcos S, Benedí-García C, Aissati S, Gonzalez-Ramos AM, **Lago CM**, Radhkrishnan A, Romero M, Vedhakrishnan S, Sawides L, Vinas M. VioBio lab adaptive optics: technology and applications by women vision scientists. Ophthalmic and Physiological Optics 2020; 40: 75-87

4. **Lago CM**, de Castro A, Marcos S. Computational simulation of the optical performance of an extended depth of focus intraocular lens in post-LASIK eyes. Journal of Cataract and Refractive Surgery (under revision)

In preparation

5. **Lago CM**, de Castro A, Marcos S. Computational simulations. As a predictor of the performance of a new refractive IOL design: Isopure IOL

6. **Lago CM,** Siso-Fuertes I, Zaytouny A, Dorronsoro C, Arba-Mosquera S, Sawides L. SimVis simulation of LASIK corneal ablation patterns for presbyopia correction: Computational, on-bench and clinical validations.

Proceeding

1. Sawides L, de Castro A, **Lago CM**, Barcala X, Zaytouny A, Marcos S, Dorronsoro C. SimVis simulations of multifocal IOL designs based on public-literature data. In: Optical Design and Engineering VIII. SPIE, 2021; 122-132

Congress contributions

Personally presented

1. Carmen M Lago, Alberto de Castro, Susana Marcos. Optical design: Extended depth of focus intraocular lens and corneal shape influence. International OSA Network of Students (Barcelona 2019). *Oral contribution.*

2. Carmen M Lago, Alberto de Castro, Susana Marcos, Lucie Sawides. From real lens design to simulation in SimVis Gekko. Optics and Photonics for Scientific progress (On line 2021). *Poster.*

3. Carmen M Lago, Alberto de Castro, Lucie Sawides, Susana Marcos. Simulated assessment of Presbyopia correction IOLS in post-LASIK patients. ARVO anual meeting 2021, Investigative Ophtalmology & visual sciences (On line 2021). *Oral contribution.*

4. Carmen M Lago, Alberto de Castro, Lucie Sawides, Sara Aissati, Clara Benedí-García, María Viñas, Carlos Dorronsoro, Susana Marcos. Reunión Nacional de Óptica (On line 2021). *Oral contribution.*

5. Carmen M Lago. Extendiendo el foco, Isopure 1, 2, 3. FacoElche (Elche 2021). *Invited talk*

6. Carmen M Lago. Principios ópticos, Isopure 1, 2, 3. FacOPTOM (Elche 2021). *Invited talk*

7. Carmen M Lago. Del diseño de lentes intraoculares reales a la simulación en SimVis Gekko. Jornada de Doctorandos UCM (On line 2020).

Presented by collaborators.

1. Susana Marcos, Carmen M Lago, Alberto de Castro. Pseudophakic IOLs: Enlarged-Depth-of-focus. European Society of Cataract and Refractive Surgery. (Paris 2019). *Poster contribution*

2. Clara Benedí-García, María Viñas, Carmen M Lago, Carlos Dorronsoro, Susana Marcos. Optical and visual quality of real intraocular lenses physically

projected on the patient's eye. ARVO annual meeting 2020, Investigative Ophthalmology & visual sciences (on line 2020). *Oral contribution.*

3. Susana Marcos, Carmen M Lago, Alberto de Castro, Nicolas Alejandre. Predicted optical quality and halos with the AcrySof IQ Vivity® EDF IOL in post-LASIK patients. European Society of Cataract and Refractive Surgeons (Amsterdam, 2021). *Poster contribution.*

4. Lucie Sawides, Alberto de Castro, Carmen M Lago, Xoana Barcala, Amal, Zaytouny, Susana Marcos, Carlos Dorronsoro. SimVis simulations of multifocal IOL designs based on public-literature data. Optical Design and Engineering VIII 11871, 122-132. (Madrid 2021) *Oral contribution.*

5. Irene Sisó-Fuertes, Carmen M Lago, Amal Zaytouny, Carlos Dorronsoro, V Dehartunian, Samuel Arba-Mosquera, Lucie Sawides. Simvis Simulation of LASIK Corneal Ablation Patterns For Presbyopia Correction - Computational, On-Bench and Clinical Validations. European Society of Cataract and Refractive Surgeons (Amsterdam 2022). *Poster contribution.*

Invited talks

From real IOLs designs to simulations. Optical Society of America vision and color summer data blast (On Line 2021).

Honors

ARVO International Travel Grant. These grants, from the Association for Research in Vision and Ophthalmology (ARVO), are awarded to PhD students attending and presenting their scientific work at the 2021 ARVO Annual Meeting (on line 2021).

IONS Travel Grant. These grants from International Optical Society of America (OSA) Network of Students, are awarded to PhD students attending and presenting their scientific work at IONS 2019 annual meeting, (Barcelona 2019).

Other relevant information

Member of the IO-CSIC Student chapter of the Optical Society of America (OPTICA), IOSA and now named IOPTICA. Charges of secretary 2019 and 2020. President in 2021. We organized internal seminars, talks, courses and participate in outreach programs as Ciencia en el barrio, 11F, LGTBI+ in STEM, Scientifics seminars, Ciudad Ciencia, International Day of Light or Week of sciences.

Member of area of women in optics and photonics of SEDOPTICA (Sociedad Española de Óptica). Organizing coffees, mentoring, monthly interviews in “conoce a las investigadoras” program.

Organizing committee of I Workshop women, Optics and Photonics (Madrid 2019) and chair. Actually, Organizing committee, the II Workshop women, Optics and Photonics (Salamanca 2023).

Teaching course introduction to research in Optics 2020.

11 Bibliography

Aissati S, Vinas M, Benedi-Garcia C, Dorronsoro C, Marcos S. Testing the effect of ocular aberrations in the perceived transverse chromatic aberration. Biomedical Optics Express 2020; 11: 4052-4068

Aissati S, Benedi-Garcia C, Vinas M, de Castro A, Marcos S. Matching convolved images to optically blurred images on the retina. Journal of vision 2022; 22: 12-12

Akondi V, Dorronsoro C, Gambra E, Marcos S. Temporal multiplexing to simulate multifocal intraocular lenses: theoretical considerations. Biomedical optics express 2017; 8: 3410-3425

Akondi V, Sawides L, Marrakchi Y, Gambra E, Marcos S, Dorronsoro C. Experimental validations of a tunable-lens-based visual demonstrator of multifocal corrections. Biomedical Optics Express 2018; 9: 6302-6317

Alba-Bueno F, Vega F, Millán M. Halos and multifocal intraocular lenses: origin and interpretation. Archivos de la Sociedad Española de Oftalmología (English Edition) 2014; 89: 397-404

Alcon. Technical product information. https://www.alcon.com/eye-care-products.

Alcon. Acrysof IQ Vivity and Vivity toric IOLs technical specifications. June 2020. https://www.alcon-kongresse.com/wp-content/uploads/2021/02/acrysof-iq-vivity-technical-specifications_en.pdf

Ale JB. Intraocular lens tilt and decentration: a concern for contemporary IOL designs. Nepalese Journal of Ophthalmology 2011; 3: 68-77

Alio JL, Grzybowski A, El Aswad A, Romaniuk D. Refractive lens exchange. Survey of ophthalmology 2014; 59: 579-598

Alio JL, Plaza-Puche AB, Férnandez-Buenaga R, Pikkel J, Maldonado M. Multifocal intraocular lenses: an overview. Survey of ophthalmology 2017; 62: 611-634

Anera RG, Jiménez JR, Del Barco LJ, Bermúdez J, Hita E. Changes in corneal asphericity after laser in situ keratomileusis. Journal of Cataract & Refractive Surgery 2003; 29: 762-768

Aramberri J. Intraocular lens power calculation after corneal refractive surgery: double-K method. Journal of Cataract & Refractive Surgery 2003; 29: 2063-2068

Artal P. Optics of the eye and its impact in vision: a tutorial. Advances in Optics and Photonics 2014; 6: 340-367

Artal P. The eye as an optical instrument. In: Optics in Our Time. Springer, Cham, 2016; 285-297

Atchison DA, Thibos LN. Optical models of the human eye. Clinical and Experimental Optometry 2016; 99: 99-106

Bala C, Poyales F, Guarro M, Mesa RR, Mearza A, Varma DK, Jasti S, Lemp-Hull J. Multicountry clinical outcomes of a new nondiffractive presbyopia-correcting IOL. Journal of Cataract & Refractive Surgery 2022; 48: 136-143

Baloh R, Jacobson K, Socotch T. The effect of aging on visual-vestibuloocular responses. Experimental brain research 1993; 95: 509-516

Barcala X, Vinas M, Hidalgo F, Ruiz S, Nankivil D, Karkkainen T, Chehab K, Dorronsoro C, Marcos S. Comparison of vision with multifocal contact lenses and SimVis Gekko simulations in a clinical site. Investigative Ophthalmology & Visual Science 2020; 61: 579-579

Barcala X. Binocular simultaneous vision simulator: validation and implementation of the Sim+Vis technology in the clinic. In: Universidad Complutense de Madrid, 2021

Barcala X, Vinas M, Ruiz S, Hidalgo F, Nankivil D, Karkkainen T, Gambra E, Dorronsoro C, Marcos S. Multifocal contact lens vision simulated with a clinical binocular simulator. Contact Lens and Anterior Eye 2022: 101716

Barcala X, Zaytouny A, Rego-Lorca D, Sanchez-Quiros J, Sanchez-Jean R, Martinez-de-la-Casa JM, Dorronsoro C, Marcos S. Visual simulations of presbyopic corrections through cataract opacification. Journal of Cataract & Refractive Surgery 2022: 10.1097

Baudu P, Penin F, Mosquera SA. Uncorrected binocular performance after biaspheric ablation profile for presbyopic corneal treatment using AMARIS with the PresbyMAX module. American journal of ophthalmology 2013; 155: 636-647. e631

Beiko GH, Haigis W, Steinmueller A. Distribution of corneal spherical aberration in a comprehensive ophthalmology practice and whether keratometry can predict aberration values. Journal of Cataract & Refractive Surgery 2007; 33: 848-858

Benard Y, Lopez-Gil N, Legras R. Subjective depth of field in presence of 4th-order and 6th-order Zernike spherical aberration using adaptive optics technology. Journal of Cataract & Refractive Surgery 2010; 36: 2129-2138

Benard Y, Lopez-Gil N, Legras R. Optimizing the subjective depth-of-focus with combinations of fourth-and sixth-order spherical aberration. Vision research 2011; 51: 2471-2477

Benedi-Garcia C, Vinas M, Lago CM, Aissati S, De Castro A, Dorronsoro C, Marcos S. Optical and visual quality of real intraocular lenses physically projected on the patient's eye. Biomedical Optics Express 2021; 12: 6360-6374

Blum M, Büeler M, Grätzel C, Aschwanden M. Compact optical design solutions using focus tunable lenses. In: Optical Design and Engineering IV. International Society for Optics and Photonics, 2011; 81670W

Borgo M, Soranzo A, Grassi M. MATLAB for Psychologists. Springer Science & Business Media, 2012

Borkenstein AF, Borkenstein E-M, Luedtke H, Schmid R. Optical Bench Analysis of 2 Depth of Focus Intraocular Lenses. Biomedicine hub 2021; 6: 77-85

Bova A, Vita S. Clinical and Aberrometric Evaluation of a New Monofocal IOL with Intermediate Vision Improvement. Journal of Ophthalmology 2022; 2022

Brainard DH, Vision S. The psychophysics toolbox. Spatial vision 1997; 10: 433-436

Brezna W, Lux K, Dragostinoff N, Krutzler C, Plank N, Tobisch R, Boltz A, Garhöfer G, Told R, Witkowska K. Psychophysical vision simulation of diffractive bifocal and trifocal intraocular lenses. Translational Vision Science & Technology 2016; 5: 13-13

Campbell FW. The depth of field of the human eye. Optica Acta: International Journal of Optics 1957; 4: 157-164

Cano D, Barbero S, Marcos S. Comparison of real and computer-simulated outcomes of LASIK refractive surgery. JOSA A 2004; 21: 926-936

Charman W, Whitefoot H. Pupil diameter and the depth-of-field of the human eye as measured by laser speckle. Optica Acta: International Journal of Optics 1977; 24: 1211-1216

Charman W. Wavefront aberration of the eye: a review. Optometry and vision science: official publication of the American Academy of Optometry 1991; 68: 574-583

Charman WN. Developments in the correction of presbyopia I: spectacle and contact lenses. Ophthalmic and Physiological Optics 2014; 34: 8-29

Chen CC, Izadshenas A, Rana MAA, Azar DT. Corneal asphericity after hyperopic laser in situ keratomileusis. Journal of Cataract & Refractive Surgery 2002; 28: 1539-1545

Chen M, Yoon G. Posterior corneal aberrations and their compensation effects on anterior corneal aberrations in keratoconic eyes. Investigative ophthalmology & visual science 2008; 49: 5645-5652

Cheng X, Bradley A, Thibos LN. Predicting subjective judgment of best focus with objective image quality metrics. Journal of Vision 2004; 4: 7-7

da Costa H. Ensaios mecánicos. SESES, RJ, 2019

Dartnall HJ, Bowmaker JK, Mollon JD. Human visual pigments: microspectrophotometric results from the eyes of seven persons. Proceedings of the Royal society of London Series B Biological sciences 1983; 220: 115-130

Davis G. The evolution of cataract surgery. Missouri medicine 2016; 113: 58

de Castro A, Rosales P, Marcos S. Tilt and decentration of intraocular lenses in vivo from Purkinje and Scheimpflug imaging: validation study. Journal of Cataract & Refractive Surgery 2007; 33: 418-429

de Gracia P, Dorronsoro C, Sánchez-González Á, Sawides L, Marcos S. Experimental simulation of simultaneous vision. Investigative ophthalmology & visual science 2013; 54: 415-422

de la Hoz A, Germann J, Martinez-Enriquez E, Pascual D, Bekesi N, Alejandre-Alba N, Dorronsoro C, Marcos S. Design and ex situ performance of a shape-changing accommodating intraocular lens. Optica 2019; 6: 1050-1057

Delori FC, Webb RH, Sliney DH. Maximum permissible exposures for ocular safety (ANSI 2000), with emphasis on ophthalmic devices. JOSA A 2007; 24: 1250-1265

Díaz-Doutón F, Benito A, Pujol J, Arjona M, Güell JL, Artal P. Comparison of the retinal image quality with a Hartmann-Shack wavefront sensor and a double-pass instrument. Investigative ophthalmology & visual science 2006; 47: 1710-1716

Dorronsoro C, Barcala X, Gambra E, Akondi V, Sawides L, Marrakchi Y, Rodriguez-Lopez V, Benedi-Garcia C, Vinas M, Lage E. Tunable lenses: dynamic characterization and fine-tuned control for high-speed applications. Optics express 2019; 27: 2085-2100

Dorronsoro C, Cano D, Merayo-Lloves J, Marcos S. Experiments on PMMA models to predict the impact of corneal refractive surgery on corneal shape. Optics Express 2006; 14: 6142-6156

Dorronsoro C, Merayo–Lloves J, Marcos S. An Experimental Correction Factor of Radial Laser Efficiency Losses in Corneal Refractive Surgery. Investigative Ophthalmology & Visual Science 2006; 47: 3611-3611

Dorronsoro C, Marcos S. Instrument for simulating multifocal ophthalmic corrections. 2010

Dorronsoro C, Radhakrishnan A, Alonso-Sanz JR, Pascual D, Velasco-Ocana M, Perez-Merino P, Marcos S. Portable simultaneous vision device to simulate multifocal corrections. Optica 2016; 3: 918-924

Dorronsoro C, Radhakrishnan A, de Gracia P, Sawides L, Marcos S. Perceived image quality with simulated segmented bifocal corrections. Biomedical optics express 2016; 7: 4388-4399

Dorronsoro C, Rodriguez-Lopez V, Barcala X, Akondi V, Sawides L, Marrakchi Y, Lage E, Geisler WS, Marcos S. Perceptual and physical limits to temporal multiplexing simulation of multifocal corrections. Investigative Ophthalmology & Visual Science 2019; 60: 6465-6465

Duane A. Studies in monocular and binocular accommodation, with their clinical application. Transactions of the American Ophthalmological Society 1922; 20: 132

Dubbelman M, Weeber HA, Van Der Heijde RG, Völker-Dieben HJ. Radius and asphericity of the posterior corneal surface determined by corrected Scheimpflug photography. Acta Ophthalmologica Scandinavica 2002; 80: 379-383

Eppig T, Scholz K, Löffler A, Meßner A, Langenbucher A. Effect of decentration and tilt on the image quality of aspheric intraocular lens designs in a model eye. Journal of Cataract & Refractive Surgery 2009; 35: 1091-1100

Evans BJ. Pickwell's Binocular Vision Anomalies E-Book. Elsevier Health Sciences, 2021

Fernández D, Barbero S, Dorronsoro C, Marcos S. Multifocal intraocular lens providing optimized through-focus performance. Optics Letters 2013; 38: 5303-5306

Fernández EJ, Artal P. Study on the effects of monochromatic aberrations in the accommodation response by using adaptive optics. JOSA A 2005; 22: 1732-1738

Fernández EJ, Prieto PM, Artal P. Binocular adaptive optics visual simulator. Optics letters 2009; 34: 2628-2630

Fernández J, Rodríguez-Vallejo M, Burguera N, Rocha-de-Lossada C, Piñero DP. Spherical aberration for expanding depth of focus. Journal of Cataract & Refractive Surgery 2021; 47: 1587-1595

Fernández-Vega-Cueto L, Madrid-Costa D, Alfonso-Bartolozzi B, Vega F, Millán MS, Alfonso JF. Optical and Clinical Outcomes of an Extended Range of Vision Intraocular Lens. Journal of Refractive Surgery 2022; 38: 168-176

Fisher B, Potvin R. Clinical outcomes with distance-dominant multifocal and monofocal intraocular lenses in post-LASIK cataract surgery planned using an intraoperative aberrometer. Clinical & Experimental Ophthalmology 2018; 46: 630-636

Glasser A, Campbell MC. Presbyopia and the optical changes in the human crystalline lens with age. Vision research 1998; 38: 209-229

Grzybowski A, Markeviciute A, Zemaitiene R. A review of pharmacological presbyopia treatment. Asia-Pacific Journal of Ophthalmology (Philadelphia, Pa) 2020; 9: 226

Guillon M, Dumbleton K, Theodoratos P, Gobbe M, Wooley CB, Moody K. The effects of age, refractive status, and luminance on pupil size. Optometry and vision science 2016; 93: 1093

Gundersen KG, Potvin R. Clinical outcomes and quality of vision associated with bilateral implantation of a wavefront shaping presbyopia correcting intraocular lens. Clinical Ophthalmology (Auckland, NZ) 2021; 15: 4723

Gundersen KG, Potvin R. The effect of spectacle-induced low myopia in the non-dominant eye on the binocular defocus curve with a non-diffractive extended vision intraocular lens. Clinical Ophthalmology (Auckland, NZ) 2021; 15: 3541

Hampson KM. Adaptive optics and vision. Journal of Modern Optics 2008; 55: 3425-3467

Hermans EA, Terwee TT, Koopmans SA, Dubbelman M, van der Heijde RG, Heethaar RM. Development of a ciliary muscle–driven accommodating intraocular lens. Journal of Cataract & Refractive Surgery 2008; 34: 2133-2138

Hart RW, Farrell RA. Light scattering in the cornea. JOSA 1969; 59: 766-774

Helmholtz Hv. Ueber die accommodation des auges. Archiv für Ophthalmologie 1855; 1: 1-74

Hervella L, Villegas EA, Prieto PM, Artal P. Assessment of subjective refraction with a clinical adaptive optics visual simulator. Journal of Cataract & Refractive Surgery 2019; 45: 87-93

Hervella L, Villegas EA, Robles C, Artal P. Spherical aberration customization to extend the depth of focus with a clinical adaptive optics visual simulator. Journal of Refractive Surgery 2020; 36: 223-229

Iijima K, Kamiya K, Shimizu K, Igarashi A, Komatsu M. Demographics of patients having cataract surgery after laser in situ keratomileusis. Journal of Cataract & Refractive Surgery 2015; 41: 334-338

Iskander DR. Computational aspects of the visual Strehl ratio. Optometry and Vision Science 2006; 83: 57-59

Iyer KK, Bradley AP, Wilson SJ. Conducting shorter VEP tests to estimate visual acuity via assessment of SNR. Documenta Ophthalmologica 2013; 126: 21-28

Jung SW, Kim MJ, Park SH, Choun-Ki Joo M. Multifocal corneal ablation for hyperopic presbyopes. Journal of Refractive Surgery 2008; 24: 903

Klyce SD. Corneal topography and the new wave. Cornea 2000; 19: 723-729

Kohnen T, Mahmoud K, Bühren J. Comparison of corneal higher-order aberrations induced by myopic and hyperopic LASIK. Ophthalmology 2005; 112: 1692. e1691-1692. e1611

Kohnen T, Suryakumar R. Extended depth-of-focus technology in intraocular lenses. Journal of Cataract & Refractive Surgery 2020; 46: 298-304

Kohnen T, Petermann K, Böhm M, Hemkeppler E, Ahmad W, Hinzelmann L, Pawlowicz K, Jandewerth T, Lwowski C. Nondiffractive wavefront-shaping extended depth-of-focus intraocular lens: visual performance and patient-reported outcomes. Journal of Cataract & Refractive Surgery 2022; 48: 144-150

Liang J, Williams DR, Miller DT. Supernormal vision and high-resolution retinal imaging through adaptive optics. JOSA A 1997; 14: 2884-2892

Liu Z, Pflugfelder SC. Corneal thickness is reduced in dry eye. Cornea 1999; 18: 403-407

Lourdes Llorente O, Barbero S, Merayo J, Marcos S. Total and Corneal Optical Aberrations Induced by Laser in situ Keratomileusis for Hyperopia. Journal of Refractive Surgery 2004; 20: 203-216

Lu Z-L, Dosher B. Visual psychophysics: From laboratory to theory. MIT Press, 2013

Luger MH, Ewering T, Arba-Mosquera S. 3-Month experience in presbyopic correction with bi-aspheric multifocal central presbyLASIK treatments for hyperopia and myopia with or without astigmatism. Journal of Optometry 2012; 5: 9-23

Luger MH, Ewering T, Arba-Mosquera S. Nonwavefront-guided Presby reversal treatment targeting a monofocal cornea after bi-aspheric ablation profile in a patient intolerant to multifocality. Journal of Refractive Surgery 2014; 30: 214-216

Luger MH, McAlinden C, Buckhurst PJ, Wolffsohn JS, Verma S, Mosquera SA. Presbyopic LASIK using hybrid bi-aspheric micro-monovision ablation profile for presbyopic corneal treatments. American Journal of Ophthalmology 2015; 160: 493-505

Luger MH, McAlinden C, Buckhurst PJ, Wolffsohn JS, Verma S, Arba-Mosquera S. Long-term outcomes after LASIK using a hybrid bi-aspheric micro-monovision ablation profile for presbyopia correction. Journal of Refractive Surgery 2020; 36: 89-96

Mannos J, Sakrison D. The effects of a visual fidelity criterion of the encoding of images. IEEE transactions on Information Theory 1974; 20: 525-536

Marcos S, Moreno E, Navarro R. The depth-of-field of the human eye from objective and subjective measurements. Vision research 1999; 39: 2039-2049

Marcos S, Barbero S, Llorente L, Merayo-Lloves J. Optical response to LASIK surgery for myopia from total and corneal aberration measurements. Investigative ophthalmology & visual science 2001; 42: 3349-3356

Marcos S. Image quality of the human eye. International ophthalmology clinics 2003; 43: 43-62

Marcos S, Ortiz S, Pérez-Merino P, Birkenfeld J, Durán S, Jiménez-Alfaro I. Three-dimensional evaluation of accommodating intraocular lens shift and alignment in vivo. Ophthalmology 2014; 121: 45-55

Marcos S, Werner JS, Burns SA, Merigan WH, Artal P, Atchison DA, Hampson KM, Legras R, Lundstrom L, Yoon G. Vision science and adaptive optics, the state of the field. Vision research 2017; 132: 3-33

Marcos S. Isofocal IOL Concept. International Society Of Presbyopia 2019

Marcos S, Benedí-García C, Aissati S, Gonzalez-Ramos AM, Lago CM, Radhkrishnan A, Romero M, Vedhakrishnan S, Sawides L, Vinas M. VioBio lab adaptive optics: technology and applications by women vision scientists. Ophthalmic and Physiological Optics 2020; 40: 75-87

Marcos S, Martinez-Enriquez E, Vinas M, de Castro A, Dorronsoro C, Bang SP, Yoon G, Artal P. Simulating outcomes of cataract surgery: important advances in ophthalmology. Annual Review of Biomedical Engineering 2021; 23: 277-306

Marcos S, Artal P, Atchison DA, Hampson K, Legras R, Lundström L, Yoon G. Adaptive optics visual simulators: a review of recent optical designs and applications. Biomedical Optics Express 2022; 13: 6508-6532

Marín MCP. Óptica fisiológica. Editorial Complutense, 2006

Marsack JD, Thibos LN, Applegate RA. Metrics of optical quality derived from wave aberrations predict visual performance. Journal of vision 2004; 4: 8-8

Martinez-Enriquez E, Pérez-Merino P, Velasco-Ocana M, Marcos S. OCT-based full crystalline lens shape change during accommodation in vivo. Biomedical optics express 2017; 8: 918-933

McCabe C, Berdahl J, Reiser H, Newsom TH, Cibik L, Koch D, Lemp-Hull J, Jasti S. Clinical outcomes in a US registration study of a new EDOF intraocular lens with a nondiffractive design. Journal of Cataract & Refractive Surgery 2022; 48: 1297-1304

McCabe C, Martinez AA. Visual Outcomes and Quality of Vision After Implantation of a New Presbyopia-Correcting Intraocular Lens with a Non-diffractive Design. In: 2021 ASCRS ASOA Annual Meeting. ASCRS, 2021

McLellan JS, Marcos S, Burns SA. Age-related changes in monochromatic wave aberrations of the human eye. Investigative ophthalmology & visual science 2001; 42: 1390-1395

Metcalf H. Stiles–Crawford apodization. JOSA 1965; 55: 72-74

Moarefi MA, Bafna S, Wiley W. A review of presbyopia treatment with corneal inlays. Ophthalmology and therapy 2017; 6: 55-65

Moreno-Barriuso E, Lloves JM, Marcos S, Navarro R, Llorente L, Barbero S. Ocular aberrations before and after myopic corneal refractive surgery: LASIK-induced changes measured with laser ray tracing. Investigative Ophthalmology & Visual Science 2001; 42: 1396-1403

Morgan JI, Hunter JJ, Masella B, Wolfe R, Gray DC, Merigan WH, Delori FC, Williams DR. Light-induced retinal changes observed with high-resolution autofluorescence imaging of the retinal pigment epithelium. Investigative ophthalmology & visual science 2008; 49: 3715-3729

Munnerlyn CR, Koons SJ, Marshall J. Photorefractive keratectomy: a technique for laser refractive surgery. Journal of Cataract & Refractive Surgery 1988; 14: 46-52

Naseri A, McLeod SD. Cataract surgery after refractive surgery. Current opinion in ophthalmology 2010; 21: 35-38

Navarro R, Santamaria J, Bescós J. Accommodation-dependent model of the human eye with aspherics. JOSA A 1985; 2: 1273-1280

Nemeth G, Vajas A, Kolozsvari B, Berta A, Modis Jr L. Anterior chamber depth measurements in phakic and pseudophakic eyes: Pentacam versus ultrasound device. Journal of Cataract & Refractive Surgery 2006; 32: 1331-1335

Norrby S, Piers P, Campbell C, van der Mooren M. Model eyes for evaluation of intraocular lenses. Applied optics 2007; 46: 6595-6605

Olsen T. Calculation of intraocular lens power: a review. Acta Ophthalmologica Scandinavica 2007; 85: 472-485

Oltrup T, Bende T, Al-Mohamedi H, Cayless A, Bende M, Leitritz MA, Schmidt K-UB. Comparison of spherical and aspherical intraocular lenses with decentration and tilt error using a physical model of human contrast vision and an image quality metric. Zeitschrift für Medizinische Physik 2021; 31: 316-326

Pastor-Pascual F, Gómez-Gómez A, Montés-Micó R, Ruiz-Mesa R, Tañá-Rivero P. Polychromatic through-focus image quality in a wavefront-shaping presbyopia correcting intraocular lens. Expert Review of Ophthalmology 2022; 17: 75-79

Perez GM, Manzanera S, Artal P. Impact of scattering and spherical aberration in contrast sensitivity. Journal of Vision 2009; 9: 19-19

Pérez-Gracia J, Ávila FJ, Ares J, Vallés JA, Remón L. Misalignment and tilt effect on aspheric intraocular lens designs after a corneal refractive surgery. Plos one 2020; 15: e0243740

Pérez-Gracia J, Varea A, Ares J, Vallés JA, Remón L. Evaluation of the optical performance for aspheric intraocular lenses in relation with tilt and decenter errors. PloS one 2020; 15: e0232546

Pérez-Merino P, Marcos S. Effect of intraocular lens decentration on image quality tested in a custom model eye. Journal of Cataract & Refractive Surgery 2018; 44: 889-896

Petrash JM. Aging and age-related diseases of the ocular lens and vitreous body. Investigative ophthalmology & visual science 2013; 54: ORSF54-ORSF59

Pieh S, Artmayr C, Pai V, Schartmüller D, Kriechbaum K. Through-Focus Response of Extended Depth of Focus Intraocular Lenses. Journal of Refractive Surgery 2022; 38: 497-501

Piers PA, Fernandez EJ, Manzanera S, Norrby S, Artal P. Adaptive optics simulation of intraocular lenses with modified spherical aberration. Investigative ophthalmology & visual science 2004; 45: 4601-4610

Piers PA, Manzanera S, Prieto PM, Gorceix N, Artal P. Use of adaptive optics to determine the optimal ocular spherical aberration. Journal of Cataract & Refractive Surgery 2007; 33: 1721-1726

PMA P930014/S126: FDA Summary of Safety and Effectiveness Data: https://www.accessdata.fda.gov/cdrh_docs/pdf/P930014S126B.pdf

Pop M, Payette Y. Correlation of wavefront data and corneal asphericity with contrast sensitivity after laser in situ keratomileusis for myopia. In: SLACK Incorporated Thorofare, NJ, 2004; S678-S684

Porter J, Queener H, Lin J, Thorn K, Awwal A. Adaptive optics for vision science. 2006

Radhakrishnan A, Pascual D, Marcos S, Dorronsoro C. Vision with different presbyopia corrections simulated with a portable binocular visual simulator. PLoS One 2019; 14: e0221144

Rampat R, Gatinel D. Multifocal and extended depth-of-focus intraocular lenses in 2020. Ophthalmology 2021; 128: e164-e185

Reinstein DZ, Archer TJ, Gobbe M. The history of LASIK. Journal of Refractive Surgery 2012; 28: 291-298

Rocha KM, Soriano ES, Chamon W, Chalita MR, Nosé W. Spherical aberration and depth of focus in eyes implanted with aspheric and spherical intraocular lenses: a prospective randomized study. Ophthalmology 2007; 114: 2050-2054

Rocha KM, Vabre L, Chateau N, Krueger RR. Expanding depth of focus by modifying higher-order aberrations induced by an adaptive optics visual simulator. Journal of Cataract & Refractive Surgery 2009; 35: 1885-1892

Rocha KM, Vabre L, Chateau N, Krueger RR. Enhanced visual acuity and image perception following correction of highly aberrated eyes using an adaptive optics visual simulator. Journal of Refractive Surgery 2010; 26: 52-56

Roorda A. Adaptive optics for studying visual function: a comprehensive review. Journal of vision 2011; 11: 6-6

Rosales P, Marcos S. Phakometry and lens tilt and decentration using a custom-developed Purkinje imaging apparatus: validation and measurements. JOSA A 2006; 23: 509-520

Rosales P, Marcos S. Customized computer models of eyes with intraocular lenses. Optics Express 2007; 15: 2204-2218

Rosales P, Marcos S. Pentacam Scheimpflug Quantative Imaging of the crystalline lens and intraocular lens. 2008

Rosales P, De Castro A, Jiménez-Alfaro I, Marcos S. Intraocular lens alignment from purkinje and Scheimpflug imaging. Clinical and Experimental Optometry 2010; 93: 400-408

Ryan A, O'Keefe M. Corneal approach to hyperopic presbyopia treatment: six-month outcomes of a new multifocal excimer laser in situ keratomileusis procedure. Journal of Cataract & Refractive Surgery 2013; 39: 1226-1233

Sawides L, De Gracia P, Dorronsoro C, Webster MA, Marcos S. Vision is adapted to the natural level of blur present in the retinal image. PloS one 2011; 6: e27031

Sawides L. Correction and control of ocular aberrations with adaptive optics: effects on human vision. In: Universidad de Valladolid, 2013

Sawides L, de Castro A, Lago CM, Barcala X, Zaytouny A, Marcos S, Dorronsoro C. SimVis simulations of multifocal IOL designs based on public-literature data. In: Optical Design and Engineering VIII. SPIE, 2021; 122-132

Schallhorn JM. Multifocal and extended depth of focus intraocular lenses: a comparison of data from the united states food and drug administration premarket approval trials. Journal of Refractive Surgery 2021; 37: 98-104

Schwiegerling J. Scaling Zernike expansion coefficients to different pupil sizes. JOSA A 2002; 19: 1937-1945

Shetty R, Brar S, Sharma M, Dadachanji Z, Lalgudi VG. PresbyLASIK: A review of PresbyMAX, Supracor, and laser blended vision: Principles, planning, and outcomes. Indian Journal of Ophthalmology 2020; 68: 2723

Stodulka P, Slovak M. Visual Performance of a Polynomial Extended Depth of Focus Intraocular Lens. Open Journal of Ophthalmology 2021; 11: 214-228

Studený P, Hlaváček J, Chaloupka R, Veselý, and Baxant A. D. Virtiol – Simulation of vision guality with multifocal and edof intraocular lenses. Ces. a Slov. Oftalmol 2018; vol. 74, no. 6, pp. 219–225.

Sun M, de Castro A, Ortiz S, Perez-Merino P, Birkenfeld J, Marcos S. Intraocular lens alignment from an en face optical coherence tomography image Purkinje-like method. Optical Engineering 2014; 53: 061704

Sun M, Pérez-Merino P, Martínez-Enríquez E, Velasco-Ocana M, Marcos S. Full 3-D OCT-based pseudophakic custom computer eye model. Biomedical optics express 2016; 7: 1074-1088

Tabernero J, Piers P, Benito A, Redondo M, Artal P. Predicting the optical performance of eyes implanted with IOLs to correct spherical aberration. Investigative ophthalmology & visual science 2006; 47: 4651-4658

Thibos LN, Wheeler W, Horner D. Power vectors: an application of Fourier analysis to the description and statistical analysis of refractive error. Optometry and vision science: official publication of the American Academy of Optometry 1997; 74: 367-375

Thibos LN, Applegate RA, Schwiegerling JT, Webb R. Standards for reporting the optical aberrations of eyes. In: Slack Incorporated Thorofare, NJ, 2002; S652-S660

Thibos LN, Hong X, Bradley A, Applegate RA. Accuracy and precision of objective refraction from wavefront aberrations. Journal of vision 2004; 4: 9-9

Titiyal J, Kaur M, Nair S. Current concepts in Refractive Surgery : Comprehensive Guide to Decision Making & Surgical Techniques. 2021

Tscherning MHE. Physiologic Optics; Dioptrics of the Eye, Functions of the Retina, Ocular Movements and Binocular Vision. Keystone, 1904

Uhlhorn SR, Borja D, Manns F, Parel J-M. Refractive index measurement of the isolated crystalline lens using optical coherence tomography. Vision research 2008; 48: 2732-2738

Unterhorst HA, Rubin A. Ocular aberrations and wavefront aberrometry: A review. African Vision and Eye Health 2015; 74: 6

Uthoff D, Pölzl M, Hepper D, Holland D. A new method of cornea modulation with excimer laser for simultaneous correction of presbyopia and ametropia. Graefe's Archive for Clinical and Experimental Ophthalmology 2012; 250: 1649-1661

Van den Berg T. Light scattering by donor lenses as a function of depth and wavelength. Investigative ophthalmology & visual science 1997; 38: 1321-1332

Vargas-Fragoso V, Alió JL. Corneal compensation of presbyopia: PresbyLASIK: an updated review. Eye and Vision 2017; 4: 1-8

Vedhakrishnan S, Vinas M, Benedi-Garcia C, Casado P, Marcos S. Visual performance with multifocal lenses in young adults and presbyopes. PloS one 2022; 17: e0263659

Villegas EA, Manzanera S, Lago CM, Hervella L, Sawides L, Artal P. Effect of crystalline lens aberrations on adaptive optics simulation of intraocular lenses. Journal of Refractive Surgery 2019; 35: 126-131

Vinas M, Dorronsoro C, Gonzalez V, Cortes D, Marcos S. Testing vision with radial and angularly segmented multifocal patterns using adaptive optics. Investigative ophthalmology & visual science 2015; 56: 1358-1358

Viñas Peña M. Polychromatic adaptive optics to evaluate the impact of manipulated optics on vision. 2015

Vinas M, Dorronsoro C, Gonzalez V, Cortes D, Radhakrishnan A, Marcos S. Testing vision with angular and radial multifocal designs using Adaptive Optics. Vision Research 2017; 132: 85-96

Vinas M, Dorronsoro C, Radhakrishnan A, Benedi-Garcia C, LaVilla EA, Schwiegerling J, Marcos S. Comparison of vision through surface modulated and spatial light modulated multifocal optics. Biomedical optics express 2017; 8: 2055-2068

Vinas M, Gonzalez-Ramos A, Dorronsoro C, Akondi V, Garzon N, Poyales F, Marcos S. In vivo measurement of longitudinal chromatic aberration in patients implanted with trifocal diffractive intraocular lenses. Journal of Refractive Surgery 2017; 33: 736-742

Vinas M, Aissati S, Romero M, Benedi-Garcia C, Garzon N, Poyales F, Dorronsoro C, Marcos S. Pre-operative simulation of post-operative multifocal vision. Biomedical optics express 2019; 10: 5801-5817

Vinas M, Benedi-Garcia C, Aissati S, Pascual D, Akondi V, Dorronsoro C, Marcos S. Visual simulators replicate vision with multifocal lenses. Scientific reports 2019; 9: 1-11

Visser N, Bauer NJ, Nuijts RM. Toric intraocular lenses: historical overview, patient selection, IOL calculation, surgical techniques, clinical outcomes, and complications. Journal of Cataract & Refractive Surgery 2013; 39: 624-637

von F Z. Beugungstheorie des schneidenver-fahrens und seiner verbesserten form, der phasenkontrastmethode. physica 1934; 1: 689-704

Wang L, Dai E, Koch DD, Nathoo A. Optical aberrations of the human anterior cornea. Journal of Cataract & Refractive Surgery 2003; 29: 1514-1521

Wang X, Dong J, Wang X, Wu Q. IOL tilt and decentration estimation from 3 dimensional reconstruction of OCT image. PLoS One 2013; 8: e59109

Watson AB, Pelli DG. QUEST: A Bayesian adaptive psychometric method. Perception & psychophysics 1983; 33: 113-120

Watson AB. Temporal sensitivity. Handbook of perception and human performance 1986; 1: 1-43

White I, Dederich H. American National Standard for Safe Use of Lasers, ANSI Z 136.1–2007. Laser Institute of America: Orlando 2007

Wizinowich P. Adaptive optics in astronomy. Contemporary Physics 2015; 56: 432-450
188 Xia T, Martinez CE, Tsai LM. Update on intraocular lens formulas and calculations. Asia-Pacific journal of ophthalmology (Philadelphia, Pa) 2020; 9: 186

Xu R, Bradley A, Lopez Gil N, Thibos LN. Modelling the effects of secondary spherical aberration on refractive error, image quality and depth of focus. Ophthalmic and Physiological Optics 2015; 35: 28-38

Yi F, Iskander DR, Collins MJ. Estimation of the depth of focus from wavefront measurements. Journal of Vision 2010; 10: 3-3

Yi F, Iskander DR, Collins M. Depth of focus and visual acuity with primary and secondary spherical aberration. Vision research 2011; 51: 1648-1658

Young T. II. The Bakerian Lecture. On the mechanism of the eye. Philosophical Transactions of the Royal Society of London 1801: 23-88

Zabihian A, Maghami M, Asgarian F, Sodagar AM, Hudak R, Penhaker M, Majernik J. Implantable biomedical devices. Biomedical Engineering, Technical Applications in Medicine, Rijeka: InTech 2012: 157-190

Zheleznyak L, Kim MJ, MacRae S, Yoon G. Impact of corneal aberrations on through-focus image quality of presbyopia-correcting intraocular lenses using an adaptive optics bench system. Journal of Cataract & Refractive Surgery 2012; 38: 1724-1733

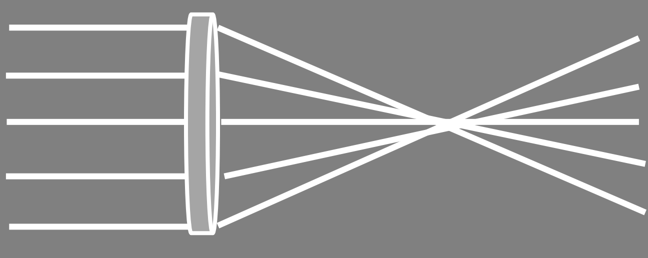

Madrid, 2023